

Technical Report

TR-01-24

# First TRUE Stage – Transport of solutes in an interpreted single fracture

Proceedings from the 4th International Seminar Äspö, September 9–11, 2000

Svensk Kärnbränslehantering AB

August 2001

**Svensk Kärnbränslehantering AB**

Swedish Nuclear Fuel  
and Waste Management Co  
Box 5864

SE-102 40 Stockholm Sweden

Tel 08-459 84 00  
+46 8 459 84 00

Fax 08-661 57 19  
+46 8 661 57 19



# **First TRUE Stage – Transport of solutes in an interpreted single fracture**

**Proceedings from the 4th International Seminar Äspö, September 9–11, 2000**

Svensk Kärnbränslehantering AB

August 2001

# Contents

	Page
<b>Session 1 – Introduction</b>	<b>5</b>
<b>Session 2 – SKB project team interpretation of experimental results</b>	<b>7</b>
<b>Session 3 – Alternative evaluation of TRUE-1 results and related studies</b>	<b>8</b>
<b>Session 4 – Understanding of retention processes in a single fracture</b>	<b>9</b>
<b>Conclusions of the seminar</b>	<b>12</b>
<b>APPENDICES:</b>	<b>209</b>
Appendix A: References	211
Appendix B: Agenda of seminar	216
Appendix C: List of participants	219

# Session 1. Introduction

The First Stage of the Tracer Retention Understanding Experiments (TRUE-1) was initiated in 1994 and the experimental activities were officially concluded in December 1998 with the termination of the final test with radioactive sorbing tracers. The programme also included a laboratory programme focused on both generic (Äspö HRL) and site-specific (Feature A) geological material. Modelling, both scopings, predictions and evaluation of the final tests with sorbing tracers has been performed parallel to the experimental work. The work and conclusions of the SKB TRUE project team have been published in a SKB technical report /Winberg et al., 2000/. The TRUE-1 experiments have also been subject to blind prediction and evaluation by an international group of modelling teams within the auspices of the Äspö Task Force on Groundwater on Modelling of Groundwater Flow and Solute Transport. A list of relevant reports and publications related to the First TRUE Stage are presented in Appendix A.

The present seminar provides a venue to present and discuss the results of the TRUE-1 experiments in terms of identified transport and retention processes and concepts/ approaches used to model. However, given the fact that many international programs, including that of SKB, are either underway or preparing for site characterisation programs, the seminar provides a possibility to discuss research priorities and the specific data needs for development of a geological repository.

In his opening address, the director of the Äspö Hard Rock Laboratory Olle Olsson emphasised the need to carefully integrate available experience from other research sites, e.g. Grimsel (Switzerland), Stripa (Sweden) and El Berrocal (Spain). The two important questions to be asked are;

- What do we know?
- What is the way forward?

For the subsequent discussions four different discussion themes were identified;

1. Identification of transport processes.
2. Model concepts.
3. Site-specific data needs for a geological repository.
4. Research priorities.

## **1. Identification of transport processes**

- Have the dominant transport processes active on the TRUE-1 spatial and temporal scales been identified?!
- If not, what alternative/new transport processes need to be resolved?!
- Have the relevant parameters been collected from field tests, and in sufficient amounts (statistical aspects)?!
- If not, what complementary data are required?!

## **2. Model concepts**

- A conductive single fracture is by necessity connected to a surrounding fracture network. Under what conditions do this surrounding network have to be taken into account!? Do we need to improve understanding of the altered rim zone around a fracture? If so, what are the urgent needs?
- How handle the unknown parts of the flow paths between borehole intercepts?
- Are the modelling concepts based on realistic descriptions of fractured rock, and can adequate data be collected in the field?!
- Are the modelling approaches feasible and useful for modelling of radionuclide migration and retention?!

## **3. Site-specific data needs for a geological repository**

- TRUE-1 has shown that the detailed characteristics of altered rim zone of the studied feature needs to be considered in order to account for the noted retention over the spatial and time scales of the TRUE-1 experiments. To what extent do we need to consider the characteristics of fracture rim zones for the time perspective of a geological repository?
- To what extent can the results and data from TRUE-1 be extrapolated?! This applies both to Äspö itself (including upscaling to larger scales) and transferability to other sites.
- Tracer tests are time and resource intensive elements of site characterisation. For future site characterisation, what types of tests are required to fulfil the data needs of PA (spatial and temporal scales)?!
- Breakthrough curves are an integrated/averaged result of the transport phenomena studied. Detailed information on the flow path geometry and its variability are required to fully differentiate/distinguish effects of transport processes from effects introduced by geometry, e.g. channelling. How far do we need to push the detailed characterisation of a potential repository site? Is it satisfactory to rely on data /extrapolation from detailed pore space information from e.g. the TRUE-1 site?

## **4. Research priorities**

- Is the relation between (the needs of) PA and the TRUE programme satisfactory met?
- Are additional laboratory transport data required?! If yes, of what and in what quantities are data required? In this context, what are the prospects of assessing diffusion properties and variability from electrical well logs.
- Integration of laboratory, detailed and block scale results are considered important to enable a adequate representation of the site scale. Regarding the issue of upscaling, what material parameters need to be addressed?
- Heterogeneity: detailed understanding of pore space of fractures (epoxy resin impregnation), assessment of relative role of internal heterogeneity of fractures relative to that introduced by fracture intersections!
- Improvements in future field tracer experiments.
- Characterisation techniques and methodology.

- Testing techniques (development of single hole tracer test techniques!?)
- Duration of experiments.
- What should the “next” tracer experiment in the TRUE series look like?!
- Scale (integration of scales).
- Configuration of experiment (flow field).

## **Session 2. SKB project team interpretation of experimental results**

*Chairman: Peter Wikberg, SKB*

No specific written account of the results and conclusions by the SKB TRUE Project Team presented as part of Session 2 is provided here, nor is any written account of the TRUE-1 related papers presented as part of Sessions 3a /Birgersson et al./, 3c /Selroos/, and 4 /Cvetkovic/. The reader is instead referred to Winberg et al. /2000/ and the supporting reports listed in Appendix A.

In the ensuing discussion the following items were discussed;

### ***Geometry of studied feature***

The TRUE-1 tracer tests were carried out in an interpreted single fracture denoted Feature A. The investigated reactivated mylonite which makes up Feature A does not intercept the tunnel. Near its projected intersection with the tunnel, however, a dry, apparently non-reactivated mylonite is present with a more gentler slope than Feature A. This feature is visible in the major part of the northern tunnel wall and in the roof. This observation has bearing on the continuity and singularity of Feature A.

As pointed out by the project group, there exists an uncertainty in whether the studied feature is a single feature with an undulating surface, or alternatively, a hydraulic structure made up of a few sub-parallel interconnected conductive structures.

### ***Hydraulic situation***

A decrease in hydraulic head in the vicinity of the tunnel has been observed as time has progressed, and has been interpreted to be associated with drainage of the pore spaces in the immediate vicinity of the tunnel. This is also reflected in an increased gradient towards the tunnel. However, the increase in hydraulic gradient is inconsistent with the reduced inflow to the tunnel segment during the corresponding time period.

A plausible explanation for this inconsistency is that that the spatial window for the pressure registrations (TRUE-1 site, L=20 m) is much smaller than the spatial window used for monitoring of water inflow (L=100 m). This implies that activities at lower elevations in the laboratory may have affected the inflow to Zone NNW-4, assumed to

dominate the inflow to the tunnel section which include the TRUE-1 site. Alternatively, the observation may be caused by development of a low-permeable skin around the tunnel perimeter.

However, the magnitude of the pressure responses, clearly shows that disturbances in Feature A, show well defined responses in other sections including Feature A, with magnitudes significantly higher than in the remainder of the network. In addition the chemical signature in the TRUE-1 block supports the singular and well controlled nature of Feature A.

### ***Retention in the laboratory scale***

Porosities in the range of 0.3–1% have been presented for the various lithological units in the immediate vicinity of Feature A. It was argued by various parties (data from Grimsel, Stripa) that the porosity of lab specimens can be up to a factor 2 higher than a porosity measured in-situ. Diffusivity values for in-situ conditions were reported which were 1–2 orders of magnitude lower than values obtained on corresponding drill cores from in-situ diffusion experimentation at the Canadian URL.

### ***Internal structure***

The SKB project group presented the hypothesis that the studied fracture (Feature A) is either an undulating single fracture plane, partly affected by a dual intercept (cf. Borehole KXTT4), or a system of near parallel connected shorter fractures along the direction of the average orientation of the interpreted Feature A, and also aligned with a reactivated mylonite. Further, that there is a zone of altered Äspö diorite with a higher porosity. A gradient in material properties (porosity and diffusivity) has been interpreted from the fracture surface into the intact rock. Larger fragments of wall rock (Altered Äspö diorite) may exist in the fracture. Fine-grained fault gouge has not been observed. However, its existence cannot be ruled out.

## **Session 3. Alternative evaluation of TRUE-1 results and related studies**

*Chairmen: Olle Olsson and Mansueto Morosini*

Session 3a Detailed characterisation of transport-related properties, see page 13.

Session 3b Alternative evaluation of TRUE-1 results, see page 49.

Session 3c Related studies, see page 135.

## Session 4. Understanding of retention processes in a single fracture

Moderator: Johan Andersson, Streamflow AB

The moderator of the session identified the most important issues to be discussed during the concluding session;

- Do we understand the basic principles for retention in a single fracture/TRUE-1 Feature A?
- Have we seen matrix diffusion demonstrated!?
- Can we defend that values in retention parameters derived from *in situ* experiments are not over-conservative?!
- Is there a way to extrapolate the TRUE-1 results to performance assessment time scales!?
- What data/analysis are needed in the perspective of the explicit needs of performance assessment?!
- What is the role in the future of experiments of TRUE-1 type!?

### **Active processes**

It was pointed out that practically every modeller uses the Advection-Dispersion (AD) model and obtain a good fit! However, this is not necessarily a good qualifier for the validity of the AD concept. There is a need to see the transport problem at hand in other ways. Assume that matrix diffusion (MD) is non-existent. The observed retention in the TRUE-1 experiments can in such a case be explained by e.g. pure surface sorption. However, there is a need to invoke multiple parallel flow paths!

A conceptual model needs to be tested also for alternative test set ups. Otherwise it is impossible to clearly differentiate between models.

When assuming diffusion into matrix rock to be dominant we introduce a factor 30–40 discrepancy between observed laboratory and *in situ* retention parameters. Are we in fact wrong with this assumption Alternative explanations may include effects of e.g.;

- zones of stagnant water with fracture in-fills,
- non-correct flow rates,
- fracture network effects (intersecting fractures).

The above list of alternative processes/effects may according to one analyst explain up to a factor 10–20 of the noted discrepancy between laboratory and *in situ* retention. It was concluded that a number of alternative explanations are available and it was recommended that the Project Team should pursue their plans for resin injection and subsequent excavation and detailed analysis of the excavated material. Three-dimensional effects could be analysed and Cs would still be detectable in the fracture. There is a clear need for independent information to assess the relative effects of different processes/properties.



It was further commented that the internal structure of the flow path is important and could result in an enhanced flow wetted surface area, and if fault gouge is present, it could play an important role. However, the collected breakthrough curves from the experiments (with  $-3/2$  slopes) support the existence of matrix diffusion effects.

It was emphasised that the observed retention is likely to be the result of a combination of effects. It is not a question of either or, with regards to active processes and/or effects! Further, indications of limited or unlimited diffusion can be derived from deviations from the  $-3/2$  slope in a breakthrough curve. Fault gouge could in this context (depending on sorptivity of the individual radionuclide) result in limited diffusion. This type of information can be obtained by extending the experiment duration.

Fault gouge has not been collected from Feature A. However, the amount of gouge material to be expected in a typical fracture at Äspö as observed in the REX experiment is estimated at about  $110 \text{ mg/cm}^2$ .

It was concluded that fault gouge present or not, the internal structure of Feature A still needs to be resolved. Another issue is to what extent the values on flow wetted surface area as determined from the TRUE-1 experiments are relevant for performance assessment (PA)? However, it is important to note that higher retention than assumed in PA has been observed in the TRUE-1 experiments! The discussion theme was then oriented from assessment of understanding of the TRUE-1 experiments towards what type of experiments that should be part a site characterisation programme, and what experiments (at Äspö or elsewhere) that should be made in support of PA.

The principal challenges are to;

- show that the modelling concepts used are defensible,
- assess retention in the long-term perspective,
- understand implications of (modelling results for) extrapolation to longer spatial and temporal scales,
- assess whether additional experiments of TRUE type are necessary?
- come to some kind of common agreement on the above issues.

### ***Flow wetted surface***

It was argued that the water residence time in the PA time perspective is irrelevant. Further that the flow wetted surface (FWS) can be obtained from borehole logs where the FWS per volume of rock  $a_r \sim 4/H$ , where H is the average distance between conductive fractures along the borehole. It was commented that the latter approach to assess FWS from flow data in boreholes has been adopted in the SKB SR 97 study. The question is whether this approach can be defended.

In this context it was argued that the quotient FWS cannot be dissociated with the acting flow Q (FWS/Q). The notion that  $a_r [L^2/L^3]$  alone provide the necessary entity is wrong!

It was added that upscaling of FWS/Q involves both time and space, i.e. it is a scale-dependent parameter. In addition the TRUE-1 has been a series of experiments which have been driven towards minimising mixing. Of interest is to revisit the ideas previously brought forward by Ivars Neretnieks during the planning stages of TRUE Block

Scale where mixing is promoted e.g. by introducing a line sink (e.g. gallery of boreholes) providing multiple breakthrough points.

It was concluded that there exists a need on the part of SKB to unify the views and concepts related to the flow-wetted surface (FWS/Q,  $a_r$ ,  $a_w$  or k) and its estimation.

### ***Internal structure of Feature A***

It was observed that in the event the feature A is characterised by a number of parallel flow channels/fractures, the apertures of these fractures would be in the order of 0.1 mm. In that case it is not important to characterise the aperture distribution of the fracture in detail, i.e. retention will not be governed by aperture variability (and the  $\beta$  parameter as used by the SKB project team). In response it was stated that small scale characteristics and their variability should not be discarded before understanding has been demonstrated.

### ***Relevance to repository performance assessment***

It was pointed out that the step to performance assessment scale is foremost a problem of extrapolation in time. The planned resin impregnation at the TRUE-1 site will shed light on the internal structure of the studied feature, but will not provide the answer to the problem of the time aspect.

### ***Implications for site characterisation***

The discussion was then shifted to the implications of the TRUE-1 results for site characterisation (SC) and the performance of possible new “TRUE-type” experiments.

It was stated that there is no need for tracer tests at SC spatial scales (kilometres), at least not under the early phases of site characterisation.

In this context the correlation between hydro(geo)logy and transport was emphasised in the SC perspective. The question is to what extent hydraulic information can be used to infer about transport.

One should during SC collect whatever information possible with regards to flow/flow distribution in boreholes. In this context Peter Andersson provided an outline of what is planned for SKB tracer experimentation during future SC. One large scale (LPT-2 type (Äspö)) tracer experiment has been proposed with the objective to improve geoscientific understanding, and to provide parameters. In addition, the potential of single hole injection-withdrawal (push-pull) tests is being explored.

In this context the use of environmental tracers as natural analogues for understanding transport in the site scale should not be overlooked. A recent example is the support provided by hydrogeochemistry as part of the analysis of Task 5 of the Äspö Task Force.

Careful “sniffing” of CFCs during long-term pumping tests was suggested as an alternative/complement.

## ***Need for complementary investigations at the TRUE-1 site***

More boreholes (test sections) and additional tracer dilution measurements (using additional sink sections) were requested.

## **Conclusions of the seminar**

The outcome of the 4<sup>th</sup> International Äspö seminar focused on the TRUE-1 experiments can be summarised in the following main bullets;

- There is a general consensus that the observed retardation observed in the TRUE-1 experiments requires diffusion into geological material to be an active process. This supported by the  $-3/2$  slope noted in log-log BTCs. Whether this is due to diffusion (and subsequent sorption) in the altered matrix rock, or in possible fault gouge cannot be differentiated with available data,
- Some researchers claim that the observed enhanced retardation may be explained by diffusion into stagnant water pools, pure surface sorption, or may be due to an underestimation in the flow-wetted surface area. The latter effect may be attributed to a more complex flow path (multi-layered structure) or three-dimensional effects,
- A clear differentiation between the principal active process can only assessed by resin injection and subsequent excavation and analysis,
- It was identified that experiments of TRUE type are important for improving the understanding of retention processes. However, this type of experiment will not be part of a site characterisation programme,
- It was recommended to broaden the data base from the TRUE-1 site before characterising pore space with resin techniques. This includes tracer dilution tests using sinks in other features than Feature A.

## **End of seminar**

Olle Olsson, Peter Wikberg and Anders Winberg thanked the discussion moderator Johan Andersson and all participants for contributing to a good and stimulating discussion and concluded the seminar.

## **References**

**Winberg A, Andersson P, Hermanson J, Byegård J, Cvetkovic V, Birgersson L, 2000.** Äspö Hard Rock Laboratory. Final report of the first stage of the Tracer Retention Understanding Experiments. SKB TR-00-07, Swedish Nuclear Fuel and Waste Management Co.

## **Session 3a**

**Detailed characterisation of  
transport-related properties**

# Contents

	Page
<b>Session 3 a Detailed characterisation of transport-related properties</b>	
Alteration and diffusion profiles in two drill cores from Äspö	15
Uncertainty in rock properties: Implications for analysis of radionuclide migration in heterogeneous bedrock	19
Visualization and quantification of heterogeneous diffusion rates in granodiorite samples by X-ray absorption imaging	31

# Alteration and diffusion profiles in two drill cores from Äspö

Ove Landström

Eva-Lena Tullborg, Terralogica AB, Gråbo

## Executive summary

The effect of hydrothermal and subsequent low temperature alteration/diffusion, and glacial/post-glacial weathering and diffusion have been studied in two cores of quartz monzodiorite. One core (YA 1192) was drilled into the hydrothermally altered wall rock of a water conducting fracture exposed at 170 m depth in the access tunnel to the Äspö Hard Rock Laboratory. The other one (BAS 1) was drilled from an outcrop with a glacially polished surface, 1 km north of the YA 1192 site, c f Figure 3a-1. Both drill cores were sectioned into mm thick slices perpendicular to the core axis. The fracture filling of the YA 1192 core, the weathered surface of the BAS 1 core and the different slices were analysed for major and trace elements and isotopes of U and Th.

This presentation summarises the major findings from the study reported by Landström et al. /2001/.

## **The YA 1192 core**

The altered zone of the YA 1192 core extends to approx. 2.5 cm from the fracture surface. Alteration of plagioclase (plagioclase → albite + sericite + epidote + +/-calcite) dominates, and has resulted in a higher porosity and in formation of secondary minerals with high sorption capacity (e.g. sericite). Br, Cs and the  $^{234}\text{U}/^{238}\text{U}$  activity ratios are increased in the alteration zone, relative to the host rock, indicating saline water (Br) in pores and micro fractures (i.e. an indication of diffusion medium) and diffusion of U and Cs from fracture groundwater (and probably subsequent sorption). The U migration is geologically recent (< 1 Ma). The 2.5 cm altered zone (corresponding to the zone of active matrix diffusion) significantly exceeds the visible red staining zone (0.5 cm) caused by hematite/FeOOH micrograins, emphasising the need of microscopy to identify zones of alteration.

## **Matrix diffusion – comparison with other studies**

Similar results were obtained in analyses of a drill core crosscutting a water-conducting fracture at 317 m depth in the nearby Götömar granite;  $^{234}\text{U}/^{238}\text{U} > 1$  and increase in Cs relative to host rock in the 0–3 cm zone adjacent to the fracture /Smellie et al., 1986 and discussed in Alexander et al., 1990/. The uranium data suggested a recent (< 1 Ma) deposition of U and that at least part of the U originated in fracture groundwater; i.e. by processes similar to those suggested for YA 1192. In a corresponding study from the Kamaishi site in Japan, Ota et al. /1997/ report on a hydrothermally altered zone adjacent to a water-conducting fracture, extending 5 cm into the granodioritic wall rock. The zone is characterised by connected porosity, decreasing with distance from the fracture. They interpreted the increase in U,  $^{234}\text{U}/^{238}\text{U}$  activity ratios > 1 and  $^{230}\text{Th}/^{234}\text{U}$  activity ratios < 1 as diffusion of U into the altered zone, occurring within the last 300 ka. A

correspondence between the extent of alteration zones adjacent to water conducting fractures and in-diffusion of U, evidenced by uranium series measurements, have also been reported from several other sites e.g. Böttstein and Grimsel in Switzerland /Smellie et al., 1986/, El Berrocal in Spain /Heath and Montoto, 1996/ and Eye-Dashwa Lakes granite pluton in Canada /Gascoyne and Schwarcz, 1986/. Miller et al. /1994/ conclude in their review that; “Comprehensive geochemical and petrophysical characterisation reveals that the region of enhanced trace element mobility in the vicinity of a fracture often corresponds to zones of physical or hydrothermal alteration”

The studies cited above support the concept of matrix diffusion as a retardation mechanism for uranium. They also emphasise that alteration processes in the rock adjacent to fractures are, if not a prerequisite, crucial in creating conditions favourable to matrix diffusion; e.g., increased porosity and secondary minerals susceptible to sorption.

### ***The BAS-1 core***

The conspicuous weathering at the BAS-1 site is confined to a narrow rim of the bedrock surface (approx. 0.2–0.5 cm thick). Mass balance calculations for this rim zone (based on immobility of K) indicate that mechanical erosion has dominated over chemical dissolution processes (roughly 10 times greater). The chemical weathering has affected mainly plagioclase and chlorite resulting in slight dissolution of these minerals. Quartz and K-feldspar have remained almost unaltered. Pyrite grains in the outer 2 mm show different degrees of oxidation whereas pyrite grains at 1.5 cm are unaltered. Besides the thin weathered surface rim, slight alteration of plagioclase and increase in porosity is indicated in the 2–3 cm zone below the surface. Decrease of U and Cs concentrations in this zone is then interpreted as being due to leaching/diffusion processes, confined to the Weichselian glaciation (< 100 ka). The  $^{234}\text{U}/^{238}\text{U}$  is close to unity indicating bulk leaching of U under oxic conditions. This is in accordance with results obtained from similar studies in Palmottu /Suksi and Raisilainen, 2000/ and Lac de Bonnet /Gascoyne and Cramer, 1987/. It is suggested that alteration of pyrite and bulk leaching of U are common results of interaction between oxygenated water and the uppermost surface of the bedrock or in near surface fractures in areas exposed to the last glaciation.

### ***Indications of oxygenated glacial melt water***

The deposition of U in Ya 1192 and leaching of U from BAS 1 are coeval to quaternary glacial, interstadial and interglacial periods during which the hydrogeological and geochemical conditions changed significantly. A main question in performance assessment is whether oxygenated glacial melt water can penetrate to the repository depth (500 m) and modify the redox conditions. We conclude that the bedrock surface at BAS 1 has been in contact with glacial melt water as well as meteoric water, resulting in oxidation/alteration of pyrite, oxidation/mobilisation of U, and probably also desorption/mobilisation of Cs. In contrast, no signs of oxygenated glacial melt water influence were found in the YA 1192 core (170 m depth). In fact, the absence of Fe-oxyhydroxides but presence of fresh pyrite in the fracture filling and the altered zone at YA 1192 as well as deposition of U are contradictory to interactions with oxidising glacial melt water from the late glaciations. It is concluded that components of groundwater with glacial melt water signature ( $\delta^{18}\text{O}$  values varying from –15.8 to –13.6 ‰) found at depths from 134 to 450 m at Äspö /Laaksoharju et al., 1999/ are not associated with oxidations processes at these depths (results from this study and mineralogical results

## Äspö - Leaching and deposition of elements

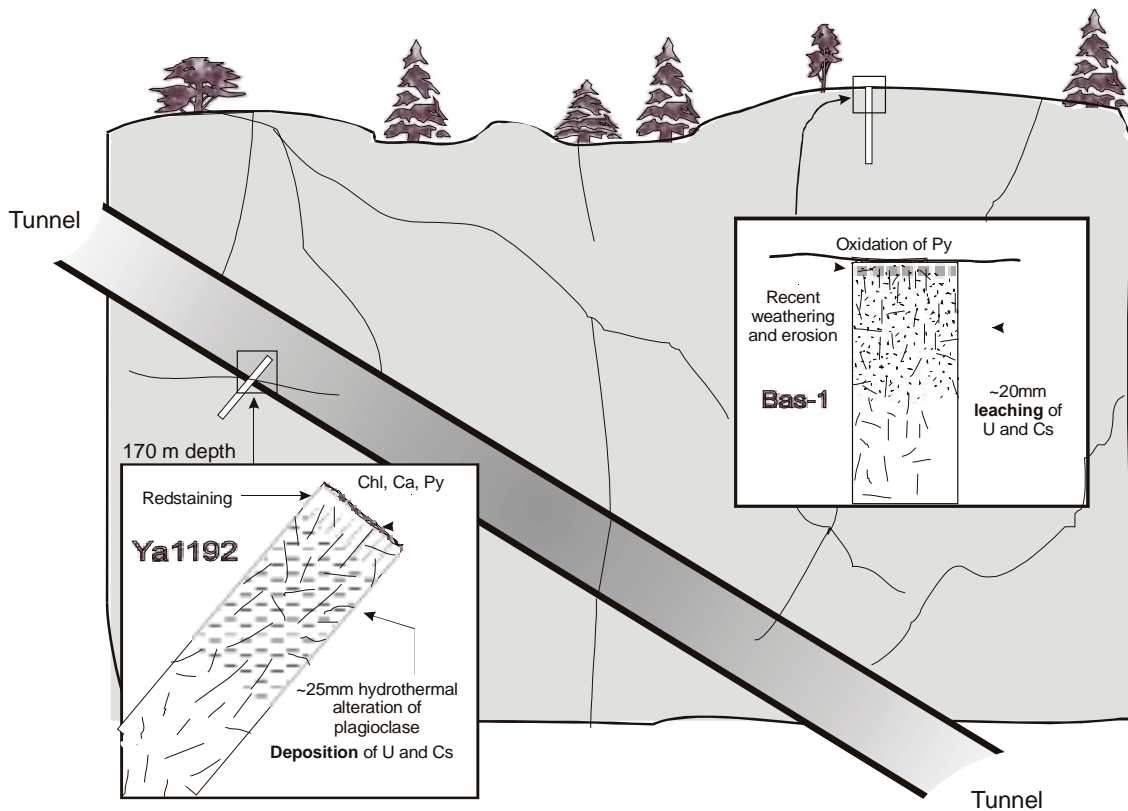


**Figure 3a-1.** Schematic view of the two boreholes; Bas-1 at the surface of Äspö and YA 1192 intersecting a fracture surface at 170 metres depth in the access tunnel to the Äspö Hard Rock Laboratory.

compiled in Tullborg /1997/ and references therein). This means that previous suggestions about a high O<sub>2</sub> content in glacial melt waters may be over-estimated and/or that the O<sub>2</sub> was consumed already in the near surface zone.

## References

**Alexander W R, McKenzie A B, Scott R D, McKinley IG, 1990.** Natural analogue studies in crystalline rock: the influence of water-bearing fractures on radionuclide immobilization in granitic rock repository. NAGRA Technical Report, MTB 87-08, NAGRA, Wettingen, Switzerland.

**Gascoyne M, Cramer J J, 1987.** History of actinide and minor element mobility in an Archean granitic batholith in Manitoba, Canada. *Applied Geochemistry*, 2, 37–54.

**Gascoyne M, Schwarcz H P, 1986.** Radionuclide migration over recent geologic time in a granitic pluton. *Isotope Geoscience*, 59, 75–85.



**Heath M J, Montoto M, 1996.** Rock matrix diffusion as mechanism for radionuclide retardation: Natural radio-element migration in relation to the microfractography and petrophysics of fractures crystalline rock. EU-report EUR 17121 EN.

**Laaksoharju M, Tullborg E-L, Wikberg P, Wallin B, Smellie J, 1999.** Hydrogeochemical conditions and evolution at the Äspö HRL, Sweden. *Applied Geochemistry*, 14, 835–859.

**Landström O, Tullborg E-L, Eriksson G, Sandell Y, 2001 (in press).** Effects of glacial/post glacial weathering compared with hydrothermal alteration – implications for matrix diffusion. Results from drillcore studies in porphyritic quartz monzodiorite from Äspö SE, Sweden. SKB R-01-37, Swedish Nuclear Fuel and Waste Management Co.

**Miller W, Alexander R, Chapman N, McKinley I, Smellie J, 1994.** Natural analogue studies in the geological disposal of radioactive waste. *Studies in Environmental Science* 57. Elsevier, Amsterdam. ISBN 0-444-81755-7.

**Ota K, Amano K, Ando T, Sato H, Shibutani T, Tachi Y, 1997.** In situ Matrix Diffusion in Fractured Crystalline rock, Kamaishi, in situ test site, North-East Japan. In: 6th International Conference on the Chemistry and Migration Behaviour of Actinides and Fission Products in Geosphere. Abst. Migration '97, Sendai, Japan, 26–31 Oct. 1997, 98–99.

**Smellie J A T, McKenzie AB, Scott R D, 1986.** An analogue validation study of natural radionuclide migration in crystalline rocks using uranium-series disequilibrium studies. *Chemical Geology*, 55, 233–254.

**Suksi J, Rasilainen K, 2000.** Isotopic fractionation of U in rocks reflecting redox conditions around a groundwater flow route. *Mat. Res. Soc. Symp. Proc.* (in print).

**Tullborg E-L, 1997.** Recognition of low temperature processes in the Fennoscandian shield. Ph D thesis, Earth Science Centre A17, Göteborg University, ISSN 1400-3813.

# Uncertainty in rock properties: Implications for analysis of radionuclide migration in heterogeneous bedrock

*Anders Wörman and Shulan Xu,  
Department of Earth Sciences, Uppsala University, Sweden*

## Abstract

A basic rationale for the current study is that site investigations in connection with the planning of the final repository for high radioactive waste will provide only fragmentary (discrete) information of the bedrock properties. Since the bedrock displays generally a significant heterogeneity in most properties of relevance to radionuclide migration, there will be uncertainties about the barrier effect provided by the bedrock towards accidental leakage of radionuclides from the repository.

This paper shows how the heterogeneity in the bedrock properties has two fundamentally different implications for an analysis of radionuclide transport. Firstly, the actual variation of bedrock properties causes migrating nuclides to encounter a certain (known) distribution of properties along their transport path. The associated effect does not depend on the spatial correlation of properties (auto-covariance), but does depend on the variance and cross-correlation between the properties. A second effect is due to the uncertainty about the statistical representativity of properties along an individual transport path, which is related to the discrete measuring technique. This effect can, generally, be considered to be the main effect of the heterogeneity of the bedrock on analysis of solute transport. By analysis of an ensemble of equally probable realisations of the transport along an individual path we were able to express the expected values of the mean and variance of the residence time PDF for radionuclides travelling in a single fracture. The 'uncertainty effect' is significant if a certain sum of H-terms is much larger than unity.

Based on geostatistical information for the Swedish granitic bedrock, the effect of uncertainty of bedrock properties on the transport of radionuclides can be important for fractures thinner than about 0.1 mm. The geostatistical information was obtained through sampling drill-cores at the Äspö Hard Rock Laboratory and performing a large number of batch tests in sub-samples taken in a certain pattern in the cores.

## 1 Introduction

One component in the system for disposal of radioactive waste in geological formations is the bedrock itself. Migrating radionuclides (RNs) is assumed to be retarded by diffusion into stagnant pore water (in micro-fissures and matrix pores) and adsorption onto solid surfaces. A significant problem, however, in a performance assessment is to estimate the barrier effect of the geosphere. The significant spatial variability of the rock properties implies that migrating RNs encounter a distribution of bedrock properties and mass-transfer mechanisms in different proportions along the transport paths. For practi-

cal reasons, we will never be able to know exactly this distribution of properties by performing a reasonable amount of measurements in a site investigation.

On the contrary, recent experimental studies reveal that crystalline bedrock can possess a marked heterogeneity of various physical and geochemical properties /Hakami and Barton, 1990; Siitari-Kauppi et al., 1997; Xu and Wörman, 1998/ that potentially may have a certain impact on the transport of RNs in fractured bedrock. Also current field investigation techniques provide only fragmentary information of the properties of the geosphere. This is a basic motivation for treating flows of water and solute elements in groundwaters by means of stochastic continuum models /Gelhar et al., 1974; Dagan, 1989; Gutjahr et al. 1978; Gelhar et al., 1979; Gelhar and Axness, 1983/. The problem is stated mathematically as a system of partial differential equations (PDE) with spatially stochastic perturbations introduced in the coefficients. In such an approach we recognise the spatial variability in bedrock properties along a specific pathway but also a distribution of equally probable pathways that reflects our uncertainty of the bedrock. Solution to the ensemble average of the transport along the distribution of pathways and estimation of the uncertainty of the averaged solution are the aims of the stochastic approach.

The stochastic analysis is based on the idea that we know only certain point values of the property fields and use this information to estimate intermediate values. If we were able to estimate the exact distribution of values from a large number of samples it would be relevant to perform a deterministic analysis of the transport. Consequently, there are two important problems (at least) related to the spatial variability of rock properties, effects of the actual (real) spatial parameter variability along the pathway and effects due to the uncertainty in our knowledge of the heterogeneous rock properties. The first problem can be analysed based on a deterministic description of the parameter variability, whereas the second problem requires a stochastic approach. The purpose of this paper is to outline the implications of the two approaches and to show how the stochastic approach can be supported by geo-statistical data obtained from rock samples. The solute transport is assumed to occur in a single fracture and diffusion and equilibrium sorption in the rock matrix affect the transport.

In this paper we show also how rock samples taken at Äspö are analysed with respect to effective diffusivity, porosity and sorption properties. The data is analysed and represented in the form of basic semi-variograms for Äspö diorite and Smålands granite.

## 2 General formulation of the problem

Transport of radionuclides in a single fracture in bedrock can be expressed as /Neretnieks, 1980/:

$$\frac{\partial \tilde{c}}{\partial t} + \tilde{u} \frac{\partial \tilde{c}}{\partial x} - 2 \frac{\tilde{\varepsilon}_t \tilde{D}_p}{\tilde{h}} \frac{\partial \tilde{c}_m}{\partial z} \Big|_{z=0} = 0 \quad (1)$$

$$(1+K_D) \frac{\partial \tilde{c}_m}{\partial t} - \frac{\tilde{\varepsilon}_t}{\tilde{\varepsilon}} D_p \frac{\partial^2 \tilde{c}_m}{\partial z^2} = 0 \quad (2)$$

where  $c$  is the concentration of solute per unit volume of water [ $\text{kg}/\text{m}^3$ ],  $c_m$  is the dissolved solute mass per unit volume of pore water in the rock matrix [ $\text{kg}/\text{m}^3$ ], the pore diffusivity  $D_p = D\delta_D/\tau^2$  [ $\text{m}^2/\text{s}$ ],  $D$  is the molecular (ionic) diffusion coefficient [ $\text{m}^2/\text{s}$ ],  $\delta_D$  is the constrictivity,  $\tau$  is the tortuosity,  $u$  is the advection velocity of the solute [ $\text{m}/\text{s}$ ],  $t$  is the time [ $\text{s}$ ],  $x$  is a length co-ordinate,  $h$  is the fracture aperture [ $\text{m}$ ],  $\epsilon$  is the total porosity of rock matrix,  $\epsilon_t$  is the porosity of rock matrix available to matrix diffusion,  $\rho$  is the density of the rock [ $\text{kg}/\text{m}^3$ ] and the partition coefficient  $K_D = (\rho/\epsilon)(c_w/c_m)$ . This formulation deviates from the one proposed by Neretnieks /1980/ in that we have decided to differentiate between the porosity available to transport and the total porosity (important to the accumulation capacity). Further, variables marked with a tilde '~' are assumed to be spatially variable in the  $x$ -direction (either randomly or deterministically).

We chose to analyse a case in which a short pulse is introduced at the upstream side of the fracture, i.e. the boundary conditions are defined as:

$$\tilde{c}(x=0, t) = \delta(t) \frac{M}{Q} \quad (3)$$

$$\tilde{c}_m(z=0, t) = \tilde{c}(x, t) \quad (4)$$

$$\tilde{c}_m(z=\infty, t) = 0 \quad (5)$$

where  $M$  is total solute mass [ $\text{kg}$ ],  $Q$  is discharge [ $\text{m}^3/\text{s}$ ] and  $\delta$  is Diracs delta function [ $\text{s}^{-1}$ ]. By solving the problem in the Laplace domain with zero initial concentration and using a standard transform /e.g. Rådhe and Westgren, 1989/ we obtain the solution on the form:

$$c(x, t) = \frac{M}{Q} \frac{x \epsilon_t}{u h} \sqrt{\frac{\epsilon D_p (1 + K_D)}{\pi (t - x/u)^3 \epsilon_t}} \exp\left[-\frac{\epsilon_t \epsilon D_p (1 + K_D) x^2}{h^2 u^2 (t - x/u)}\right] \theta(t - x/u) \quad (6)$$

where  $\theta$  is the Heaviside unit function.

### 3 Deterministic analysis of solute transport with spatially variable rock properties

A purpose of this section is to analyse the effect of a deterministic (known) variability of rock properties on the solute transport in a single fracture. Such a solution is important in order to understand the different effects of parameter heterogeneity related to the actual (real) spatial variability along a specific transport path and the effect related to our uncertainty of the exact variability.

For simplicity we start by consider a fracture that is divided in two parts of equal size. Since there is no diffusive term in (1) we can obtain the solution  $S$  at the distance  $x=X$  by using the solution from the first half ( $x=X/2$ ) as a boundary condition for solving the

transport in the second half. Formally, the solution can be expressed as a convolution  $S = S_1 \cdot S_2$  where the subscripts 1 and 2 denote the first and second halves of the fracture and  $\cdot$  is the convolution operator. In terms of the solution (6), the result is;

$$c(x,t) = \frac{M}{Q} \int_0^{\infty} \frac{X/2 \varepsilon_{t2}}{u_2 h_2} \sqrt{\frac{\varepsilon_2 D_{p2} (1 + K_{D2})}{\pi (t - \tau - (X/2)/u_2)^3 \varepsilon_{t2}}} \exp\left[-\frac{\varepsilon_{t2} \varepsilon_2 D_{p2} (1 + K_{D2}) (X/2)^2}{h_2^2 u_2^2 (t - \tau - (X/2)/u_2)}\right] \theta(t - \tau - (X/2)/u_2) \\ \frac{X/2 \varepsilon_{t1}}{u_1 h_1} \sqrt{\frac{\varepsilon_1 D_{p1} (1 + K_{D1})}{\pi (t - (X/2)/u_1)^3 \varepsilon_{t1}}} \exp\left[-\frac{\varepsilon_{t1} \varepsilon_1 D_{p1} (1 + K_{D1}) (X/2)^2}{h_1^2 u_1^2 (t - (X/2)/u_1)}\right] \theta(t - (X/2)/u_1) d\tau \quad (7)$$

We can see directly from convolution principles that the convolution (7) is identical to the convolution in which the solutions  $S_1$  and  $S_2$  are interchanged with each other; i.e.  $S_1 \cdot S_2 = S_2 \cdot S_1$ . The same conclusion can be reached by recognising the convolution as an inversion rule for Laplace transforms, i.e.  $L[S] = L[S_1] L[S_2]$ , and analysing the appearance of the solution in the Laplace domain /Hautojärvi A, Poteri A, Personal communication/. The implication is that the spatial order of the two halves does not affect the convoluted solution. However, the variance of the properties affects the solution. Since the different properties form a lumped parameter  $P$  that is a function of the different variables  $P(K_p; \varepsilon; \varepsilon_t; u; h)$ , we cannot unconditionally use the expected values of the individual parameters, i.e.  $E[P] \neq P(E[K_p]; E[\varepsilon]; E[\varepsilon_t]; E[u]; E[h])$ . This is because of both possible cross-covariance between parameters and the fact that the expected value of a function of a single stochastic variable is not generally the function of the expected value of the stochastic variable.

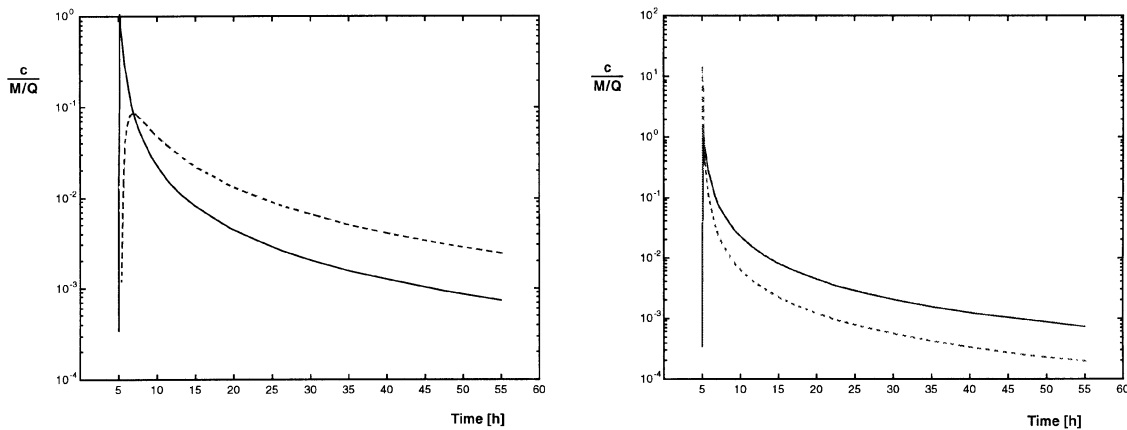


**Figure 3a-2.** Solution according to (7) to transport in a fracture in which the properties are different in two half-parts (solid curves) and the solution according to (6) with expected value of the individual parameters (dashed curve). In the left-hand diagram the effective diffusivity  $D_p$  varies a factor 10 between the two half-parts. In the right-hand diagram the fracture aperture  $h$  varies a factor 10 between the two half-parts. The largest values of  $D_p$  and  $h$  were  $3.6 \times 10^7 \text{ m}^2/\text{h}$  and  $5 \times 10^{-4} \text{ m}$ . Further,  $u = 0.198 \text{ m/h}$ ,  $K_p = 540$ ,  $\varepsilon_1 = 0.004$  and  $\varepsilon_2 = 0.006$ .

The convolution can be performed for any arbitrary number of parts of any arbitrary lengths, which means that the above conclusions can be generalised to a continuum. Consequently, if we were able to take samples from the bedrock to the extent that we are sure what properties migrating RNs will encounter, the auto-correlation of a rock property would not be important. However, the variance of the properties could be important. Figure 3a-2 shows how the solution varies between a case in which when we consider the variance in the properties (solution is obtained as  $E[S]$ ) and when the properties are represented using expected values (solution is obtained as  $S(E[K_p]; E[\epsilon]; E[\epsilon]; E[u]; E[h])$ ). The difference is generally not so great even if all properties vary and, for moderate variances, we can use the expected values of the properties as approximations.

#### 4 Stochastic approach to account for parameter variability

From the previous section we have seen that there is a difference in the solution to the RN transport in a rock fracture when we use mean values of the properties and when we consider a known sequence of the properties. A purpose of this section is to express the solution using effective values of the rock properties. Following the deterministic approach of the previous section could lead to the objective, but this would require that we ignore the uncertainty of the rock properties that is associated with a discrete information of the bedrock. However, analysing an ensemble of equally probable realisations of the real case can represent the uncertainty in the solution, where the ensemble of realisations satisfies certain statistical requirements of the bedrock.

By assuming that the properties (denoted by tilde in (1) and (2)) are spatially random, we are able to express both the expected value of the solution  $E_e[S]$  and the uncertainty of the solution in terms of the variance  $Var_e[S]$ , where subscript e denotes evaluation over the 'ensemble'. In order to do this, we de-couple the two-dimensional flow problem from the one-dimensional mass-transfer problem using a Lagrangian way of description /e.g. Cvetkovic and Selroos, 1999/. The one-dimensional solution applies along individual transport paths or for a case in which the flow is uniform. By assuming small perturbations and exponential covariance functions of all rock properties, we are able to solve the mass-transfer problem in terms of the expected values of the mean and the variance of the residence times in the fracture /Wörman et al., 2000/ (cf. Figure 3a-3). These quantities have been appointed as relevant performance indices by Cvetkovic and Selroos /1999/.

Microstructural evidences and historical records of matrix diffusion indicate that the diffusion is limited to a narrow zone adjacent to water conducting fractures /Heath and Montoto, 1996/. From observations of the uranium series concentration profiles adjacent to a fracture they concluded that the penetration seems to be limited to the order of millimetres or tens of millimetres from the main fracture plane /Heath et al., 1992/. Therefore, it seems justified to replace the boundary condition (5) with a no-flux condition at a depth in the rock matrix equal to  $Z$  [m]. The solutions are then obtained in the forms

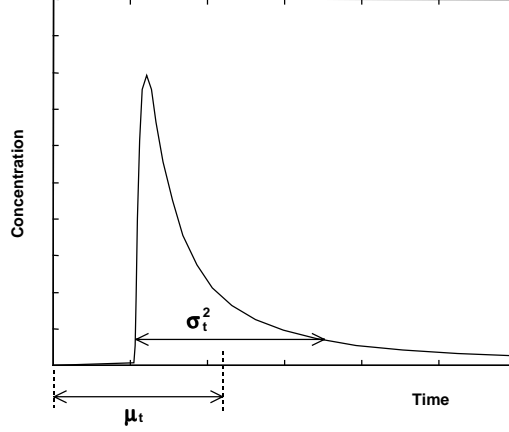


**Figure 3a-3.** Principal sketch of how a breakthrough is characterised by the expected value and the variance of the breakthrough (residence time probability density function).

$$\mu_t = \frac{x}{u} E[\eta_1] (1 + E[\eta_2] R) \quad (8)$$

$$\sigma_t^2 = \frac{2}{3} \frac{x}{u} R T E[\eta_1] E[\eta_2] \left[ 1 + 3 R \left( \frac{(1 + R)^2 E[\eta_2]}{R^2} H_1 + \sum_{i=2}^7 H_i \right) \right] \quad (9)$$

in which  $\mu_t$  = expected value of residence time PDF,  $\sigma_t^2$  = variance of residence time PDF,  $R = (1 + K_D) (2 Z \epsilon) / h$ ,  $T = (\epsilon / \epsilon_t) (Z^2 / D_p) (1 + K_D)$  [s],  $H_i = (I_i b_i) / (E[\eta_1] E[\eta_2] u T)$ ,  $\eta_1 = u / \tilde{u}$ ,  $\eta_2 = (D_p / D_p)^{0.5} (\tilde{\epsilon}_t \tilde{\epsilon} / \epsilon_t \epsilon)^{0.5} ((1 + K_D) / (1 + K_D))^{0.5} h / \tilde{h}$  and variables without a tilde should be regarded as expected values (e.g.  $u = E[u]$ ). The correlation lengths  $I_i$  and variances  $b_i$  are defined in Table 3a-1. The uncertainty of (8) and (9) can be expressed in terms of their variances in the Laplace domain and inverted numerically /Wörman et al., 2000/.

Consequently, there are three typical parameters governing the RN transport. The R-parameter can be viewed as a retardation factor, the T-parameter is a typical residence time for RNs in the rock matrix and the seven H-terms reflect the effect of the uncertainty of the heterogeneous rock properties (i.e. the uncertainty of the rock properties along a single arbitrary transport path). If the rock properties are completely spatially uncorrelated ( $I_i = 0$ ), there is no uncertainty of the distribution of parameters along a transport path. In all realisations of the transport we will then have a complete representation of all properties and, in that case, their spatial correlation is of no importance (cf. previous section).

The expected values  $E[\eta_1]$  and  $E[\eta_2]$  represent the effect of the actual (known) variability in parameters that exists even if there is no uncertainty about the distribution of properties along a specific transport path. This effect is the same as that described in the previous section. These averages should be weighted by distance  $x$  and depend on the cross-correlation of the properties but not their auto-correlation. For most practical purposes, the expected values  $E[\eta_1]$  and  $E[\eta_2]$  can be regarded as being effectively unity.

To sum up, the main effect of heterogeneity of the rock properties is due to the uncertainty of the properties associated with a discrete sampling technique; this is the effect accounted for by the H-terms in (9).

**Table 3a-1. Definition of covariance function for the auxiliary variable  $\beta$  and the amplitudes (variance),  $a_i$ , of the series representation.**

$$\text{Cov}[b(s)] = \text{Cov}[b'(s)] = \sum_{i=1}^7 a_i \exp(-|s|/\lambda_i)$$

$$\tilde{M}_p = \tilde{D}_p^{0.5} (\tilde{\epsilon}_+ \tilde{\epsilon})^{0.5} (1 + \tilde{K}_D)^{0.5}$$

Definitions of coefficients  $c_1$  and  $c_2$  can be found in Appendix 1

i	$a_i$	$b_i$	$I_i$
1	$(c_1 + E[\eta_2] c_2)^2 b_i$	$\text{Var}[u/\tilde{u}]$	$I_u$
2	$(c_2)^2 b_i$	$E^2[\eta_1] E^2[h/\tilde{h}] \text{Var}[\tilde{M}_p/M_p]$	$I_M$
3	$(c_2)^2 b_i$	$E^2[\eta_1] \text{Var}[h/\tilde{h}]$	$I_h$
4	$(c_2)^2 b_i$	$E^2[\eta_1] \text{Var}[\tilde{M}_p/M_p] \text{Var}[h/\tilde{h}]$	$\frac{1}{1/\lambda_M + 1/\lambda_h}$
5	$(c_2)^2 b_i$	$\text{Var}[\tilde{M}_p/M_p] \text{Var}[u/\tilde{u}] E^2[h/\tilde{h}]$	$\frac{1}{1/\lambda_u + 1/\lambda_M}$
6	$(c_2)^2 b_i$	$\text{Var}[h/\tilde{h}] \text{Var}[u/\tilde{u}]$	$\frac{1}{1/\lambda_u + 1/\lambda_h}$
7	$(c_2)^2 b_i$	$\text{Var}[h/\tilde{h}] \text{Var}[u/\tilde{u}] \text{Var}[\tilde{M}_p/M_p]$	$\frac{1}{1/\lambda_u + 1/\lambda_h + 1/\lambda_M}$

## 5 Measuring variability of bedrock properties

Petrographic analyses of fractures in crystalline bedrock indicate that there is a significant spatial variability of the properties affecting the migration of naturally existing elements in the groundwater /Heath and Montoto, 1996/. Similarly, investigations of the variation of the aperture in rock fractures at Äspö indicate a significant variation /Hakami and Barton, 1990; Siitari-Kauppi et al., 1997/. In the stochastic theory of the previous section, these variation in the problem variables can be represented in terms of the advection velocity  $u$ , the aperture  $h$  and the matrix property  $M$  (Table 3a-1 defines  $M$ ). This separation/limitation is proposed because  $u$ ,  $h$  and  $M$  can readily be treated independently. In the theory, the cross-correlation between  $u$ ,  $h$  and  $M$  have been neglected, whereas there is a possibility to design measurements so that the cross-covariances between the parameters defining  $M$  can be taken into account.

In a real fracture, the aperture varies and distorts the flow field. The statistics of the rock properties should thus be evaluated along the stream-lines by means of numerical simulations of the flow. The general statistics of  $h$  and  $M_p$ , obtained in an arbitrary



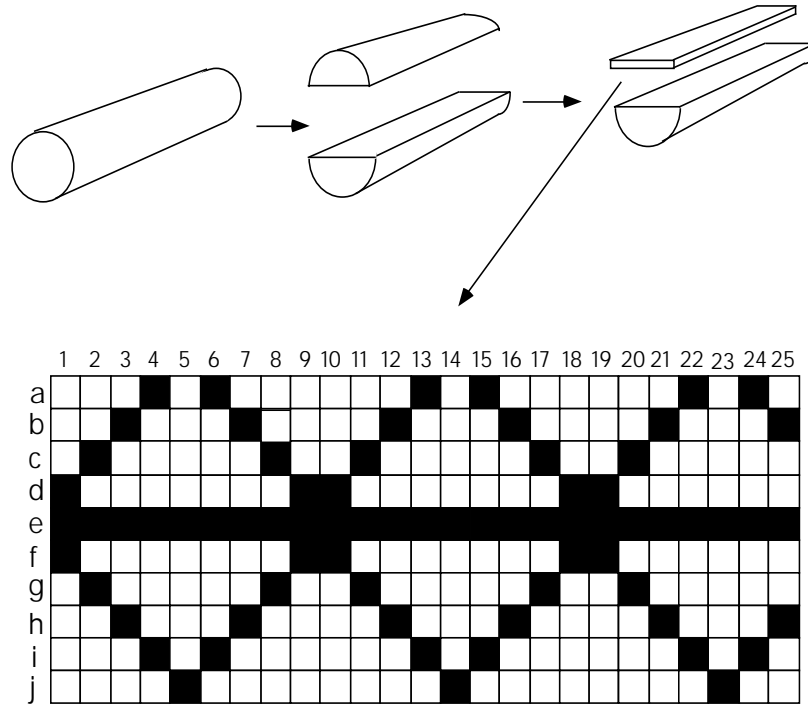


**Figure 3a-4.** Schematic of the sampling pattern used on drill cores taken at Äspö Hard Rock Laboratory. Black squares represent slabs to be investigated with regard to certain parameters.

direction, should be converted to the statistics in  $u$ ,  $h$  and  $M_p$  encountered along streamlines. In order to calculate the flow field (statistics in  $u$ ) we need to know the aperture statistics. The remaining requirement to facilitate the analysis of the solute mass transport is then to obtain the statistics in the matrix property  $M_p$ .

In order to study the statistics of  $M_p$  in granitic bedrock, nine drill cores were taken from the Äspö hard rock laboratory, Kalmar County in Sweden. The cores had a diameter of 20 cm, a length ranging from 50 to 90 cm and they were taken both in Äspö diorite and Småland granite. The drill cores were used for certain migration tests (not reported here), evaluation of mineral composition, and different batch tests like leaching, through diffusion, in-diffusion and sorption tests on crushed rock /Xu and Wörman, 1998/. The main minerals of Småland granite are quartz, potassium feldspar, muscovite and saussuritized feldspar.

Rock slabs were taken in a certain pattern (Figure 3a-4) which facilitated a reliable geostatistical analysis of the data in two dimensions. The size of each slab face was 20x20 mm and the thickness varied in the range 6–15 mm. The auto-covariance function or semi-variogram of the data (porosity, effective diffusivity and sorption properties) can be estimated from measurements on the individual slabs with appropriate separation distances. The correlation length in an arbitrary direction in the  $(x, y)$ -plane,  $I$ , was evaluated based on the assumption of isotropic conditions. Figure 3a-5 shows the auto-covariance of the matrix property  $M_p$  when the cross-correlation between properties is accounted for.

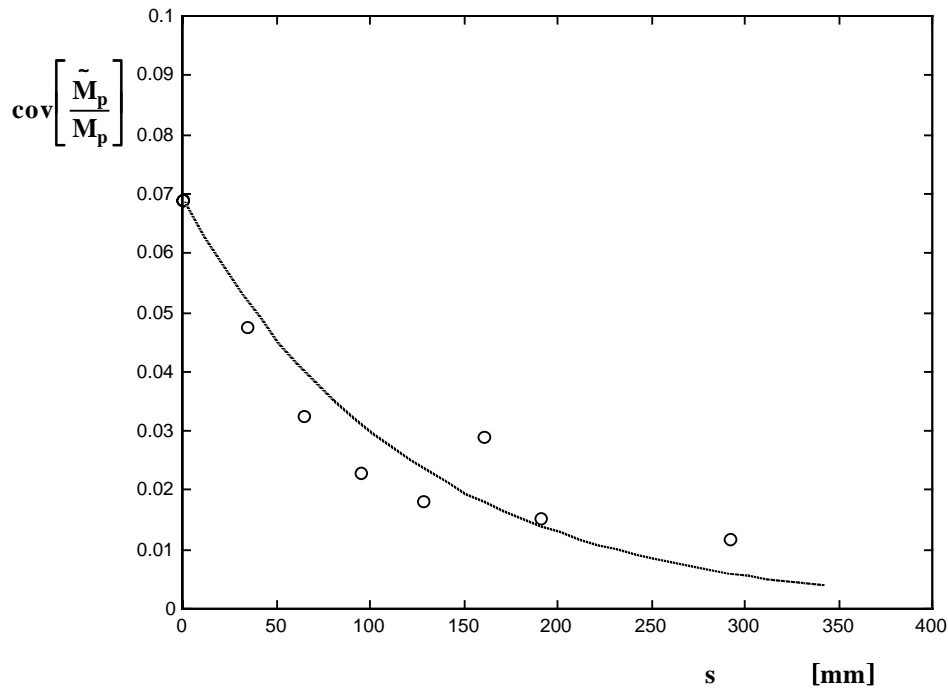


**Figure 3a-5.** Auto-covariance vs separation distance for the effective matrix parameter  $\tilde{M}_p$  obtained for a diorite taken at Äspö Hard Rock Laboratory, Sweden /Xu and Wörman, 1998, 1999/. The curve represents the exponential covariance function.

By using the data obtained in this study and the statistics of fracture aperture variation of Hakami and Barton /1990/ we found that typical statistics for Äspö diorite is given by  $\sum_{i=1}^7 \lambda_i b_i \approx 0.21$  and  $\sum_{i=1}^7 \lambda_i^2 b_i \approx 0.032$ . Based on this statistics and a plausible relationship between fracture aperture and groundwater flow velocity, we can conclude that the effect of heterogeneity (uncertainty) in the rock properties can significantly affect the variance in the residence time PDF (cf. (9)) /Wörman et al., 2000/. The aperture needs to be thinner than about 0.1 mm for this effect to be essential.

## 6 Discussion and conclusions

The isolation of spent nuclear fuel in a deep repository in bedrock relies to a certain extent on geosphere retardation of radionuclides that accidentally escapes from the repository. In the analysis of radionuclide migration we are facing two types of problems related to the spatial variability of the bedrock properties. Firstly, a known sequence of different values of the rock properties affects the solution. This is because of both possible cross-covariance between parameters and the fact that the expected value of a function of a single stochastic variable is not generally the function of the expected value of the stochastic variable. In this case, where the exact distribution of rock properties is known, the solution is independent, however, on the spatial correlation between properties.

This type of “deterministic/actual” heterogeneity effect appears both in a deterministic analysis of the spatial variability of the properties and in an analyses in which the properties are assumed to be spatially random. The latter approach reflects the fact that

there is also an uncertainty about the exact appearance of the property fields, which in many cases can be significant. Field investigations provide generally only discrete (and sparse) information that implies marked uncertainties in the analysis of solute transport.

By means of a stochastic analysis we were able to represent the effect of the uncertainty of the rock properties on the mean value solution and the uncertainty of the solution. This additional effect of heterogeneity of the properties is generally more pronounced than that due to a known sequence of the properties  $\sum_{i=1}^7 \lambda_i b_i / (u T) \gg 1$ , we need to consider the uncertainty in the rock properties, where  $u$  is advection velocity,  $T$  is residence time in the rock matrix,  $I_i$  is correlation lengths and  $b_i$  are variances defined in Table 3a-1. As a rule of thumb for conditions typical to the Swedish bedrock at a depth of 500 m, the aperture needs to be thinner than about 0.1 mm for the effect of heterogeneity (uncertainty) in rock properties to have an essential impact on the variance in the residence time PDF.

## 7 Acknowledgements

This paper presents the outcome of a project that was initiated by Björn Dverstorp at the Swedish Nuclear Power Inspectorate in order to study how geosphere retardation can be considered in a performance assessment of a repository for spent nuclear fuel that is placed in a heterogeneous bedrock. The project started in July of 1994 and will be completed in February of 2001. It was the basis for a PhD-dissertation of the second author /Xu, 2000/.

## References

- Cvetkovic V, Selroos J-O, 1999.** Geosphere performance indices: Comparative measures for site selection and safety assessment of deep waste repositories SKB Rapport R-99-01, Swedish Nuclear Fuel and Waste Management Co.
- Gelhar L W, Ko P Y, Kwai H H, Wilson J L, 1974.** Stochastic Modelling of Ground-water System, Rep. 189, R. M. Parsons Lab. for Water Resour. and Hydrodyn., Mass. Inst. of Technol., Cambridge.
- Gelhar L W, Gutjahr A L, Naff R L, 1979.** Stochastic Analysis of Macrodispersion in a Stratified Aquifer, Water Resources Res., 15(6), 1387–1397.
- Gelhar L W, Axness C L, 1983.** Three-dimensional Stochastic Analysis of Macrodispersion in Aquifers, Water Resources Res., 19(1), 161–180.
- Gutjahr A L, Gelhar L W, Bakr A A, MacMillan J R, 1978.** Stochastic Analysis of Spatial Variability in Subsurface Flows, 2. Evaluation and Application. Water Resources Res. 14(5), 953–959.

**Hakami E, Barton N, 1990.** Aperture Measurements and Flow Experiments Using Transparent Replicas of Rock Joints, Proc. Int. Symp. Rock Joints, Loen, Norway, Eds. Barton and Stephansson, Balkema, Rotterdam, The Netherlands, 383–390.

**Heath M J, Montoto M, 1996.** Rock Matrix Diffusion as Mechanism for Radionuclide Retardation: Natural Radio-Elements Migration in Relation to the Microfractography and Petrophysics of Fractured Crystalline Rock, Report EUR 17121, European Commission, ISBN 92-827-3907-4.

**Heath M J, Montoto M, Rodriguez Rey A, Ruiz de Argandona V G, Menendez B, 1992.** Rock Matrix Diffusion as a Mechanism of Radionuclide Retardation: A Natural Analogue Study of El Berrocal Granite, Spain. *Radiochimica Acta* 58/59, 379–384.

**Rådhe L, Westgren B, 1989.** Mathematics Handbook for Science and Engineering, Studentlitteratur, Lund, Sweden.

**Siitari-Kauppi M, Lindberg A, Hellmuth K H, Timonen J, Väättäinen K, Hartikainen J, Hartikainen K, 1997.** The Effect of Microscale Pore Structure on Matrix Diffusion æ a Site-specific Study on Tonalite. *J. Contaminant Hydrology*, 26, 147–158.

**Wörman A, Xu S, Dverstorp B, 2000.** Kinematic Analysis of Solute Mass Flows in Rock Fractures with Spatially Random Parameters. Under review: *Water Resources Research*.

**Xu S, 2000.** Effect of uncertainty of rock properties on radionuclides transport by groundwater: Implications to performance assessments of the repository of spent nuclear fuel in heterogeneous bedrock, PhD thesis, In press: *Acta universitatis upsaliensis*, Uppsala Universitet, Sweden.

**Xu S, Wörman A, 1999.** Implications of Sorption Kinetics to Radionuclide Migration in Fractured Rock, *Water Resources Research*, 35(11), 3429–3440.

**Xu S, Wörman A, 1998.** Statistical Patterns of Geochemistry in Crystalline Rock and Effect of Sorption Kinetics on Radionuclide Migration, SKI Report 98:41, Stockholm, Sweden, ISSN 1104–1374.

## Appendix 1: Definition of coefficients Table 3a-1

$$c_1 = p/u \quad (A1)$$

$$c_2 = -\frac{2}{h u} \sqrt{p D_p \varepsilon_t \varepsilon \left(1 + K_D \frac{k_r}{p + k_r}\right)} \left( 1 - \frac{2}{1 + \exp\left(-2 Z \sqrt{\frac{p \left(1 + K_D \frac{k_r}{p + k_r}\right)}{\varepsilon_t / \varepsilon D_p}}\right)} \right) \quad (A2)$$

# Visualization and quantification of heterogeneous diffusion rates in granodiorite samples by X-ray absorption imaging

## Diffusion within gouge materials, altered rim and intact rock matrix

*Susan J Altman, Vincent C Tidwell,  
Sandia National Laboratories*

*Masahiro Uchida,  
Japan Nuclear Cycle Development Institute*

### Abstract

Matrix diffusion is one of the most important contaminant migration retardation processes in crystalline rocks. Performance assessment calculations in various countries assume that only the area of the fracture surface where advection is active provides access to the rock matrix. However, accessibility to the matrix could be significantly enhanced with diffusion into stagnant zones, fracture fillings, and through an alteration rim in the matrix. Laboratory visualization experiments were conducted on granodiorite samples to investigate and quantify diffusion rates within different zones of a Cretaceous granodiorite. Samples were collected from the Kamaishi experimental site in the northern part of the main island of Japan. Diffusion of iodine out of the sample is visualized and rates are measured using x-ray absorption imaging. X-ray images allow for measurements of relative iodine concentration and relative iodine mass as a function of time and two-dimensional space at a sub-millimeter spatial resolution. In addition, two-dimensional heterogeneous porosity fields (at the same resolution as the relative concentration fields) are measured. This imaging technique allows for a greater understanding of the spatial variability of diffusion rates than can be accomplished with standard bulk measurements. It was found that diffusion rates were fastest in partially gouge-filled fractures. Diffusion rates in the recrystallized calcite-based fracture-filling material were up to an order of magnitude lower than in gouge-filled fractures. Diffusion in altered matrix around the fractures was over an order of magnitude lower than that in the gouge-filled fractures. Healed fractures did not appear to have different diffusion rates than the unaltered matrix.

### 1 Introduction

Matrix diffusion is one of the most important retardation processes in fractured rocks. A traditional Performance Assessment (PA) assumption for modeling matrix diffusion assumes radionuclides only diffusion into the matrix adjacent to the advective path or channel in the fractures. This available area for matrix diffusion is called the flow-wetted surface (FWS) and the ratio of FWS is commonly 20 to 50% of the fracture surface area. In many cases, a limited depth of rock matrix is assumed to be accessible

by diffusion. Thus, traditional PA assumes a limited volume of rock matrix is accessible for matrix diffusion.

However, geologic examination of crystalline rocks commonly shows an altered rim (or halo) along the entire fracture surface indicated by orange, pink or white coloring. The presence of this altered matrix gives evidence that there is access via diffusion along the entire gouge-filled fracture surface. Therefore, the FWS could be assumed to be 100% due to diffusion in geologic time.

Besides open void space in a fracture, there usually exist finely crushed materials, called fault gouge and/or breccia, as well as calcite-based recrystallized material. The porosity of these materials may be high relative to the rock matrix. However, these materials are fragile and cover small areas and are thus difficult to measure.

The Japan Nuclear Cycle Development Institute (JNC) decided to apply a novel technique developed by Sandia National Laboratories (SNL) using non-destructive X-ray absorption imaging to observe the porosity and tracer migration in fractured granite rock at a sub-millimeter spatial resolution /Tidwell and Glass, 1994/. This method was originally applied to the dolomite samples from the Waste Isolation Pilot Plant, the U. S. Department of Energy's deep geologic repository for transuranic nuclear waste site in New Mexico, to observe and quantify heterogeneous tracer migration /Tidwell et al., 2000/. However, prior to this study, this method had not been tested on crystalline rock.

The following objectives were defined for the preliminary experiments:

1. Test and refine the X-ray absorption experimental technique for optimal imaging of diffusion processes occurring in fractured crystalline rock, specifically in fracture-filling material, altered granodiorite and unaltered granodiorite. Of special interest is whether the technique will be effective for the matrix samples with extremely low-porosity.
2. Obtain qualitative and possibly quantitative information on the relative diffusion rates of the different materials (gouge-filled fracture, recrystallized fracture filling, altered and unaltered matrix).

These experiments are described in more detail in Altman et al. /2001/.

## **2 Experimental description**

### ***Sample descriptions***

A core approximately 15 cm in diameter and a block, approximately 50 cm on a side, taken from the Kamaishi mine in the northern part of the main island of Japan, were used in this study. The core sample consisted of fracture-filling material as well as altered and unaltered matrix. The fracture in the core was characterized as a Type-B fracture, meaning it contains a zone of fracture fillings, altered and unaltered matrix /Osawa et al, 1995/. Damage from shipping and handling of the core might have caused fracturing in the fracture-filling material along the plane of the fracture. Samples KC1c-FF, KC1a-alt and KC1a-unalt (Figure 3a-6) were taken from this core.

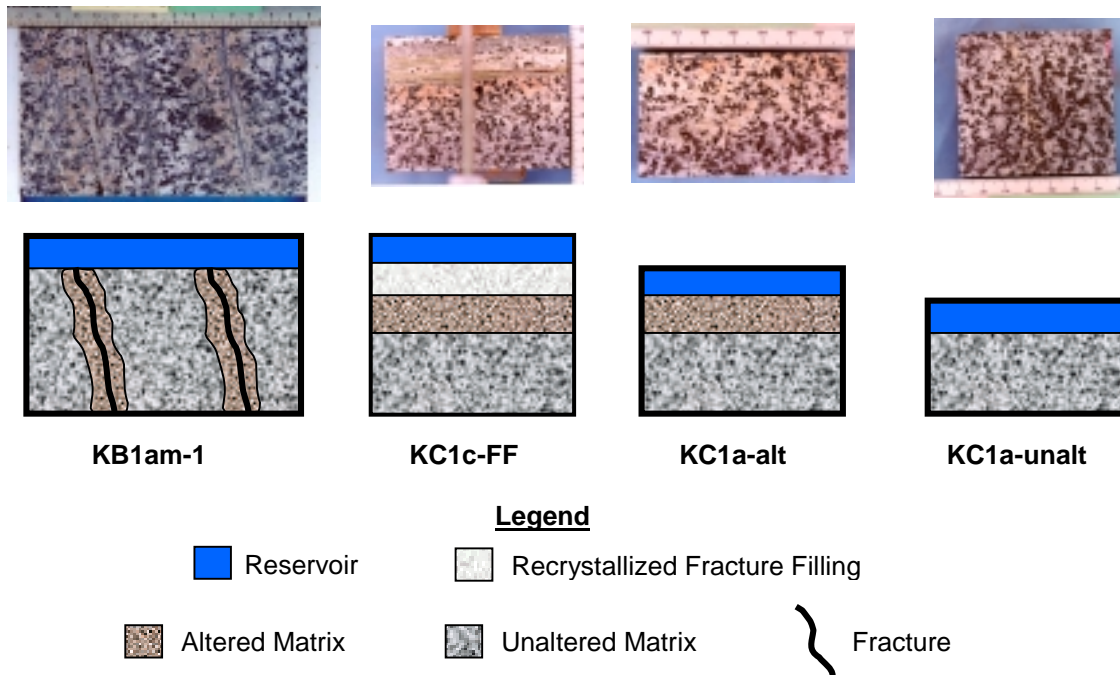


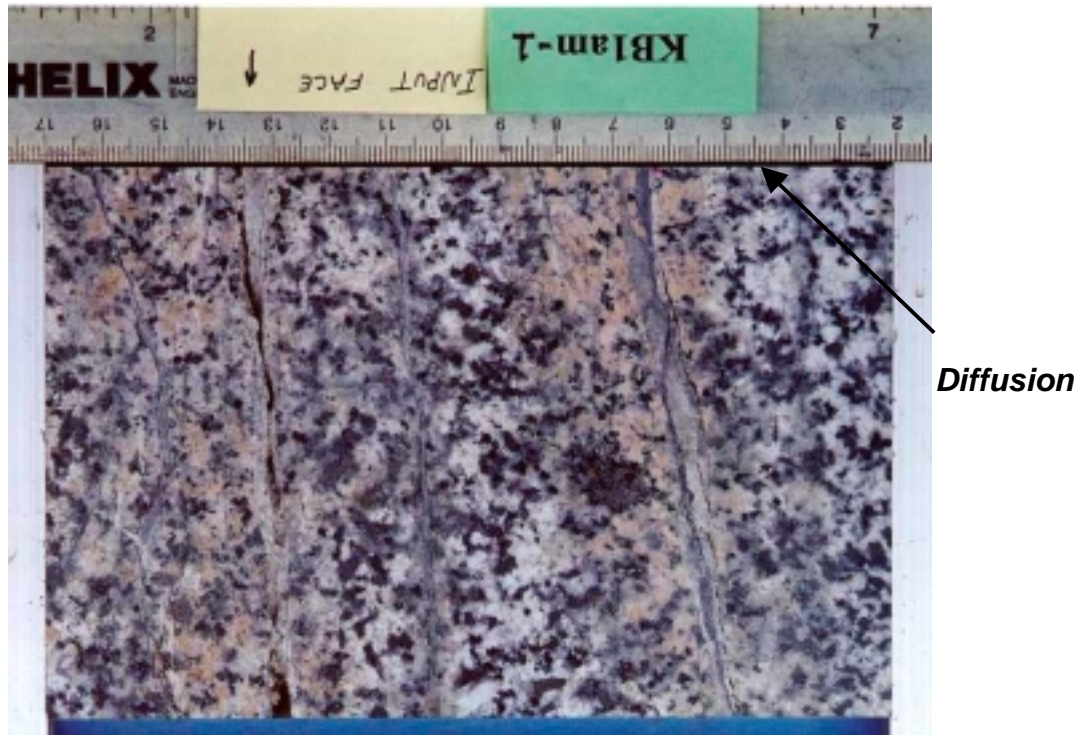
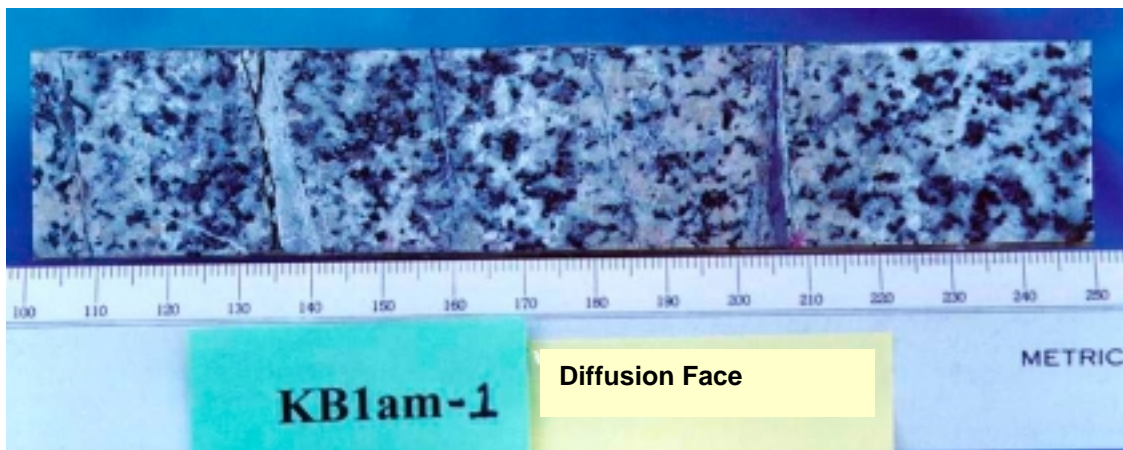
**Figure 3a-6.** Rock samples and schematic of the different test cells for the experiments showing how the configuration of the materials with the source terms differ. Scales are in centimeters.

The block contained several fractures running perpendicular to the diffusion face. Some of the fractures were filled with high-porosity fault gouge and others were recrystallized. Rock bolts were used to protect the integrity of the fractures during shipping. Altered matrix was also present in the sample in the vicinity of several of the fractures. One of the advantages of this block over the original core, described above, is that there was less damage to the block during shipping. Therefore, the fractures have been left intact and disturbance or loss of the fracture-filling material, especially the high-porosity gouge material, was probably minimal. Sample KB1am-1 (Figures 3a-6 and 3a-7) was taken from this block. The dimensions of each sample are listed in Table 3a-2.

**Table 3a-2. Dimensions of samples.**

Sample ID	Description	Length (cm)	Width (cm)	Thickness (cm)	Volume (cm <sup>3</sup> )
KB1am-1	Fractured sample	10.024	14.989	2.423	364.010
KC1c-FF	Fracture-Filling	7.840	9.241	2.289	165.787
KC1a-alt	Altered matrix	4.940	7.330	2.625	95.034
KC1a-unalt	Unaltered matrix	7.240	6.861	2.641	131.187



**A****B**

**Figure 3a-7.** Photograph of two faces of sample for test cell KB1am-1. The upper face is the face over which the X-ray images are taken (A). The lower face is the face where the diffusion boundary is located (B). The scale is in centimeters.

Four samples were selected for the purpose of gaining an understanding of the variation in diffusion rates in different materials (Figure 3a-6). Use of KC1c-FF focused on evaluating diffusion rates through the recrystallized fracture-filling. Test cells KC1a-alt and KC1a-unalt were selected to assess diffusion through the altered matrix and unaltered matrix, respectively. Results from KB1am-1 were used to look at diffusion through partially gouge-filled fractures. Note that the two predominant fractures in KB1am-1 were partially opened and partially filled with gouge material. There were also recrystallized fractures in the sample.

### Test cell preparation

A schematic of the test system used in the diffusion experiment is shown in Figure 3a-8. Each sample was housed in a separate test cell. Four bars of aluminum were cut to fit around the four edges of each sample. The frame was used to provide rigidity to the test cell and minimize X-ray scatter around the edges of the sample. A reservoir, used for a controlled concentration boundary condition, was milled out of one of the aluminum bars. The aluminum bars at the base of the test cell, consisted of two pieces. The piece in contact with the sample has a hole providing access to tracer during saturating process (Figure 3a-8, Piece A). The second piece was constructed so that it would fit in the hole for final assembly (Figure 3a-8, Piece B). By inserting plumber's putty (a very low conductivity material) along the end of the sample, in contact with the area where the two pieces join, a no-flow boundary was created.

Once the aluminum bars were constructed the frame and samples were potted in epoxy. The epoxy was used so as to form no flux boundaries along the faces and edges of the sample. A high viscosity epoxy was used to minimize inhibition into the rock. One drawback of using the high viscosity epoxy was that air bubbles formed in the epoxy.

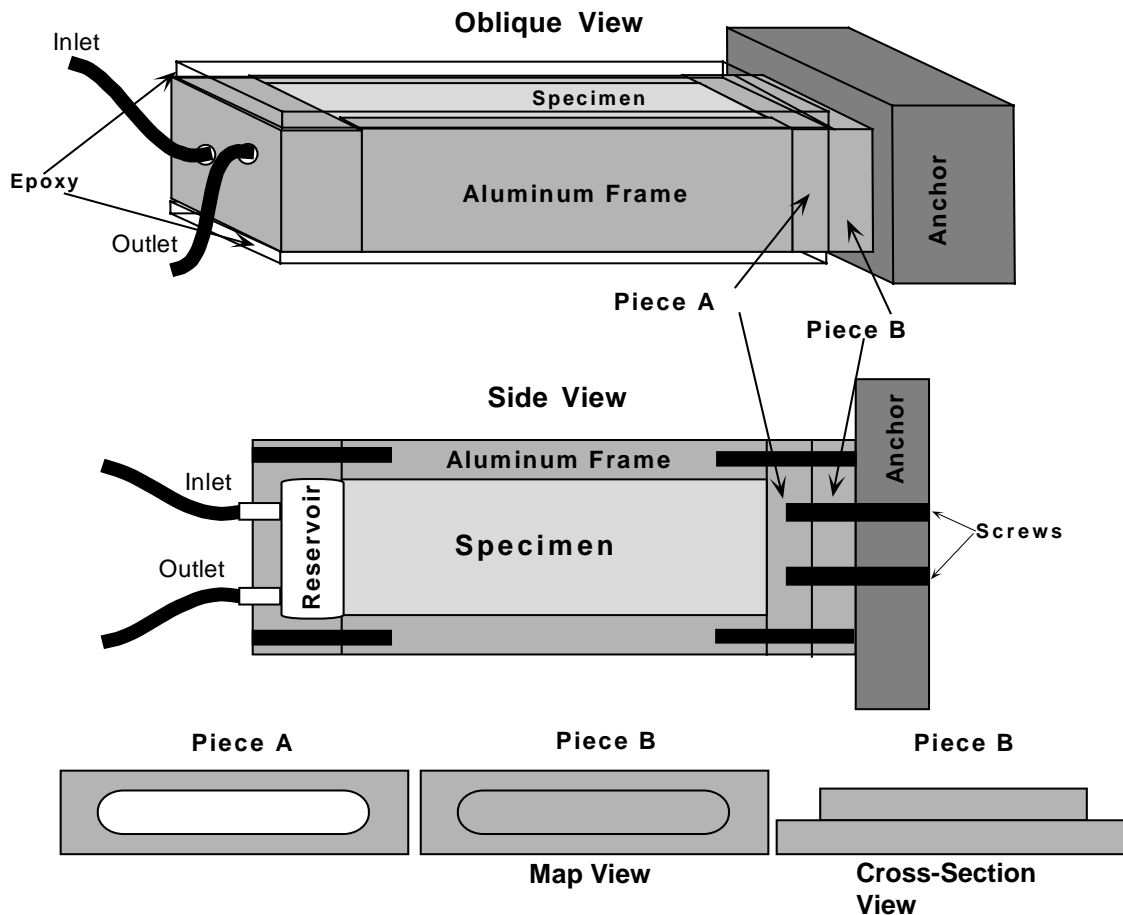


**Figure 3a-8.** Schematic of a test cell showing oblique and side views. Pieces A and B comprise the bottom aluminum bar on the test cell. Piece A, with its open center is attached with epoxy directly onto the sample. This end remains open during the saturation period. Piece B fits into the open slot of piece A. When inserted with plumber's putty the end now becomes a no-flux boundary.

### ***Tracer solution***

The iodide ion was selected as a tracer because it is geochemically conservative and has favorable X-ray absorption characteristics /Tidwell et al., 2000/. Ten-weight-percent potassium iodide (KI) was used as the tracer solution. Albuquerque, New Mexico tap water was used as the solution and the zero-concentration circulated fluid because the chemistry of the tap water appears to be similar to the chemistry of the groundwater where the samples were obtained.

### ***Saturating samples***

After the samples were epoxied in their aluminum frame they were ready for saturating. The dry samples were weighed then placed in a vacuum chamber. The samples were first saturated with CO<sub>2</sub> to minimize the possibility of entrapped air. The tracer was then introduced and the samples were saturated under vacuum conditions. The samples were left in tracer solution under vacuum conditions until the weight of the samples with tracer stabilized (49 days).

### ***X-ray absorption imaging set-up***

High-resolution, X-ray absorption images were acquired by directing a beam of X-rays at the face of the test cells while recording the transmitted X-rays on film secured in a cassette behind the test system. The X-ray source was located at a sufficient distance from the film (approximately 2.8 m) to expose the entire film while minimizing parallax. X-ray source parameters used in imaging were tuned to the absorption characteristics of the tracer. A source intensity of 60 kV at 26.6 mA was used. The accompanying exposure time is set to maximize image contrast, which is a function of sample thickness and tracer concentration. Exposure time determined by trial-and-error was 17 minutes for samples KC1a-alt and KC1a-unalt and 13 minutes for KB1am-1 and KC1c-FF. X-ray images were taken of the dry samples, saturated samples and samples over time during the duration of the experiment.

### ***Diffusion experiment***

Once the samples are saturated, the diffusion experiment is ready to begin. The finished test cells were mounted side by side on a steel frame (Figure 3a-9). A fixed density wedge was also mounted to the frame. The test cells were arranged so that the reservoirs were above the rock sample. This position was chosen so that the less dense fluid that circulated through the reservoir was above the more dense tracer solution used to saturate the rock sample. Therefore, mixing due to density differences was not expected.

A constant-tracer-concentration-boundary condition was achieved by circulating fluid (tap water) through the reservoir (Figure 3a-10). Note the samples were originally saturated with a KI tracer and therefore the concentration boundary condition is  $C = 0$ . Therefore, the experiment visualizes diffusion out of the samples. The experiments commenced with the circulation of clean water. After starting circulation, X-ray images were taken periodically over a period of 202 days.

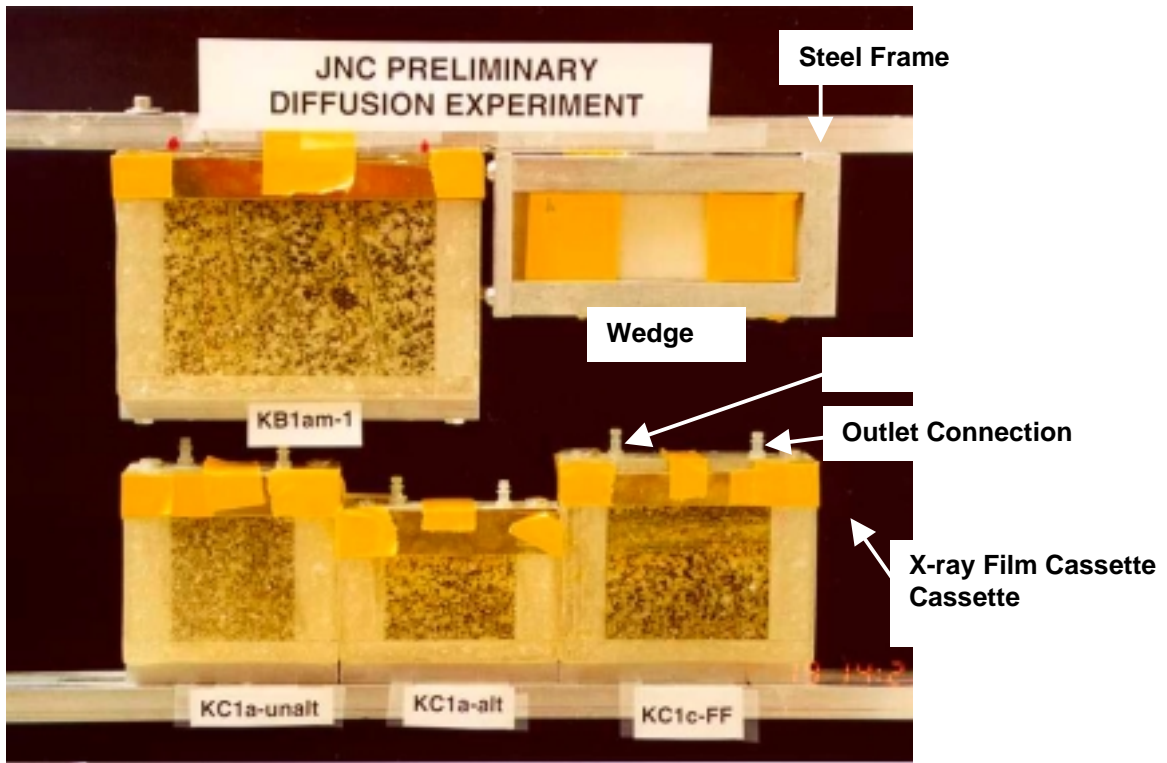


Figure 3a-9. Photograph of test cells mounted on steel frame and in position for X-ray imaging.

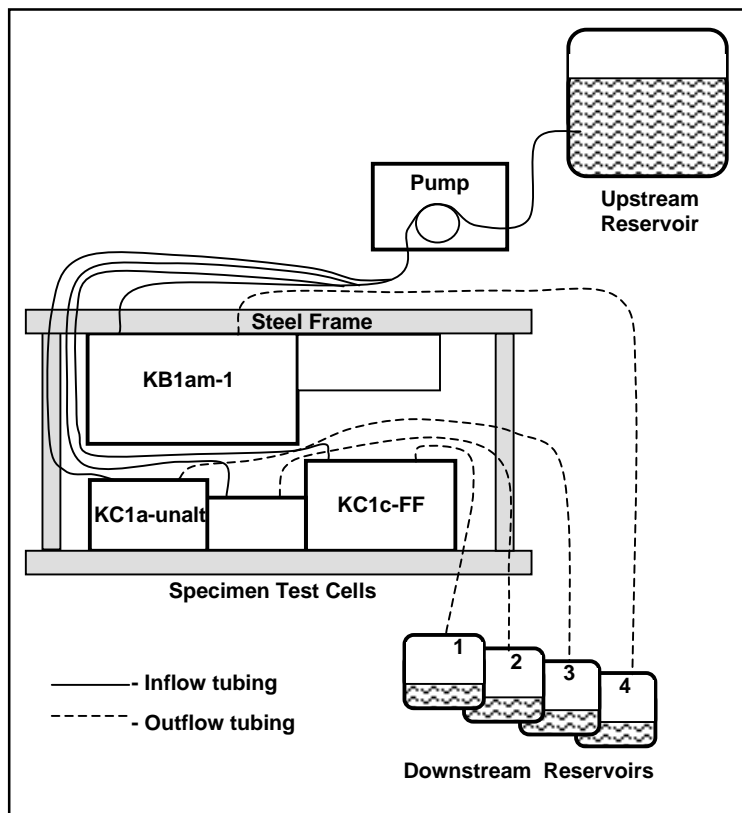


Figure 3a-10. Schematic of experimental system.

### 3 Analyses of images

Spatial variation in solute concentration within each sample was recorded as differences in film density. To quantify these differences, digital imaging was employed. This was accomplished by placing the exposed X-ray film in front of a diffused bank of high-frequency (60 MHz), high-output fluorescent lights. A computer-controlled feedback loop was used to maintain consistent light intensity during imaging. Variation in the transmitted light intensity field, corresponding to differences in film density and hence the solute concentration, was recorded by means of a charge-coupled device (CCD) camera focused on the front of the X-ray film. The CCD camera output was digitised into an array of at least 1024 x 1024 points, with each point assigned a gray level value between zero and 4095 according to the transmitted light intensity. The array size of the camera and the size of the test system determine the spatial resolution of the acquired image. For this experiment each pixel will be measured approximately 0.3 mm on a side.

Because data from multiple images are required to calculate the relative concentration, total mass, and porosity at a given point, care in registering images is required. To aid in this process, lead reference marks were strategically affixed to the test system.

To determine the relative tracer concentration at each point in the X-ray image, the digitized gray-level values were modified through a two-step process. The first step adjusted the image according to the fixed-density wedge included in each image to correct for variations in the source intensity and variations in film quality. The wedge, which varies linearly in thickness, was made of a hardened epoxy/tracer suspension. This was accomplished by taking a transect through the wedge and then plotting the gray-level intensity versus wedge thickness at each pixel. This process was repeated for each image using the same transect. A polynomial function was then fit to the wedge data. One curve was chosen as the reference and all other wedge intensity data were mapped back to the reference. Once the reference mapping has taken place, the image gray-level intensities were adjusted according to the mapping.

#### **Porosity Estimates**

The porosity ( $\phi_{i,j}$ ) at each pixel is determined from the X-ray images taken of the tracerless ( $I_d$ ) and tracer saturated ( $I_s$ ) samples. The natural log transformed images are subtracted and then normalized by the mean value and scaled by the bulk porosity:

$$\phi_{i,j} = \frac{\ln(I_s)_{i,j} - \ln(I_d)_{i,j}}{E[\ln(I_s)_{i,j} - \ln(I_d)_{i,j}]} \phi_{bulk} \frac{z_{i,j}}{z_{avg}} \quad (1)$$

where  $E[\ln(I_s)_{i,j} - \ln(I_d)_{i,j}]$  is the average difference between the tracer saturated and tracerless images,  $\phi_{bulk}$  is the bulk porosity of the rock slab,  $z_{i,j}$  is the thickness of the slab at point  $i,j$ , and  $z_{avg}$  is the average thickness of the rock slab. As the samples were all ground to have an even thickness, the  $z_{i,j}/z_{avg}$  term drops out of the equation. The bulk porosity ( $\phi_{bulk}$ ) of each sample is needed to estimate the porosity distribution from the image analyses. The bulk porosity was estimated by calculating the change in mass between the dry samples and saturated sample as follows:

$$\phi_{bulk} = \frac{(M_{sat} - M_{dry} - M_{Res})}{(\rho_{tracer} V)} \quad (2)$$

where  $M_{sat}$  is the mass of the saturated sample,  $M_{dry}$  is the mass of the dry sample,  $M_{Res}$  is the mass of the tracer in the reservoir,  $\rho_{tracer}$  is the density of the tracer and  $V$  is the volume of the sample.  $M_{sat}$  and  $M_{dry}$  are measured directly.

### **Estimates of $C/C_o$ and $M/M_o$**

Relative concentration is calculated from the adjusted gray-level images by applying linear absorption theory /Tidwell and Glass, 1994/. Specifically, at each point or pixel in the image domain the following equation is applied:

$$\frac{C}{C_o} = \frac{\ln(I) - \ln(I_d)}{\ln(I_s) - \ln(I_d)} \quad (3)$$

where  $I$  is the transmitted light intensity at a fixed point,  $I_s$  is the transmitted light intensity at the same point on the image for the fully tracer saturated condition (image  $C/C_o = 1$ ), and  $I_d$  is the transmitted light intensity at the same point on the image before the sample has been saturated with tracer (image  $C/C_o = 0$ ).

To assist in the analyses, the normalized cumulative mass ( $M/M_o$ ) in the area of the fractures in KB1am-1, the fracture filling material in KC1c-FF, and the altered matrix in sample KC1a-alt was calculated as follows:

$$\left( \frac{M}{M_o} \right) = \frac{\sum_{i=1}^N \left( \frac{C}{C_o} \right)_i z_i \phi_i}{\sum_{i=1}^N z_i \phi_i} \quad (4)$$

where  $M$  is the mass of tracer in the area at a the time the X-ray image was taken and  $M_o$  is the corresponding quantity when the sample is saturated with tracer,  $z_i$  is the thickness of the slab at a given pixel,  $\phi_i$  is the corresponding porosity and  $N$  is the number of pixels in the area.

### **Diffusion coefficient estimates**

Two methods were used to estimate the diffusion coefficients for different portions of the samples: an analytical method and a numerical (semi-analytical) method employing multiple rates of mass transfer.

#### **Analytical solution**

The configuration of a constant tracer concentration boundary condition along one edge of the test sample while the other edges and faces are maintained as zero flux boundaries allows direct comparison with analytical solutions for 1-D diffusion in a finite slab. According to Crank /1975/ the relative concentration is a function of position and time  $C/C_o(x,t)$  as given by:

$$\frac{C}{C_o}(x,t) = 1 - \frac{4}{\pi} \sum_{n=0}^{\infty} \frac{(-1)^n}{2n+1} \exp\left[ \frac{-D_e(2n+1)^2 \pi^2 t}{4l^2} \right] \cos\left[ \frac{(2n+1)\pi x}{2l} \right] \quad (5)$$

where  $D_e$  is the diffusion coefficient,  $l$  is the slab length, and  $n$  is a summation index. Similarly consider  $M$  the total mass of tracer in the sample at time  $t$  and  $M_o$  the corresponding quantity when the sample is saturated, their ratio is given by:

$$\frac{M}{M_o} = 1 - \sum_{n=0}^{\infty} \frac{8}{(2n+1)^2 \pi^2} \exp\left[\frac{-D_e(2n+1)^2 \pi^2 t}{4l^2}\right] \quad (6)$$

Important assumptions made in these solutions are that the diffusion coefficient is constant (i.e., independent of solute concentration), the porous medium is homogeneous and isotropic, the tracer is conservative and the boundary conditions are constant throughout the test.

Inversion and truncation of Equation 6 provides a direct means of calculating  $D_e$  from the  $M/M_o$  profile. Crank /1975/ gives the relation:

$$D_e = \frac{0.196l^2}{t_{0.5}} \quad (7)$$

where  $t_{0.5}$  is the time for which  $M/M_o = 0.5$ . The diffusion coefficient,  $D_e$  is defined as

$$D_e = D_o \tau \quad (8)$$

where  $D_o$  is the free water diffusion coefficient and  $\tau$  is the tortuosity. The error caused by the truncation is reported to be approximately 0.001 percent.

Equations 5–7 will serve as the basis for analyzing the matrix diffusion. Specifically, the relative concentration  $C/C_o(x,t)$  and the mass removal  $M/M_o$  as measured by X-ray imaging can be compared directly to equations 5 and 6 to assess whether matrix diffusion in the JNC samples follows a constant rate. Equation 7 was used to calculate the effective diffusion rate assuming uniform diffusion.

### *Multirate modeling*

The data analysis methods of Haggerty and Gorelick /1998/ were also used to evaluate whether multiple rates of diffusion are present during the course of the experiments. To understand the multirate model of mass transfer, one can consider a system as having a distribution of diffusion rates. The scale (both time and length) of the system controls which diffusion rates are important. At large scales, for example, features contributing to fast diffusion rates may become saturated with solute and no longer contribute to the diffusive response of the system. Also at larger scales, more surface area becomes accessible for diffusion. A model of multirate diffusion has been shown to be important in the Culebra dolomite at the WIPP site /Haggerty et al., 2001/ and has potential implications for Performance Assessment (PA) calculations /McKenna et al., 2001/. A conventional model of mass transfer with only a single rate coefficient may be an adequate conceptualization only if the time and spatial scale of the experiment being modeled and the total system being assessed are the same. At the laboratory and field scale it may be possible to determine an adequate integrated single-rate diffusion coefficient. However, such measurements are often not possible at the PA scale. To more appropriately perform PA calculations one must address the scaling issues that

influence the mass transfer rate coefficients. One approach is to use a distribution of rate coefficients or calculating an integrated single-rate coefficient that accounts for the multiple rates of diffusion that are appropriate at the PA scale /McKenna et al., 2001/.

The curve-matching and Laplace transform methods described by Haggerty and Gorelick /1998/ were used to calculate the distributional properties of the diffusion coefficients (i.e., mean and variance of a log-normal distribution). Fleming /1999/ developed a code specifically to estimate both multirate and single-rate parameters from experiments with this specific set-up (referred to as static diffusion experiments). Using Fleming /1999/ approach for this analysis provides estimates of  $\mu_d$  (the mean of the natural log distribution of  $D_e$ ), and  $\sigma_d$  (the standard deviation of natural log distribution of  $D_e$ , calculated for multirate diffusion only). The assumed multirate distribution of diffusion coefficients is lognormal. The correct distribution for the materials in these experiments is currently unknown.

The code estimates  $\mu_d$  and  $\sigma_d$  by normal inversion. The code iteratively simulates the experiment and compares the log-space simulation data to the log-space observed data (M/Mo versus time). Root mean square error (RMSE) was used as a measure of fit, as log-transformed data shows a greater sensitivity to the late-time, low mass ratios at which multirate effects are greatest. The parameter estimation statistics have been provided for the multirate and single-rate interpretations. This information is a useful statistical estimate of the reliability of the modeling results, and is the primary advantage of using formal parameter estimation techniques as opposed to conventional manual calibration of the model to the data. The 95% confidence intervals presented in the results section (Section 4) represents  $\pm 2$  standard deviations about the best-fit value of the parameter.

## 4 Results of image analyses

Results at this time are focused on the fractures in sample KB1am-1, the recrystallized fracture material in sample KC1c-FF, and the altered material in sample KC1a-alt. It was determined that the porosity of the unaltered matrix was too low such that there was not enough tracer in sample KC1a-unalt to make this technique effective.

### ***Porosity estimates***

Porosity distributions of the four samples are presented in Figures 3a-11a–e. A range of 0–25% was used to emphasize the high porosity areas, specifically the gouge-filled fractures and the recrystallized fracture-filling material. When the bulk porosity as measure in Equation 2 is used to calculate the porosity distribution of KC1a-alt (Figure 3a-11d) an area of high porosity is seen in upper right-hand portion of the sample. This area is thought to be unrealistically high based on other porosity measurements of the altered matrix. It is likely that there is an error in the bulk porosity measurement. If a more realistic bulk porosity value of 3.2% /Ota, 1998/ is used, then the porosity distribution of the sample (Figure 3a-11e) seems more realistic.



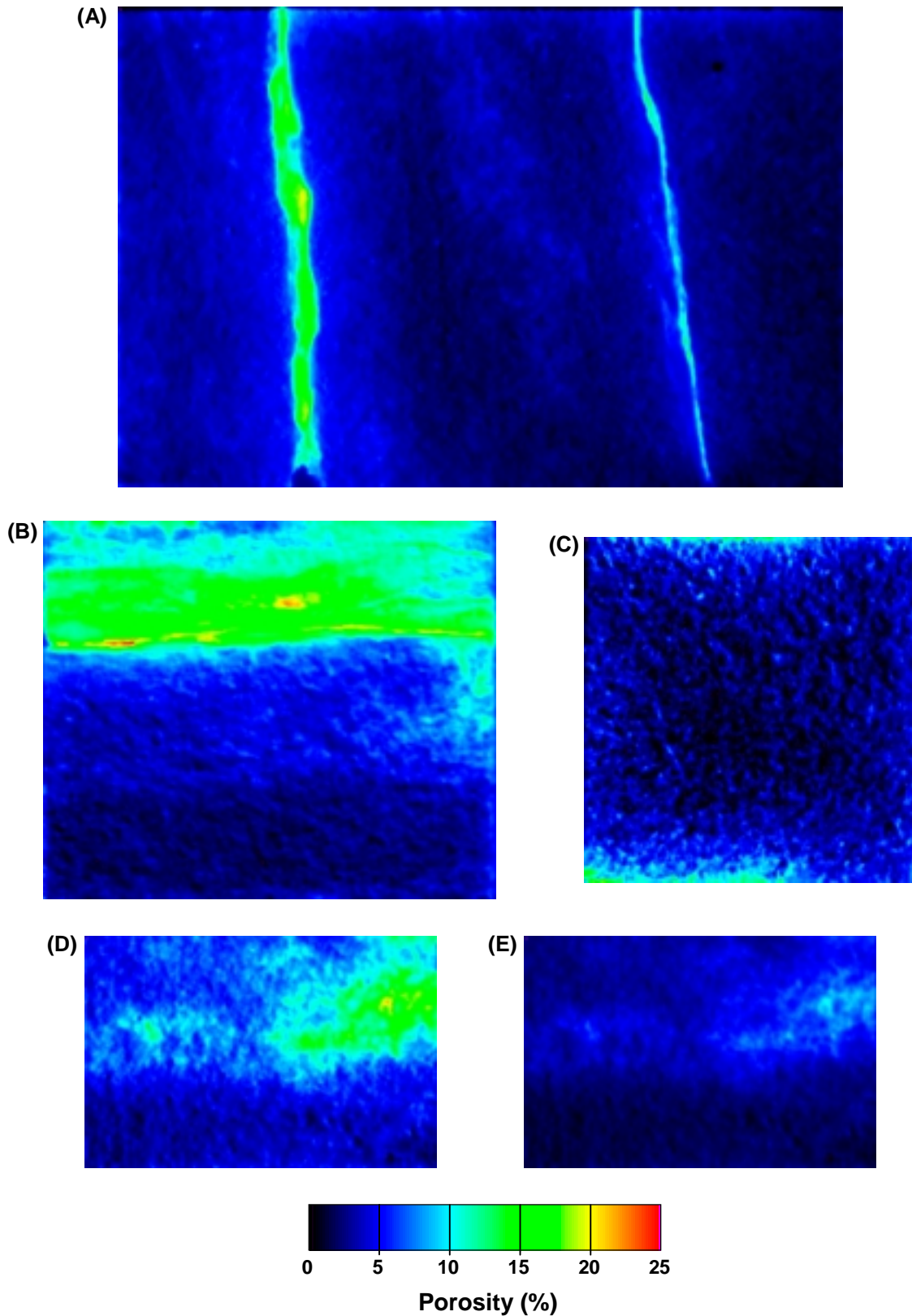


**Figure 3a-11.** Porosity distribution for each sample ((A) KB1am-1 (sample containing gouge-filled fractures), (B) KC1c-FF (sample containing recrystallized fracture-filling material), (C) KC1a-unalt (sample containing unaltered matrix), (D) KC1a-alt assuming a bulk porosity of 6.6% and (E) KC1a-alt, assuming a bulk porosity of 3.2%) (sample containing altered matrix). Note the range of porosity values shown in each image is 0–25%.

The partially gouge-filled fractures showed a range in porosity of 7–21% with an average value of 13% in the left-hand fracture and 9% in the right-hand fracture (Figure 3a-11a). The recrystallized fracture fillings showed a porosity range of 5–24% with an average value of 13% (Figure 3a-11b) and the altered matrix showed porosity ranging from 3–12% (assuming a bulk porosity of 3.2% for the whole sample) with an average porosity of 4% (Figure 3a-11e). The reason why the recrystallized fracture fillings showed higher porosity than the partially gouge filled fracture is not clear. One possible explanation is that these porosity values are calculated over the integrated sample thickness. The partially gouge-filled fractures are rather narrow in width and the fracture plane is not parallel to the X-ray beam. Thus some matrix could be included in the integration over the thickness of the sample. It is also possible that there was some sample damage to the recrystallized fracture-filling material during shipping and sample preparation leading to some inappropriately high-porosity fractures in the sample.

### ***Estimates of $C/C_0$ and $M/M_0$***

The distribution of  $C/C_0$  was calculated for all of the film that was digitized.  $C/C_0$  distributions at various times in the fractures in sample KB1am-1 are shown in Figure 3a-12. It can be seen that the iodide concentration is clearly decreasing in the fractures. In addition, the rates at which they are decreasing are different for the two fractures (note that the same times are shown for both fractures). Finally, the fractures themselves are clearly heterogeneous with areas where concentrations decrease faster than other areas. The recrystallized fracture-filling material also shows heterogeneous behavior as the concentrations decrease non-uniformly in the material through time (Figure 3a-13).

### ***Diffusion Coefficient estimates***

As stated in Section 3, two different methods were used to estimate the diffusion coefficients for different portions of the samples: an analytical method and a numerical method employing multiple rates of diffusion.

For both methods of analyses significant assumptions were made. Diffusion is assumed to be one-dimensional when in fact the materials are heterogeneous and diffusion paths could be tortuous. It is also assumed that there is no diffusion between the portion of the sample analyzed (e.g. the gouge-filled fracture) and the surrounding area. For example, it is assumed that the diffusion from the surrounding matrix to the fracture is significantly slow compared to diffusion within the fracture.

### ***Analytical Solution***

Diffusion-coefficient values calculated using the methods described in Section 3.3 are reported in Table 3a-3. The calculations were conducted for each gouge-filled fracture in KB1am-1, the recrystallized fracture-filling material in KC1c-FF and the altered matrix in KC1a-alt. Diffusion rates clearly differ between the gouge-filled fracture, recrystallized fracture filling material, and altered matrix by as much as an order of magnitude. These values are approximately an order of magnitude higher than those reported by Ota /1998/.

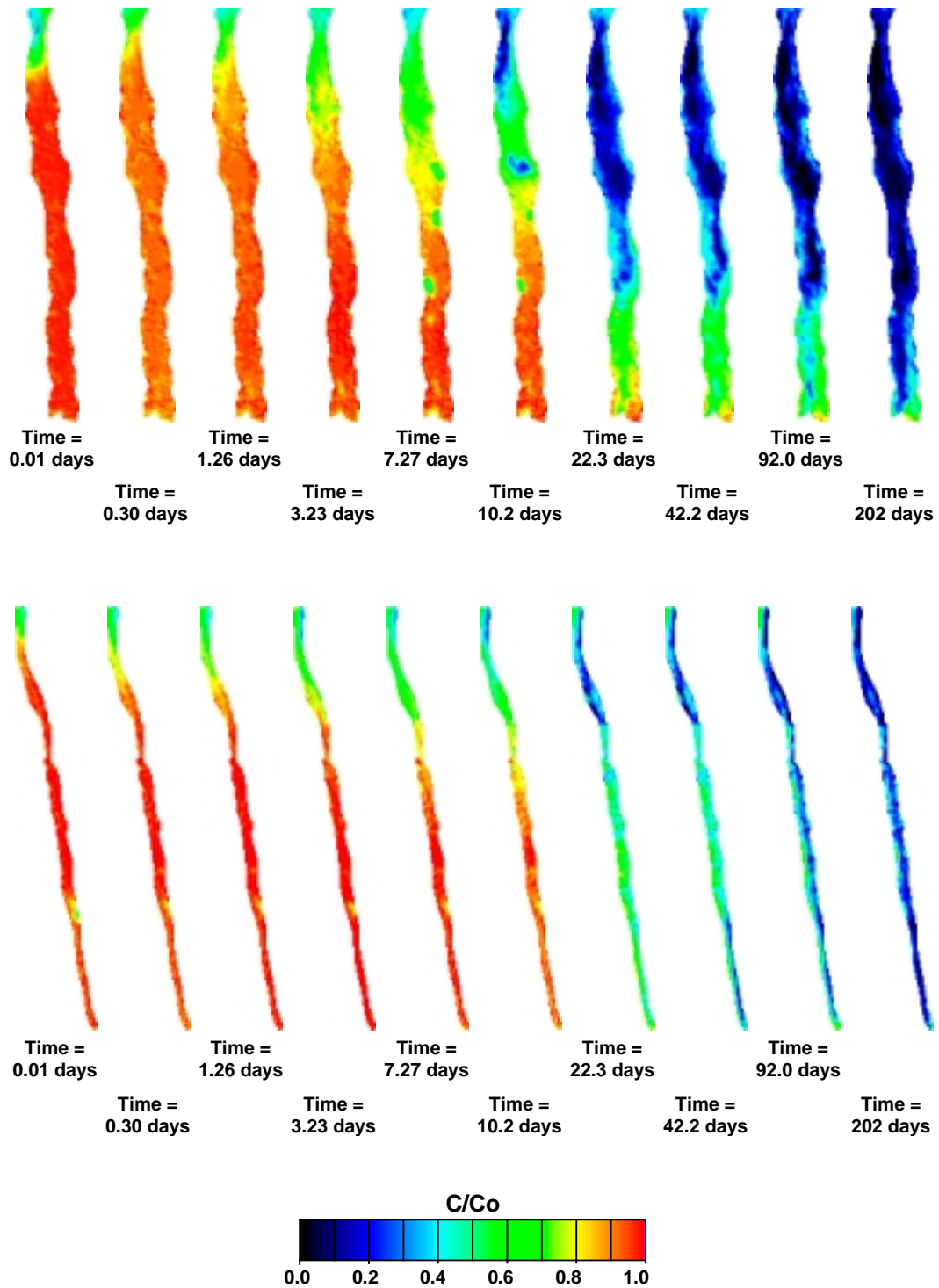


**Figure 3a-12.**  $C/C_0$  images of two fractures in sample KB1am-1. Observe diffusion out of the sample in the upward direction. For scale, each fracture is approximately 10 cm long. Pixel size is approximately 0.3 mm on a side.

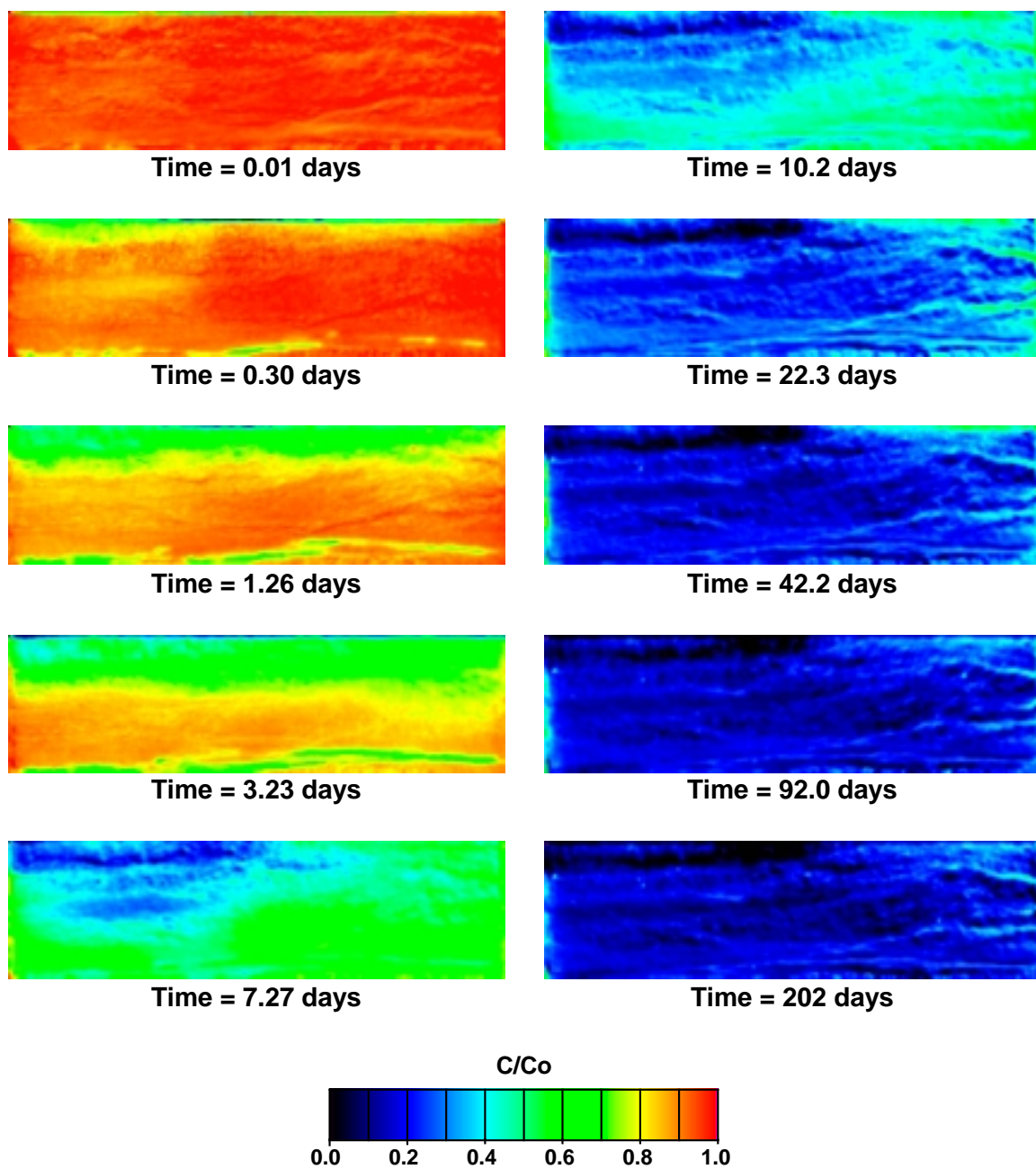


**Figure 3a-13.** *C/Co* images of recrystallized fracture-filling material in sample KC1c-FF. Observe diffusion out of the sample in the upward direction. The region shown is approximately 9.4 x 2.6 cm. Pixel size is approximately 0.3 mm on a side.

**Table 3a-3. Diffusion coefficient estimates based on analytical method described in Crank /1975/.**

	<b>KB1am-1 Left-hand fracture</b>	<b>KB1am-1 Right-hand fracture</b>	<b>KC1c-FF Fracture-filling material</b>	<b>KC1a-alt Altered material</b>
$D_e$ (m <sup>2</sup> /s)	$1.1 \times 10^{-9}$	$9.5 \times 10^{-10}$	$2.0 \times 10^{-10}$	$3.8 \times 10^{-11}$
$D_e$ , Ota /1998/	–	–	$2.4 \times 10^{-11}$	$1.8 \times 10^{-11}$

### **Multirate modeling**

Numerical modeling results are reported in Table 3a-4. In general, the inverse modeling did a good job at matching the observed data. At approximately 10 days there is a sharp break in the data that the inverse model had difficulty in matching, especially when using the single-rate model. The results from the inverse modeling approximately match the diffusion coefficients calculated using the analytical solution (see Section 5 for more discussion on the comparison).

**Table 3a-4. Diffusion coefficient estimates based on multirate inverse modeling.  $D_e$  reported in m<sup>2</sup>/s.**

	<b>KB1am-1 Left-hand fracture</b>	<b>KB1am-1 Right-hand fracture</b>	<b>KC1c-FF Fracture-filling material</b>	<b>KC1a-alt Altered matrix</b>
$D_e$ single rate	$7.5 \times 10^{-10}$	$4.5 \times 10^{-10}$	$4.3 \times 10^{-10}$	$3.6 \times 10^{-11}$
95% confidence range $D_e$ single rate	$2.9 \times 10^{-10}$ – $1.9 \times 10^{-9}$	$2.1 \times 10^{-10}$ – $9.6 \times 10^{-10}$	$1.4 \times 10^{-10}$ – $1.4 \times 10^{-9}$	$2.5 \times 10^{-11}$ – $5.1 \times 10^{-11}$
$D_e$ multirate	$1.2 \times 10^{-9}$	$6.2 \times 10^{-10}$	$9.6 \times 10^{-11}$	$3.8 \times 10^{-11}$
95% confidence range $D_e$ multirate	$4.2 \times 10^{-10}$ – $3.7 \times 10^{-9}$	$3.3 \times 10^{-10}$ – $1.1 \times 10^{-9}$	$3.4 \times 10^{-11}$ – $2.7 \times 10^{-10}$	$2.3 \times 10^{-11}$ – $6.3 \times 10^{-11}$
$\sigma_d$ multirate	1.1	1.5	1.3	0.77
95% confidence range $\sigma_d$ multirate	0.9–1.4	1.1–1.8	1.3–1.3	0–2.9
$D_e$ , Ota /1998/	–	–	$2.4 \times 10^{-11}$	$1.8 \times 10^{-11}$

There is not a significant difference between the diffusion coefficients calculated using the single-rate and multirate model for the fractures in sample KB1am-1. To more fully evaluate multirate diffusion over two orders of magnitude variation in M/Mo data are needed. These results indicate that multirate behavior may not be important within the fractures, however more late-time data is needed to be confident in this interpretation. The difference in single-rate and multirate  $D_e$  values as well as the shorter range in  $\sigma_d$  values, indicate that multirate behavior might be more important in the fracture-filling material.

## 5 Summary and discussion

These experiments have successfully demonstrated that diffusion can be an active process in the different environments of the Kurihashi granodiorite. Specifically, these experiments have provided the direct observation of diffusion in gouge-filled fractures, recrystallized fracture-filling material and altered matrix. Analogous evidence of diffusion in the Culebra dolomite at the WIPP site was important in convincing an independent oversight group (the Environmental Evaluation Group), the State of New Mexico's Attorney General's Office and the regulatory agency (the U. S. Environmental Protection Agency) that diffusion is a realistic retardation mechanism. Visualization of the relative concentration distributions supports different rates of diffusion in the three types of materials. Through X-ray absorption visualization techniques it is clear that the materials and diffusion rates are heterogeneous. Based on these interpretations, qualitative comparisons of diffusion rates in the different materials can be made (Figure 3a-14):

- diffusion rates in the fracture gouge are potentially one order of magnitude higher than diffusion rates in the recrystallized fracture-filling material,
- diffusion rates in the recrystallized fracture-filling materials are approximately a five times higher than the diffusion rates of the altered material.

There is clearly agreement between the diffusion coefficients calculated using the analytical solution and by numerical modeling. Differences between the single-rate and multirate diffusion coefficients are small, especially for the fractures in sample KB1am-1. There is a notable difference between the diffusion coefficients calculated from these experiments and those reported by Ota /1998/, which are approximately 1 to 1.5 orders of magnitude lower. There are several reasons why these experiments would lead to estimates of larger diffusion coefficients than other methods for measuring diffusion such as through diffusion experiments: 1) X-ray absorption imaging can study more fragile fracture filling materials whereas through-diffusion experiments require

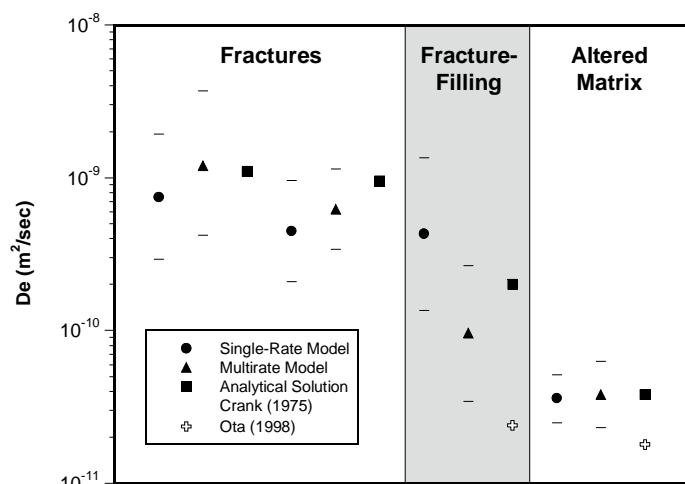


**Figure 3a-14.** Effective diffusion coefficient estimates using a single-rate and multirate model as compared to the analytical solution results.

more solid sample which allows sample fabrication, 2) through-diffusion experiments measure only that diffusion that is able to pass completely through the sample (i.e., connected porosity) whereas the visualization technique measures diffusion in all regions. The diffusion coefficients estimated by these experiments are now being used in PA-scale calculations to determine the impact of diffusion to increase the FWS on releases.

## References

- Altman S J, Uchida M, Tidwell V C, Boney C M, Chambers B P, 2001.** Visualization and quantification of heterogeneous diffusion rates in granodiorite samples by X-ray absorption imaging, SAND2001-1842, Sandia Natl. Lab., Albuquerque, NM,
- Crank J, 1975.** The Mathematics of Diffusion, Clarendon Press, Oxford.
- Fleming S W, 1999.** Single and Multiple rates of nonequilibrium diffusive mass transfer at the laboratory, field and regional scales in the Culebra Member of the Rustler Formation, New Mexico, Master Thesis from Oregon State University, June, 1999.
- Haggerty R, Fleming S W, Meigs L C, McKenna S A, 2001.** Tracer tests in a fractured dolomite, 2. Analysis of mass transfer in single-well injection-withdrawal tests, *Water Resour. Res.*, 37(5), 1129–1142.
- Haggerty R, Gorelick S M, 1998.** Modeling mass transfer processes in soil column with pore-scale heterogeneity, *Soil Sci. Soc. Am. J.*, vol. 62, 62–74.
- McKenna S A, Meigs L C, Haggerty R, 2001.** Tracer tests in a fractured dolomite, 3. Double porosity, multiple-rate mass transfer processes in convergent-flow tracer tests, *Water Resour. Res.*, 37(5), 1143–1154.
- Osawa H, Sasamoto H, Nohara T, Ota K, Yoshida H, 1995.** Development of a conceptual flow-path model of nuclide migration in crystalline rock – a case study at the Kamaishi in-situ test site, Japan, *Mat. Res. Soc. Symp. Proc.*, vol. 353, 1267–1273.
- Ota K, Amano K, Ando T, 1998.** Brief overview of in situ contaminant retardation in fractured crystalline rock at the Kamaishi in situ test site, in *Proceedings of an international workshop for the Kamaishi in situ experiments*, Japan Nuclear Cycle Development Institute, August, 1998.
- Tidwell V C, Glass Jr R J, 1994.** X ray and visible light transmission for laboratory measurement of two-dimensional saturation fields in thin-slab systems, *Water Resour. Res.*, 30(11), 2873–2882.
- Tidwell V C, Meigs L C, Christian-Frear T, Boney C M, 2000.** Effects of spatially heterogeneous porosity on matrix diffusion as investigated by X-ray absorption imaging, *J. Contam. Hydrol.*, 42, 285–302.

## **Session 3b**

**Alternative evaluation of  
TRUE-1 results**



# Contents

	Page
<b>Session 3b Alternative evaluation of TRUE-1 results</b>	
Learning from recovery: Thoughts on Feature A transport experiments	51
A simple flow channel model of TRUE-1	71
Integration of laboratory sorption and diffusivity data in modelling of sorbing tracer tests STT-1 and STT-1b	85
Evaluation of TRUE-1 tests with sorbing tracers using CHAN3D	111
Revisiting the Advection-Dispersion Model – Testing an alternative	125

# Learning from recovery: Thoughts on Feature A transport experiments

*Bill Dershowitz, Thomas Doe, Aaron Fox,  
Golder Associates Inc*

*Masahiro Uchida,  
Japan Nuclear Fuel Cycle Development Corporation*

*Trenton Cladouhous,  
WebPE.com*

## Abstract

This paper summarizes discrete fracture network (DFN) analysis of the Tracer Retention Understanding Experiments “TRUE-1” carried out at the Äspö Hard Rock Laboratory in Sweden from 1995 through 2000. These studies confirmed the ability of the DFN approach, together with conventional advection-dispersion-diffusion assumptions to calibrate and predict solute transport in a single fracture at the 5 to 10 meter scale. The analysis also indicated the possibility that alternative formulations of reactive transport constitutive laws may also be useful.

In addition to addressing issues of ADD transport, the “TRUE-1” experiment raised and addressed important issues regarding solute transport pathways and the effect of fracture network connectivity on flow and transport in fractured rock.

## 1 Introduction

Solute transport in fractured rock is controlled by unique combinations of transport properties, transport pathway geometry, and hydraulic head field. Minor changes in the head field can radically alter the transport pathways, producing completely different transport results.

The Tracer Retention Understanding Experiments (TRUE) are part of a research program at Äspö, the Swedish Hard Rock Laboratory, designed to study the transport of radionuclides in crystalline rock /Winberg, et al., 2000/. The TRUE-1 experiment was carried out in a 50-m scale block of fractured rock at the northern end of the Laboratory, at the 450 m level (Figure 3b-1). Tracer experiments focused on a geologically and hydrogeologically identified structure, “Feature A” (Figures 3b-2 and 3b-3) at the 5 to 20 meter scale. The purpose of this paper is to point out several of the interesting aspects of this experiment, particularly as they relate to improving the understanding of flow and transport in fractured rocks.



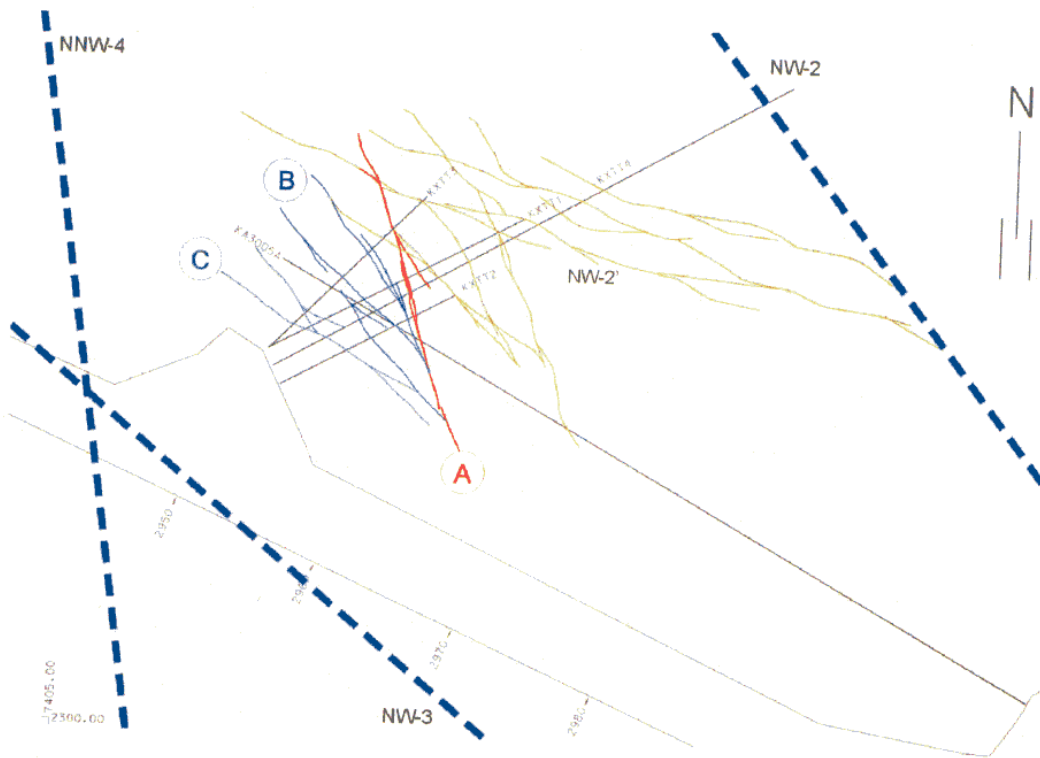


**Figure 3b-2.** Feature A in the TRUE-1 rock (after Winberg et al., 2000).

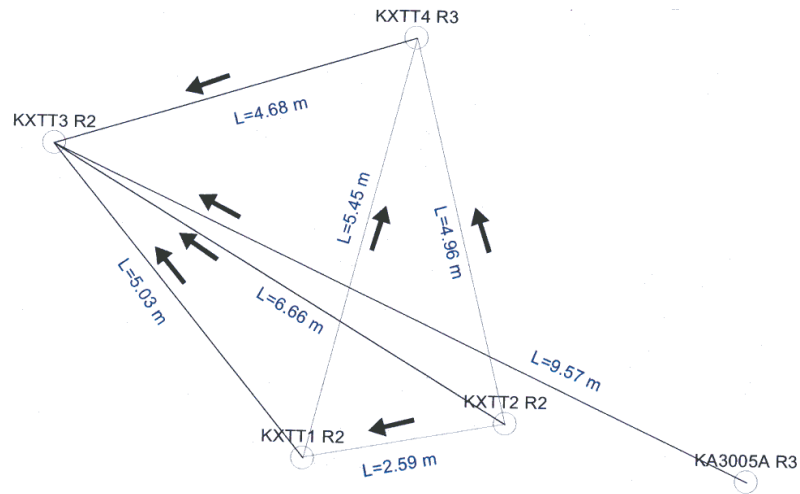


**Figure 3b-3.** Tracer test geometry in the plane of the interpreted “Feature A” /after Winberg et al., 2000/.

The JNC/Golder modeling group used stochastic discrete feature network (DFN) models for analysis and modeling of the TRUE-1 experiment /Dershowitz et al., 2000/. This effort included identification of conductive features, their geometry, and properties, stochastic discrete fracture simulations, and flow and transport modeling. Most DFN analyses were carried out using stochastic models, reflecting the underlying uncertainty in fracture geometry and properties even for as well characterized a rock block as TRUE-1. However, by the end of the project, transport was reduced to a network of less than 10 pipes between injection and collection boreholes, with deterministically calibrated properties. The details of these analyses are described in Dershowitz et al. /1996/ and Dershowitz et al. /2001/.

This paper will address four major issues which arose during the project:

1. Identification of flow and transport pathway geometry.
2. Network connectivity and head.
3. Transport process constitutive approaches.
4. Calibration and prediction.

Resolution of these issues is essential to understanding solute transport processes in fractured rock, and developing an ability to predict transport at larger time and distance scales.

## 2 Pathway geometry

Figure 3b-3 shows the geometry of tracer tests carried out in “Feature A”. Although the goal of the experiment was to test a single discrete fracture, evidence from borehole images clearly demonstrates that at the 10 meter scale of the experiment, “Feature A” is not a single fracture, but rather a structure made up of multiple fractures, intersected by and interacting with a fracture network. The orientation of “Feature A” at each of its intersections with the five experimental boreholes is illustrated in Table 3b-1. The strike of these intercepts varies from N25W to N46W, with dips between 76 and 80 degrees. Thus, even while “Feature A” is a relatively well defined feature at the scale of 10 to 50 meters, it is clearly not a single planar structure. In particular, at borehole KXTT4, “Feature A” consists two distinct fractures with hydraulic response – which indicates that at least two distinct transport pathways should not be unexpected (Figure 3b-4).

**Table 3b-1. Orientations of “Feature A” at intersections with boreholes.**

Borehole	Strike of fractures at “Feature A” intercept	Dip of fractures at “Feature A” intercept
KXTT1	N36W	78
KXTT2	N25W	76
KXTT3	N35W	78
KXTT4	N34W, N46W	76, 80

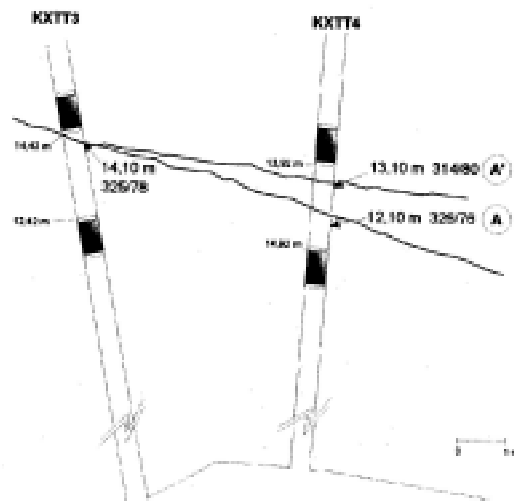


**Figure 3b-4.** Intersection of interpreted “Feature A” with boreholes KXTT3 and KXTT4 /after Winberg et al., 2000/.

Figure 3b-5 illustrates the orientation distribution of potentially conductive features identified by the project geologist, Jan Hermanson from borehole images, borehole flow logging and hydraulic interference measurements. The intensity of potentially conductive fractures in each of the boreholes defining “Feature A” is shown in Figure 3b-6. Based on this analysis, the conductive fracture intensity  $P_{32}$  in the rock block of “Feature A” is on the order of  $3.15 \text{ m}^2/\text{m}^3$ . For a five meter transport path, this results in 3 to 7 intersecting conductive fractures with transmissivities similar to “Feature A”, i.e., on the range of  $10^{-6}$  to  $10^{-8} \text{ m}^2/\text{s}$ . This is illustrated in the DFN model of Figures 3b-7 and 3b-8.

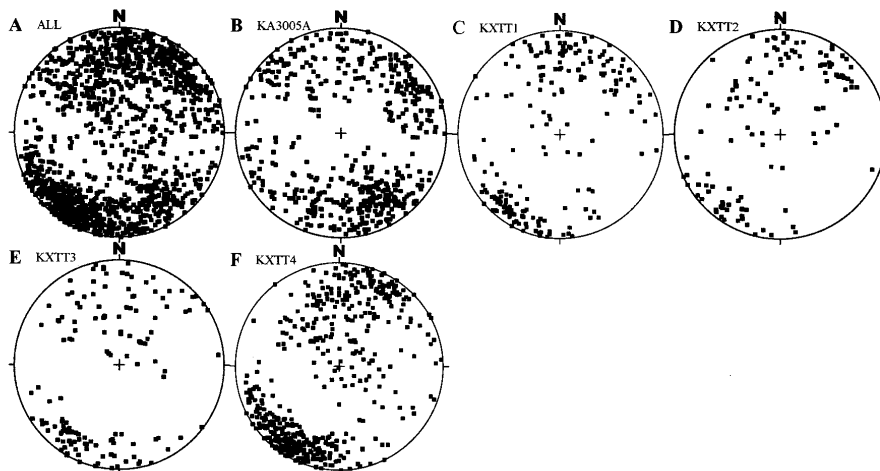


**Figure 3b-5.** Orientation of conductive fractures in boreholes transection the TRUE-1 rock block.

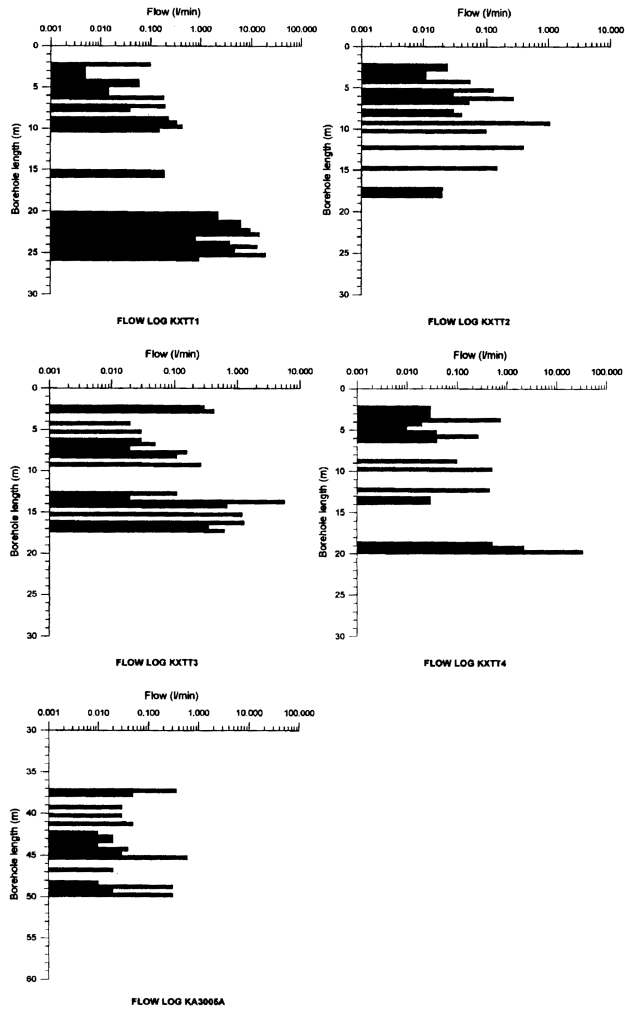


*Figure 3b-6. Results of single packer flow logging in boreholes penetrating the TRUE-1 Rock Block. If intensity is to be illustrated perhaps this figure is obsolete!?*

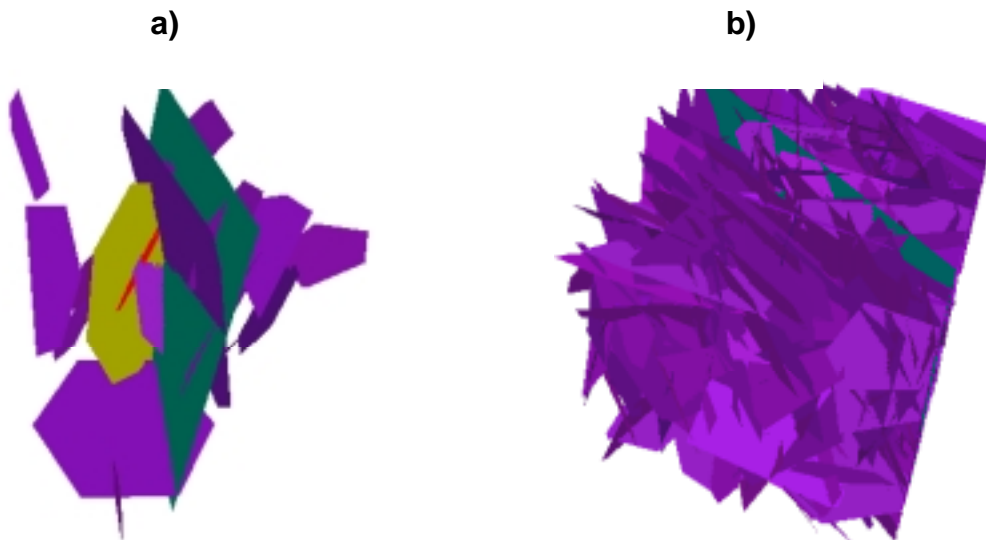


*Figure 3b-7. a) DFN Model for "Feature A", with 5% of Conductive Background Fractures., b) Fracture Network View of "Feature A" with Conductive Fractures.*

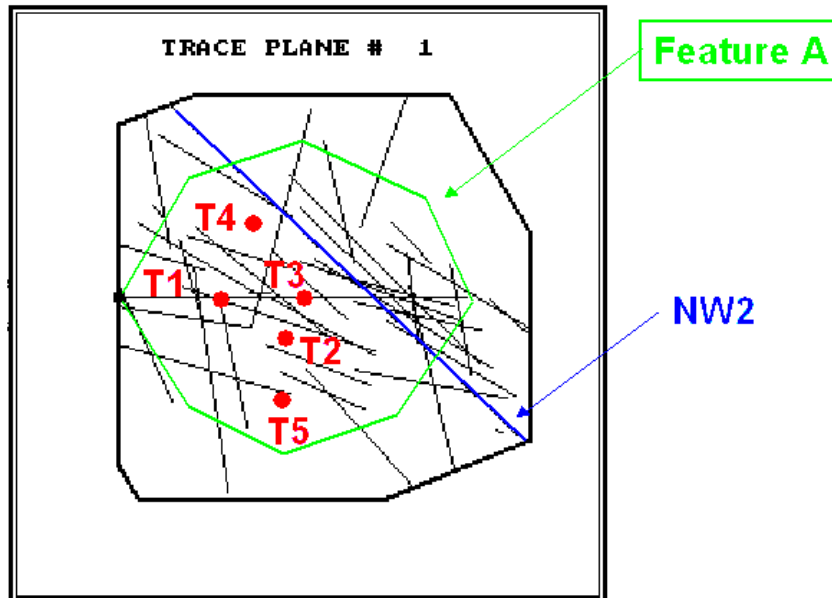


**Figure 3b-8.** DFN Model with close up of plane of “Feature A” with traces of intersecting conductive background fractures. KXT-boreholes intercepts indicated in red.

The network aspect of “Feature A” is confirmed by the results of flow dimension analysis of hydraulic tests conducted in “Feature A”. From the five boreholes intersecting “Feature A”, Dershowitz et al. /1996/ evaluated the flow dimension based on fractional dimension type curve approaches /Doe, 1991/. The flow dimension from four of five of these tests is 2.6 – indicating a leaky aquifer or fracture network behavior. Only one test, at KA3005A, away from the focus of the tracer experiments is near 2.0, the dimension for a single fracture or confined aquifer.

Given this level of structural complexity, it is to be expected that transport in “Feature A” will follow multiple pathways, and it is perhaps somewhat surprising when breakthrough exhibits only a single peak, possibly indicating a single pathway! Further, borehole intersections show that “Feature A” itself is a combination of multiple splays and coalesced fractures, as can be seen in the borehole image logs. Additional pathway structure can be provided by the internal structure of the fracture including mylonites, breccia, and gouge, as well as variations in fracture aperture (Figure 3b-9).



### CONCEPTUAL REPRESENTATION OF FEATURE A

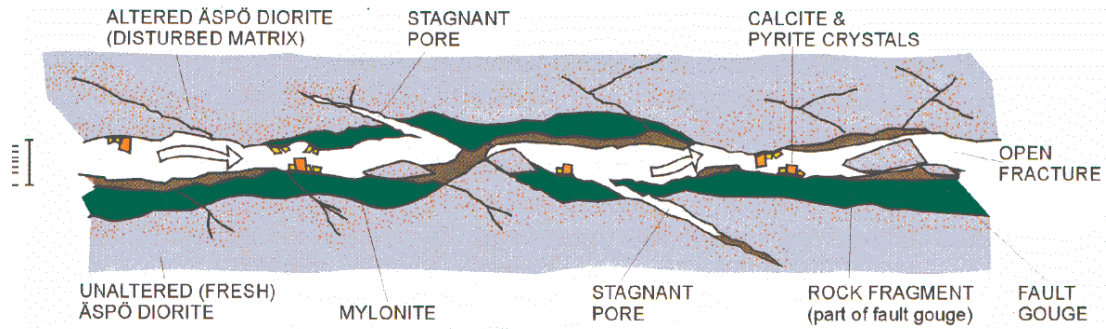


Figure 3b-9. Internal structure of “Feature A” /after Winberg et al., 2000/.

### 3 Connectivity and hydraulic head

Hydraulic interference was used to evaluate the connectivity of the rock block containing “Feature A.” This hydraulic testing indicates that “Feature A” is connected hydraulically to many of the discrete features in the surrounding 100 m scale rock volume, but is also hydraulically isolated many conductive structures within the rock block, even at distances as low as ten meters from “Feature A”. This is consistent with interference behavior observed elsewhere at Äspö and other fractured rock sites /Uchida et al., 2001/. During the tracer experiments, heads and drawdowns were to be predicted together with tracer breakthrough. In many cases, this proved to be one of the more difficult aspects of the modeling, particularly for the DFN approach. In the early tracer experiments, there was a clear “groundwater” divide within “Feature A”, caused by intersections between “Feature A” and different fractures connecting hydraulically to the Äspö tunnels. Over time, as the heads in the “Feature A” rock block equilibrated, this groundwater divide disappeared, and the natural gradient of 0.1% toward the drift was asserted throughout “Feature A”. (Figure 3b-10).

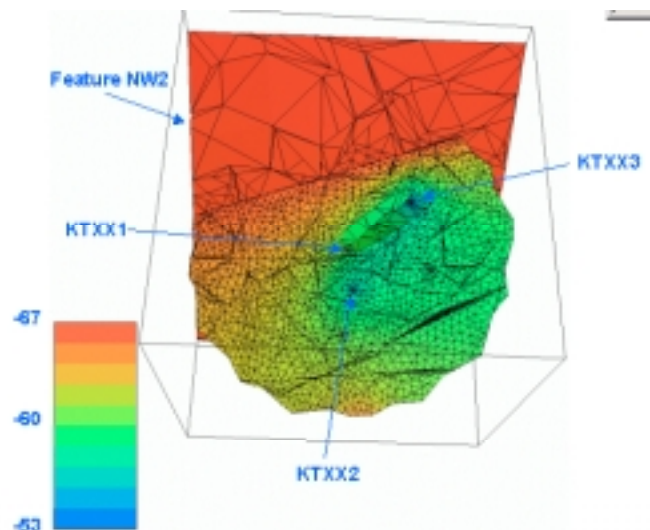
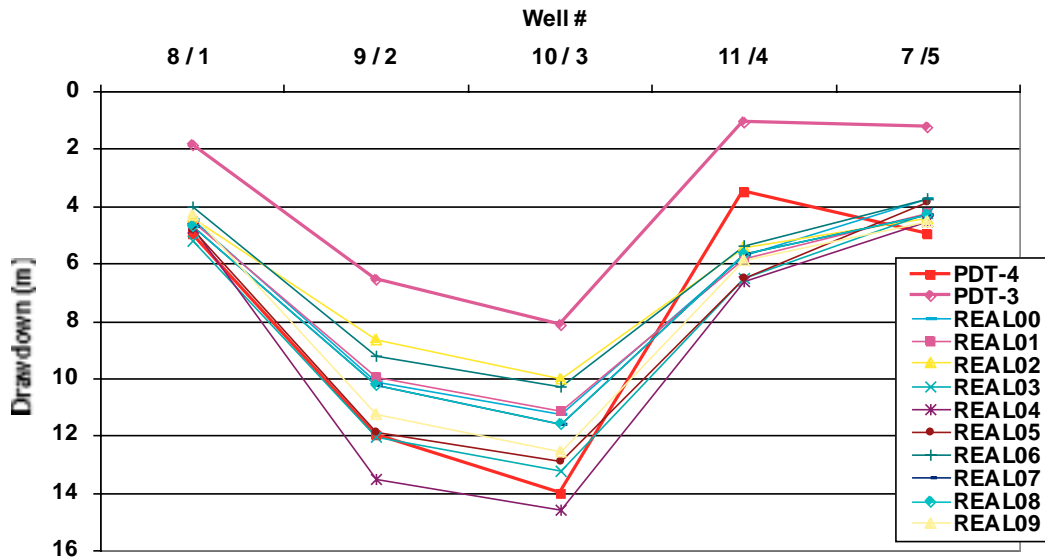


Figure 3b-10. Hydraulic head in “Feature A” during sorbing tracer test STT-2.



*Figure 3b-11. Drawdown pattern during tracer test PDT-4. In which test section?! Bad positioning of legend!*

Hydraulic responses are thus the key to understanding the connectivity of “Feature A”, and its place in the surrounding fracture network. For any realization of a discrete fracture network, stochastic fracture properties and the connectivity to boundary conditions are different. This results in differences in drawdown patterns between different DFN realizations. Figure 3b-11 illustrates drawdown patterns for 10 DFN realizations of the PDT-4 tracer test. Each of these realizations is consistent with the fracture statistics and hydraulic tests in the TRUE-1 rock block. However, each realization also produces different heads and thus significantly different gradients and flow fields within “Feature A”. This allows the quantification of the level of uncertainty in tracer prediction due to geometry and connectivity of intersecting fractures. For the purposes of “prediction” however, JNC/Golder took the DFN realization which provided the best match for the drawdown pattern of PDT-4, and used this for prediction of sorbing tracer transport along the same pathways and under the same boundary conditions.

Table 3b-2 illustrates the use of the calibrated DFN model to produce a probabilistic prediction of drawdown in response to PDT-4.

A variety of stochastic continuum approaches have been used to model “Feature A”, placing emphasis on the pattern of transmissivity and transport aperture within the single fracture, and generally ignoring connectivity to the intersecting fracture networks. This approach has the advantage of simplicity, but misses the important physical phenomena described above – it is easier to calibrate heads when you don’t need to consider the uncertainty in fracture intersections and connectivity, but it is not necessarily better!

**Table 3b-2. Calibration of head field of DFN model prior to prediction of sorbing tracer test STT-1.**

	Measured m	Calc. mean m	Difference m	Min. m	Max. m	St. Dev. m
KA3005A	-49.90	-49.58	0.32	-49.80	-49.425	0.139
KXTT1	-49.09	-49.25	-0.16	-49.32	-49.138	0.065
KXTT2	-49.36	-49.27	0.09	-49.35	-49.142	0.077
KXTT3	-48.97	-49.24	-0.27	-49.31	-49.124	0.074
KXTT4	-49.04	-49.37	-0.33	-49.49	-49.28	0.090

This is illustrated by the distance drawdown relationship from tracer tests carried out on “Feature A”. Figure 3b-12 shows the drawdown at borehole KXTT4 as a result of pumping from borehole KXTT3, only 4.7 m away. At the same pumping rate of 0.2 liters/minute, the drawdown during experiment STT-2 is four times greater than that observed in experiment PDT-2. At the same time, the recovery from PDT-2 is over 10 percent larger than for STT-2, even though the hydraulic response is smaller. The pumping rate of experiments RC-1 and PDT-3 is 0.4 liters/minute, doubled that of STT-2. However, the drawdown due to RC-1 is lower than that from STT-2, and the recovery of STT-2 is similar to that in RC-1. Neither of these behaviors can be predicted by a model which does not consider the complexity of the connectivity of the fracture network in the TRUE-1 block, and the interaction between fractures and the changing head field during the TRUE-1 experiment.

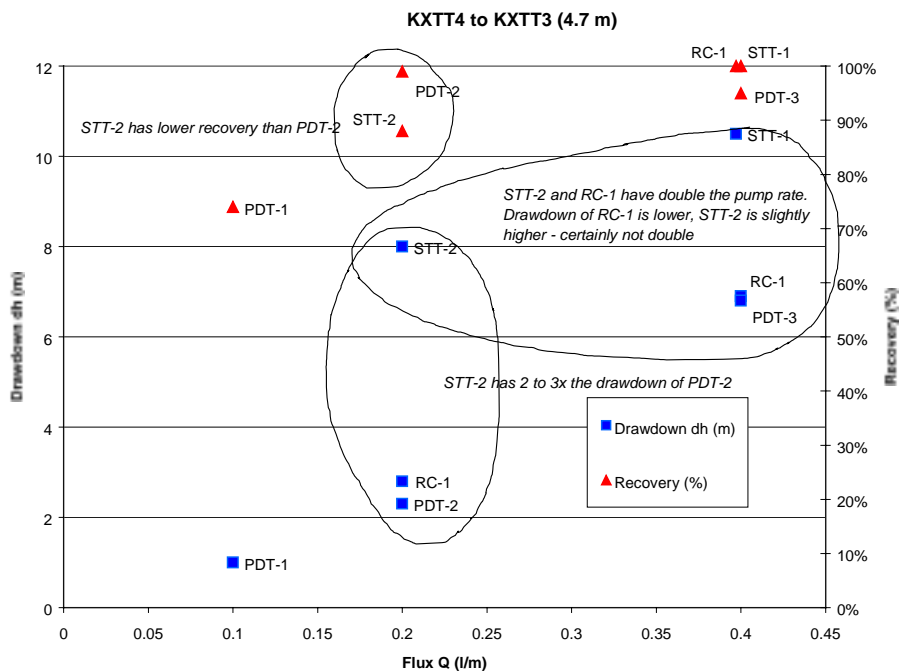


**Figure 3b-12. Hydraulic responses during tracer tests in “Feature A” between KXTT4 (source) and KXTT3 (sink).**

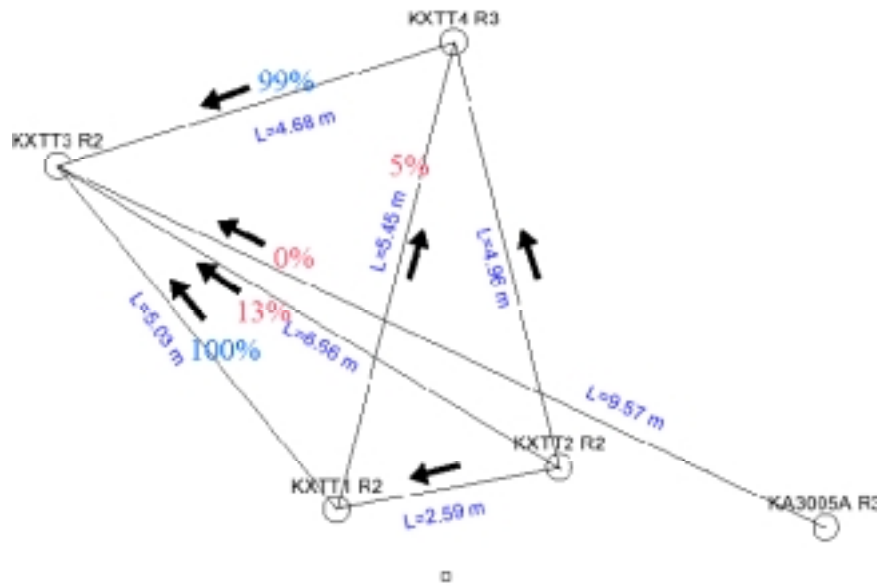


**Figure 3b-13.** Mass recovery (%) along schematic pathways between boreholes KXTT1, KXTT3, and KXTT4 in the plane of the interpreted Feature A.

This enigma of connectivity is further illustrated in Figure 3b-13. Experiments between KXTT4 and KXTT3, and between KXTT1 and KXTT3 show strong connectivity, with on the order of 90 to 100% recovery for conservative tracers. At the same time, experiments between KXTT1 and KXTT4 in Feature A show only 5% recovery! This behavior is inconsistent with the idea of pathways controlled by the stochastic pattern of apertures on fractures. However, it is reasonable, when considering that the actual connections are through the multiple fractures which make up “Feature A”, and that small changes in the head field can completely change the transport pathways in the fracture network. Clearly under the head field based on pumping in KXTT4, the transport pathways do not follow the route via KXTT3!

## 4 Transport processes

One of the goals of the TRUE-1 experiments was to improve our understanding of transport processes. It is hoped that deeper evaluation of the results from the TRUE-1 experiments will help to clarify the fundamental uncertainties regarding flow and transport in porous media:

- What is dispersion and what is the best way to parameterize dispersion to understand both symmetric (Gaussian) and non-symmetric dispersion? Can non-symmetric dispersion be explained in terms of multi-rate advection, or is it related solely to mobile-immobile exchange?
- What is the nature of exchange between mobile and immobile zones along transport pathways. Is this primarily a diffusional phenomenon, or are there other mechanisms such as locally turbulent mixing involved?

Going into the TRUE-1 project, JNC/Golder assumed that the important processes for transport are:

- Advection – transport of solutes at the same velocity as groundwater motion.
- Dispersion – variations in solute transport velocity due to variations in groundwater velocity.
- Immobile Zone exchange – exchange of mass between the mobile (advective) portions of the fracture pore-space and immobile zones such as infillings, stagnant pools, altered rock, fracture coating minerals, and the rock itself.
- Sorption – chemical attachment between certain tracers and certain minerals.

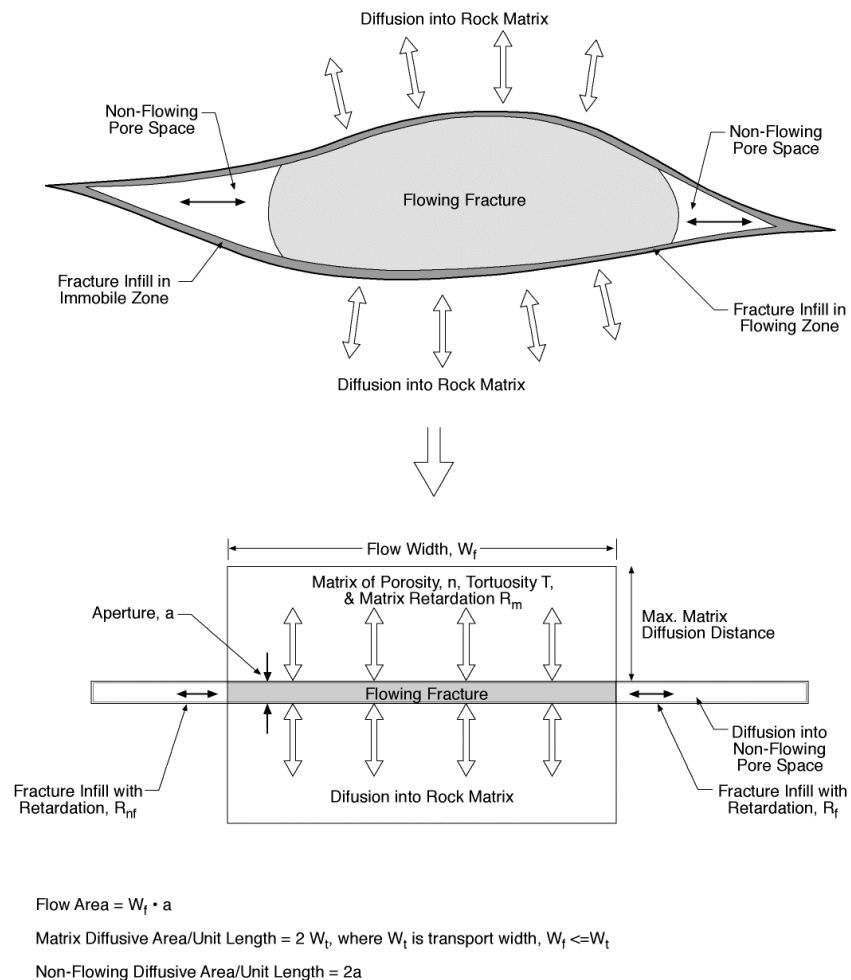


**Figure 3b-14.** Advection-Dispersion-Diffusion (ADD) transport constitutive approach for PAWorks/LTG.

Of these processes, there is the most uncertainty concerning immobile zone exchange. Is this purely a diffusive process proportional to differences in concentration, or is it the result of local turbulent mixing (advective exchange). Is immobile zone exchange controlled strictly by the available surface area, as some theorize, or is it controlled by the geological structure and material distribution within the fracture ?

JNC/Golder utilized three different solute transport approaches to examine the extent to which the important issues of immobile zone exchange can be resolved within the context of the TRUE-1 experiments: Conventional advection/dispersion/diffusion (ADD), Immobile zone exchange (IMX), and Continuous time random walk /CTRW; Berkowitz et al, 2000/.

The ADD approach is illustrated in Figure 3b-14 /Dershowitz et al., 1998/. The Laplace Transform Galerkin solution for solute transport ADD assumes steady-state flow and a second-order Galerkin approach to describe the diffusive mass transfer of a solute between the groundwater in a pipe and the multiple immobile porosity zones attached to it, the advective-dispersive transport of solute species  $n$  in a pipe network is given by /Sudicky, 1990/:

$$A \left[ R_n(\lambda) \frac{\partial C_n}{\partial t} + q(\lambda) \frac{\partial C_n}{\partial \lambda} - \frac{\partial}{\partial \lambda} D_{\lambda_n}(\lambda) \frac{\partial C_n}{\partial \lambda} + R_n(\lambda) \lambda_n C_n - R_{n-1}(\lambda) \lambda_{n-1} C_{n-1} \right] \pm \sum_{\lambda} \dot{M} \delta(\lambda - \lambda') + \sum_{\lambda^*} Q(C_n - C_n^*) \delta(\lambda - \lambda^*) + \sum_{im=1}^{IM} V_{im} \theta_{im} D_{im} \frac{\partial C_n^{im}}{\partial w} \Big|_{w=0} = 0 \quad (1)$$

where:

$n$	=	nuclide index [-]
$im$	=	immobile zone class number (note: if desired $im$ can equal 0) [-]
$IM(\lambda)$	=	total number of immobile zones attached to pipe $\lambda$ [-]
$A(\lambda)$	=	pipe cross-sectional area [ $L^2$ ]
$R_n(\lambda)$	=	retardation factor [-]
$q(\lambda)$	=	specific discharge ( $\equiv$ Pipe velocity $v$ ) [ $L/T$ ]
$D_{\lambda_n}(\lambda)$	=	dispersion coefficient = $\alpha v + D_n^o$ [ $L^2/T$ ]
$\alpha$	=	pipe longitudinal dispersivity [ $L$ ],
$D_n^o$	=	free-solution diffusion coefficient [ $L^2/T$ ]
$\lambda_n$	=	decay constant [ $1/T$ ]
$M(t)$	=	internal solute mass source/sink [ $M/T$ ]
$Q$	=	external fluid source/sink [ $L^3/T$ ]
$\delta(\lambda - \lambda')$	=	dirac delta [ $1/L$ ]
$\delta(\lambda - \lambda^*)$	=	dirac delta [ $1/L$ ]
$V_{im}$	=	block surface area per unit volume of matrix and fissures [ $1/L$ ]
$D_{im}$	=	matrix effective diffusion coefficient [ $L^2/T$ ]
$\theta_{im}$	=	immobile zone porosity for immobile zone "im"
$C_n$	=	pipe concentration [ $M/L^3$ ]
$C_n^*$	=	concentration of injectate in external fluid source [ $M/L^3$ ]
$C_n^{im}$	=	Immobile zone concentration [ $M/L^3$ ]
$\lambda$	=	Distance along interconnected pipe network [ $L$ ]
$\lambda'$	=	Location of solute mass source/sink [ $L$ ]

$\lambda^*$	=	Location of external fluid source/sink [L]
$w$	=	Distance perpendicular to plane of fracture [L]
$t$	=	time [T]

The second order approach implemented for diffusive exchange of solute mass between the pipes and any on the *im* immobile zones attached to them is described by:

$$\theta_{im}(im, \lambda) R_n^{im}(im, \lambda) \frac{\partial C_n^{im}}{\partial t} - \frac{\partial}{\partial w} \theta_{im}(im, \lambda) D_{im} \frac{\partial C_n^{im}}{\partial w} + \theta_{im}(im, \lambda) R_n^{im}(im, \lambda) \lambda_n C_n^{im} - \theta_{im}(im, \lambda) R_{n-1}^{im}(im, \lambda) \lambda_{n-1} C_{n-1}^{im} = 0 \quad (2)$$

where:

$\theta_{im}(im, \lambda)$	=	Immobile zone porosity for immobile zone “ <i>im</i> ” attached to pipe “ $\lambda$ ” [-]
$R_n^{im}(im, \lambda)$	=	Immobile zone retardation factor for immobile zone “ <i>im</i> ” attached to pipe “ $\lambda$ ” [-]
$C_n^{im}$	=	Concentration in matrix [M/L <sup>3</sup> ]
$D_{im}$	=	Matrix effective diffusion coefficient [L <sup>2</sup> /T]
	=	$D_n^0 \tau$
$D_n^0$	=	Free-solution diffusion coefficient [L <sup>2</sup> /T]
$\tau$	=	Tortuosity [-]

The above equations used for the ADD approach recognize that we do not fully understand immobile zone exchange by providing the option of multiple immobile zones, each with its own diffusion rate, thickness, tortuosity, and porosity. Providing for multiple immobile zones is particularly useful in considering transport at multiple time and distance scales. While fracture infillings may be the primary immobile zone for transport at the 5 meter and one month scale, intact rock is more likely to be the most important immobile zone for distance scales of kilometers and time scales of hundreds or thousands of years. For the purposes of the TRUE-1 experiment, only a single immobile zone is used, and this immobile zone represents the short terms, small capacity immobile zone of gouge, breccia, and altered rock which is most likely to be important in the short time and distance scale. However, the same model can be used for longer time frames by adding additional immobile zone porosities to the porosities in the TRUE-1 model.

Advective exchange (AX) /Miller, 1996/ assumes that the process of exchange between mobile and immobile zones occurs at a fixed rate of exchanges per meter of advection, rather than at a rate proportional to differences in concentration. This model is illustrated in Figure 3b-15. The approach is based on two parameters:  $\beta$ , the number of advective exchanges per meter, and  $f_{imm}$ , the ratio of the immobile zone volume to the mobile zone volume.

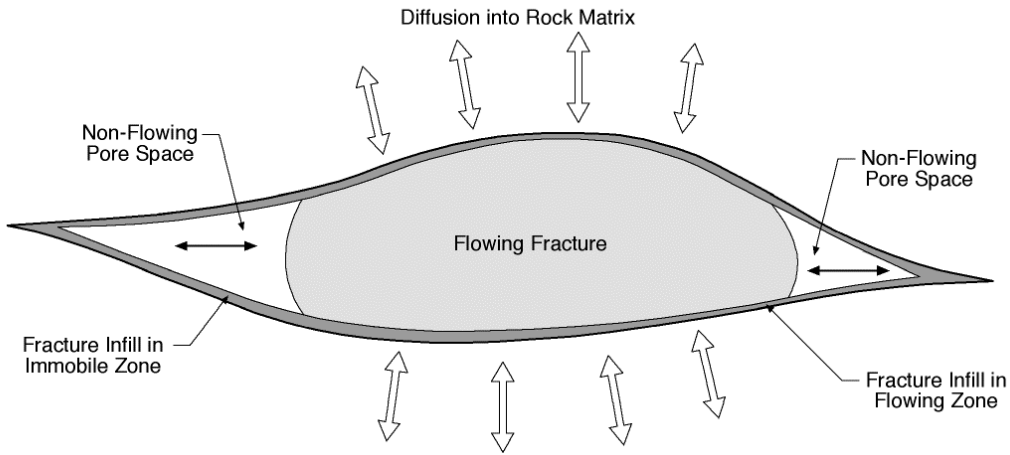


Figure 3b-15. Advective eXchange (AX) transport constitutive approach /Miller, 1996/.

Continuous Time Random Walk (CTRW) was developed by Berkowitz et al. /2000/ to explain the frequent occurrence of non-symmetrical (non-Gaussian) dispersion on the basis of multi-rate advection. CTRW treats both diffusion and Gaussian dispersion as special cases of multi-rate advection, and can reproduce both diffusive and Gaussian transport on the basis of a single parameter  $\beta$ , the power for the assumed powerlaw (Pareto) distribution of velocity. The CTRW method is summarized in Figure 3b-16 /after Berkowitz et al, 2000/.

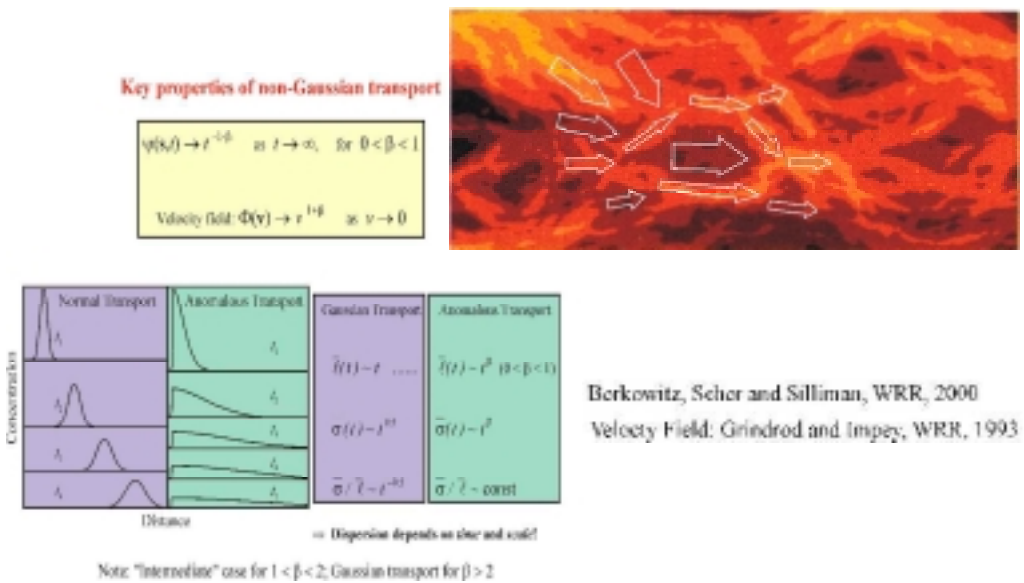


Figure 3b-16. Continuous Time Random Walk (CTRW) transport constitutive approach /Berkowitz et al., 2000/.



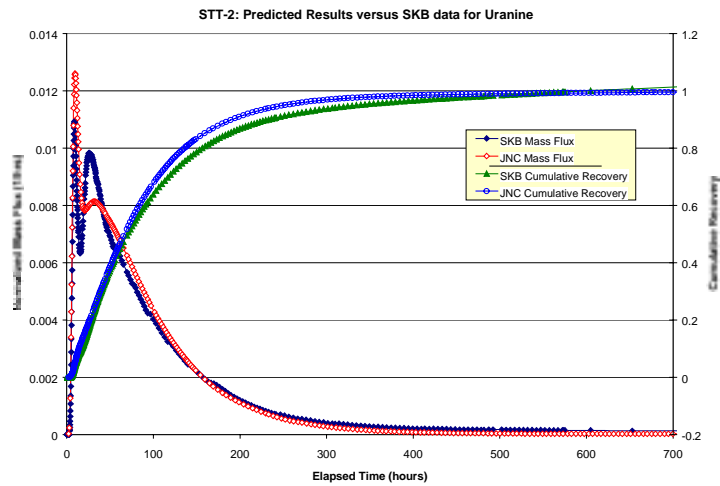


Figure 3b-17. ADD transport prediction for conservative tracer Uranine, STT-2 experiment.

While it was hoped that the TRUE-1 experiments would distinguish between different fundamental theoretical approaches to dispersion and immobile exchange, all three of the approaches implemented were able to fit experiments to some level of accuracy. Example ADD, AX, and CTRW fits to TRUE-1 experiments are shown in Figures 3b-17, 3b-18, and 3b-19. In addition, the LaSAR approach for multi-rate advection /Cvetkovic et al., 1999/ was also successful in matching the TRUE-1 experiments. The only conclusion from this is that, at present, multiple and conflicting theories about transport in fractures can reproduce the TRUE-1 experiments, and additional experiments will be required to distinguish between them.

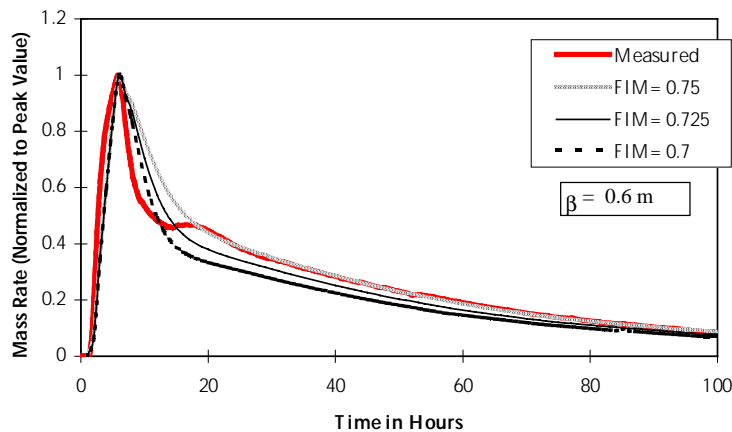


Figure 3b-18. AX transport calibration for conservative tracer Uranine, STT-2 experiment.

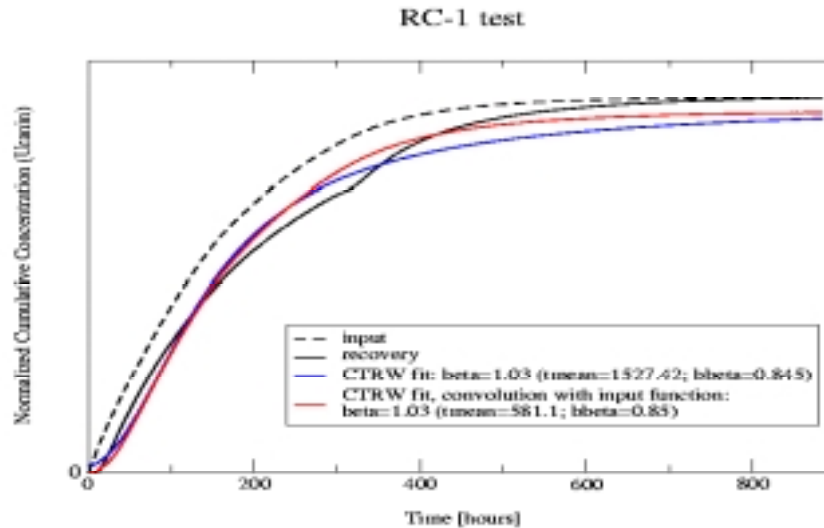


Figure 3b-19. CTRW transport calibration for conservative tracer Uranine, RC-1 experiment.

## 5 Calibration and prediction

JNC’s goal in participating in the TRUE-1 project was to improve our understanding of transport in fractures and fracture networks, not to demonstrate the predictive abilities of DFN approaches. Nevertheless, we are somewhat gratified when our calibrated DFN models demonstrate a certain degree of predictive power. The calibration process itself was quite edifying, since it showed to what extent model parameters needed to be adjusted to provide a match to transport experiments.

Over the course of four years JNC/Golder used a series of increasingly refined DFN models to produce predictions for tracer breakthrough in “Feature A”. These experiments went from the initial radially converging tests RC-1 and RC-2, dipole tests DP-1 through DP-4, and sorbing tracer experiments of the tracer retention experiment STT-1, STT-2, and STT-1b. The accuracy of calibrations and predictions improved continuously over this period, and in the end the prediction of STT-2 and STT-1b was quite accurate. Predictions for breakthrough of STT-2 tracers are illustrated in Figures 3b-17, 3b-20, 3b-21, and 3b-22. These predictions were based on calibrations to STT-1b transport behavior, and it should therefore not be too surprising that the predictions, although blind, are fairly accurate.

The key parameter which determined the success of transport calibrations and predictions was the immobile zone exchange parameters in Equation (2) above. In particular, the calibrated immobile zone retardation factor  $R_{im}$

$$R_{im} = 1 + \rho_{im} K_d' / \theta_{im} \quad (3)$$

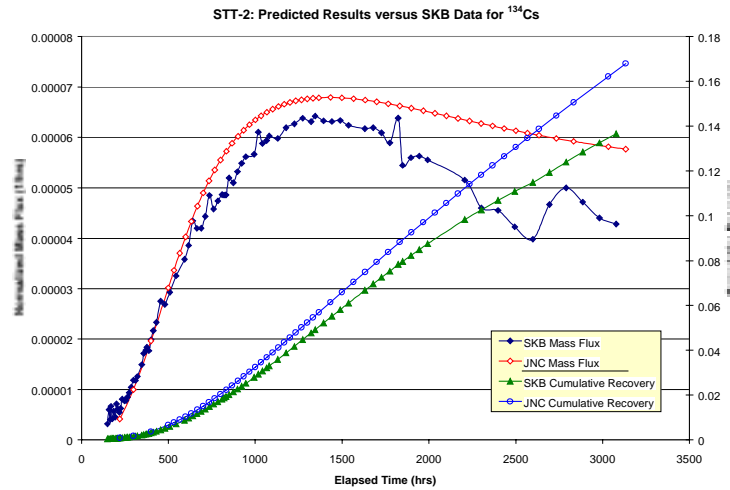


Figure 3b-20. ADD transport prediction for <sup>134</sup>Cs, STT-2 experiment.

where  $\rho_{im}$  is the immobile zone bulk density,  $\theta_{im}$  is the immobile zone porosity, and  $K_d'$  is the effective distribution coefficient for the immobile zone. The calibrated value of  $R_{im}$  indicates that either the effective distribution coefficient is 10 times the laboratory measured values, or the immobile zone porosity is on the order of 15%. Geological information /Hermanson, 2000/ indicates that the porosity of 15% is not unreasonable if immobile zone diffusion is primarily to gouge materials. This is also supported by research described in Altman et al. /2001/.

The other important immobile zone transport parameter is the perimeter of the pipe pathways. This controls the rate and amount of possible diffusion. The calibrated value for this parameter is on the order of 5 to 7 meters, for a pipe flow width of 2.5 to 3.5

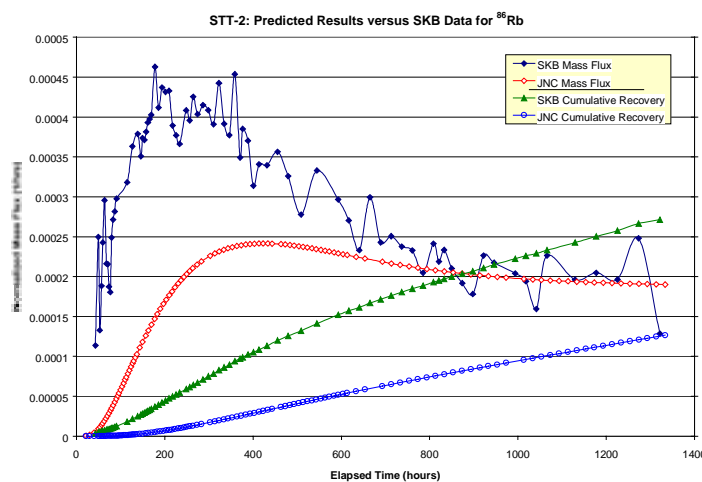


Figure 3b-21. ADD transport prediction for <sup>86</sup>Rb, STT-2 experiment.

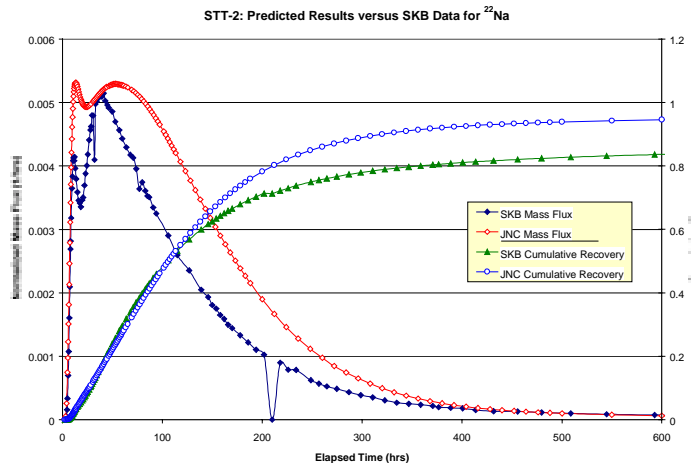


Figure 3b-22. ADD transport prediction for  $^{22}\text{Na}$ , STT-2 experiment.

meters divided by the number of surfaces on which diffusion occurs. For a simple tabular channel, the number of surfaces is 2. However, with matrix infillings, the effective number of surfaces may be much larger, resulting in effective transport path widths more on the expected order of magnitude of 0.1 to 1 m.

Unfortunately, the TRUE-1 experiments did not resolve the issue of the actual mechanism behind the parameters which work for calibrating and predicting ADD solute transport. However, they did demonstrate that, at least for “Feature A”, the ADD transport assumptions are not inconsistent with observations.

## 6 Conclusions

The TRUE-1 experiment made major progress in improving the understanding of flow and transport in fractured rock. The experiment was successful in demonstrating the usefulness of discrete fracture network methods for characterizing fracture rock and understanding the geometry of transport pathways, and the possibility of calibrating DFN models for transport predictions. The experiment did not succeed in resolving the nature of transport within fracture planes, or in resolving between competing constitutive approaches to solute transport. It is hoped that future transport experiments on single fractures and fracture networks will further advance the scientific understanding of flow and transport in fractured rock.

## References

- Altmann S, Uchida M, Tidwell V, 2001.** Visualization and Quantification of Heterogeneous Diffusion Rates in Granodiorite Samples by X-ray Absorption Imaging – Diffusion within Gouge Materials, Altered Rim and Intact Rock Matrix. Proceedings, TRUE-1 Seminar. September 2000. SKB, Stockholm.
- Berkowitz B, Scher H, Silliman S E, 2000.** Anomalous transport in laboratory-scale, heterogeneous porous media, *Water Resources Research*, Vol. 36, No. 1, pp.149–158.

**Cvertkovic V, Selroos J-O, Cheng H, 1999.** Transport of Reactive Solute in Single Fractures. *Journal of Fluid Mechanics*, Vol. 318. pp 335–356.

**Dershowitz W, Cladouhos T, Uchida M, 2001.** Tracer Tests with Sorbing Tracers. SKB International Cooperation Report ICR-2001-XX, Swedish Nuclear Fuel and Waste Management Co.

**Dershowitz W, Thomas A, Busse R, 1996.** Discrete Fracture Analysis in Support of the Äspö Tracer Retention Understanding Experiment. SKB International Cooperation Report ICR-96-05, Swedish Nuclear Fuel and Waste Management Co.

**Dershowitz W, Foxford T, Sudicky E, Shuttle D, Eiben T, 1998.** PAWorks: Pathway Analysis for Discrete Fracture Networks with LTG Solute Transport. User Documentation. Version 1.5. Golder Associates Inc, Seattle.

**Dershowitz W, Lee G, Geier J, Foxford T, LaPointe P, Thomas A, 2000.** FracMan Interactive Discrete Fracture Data Analysis, Geometric Modeling, and Exploration Simulation. User Documentation. Version 2.6. Golder Associates Inc, Seattle.

**Doe T W, 1991.** Fractional Dimension Analysis of Constant-Pressure Well Tests. Presented at the 66th Annual Technical Conference & Exhibition of the Society of Petroleum Engineers, Dallas, TX, Oct. 6–9, 1991. SPE Technical Paper No. 22702. Society of Petroleum Engineers, Richardson TX.

**Miller, 1996.** Advective Exchange: A New Conceptual Approach for Solute Transport in Fractured Rock. Internal Report. Golder Associates Inc., Seattle.

**Sudicky E A, 1990.** The Laplace Transform Galerkin Technique for Efficient Time-continuous Solution of Solute Transport in Double-porosity Media, *Geoderma*, 46, 209–232.

**Uchida M, Sawada A, Shimo M, Yamamoto H, Takahara H, Doe T, 2001.** Anisotropy, Reversibility and Scale Dependence of Transport Properties in Single Fracture and Fractured Zone – Non-sorbing Tracer Experiment at the Kamaishi Mine. Proceedings, TRUE-1 International Seminar, Swedish Nuclear Fuel and Waste Management Co.

**Winberg A, Andersson P, Hermanson J, Byegård J, Cvetkovic V, Birgersson L, 2000.** Äspö Hard Rock Laboratory. Final report of the first stage of the Tracer Retention Understanding Experiments. SKB TR-00-07, Swedish Nuclear Fuel and Waste Management Co.

# A simple flow channel model of TRUE-1

*Antti Poteri,  
VTT Energy*

*Aimo Hautajärvi,  
Posiva Oy*

## Abstract

This paper summarises the evaluation work carried out for the sorbing tracer tests STT-1 and STT-2 of TRUE-1. Transport of four different tracers (Uranine, Barium, Rubidium and Cesium) was modelled. Two different modelling approaches have been applied. First, only the equilibrium surface sorption is assumed to retard the migration. Second approach is a more comprehensive flow channel model that includes diffusion to the rock matrix, to the stagnant zones and to the fracture filling material.

The results indicate that the sorption alone can explain the transport of the sorbing tracers reasonably well. The results indicate that generally the fitted retardation coefficients for the STT-2 test were higher than for the STT-1 showing possibly some influence of the diffusive process. In the case of the Cesium the retardation was smaller in STT-2 than in STT-1. This may indicate the influence of some other process than equilibrium sorption (and matrix diffusion) in the case of the Cesium.

The breakthrough curves seem to fit to the matrix diffusion model as well. The matrix diffusion model was applied by using laboratory data for the sorption and diffusion properties, single flow velocity along the flow channel and parallel diffusive mass flux to the matrix, to the stagnant zones and to the fracture filling material. The breakthrough curves were made to fit by changing the geometry of the transport channel (width and aperture) and keeping the total flow rate through the channel fixed. The resulting alternatives for the channel geometry were about 100 channels of 0.2–1 mm width or a single channel of 0.3–0.9 m width. In the first case, the retention comes from the diffusion to the stagnant water as in the later case it comes from the diffusion to the rock matrix or filling material covering the matrix. For geometrical reasons the case of diffusion to the stagnant zones is considered more likely than diffusion to the matrix.

## 1 Introduction

The first phase of the Tracer Retention Understanding Experiment, TRUE-1, was carried out in Äspö Hard Rock Laboratory in Sweden between 1995 and 1999. The experiment included over 20 different tracer tests performed in the same fracture. Majority of the transport paths between the pumping and injection borehole sections have been only about 5 meters long. Tracer tests were performed with both conservative and sorbing tracers and also using different pumping rates.

Evaluation and modelling of the tracer tests offer a good possibility to examine different transport concepts for the fractured rock. In this paper, two different tracer tests, STT-1 and STT-2 with four differently sorbing tracers are evaluated. A simple surface sorption model and a more comprehensive matrix diffusion model were tested against the measured breakthrough curves. The goal of the evaluation was to study the sensitivity of the matrix diffusion model in the evaluation of the detailed scale tracer tests and on the other hand to evaluate the relative importance of the different processes during the transport.

## 2 Modelling concepts

### **Matrix diffusion**

Advection along fracture and diffusion to the rock matrix can be described using following equation /e.g. Neretnieks, 1980/

$$R_a \frac{\partial C_f}{\partial t} = -v \frac{\partial C_f}{\partial x} + D_e \frac{\partial C_p}{\partial z} \Big|_{z=0} \quad (1)$$

$$R_p \frac{\partial C_p}{\partial t} = D_p \frac{\partial^2 C_p}{\partial z^2} \quad (2)$$

$$C_f = C_p, \quad z = 0, x > 0 \quad (3)$$

where  $C_f$  is the solute concentration in the fracture,  $C_p$  is the solute concentration in the rock matrix,  $R_a$  is the retention coefficient in the fracture (surface sorption),  $v$  is the groundwater flow velocity,  $D_e$  is the efficient diffusion coefficient into rock matrix,  $R_p$  is the retention coefficient in the rock matrix and  $D_p$  is the diffusion coefficient in the pore water of the rock matrix. Equations (1)–(3) can be solved by applying Laplace transform, for example. Solute concentrations in the fracture and rock matrix for a continuous source are;

$$\frac{C_f}{C_0} = H\left(t - \frac{R_a x}{v}\right) \operatorname{erfc} \left( \frac{D_e x}{v} \frac{1}{2b} \sqrt{\frac{R_p}{D_p \left(t - \frac{R_a x}{v}\right)}} \right) \quad (4)$$

$$\frac{C_p}{C_0} = H\left(t - \frac{R_a x}{v}\right) \operatorname{erfc} \left( \left( \frac{D_e x}{v} \frac{1}{2b} + \frac{z}{2} \right) \sqrt{\frac{R_p}{D_p \left(t - \frac{R_a x}{v}\right)}} \right) \quad (5)$$

where H is the Heaviside's unit function.

### **Dimensionless form**

Fitting of the experimental breakthrough curves is much simpler when the Equation (4) is rewritten in the dimensionless form. Equation (4) can be expressed with three dimensionless parameters: dimensionless time  $\tau = t/t_w$ , where  $t_w$  is the groundwater transit time ( $=L/v$ ), retardation coefficient  $R_a$  and parameter  $U$  that controls the strength of the matrix diffusion. The parameter  $U$  is defined as;

$$U = \frac{\sqrt{D_e \varepsilon R_p t_w}}{2b} \quad (6)$$

where identities

$$t_w = \frac{x}{v} \quad (7)$$

$$D_e = D_p \varepsilon \quad (8)$$

have been used. Equation (4) can now be expressed with  $U$ ,  $\tau$  and  $R_a$  as

$$\frac{C_f}{C_0} = H(\tau - R_a) \operatorname{erfc}\left(\frac{U}{\sqrt{\tau - R_a}}\right) \quad (9)$$

Equation (9) can be used to calculate the breakthrough curve for the Dirac delta function input. In this case the breakthrough is;

$$j_f = \frac{U}{\sqrt{\pi}(\tau - R_a)^{3/2}} e^{-\frac{U^2}{\tau - R_a}} \quad (10)$$

where  $j_f$  is the tracer mass flux for the released unit mass of the tracer.

### **Parallel diffusion routes**

Equation (1) is based on the assumption, that there is only a single one dimensional diffusion process between the migrating solute in the fracture and the surroundings. In reality the flow is probably channelled and adjacent to the channel there are the rock matrix, stagnant zones of the flow field and the fracture filling material. All these are available for the diffusion at the same time. Assuming that the diffusion to the different environments are independent the Equations (1)–(3) can be rewritten with additional diffusional couplings. For two different diffusion environments we can write;

$$R_a \frac{\partial C_f}{\partial t} = -v \frac{\partial C_f}{\partial x} + D_e \frac{2}{2b} \frac{\partial C_p}{\partial z} \Big|_{z=0} + D'_e \frac{2}{2b'} \frac{\partial C'_p}{\partial y} \Big|_{y=0} \quad (11)$$



$$R_p \frac{\partial C_p}{\partial t} = D_p \frac{\partial^2 C_p}{\partial z^2} \quad (12)$$

$$R'_p \frac{\partial C'_p}{\partial t} = D'_p \frac{\partial^2 C'_p}{\partial y^2} \quad (13)$$

$$C_f = C_p = C'_p, \quad z = 0, y = 0, x > 0 \quad (14)$$

Where parameter with apostrophe refer to environment 1 and without apostrophe to environment 2. Equations (11)–(14) can be solved in the same way as Equations (1)–(3). In this case the dimensionless parameter  $U$  defined in Equation (6) is replaced by

$$U_{tot} = U + U' \quad (15)$$

where  $U$  is defined in Equation (6) and  $U'$  is defined by equation;

$$U' = \frac{\sqrt{D'_e \varepsilon' R'_p t_w}}{2b'} \quad (16)$$

This can be generalised to any number of parallel diffusion routes. The influence of the parallel diffusion routes changes only the dimensionless parameter  $U$  so that it will be a sum of the individual parameter  $U$  values of the different processes.

### **Diffusion to stagnant zones**

Stagnant zones of the flow field are regions in the fracture plane where the groundwater flow rate is very small. The stagnant zones of the flow field are located in the fracture plane itself and the parameter  $U$  presented in Equation (6) cannot directly be applied. In this case, the diffusion takes place in the fracture plane and not in the direction of the fracture aperture.

Straightforward analogy to the matrix diffusion case can be defined for the channelled flow. The flow channel is limited by the rock matrix from the top and bottom walls and by the stagnant water zones from the side walls. It is clear that diffusion into stagnant water is analogous to the matrix diffusion if following substitutions are done

$$\begin{array}{lcl} D_e & \rightarrow & D_w \\ b & \rightarrow & a \\ \varepsilon & \rightarrow & \varepsilon_s \\ R_p & \rightarrow & R_a \end{array} \quad (17)$$

where  $D_w$  is the molecular diffusion coefficient in water,  $a$  is the half width of the channel and  $\varepsilon_s$  is the proportion of the stagnant water available for the diffusion along the channel wall. Transport equation can be written as;

$$R_a \frac{\partial C_f}{\partial t} = -v \frac{\partial C_f}{\partial x} + \varepsilon_s D_w \frac{2}{2a} \frac{\partial C_p}{\partial z} \Big|_{z=0} \quad (18)$$

$$R_{az} \frac{\partial C_p}{\partial t} = D_w \frac{\partial^2 C_p}{\partial z^2} \quad (19)$$

$$C_f = C_p, \quad z = 0, x > 0 \quad (20)$$

where  $R_{az}$  is the retardation coefficient in the stagnant zones (in practice  $R_{az} = R_a$ ). Based on the Equations (18) and (19) the parameter  $U$  can be rewritten for the case of the stagnant zone as;

$$U_{stagnant} = \frac{\sqrt{D_w \varepsilon_s^2 R_{az} t_w}}{2a} \quad (21)$$

### Surface sorption

Advection and sorption on the fracture surface leads to retention in the breakthrough time of the migrating solute. If the breakthrough time of a non-sorbing tracer is  $t_w$  then the breakthrough time of a sorbing tracer will be;

$$t_r = R_a t_w \quad (22)$$

where  $R_a$  is the retardation coefficient. In reality there is always a distribution of the breakthrough times corresponding to different streamlines of the flow field. Let us now assume that the distribution of the groundwater transit times is  $f(t_w)$ . Then the breakthrough of a sorbing tracer can be written as;

$$\int f(t_w) \delta(t - R_a t_w) dt_w = \frac{1}{R_a} f\left(\frac{t}{R_a}\right) \quad (23)$$

indicating that the functional form of the breakthrough curve does not change and that the breakthrough curve of the sorbing tracer can be obtained from the non-sorbing breakthrough by scaling it with the retardation coefficient. In the evaluation of the TRUE tests this can be applied in the opposite direction. We make a hypothesis that all the tracers follow the same streamlines and the sorption is the only retarding mechanism. In this case it should be possible to scale all breakthrough curves to non-sorbing breakthrough and the scaling factors equal the retardation coefficients. If the transformation cannot bring some of the breakthrough curves on the non-sorbing breakthrough then the sorption alone cannot explain the retardation of that tracer.

The effect of the matrix diffusion can also be estimated in the similar way. It can be derived from the Equation (10) that for the delta function input the peak time of the breakthrough curve in the case of the matrix diffusion is;

$$\tau_{peak} = R_a + \frac{2}{3}U^2, \quad (24)$$

where  $\tau_{peak}$  is the peak time in the dimensionless time  $\tau=t/t_w$  and  $U$  is defined in Equation (6). Investigation of the Equation (24) shows that when the effect of the matrix diffusion is small the peak time scales with constant coefficient,  $R_a$ , independently of the groundwater transit time. The matrix diffusion affects the breakthrough time through the parameter  $U$ . According to the Equation (6) the  $U$  depends on the square root of the groundwater transit time  $t_w$ . This means that the scaling factor of the peak breakthrough time is not anymore constant but it increases linearly when groundwater transit time increases (for the same transport path). In the evaluation of the tracer tests this can be seen as increasing  $R_a$  between the tracer tests performed with different pumping rates. It should be noted that the shape of the breakthrough curve will also change and it is not anymore possible to scale the more retarded breakthrough curve exactly to the less retarded breakthrough curve. However, these changes may not be very prominent in the somewhat fluctuating experimental results.

The breakthrough curves evaluated from the STT-1 and STT-2 tests are tested using the linear transformation in Equation (23) to assess the significance of the surface sorption alone. This evaluation is presented in Section 3.1.

### 3 Evaluation of the STT-1 and STT-2 tests

Four different tracers were selected for the evaluation: Uranine, Barium, Rubidium and Cesium. They cover the span of the retention properties of the sorbing tracers that were applied in the tracer tests. Uranine is a conservative tracer and Cesium is the most strongly sorbing tracer used in the experiments.

Evaluation of the tracer tests was based on the application of two different models. It was studied if the equilibrium sorption alone can explain the breakthrough curves. In addition, the experiments were examined using matrix diffusion model. The matrix diffusion model is based on the laboratory data of the sorption and diffusion properties. The matrix diffusion equations are applied in the dimensionless form (Equation (9)) to estimate the strength of the matrix diffusion. The results of the matrix diffusion model are illustrated by the geometry of the flow path that is required to achieve the measured retention of the tracers.

#### ***Equilibrium surface sorption the only active retention process?***

It is possible that only the advective flow field and surface sorption mainly cause the retention of the tracers. In this case the breakthrough curves of different tracers differ by fixed scaling factors that are proportional to the surface retardation factors of the tracers (see section of the surface sorption in modelling concepts). Strictly, this is true if the influence of the source term is first deconvoluted away from the breakthrough curves. In this study this has not been done and the uncertainty caused by the source terms must be remembered when the results are interpreted.

The breakthrough curves were normalised to the injected mass before the scaling. The injected masses of the tracers were calculated by integrating numerically the injection

curves. The flow rates applied for the injection sections were 40 ml/h in STT-1 and 28 ml/h in STT-2. The calculated recoveries are presented in Table 3b-3. The scaling of the breakthrough curves was done by keeping both the scaling of the time axis and the normalising factor of the breakthrough curve as fitting parameters. When the scaling factors ( $R_a$ ) were obtained the breakthrough curves were plotted applying the scaling law in Equation (23). This means that the scaled breakthrough curves obey the same recovery as the measured curves. The results of the scaling are presented in Figure 3b-23.

The fitted retardation coefficients do not stay constant between STT-1 and STT-2 tests. The fitted retardation coefficients for the examined tracers are plotted in Figure 3b-24 as a function of the inverse of the injection flow rate. Barium and Rubidium behave consistently and the retardation coefficient increases from STT-1 to STT-2. However, it is difficult to determine from these two tests alone that is the increase in the retardation coefficient following the Equation (24), i.e. caused by diffusive mass transfer, or is it only uncertainty related to the source terms, for example. Cesium behaves quite oddly in the scaling. The retardation coefficient is even smaller in STT-2 test than in the STT-1 test.

**Table 3b-3. Recoveries calculated from the injection curves using injection flow rates 40 ml/h for STT-1 and 28 ml/h for STT-2. The 105% recovery for the Uranine in the STT-2 test indicate that the injection flow rate should probably be higher than the applied 28 ml/h. The influence of the error to the results presented in this paper is negligible. The measured recoveries are taken from Andersson et al. /1998/ and Andersson et al. /1999/.**

	STT-1 (%)		STT-2 (%)	
	Calculated	Measured	Calculated	Measured
Uranine	100	100	105	96
Barium	84	82	57	56
Rubidium	63	60	50	49
Cesium	25	26	12	11

### ***Diffusion to rock matrix, stagnant zones and fault gauge***

The matrix diffusion model is based on the flow channel concept. The applied hydrological model includes only advection. Hydrodynamic dispersion in the flow channel is not taken into account. It is likely that the influence of the dispersion and the advective flow field in general are greatest for the non-sorbing tracer (Uranine). Accordingly, the Uranine has the worst fit among the fitted breakthrough curves (Figure 3b-26).

The matrix diffusion model was fitted to the breakthrough curve by dividing the source terms into square pulses and applying Equation (9). The retardation coefficient ( $R_a$ ) were calculated from the laboratory data by assuming 1 mm aperture. This means that the parameter  $U$  was the only fitting parameter. The fitting process resulted a set of parameter  $U$  values. The fitted  $U$  values were interpreted by assuming that there exist

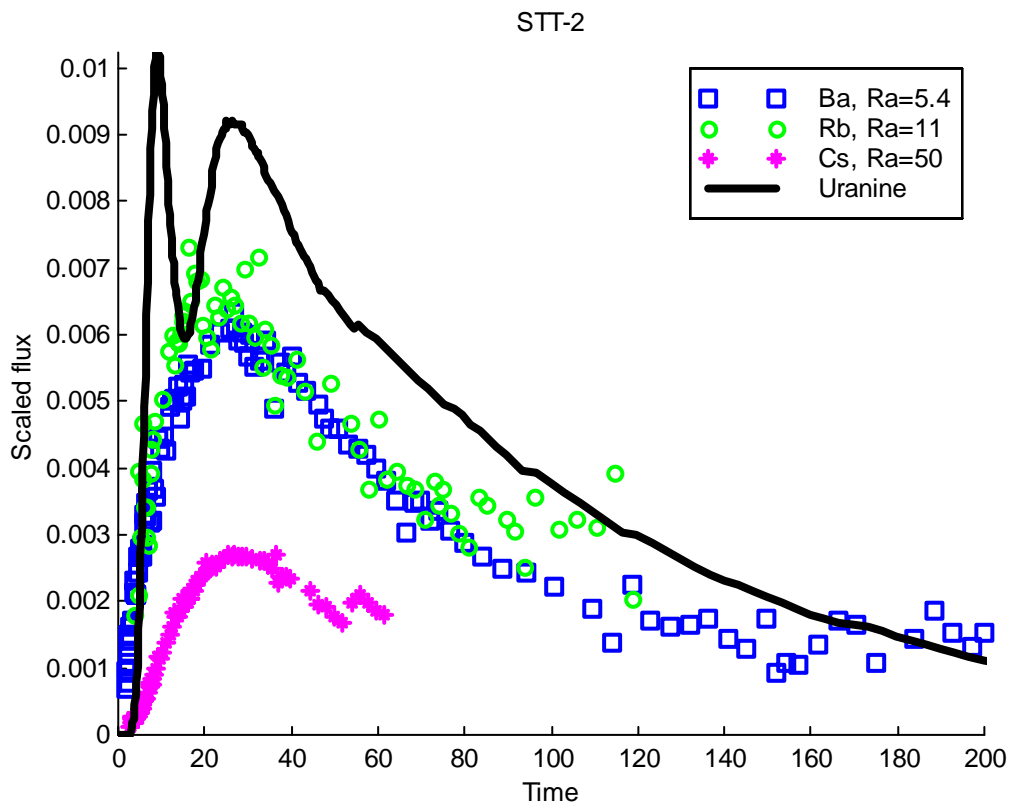
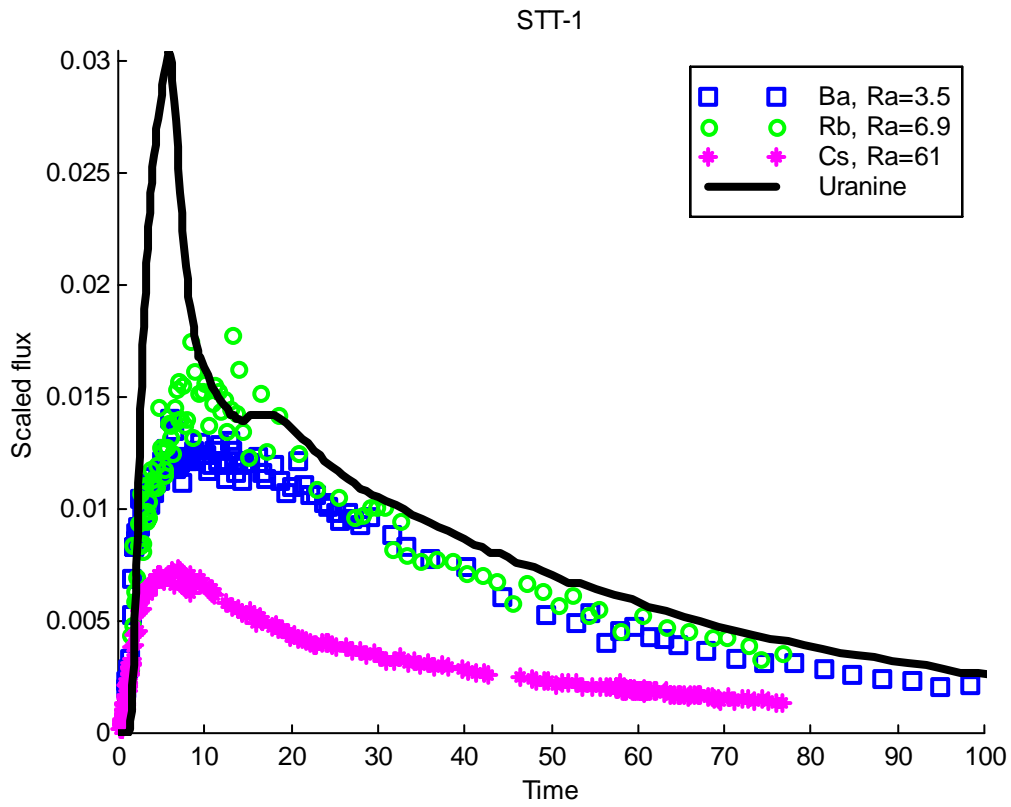


**Figure 3b-23.** Sorbing tracers breakthrough curves scaled on the Uranine breakthrough for the STT-1 and STT-2 tests.

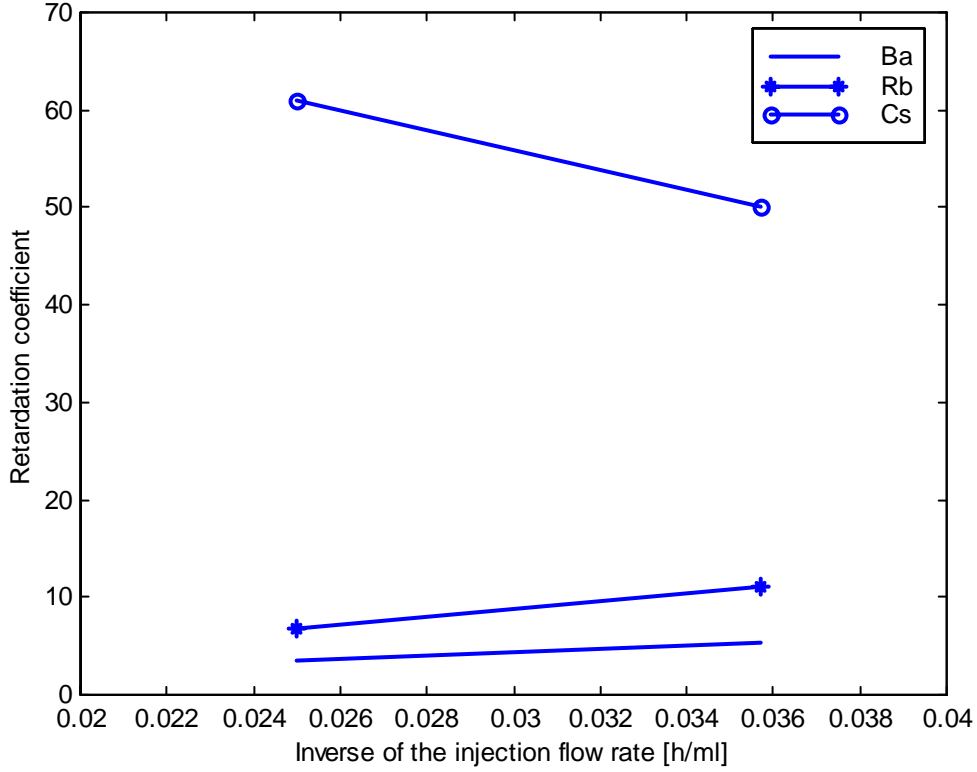


**Figure 3b-24.** Fitted retardation coefficients as a function of the inverse of the injection flow rate.

three independent and parallel diffusion processes along the flow channel. These are diffusion to the stagnant zones, to the fracture filling material and to the rock matrix. Each of these processes are characterised by their own parameter  $U$  value and the fitted model parameter  $U_{tot}$  is a sum of the three parameters;

$$U_{tot} = U_{stagnant} + U_{infilling} + U_{rock} \quad (25)$$

By substituting the representation of the parameters  $U$  from Equations (6) and (20) gives;

$$U_{tot} = \sqrt{\frac{D_w \varepsilon_s^2 R_a}{t_w} \frac{bL}{Q}} + \sqrt{\frac{D_f (1 - \varepsilon_s) \varepsilon_f R_f}{t_w} \frac{bL}{Q}} + \sqrt{\frac{D_e \varepsilon_{mf} \varepsilon_m R_p}{t_w} \frac{WL}{Q}} + \sqrt{\frac{D_f (1 - \varepsilon_{mf}) \varepsilon_f R_f}{t_w} \frac{WL}{Q}} \quad (26)$$

where  $\varepsilon_s$  and  $\varepsilon_{mf}$  are the proportions of the channel walls covered by the filling material compared to the stagnant water and to the rock matrix, respectively. This is explained more in detailed in Section 3.2.1. Subscript  $s$  denotes stagnant water,  $f$  denotes fracture filling material and  $m$  denotes rock matrix. The sorption properties of the fracture filling

material are assumed to be the same as for the rock matrix except that the porosity, the density and the effective diffusion coefficient follow the equations below.

$$\varepsilon_f = 10\varepsilon_m, \quad \frac{D_f}{D_m} = \frac{\varepsilon_f}{\varepsilon_m}, \quad \frac{\rho_f}{\rho_m} = \frac{1-\varepsilon_f}{1-\varepsilon_m}, \quad (27)$$

i.e. the porosity of the fracture filling material is assumed to be ten times higher than in the rock matrix. Both diffusivity and density are scaled accordingly.

Tracer tests STT-1 and STT-2 were performed in the radially converging flow field and applying passive tracer injection. It was decided reasonable to assume that major part of the tracers migrate through a single flow path. In addition, the evaluation of the tracer tests was based on the assumption, that the same flow channel dominates the transport both in STT-1 and STT-2 test.

The flow channel is modelled as a rectangular tube with constant aperture and constant width. The channel is surrounded by stagnant pools and fracture filling material (see Figure 3b-25). The amount of the fracture filling material is defined as the proportion of the surface area of the rock matrix ( $W \cdot L$ ) and the proportion of the surface area of the channel side walls ( $b \cdot L$ ) that are covered by the fracture filling material. These portions are presented in Equation (26) as porosities  $\varepsilon_s$  and  $\varepsilon_{fm}$ . The  $\varepsilon_s$  means the percentage of the stagnant areas on the channel side walls (area of the filling material is then  $1 - \varepsilon_s$ ) and  $\varepsilon_{fm}$  gives the percentage of the channel top and bottom walls that is not covered by the filling material.

Sorption and diffusion parameters applied in the calculations were based on the laboratory data from the Äspö Hard Rock Laboratory /Andersson et al., 1997/. Modelling parameters are collected in three different tables that are presented below. Table 3b-4 contains tracer dependent sorption and diffusion data. Table 3b-5 contains geometrical and tracer test dependent information and Table 3b-6 contains parameters that were not measured but more or less arbitrarily selected.

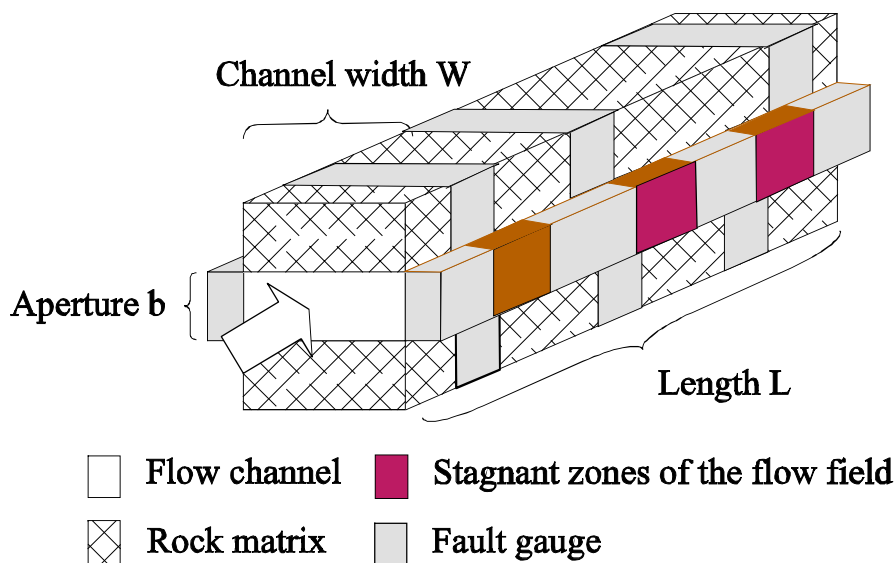


Figure 3b-25. Schematic illustration of the channel concept.

**Table 3b-4. Laboratory data on the sorption and diffusion properties of the tracers /Andersson et al., 1997/.**

	$D_e$ (m <sup>2</sup> /s)	$K_d$ (m <sup>3</sup> /kg)	$K_a$ (m)
Uranine	10 <sup>-13</sup>	0	0
Ba	4.2·10 <sup>-14</sup>	1.2·10 <sup>-3</sup>	2·10 <sup>-4</sup>
Rb	10 <sup>-13</sup>	1.4·10 <sup>-3</sup>	5·10 <sup>-4</sup>
Cs	10 <sup>-13</sup>	1.4·10 <sup>-2</sup>	8·10 <sup>-3</sup>

**Table 3b-5. General geometrical and tracer test dependent data /Andersson et al., 1998; 1999/.**

$D_w$ (m <sup>2</sup> /s)	L (m)	Q (ml/h) STT-1	Q (ml/h) STT-2
2·10 <sup>-9</sup>	4.68	40	28

**Table 3b-6. Composition of the flow channel. This data has not been measured but it has been selected for the model calculations.**

	$\rho$ (kg/m <sup>3</sup> )	$\epsilon$ (%)
Matrix	2300	0.5
Fracture filling	2196	0.50 · 5 = 2.5
Stagnant pools	–	50

Both the modelled and measured breakthrough curves were normalised during the fitting. This means that the curve fitting procedure does not care about the recoveries of the tracers, but it is only based on the shape of the curves. Table 3b-7 summarizes the results of the parameter  $U$  values that were determined for the different tracers. Fitted and measured breakthrough curves are presented in Figure 3b-26. The rather poor fit of the measured breakthrough at early times seems to become more significant when the sorption increases (cf. Cesium). It seems also that the breakthrough at early times for the non-sorbing (Uranine) tracer has been affected by the lack of the hydrodynamic dispersion in the model.

The unsatisfactory fit at the early breakthrough times cannot be improved without using different flow velocities. This seems to be the weakest point of this modelling approach and this need to be taken into account in the models applied in the future.

**Table 3b-7. Fitted parameter  $U$  values for the evaluated tracer tests.**

	U (-) STT-1	U (-) STT-2
Uranine	0.2	0.3
Ba	3.5	4.5
Rb	5	8
Cs	12	17



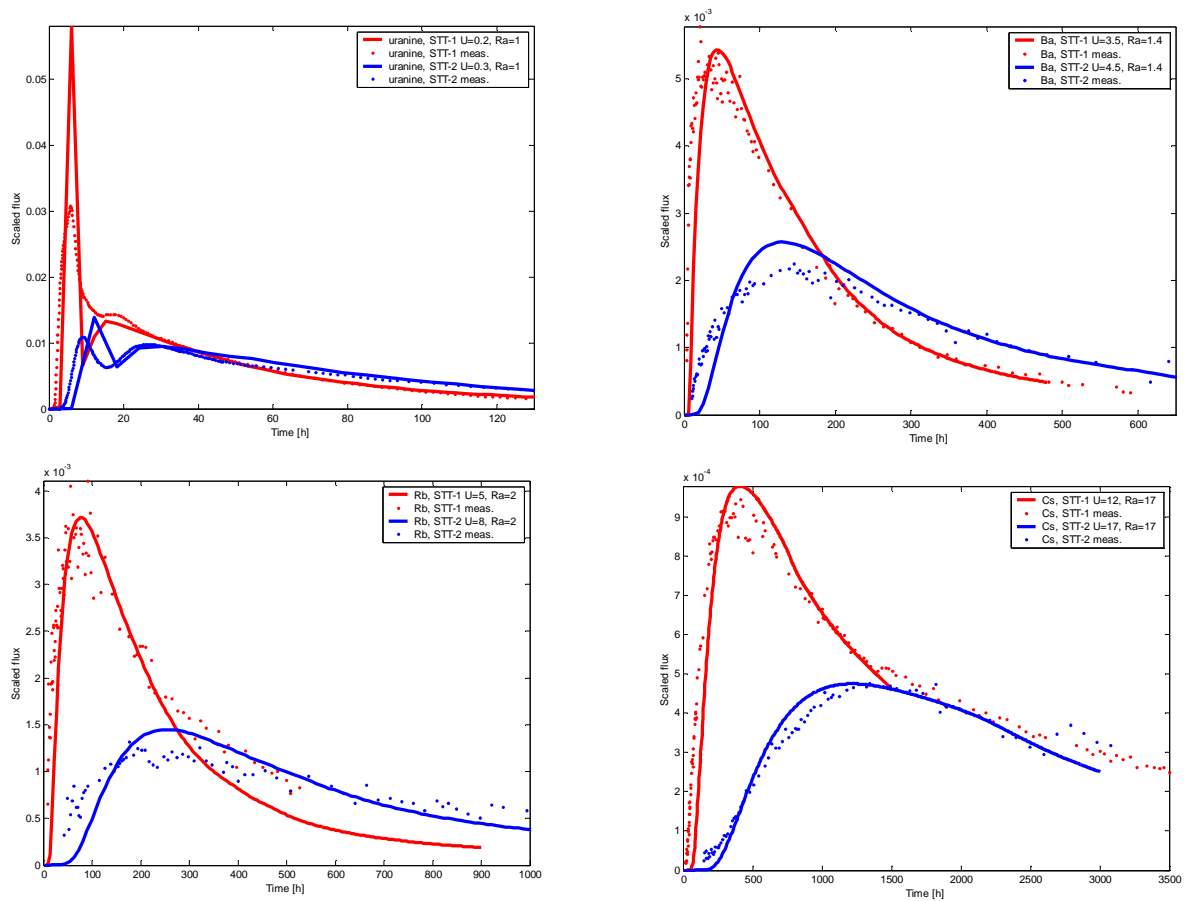


**Figure 3b-26.** Fitted breakthrough curves for tests STT-1 and STT-2.

The main part of the evaluation was to examine the set of the fitted  $U$ -parameter values against the flow channel concept. Parameter data in Tables 3b-4–3b-6 is applied in Equation (26) and the width and aperture of the flow channel were then varied. The results are presented in Figure 3b-27. The coloured lines represent the fitted  $U$ -parameter values for different tracers. The black lines represent the measured flow rate through the injection section. The points where these lines intersect give channel widths and apertures that agree both with the measured injection flow rate and the fitted parameter  $U$  value.

According to the results in Figure 3b-27 there exist two different cases that can best explain the measured breakthrough curves. The transport channel can be very wide with narrow aperture. The aperture should be in the range of  $2\text{--}10\cdot 10^{-5}$  m and the width of the channel is about 30–90 cm. In this case the retardation is caused by the diffusion to the rock matrix and filling material covering the matrix. The other channel geometry favours diffusion to the stagnant zones as retardation process. In this case, the transport channel has large aperture and narrow width. This geometry can also be interpreted as many parallel narrow channels that have stagnant water and fault gauge in between them. In this case, about 100 parallel channels that are about 0.2–1 mm wide and have also 0.2–1 mm aperture can explain the retardation. In the optimal case all different tracers support the same channel geometry. This would be reflected in Figure 3b-27 so that all the lines intersect at the same point. This seems not to be the case. The uncertainty in the case where the principal retardation mechanism is diffusion to the stagnant water seems to be larger than in the matrix diffusion case. However, the width of the transport channel for the matrix diffusion case sounds unrealistic large for the radially converging

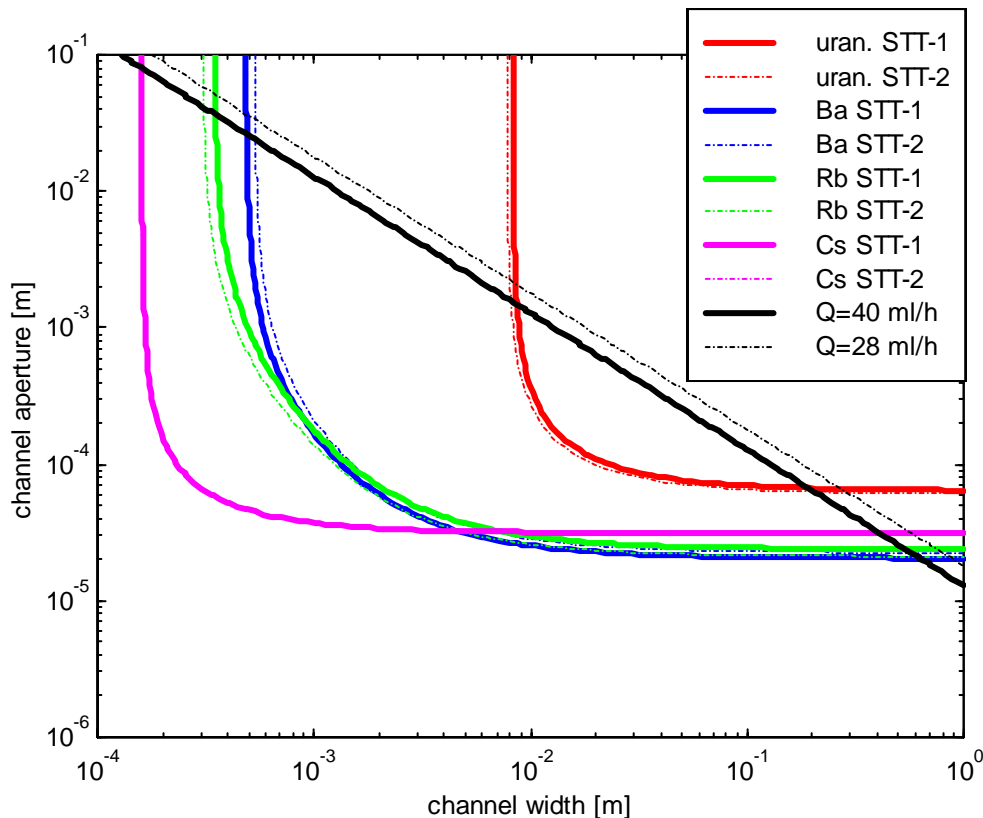


**Figure 3b-27.** Flow rate through the flow channel and parameter  $U$  values as a function of the channel width and aperture according to the Equation (26). Solid lines are for the STT-1 test and dashed for the STT-2 test. Black lines correspond to the measured flow rate through the injection sections in STT-1 and STT-2 tests. Coloured lines represent the fitted  $U$ -parameter values for different tracers: red for Uranine, blue for Barium, green for Rubidium and magenta for the Cesium.

flow field and passive tracer injection. It should be remembered that at the injection point the width of the tracer plume should be in the order of the width of the borehole, i.e. about 5–10 cm. In the matrix diffusion case the width of the flow channel should then somehow become 6–10 times larger between the injection and pumping points. In the stagnant water case the total width of the flow channels is in the order of 10–20 cm.

## Conclusions

Evaluation of the tracer tests indicate that large uncertainties may be connected to the interpretation of the diffusive mass transfer in the STT-1 and STT-2 tests. According to the evaluation equilibrium sorption alone can explain the retardation reasonably well. However, the retardation coefficients do not stay constant between STT-1 and STT-2 tests, indicating that there might exist some diffusive mass transfer also. Interpretation of the tests by assuming that the sorption is the principal retardation process and that in addition there exists diffusive process was not tested in this study, but it would offer an interesting alternative to explain the transport with reasonable parameter values. Matrix diffusion as the major retardation process fits also to the breakthrough curves, but in that case the parameter values should be extended to rather unrealistic range. Diffusion to the stagnant water or fracture filling material seems more realistic in this concept.

However, in this case the flow channel need to be filled by a large amount of fault gouge to produce the stagnant pools needed.

The behaviour of the Cesium has not been consistent. Retardation of the Cesium is not depending on the flow rate as the equilibrium sorption or matrix diffusion model is predicting. In addition to these there may exist other important process for Cesium, like sorption kinetics. The influence of the background flow field is also unknown. It is possible that due to the background flow field the STT-1 and STT-2 experiments do not test the same flow path. From the modelling point of view additional tracer tests performed with different pumping rates than applied in STT-1 and STT-2 (but testing the same flow path) are beneficial.

## References

**Andersson P, Byegård J, Cvetkovic V, Johansson H, Nordqvist R, Selroos J-O, Winberg A, 1997.** TRUE 1st Stage Test Programme. Experimental Plan for Tests with Sorbing Tracers at the TRUE-1 Site. Äspö Hard Rock Laboratory, SKB PR HRL-97-07, Swedish Nuclear Fuel and Waste Management Co.

**Andersson P, Johansson H, Nordqvist R, Skarnemark G, Skålberg M, Wass E, 1998.** TRUE 1st Stage Tracer Test Programme. Tracer Tests with Sorbing Tracers, STT-1, Experimental Description and Preliminary Evaluation. Äspö Hard Rock Laboratory, Technical Note TN-98-10t, Swedish Nuclear Fuel and Waste Management Co.

**Andersson P, Wass E, Byegård J, Johansson H, Skarnemark G, 1999.** TRUE 1st Stage Tracer Test Programme. Tracer Tests with Sorbing Tracers, STT-2, Experimental Description and Preliminary Evaluation. Äspö Hard Rock Laboratory, International Progress Report IPR-99-15, Swedish Nuclear Fuel and Waste Management Co.

**Neretnieks I, 1980.** Diffusion in the Rock Matrix: An Important Factor in Radionuclide Retardation? *Journal of Geophysical Research*, vol. 85, No. B8, pages 4379–4397. August 1980.

# Integration of laboratory sorption and diffusivity data in modelling of sorbing tracer tests STT-1 and STT-1b

*Henrik Widestrand, Johan Byegård, Mats Skålberg,  
Dept. of Nuclear Chemistry, Chalmers University of Technology, Göteborg,  
Sweden*

*Roy Haggerty,  
Dept. of Geosciences, Oregon State University, Corvallis, USA*

## Abstract

Tracer migration experiments at the 5 m scale have been performed in a single fracture at the Äspö Hard Rock Laboratory, Sweden. The tracers used in the well-to-well tests were non-sorbing HTO and sorbing  $^{22}\text{Na}^+$ ,  $^{58}\text{Co}^{2+}$ ,  $^{85}\text{Sr}^{2+}$ ,  $^{86}\text{Rb}^+$ ,  $^{133}\text{Ba}^{2+}$  and  $^{137}\text{Cs}^+$ . In support of the in situ experiments, sorption and diffusion properties of the tracers have been measured in parallel laboratory experiments. In this work, we use the laboratory sorption and diffusion data to model these tracers in 11 breakthrough curves (BTCs) from two different well pairs. BTCs were evaluated using a modified double porosity model assuming mass transfer into the rock matrix and mass transfer into stagnant zones of water. The majority of parameters in the model were obtained directly from laboratory and field measurements. A total of 4 transport parameters were estimated simultaneously from 4 of the BTC data sets. By doing this, it was possible to estimate a consistent set of transport parameters for all tracers, using laboratory-estimated sorption distribution coefficients. Forward simulations with no estimated parameters (for Ba, Cs and Co) were also carried out.

Sorption coefficients measured in the laboratory were sufficient, for most tracers, to adequately model field data. While improved fits were possible using sorption coefficients fitted to field data, a good agreement between laboratory-derived and fitted sorption coefficients was observed. Limited sorption reversibility was needed in the model to fit Cs and Co data. The tails of the breakthrough curves could not be modelled using diffusion into the wall rock only. Diffusion into stagnant zones of water within the fracture plane was used for modeling and also interpreted as the main cause for the observed tailing in the breakthrough curves. The flow path was interpreted as being channelled, with a channel width of a few centimetres.

## 1 Introduction

In Sweden and many other countries, deep geological repositories are planned for the disposal of high-level radioactive waste. des) over long periods of time. In the event of leakage, dissolved radionuclides will be transported by groundwater along fractures in the rock. However, transport is expected to be significantly retarded for a majority of radionuclides. The main retardation processes are sorption onto the fracture walls and diffusion into micropores within the rock matrix, which enables further sorption

on surfaces within the rock matrix /Neretnieks, 1980/. Many *in situ* experiments using non-sorbing tracers have been performed in fractured rock /e.g., Birgersson et al., 1992; D' Alessandro et al., 1997; Haggerty et al., 1998; Himmelsbach et al., 1998/. Among the much fewer experiments using sorbing tracers are e.g. the *in situ* migration studies at Studsvik, Sweden /Landström et al., 1982/, at Finnsjön, Sweden /Byegård et al., 1991/ and the extensive migration experiments at Grimsel, Switzerland /Hadermann and Heer, 1996; Heer and Hadermann, 1994/.

The Swedish Nuclear Fuel and Waste Management Co. (SKB) operates the Äspö Hard Rock Laboratory (Äspö HRL), near Oskarshamn in south-east Sweden, with the main tasks to develop site characterisation methods, demonstrate the technical feasibility of repository techniques and to perform research on the different barrier functions of a repository. In the First TRUE (Tracer Retention Understanding Experiments) Stage (TRUE-1) project /Winberg et al., 2000/, transport experiments were performed using sorbing and non-sorbing tracers within a single fracture at a depth of 400 m in Äspö HRL. A radially converging geometry and approximately 5 m travel distance was used in the experiments. In support of the *in situ* experiments, sorption and diffusion properties of the utilised tracers have been studied in parallel laboratory experiments using site-specific fracture material and generic Äspö materials /Widestrand et al., 2000/.

The focus of this paper is on the application and interpretation of laboratory sorption and diffusion data in modeling of two Sorbing Tracer Tests (STT-1 and STT-1b) at Äspö HRL. The tracers used are HTO (tritiated water, as a non-reactive tracer) and in increasing order of sorptivity:  $^{22}\text{Na}^+$ ,  $^{85}\text{Sr}^{2+}$ ,  $^{133}\text{Ba}^{2+}$ ,  $^{86}\text{Rb}^+$ ,  $^{58}\text{Co(II)}$  and  $^{137}\text{Cs}^+$ . First, a short description of the laboratory and field experiments and an outline of the model used is presented. In the next part the model is applied to analyse the *in situ* experiments, using a parameter estimation method that utilizes multiple data sets simultaneously. Finally, a comparison between laboratory and *in situ* sorption data is made.

## 2 Experimental

### **Overview of field site**

Only a brief summary of the characteristics of the field site is given here. A more detailed description of the structure and hydraulics of the site is given by Winberg et al. /1996; 2000/. Specific test details and parts of the results are presented by Widestrand et al. /2000/ and by Winberg et al. /2000/.

The fracture used for *in situ* tracer experiments, the so called “Feature A”, is located 400 m below sea level at Äspö HRL and comprise a reactivated mylonite lying within Äspö diorite. The mylonite has undergone secondary brittle deformation along one, or alternatively, two sub-parallel fault planes /Winberg et al., 2000/. Mineralogically the mylonite is characterised by very fine-grained epidote, quartz, K-feldspar and albite. Biotite is replaced with chlorite and epidote in most samples collected /Byegård et al., 1998/. The bedrock at the experimental level is mainly Äspö diorite, which is a medium-grained porphyritic quartz-monzodiorite with K-feldspar megacrysts. A conceptual representation of Feature A is shown in Figure 3b-28.

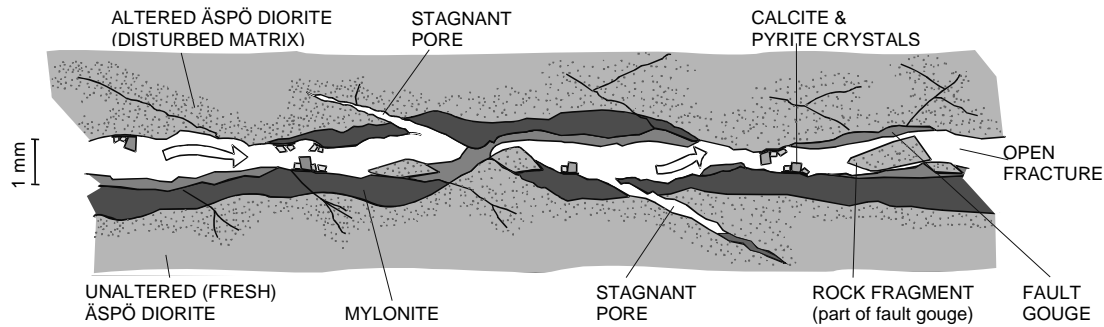


**Figure 3b-28.** Conceptual visualisation of Feature A. Fracture aperture is approximately in the mm-scale, the thickness and sizes of the other constituents are not shown in scale /Winberg et al., 2000/.

SEM/EDS (Scanning Electron Microscopy with Energy Dispersive (X-ray) Spectroscopy) microprobe analysis show that the fracture planes are coated with calcite, chlorite and to some extent clay minerals. Fault gouge may be present in Feature A. However, no gouge material has been collected.

The flow aperture is approximately 1.5 mm /Winberg et al., 2000/ and it was evaluated from hydraulic pumping tests using the mass balance method /Gustafsson and Klockars, 1981/. The width of Feature A (including mylonite and altered rim zone) varies between 0.05 and 0.09 m.

The groundwater in Feature A is saline and is dominated by sodium (1740 mg/L), calcium (1310 mg/L) and chloride (5400 mg/L) /Nilsson, 1997/.

Five boreholes with lengths from 20 to 60 m were drilled from the main tunnel into the rock volume used for the TRUE-1 experiment, which contains several conductive and connected fractures, including Feature A. The boreholes were packed off where they intersect Feature A, allowing water to be injected to and extracted from Feature A at those locations. A radially converging flow field was created by pumping water from one borehole. The pumping flow rate was 0.4 L/min.

Injection was done by circulating a tracer solution in a borehole section and allowing the tracers to be transported within the flow field caused by pumping in an adjacent borehole. The injection procedure was aimed to obtain a square injection concentration function. After 4 hours, the injection was terminated by replacing the groundwater containing the tracers with pure groundwater. Two different injection boreholes were used in the tests. The sorbing tracer test labelled STT-1 had a distance of 4.6 m, while the test labelled STT-1b had a distance of 5.1 m between the borehole sections used in respective experiments.

The injection solutions consisted of synthetic groundwater and the radioactive tracers, which were then mixed with natural groundwater in the injection system. By using a synthetic groundwater and radioactive tracers of sufficiently high specific activity for the injection solution, chemical concentrations very similar to the natural groundwater composition could be obtained, minimizing non-linear sorption effects. A speciation calculation of the groundwater using PHREEQE /Parkhurst et al., 1980/ and the database Hatches 5.0 /Bond et al., 1992/ showed that all tracers exist in non-complexed ionic forms, with the exception of Co. According to the calculation, the Co species

may be dominated of  $\text{Co}^{2+}$ , whereas  $\text{CoSO}_4$  and  $\text{CoCl}^+$  co-exist to a relatively large degree. The notation Co hereafter refers to the total concentration of all Co species.

### Tracer injection data

The concentrations of the tracers were measured using  $\gamma$ -spectrometry (HPGe-detectors, EG&G, ORTEC). On-line measurements of the injection loop and laboratory measurements of collected samples were performed. The pure  $\beta$ -emitter tritium in HTO was measured by liquid scintillation counting (Wallac 1414 Guardian, EG&G), /Widestrand et al., 2000/.

The injection concentrations for STT-1 and STT-1b are plotted in Figure 3b-29. The second peak in the injection concentrations (see STT-1 at 9 h and STT-1b at 6 h) was caused by poor mixing in the packed off section in the injection borehole. To improve the injection, a second flush with groundwater was performed in STT-1b, which caused the third concentration peak, see Figure 3b-29 (right).

Sorption of Cs, Co and to some extent Rb and Ba was observed during the 4 h injection period (see Figure 3b-29). A time-delay in the HTO sampling equipment caused the deviation observed in early-time HTO data.

The mass recoveries of the different tracers are given in Table 3b-8, obtained by taking the difference between the integrated injection and breakthrough curves. It should be noted that the Rb, Ba, Cs and Co lack some mass in the integrated breakthrough data.

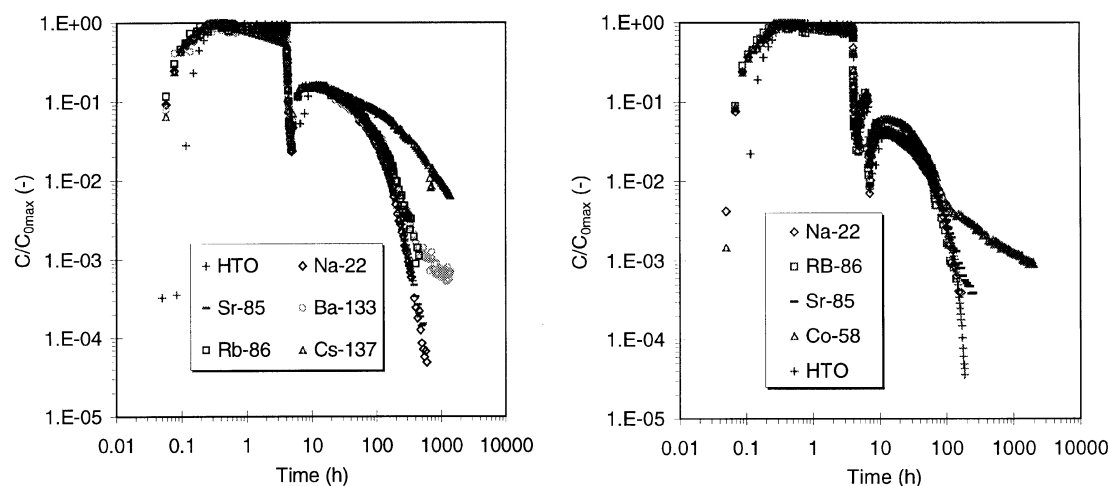


**Figure 3b-29.** Injection concentrations for STT-1 (left) and STT-1b (right). All concentrations are normalized to  $C_{0max}$ , which is the maximum concentration of a specific radionuclide in the injection loop, measured after about 0.3 h.

**Table 3b-8. Approximate tracer mass recoveries based on integration of concentration curves /Widestrand et al., 2000/. The integration time is given within parenthesis.**

Tracer	STT-1	STT-1b
HTO	96% (360 h)	94% (333 h)
<sup>22</sup> Na <sup>+</sup>	97% (1242 h)	96% (1292 h)
<sup>85</sup> Sr <sup>2+</sup>	98% (960 h)	82% (505 h)
<sup>86</sup> Rb <sup>+</sup>	64% (527 h)	79% (553 h)
<sup>133</sup> Ba <sup>2+</sup>	87% (1350 h)	not used
<sup>137</sup> Cs <sup>+</sup>	33% (7005 h)	not used
<sup>58</sup> Co	not used	29% (3622 h)

The time that breakthrough could be followed was limited due to concentrations near the detection limits, relatively short half-lives for some radionuclides and by the experimental time available. The mass recoveries for these elements are thus the lower limits obtained in these experiments.

### **Supporting laboratory data**

Laboratory experiments with host rock (Äspö diorite) and site-specific Feature A material were performed using a synthetic groundwater in inert atmosphere to measure parameters to be used for modeling of the tracer tests. Matrix sorption coefficients,  $K_d$ , surface sorption coefficients,  $K_a$ , effective diffusivity,  $D_e$ , and matrix porosity,  $\phi_{m,tot}$ , were the primary parameters determined. More specific test details of the laboratory experiments can be found in Johansson et al. /1997; 1998/ and in Byegård et al. /1998/.

Interpretation of the laboratory data to obtain data representative for the *in situ* conditions is not a straightforward task, primarily due to material disturbances caused by e.g. stress release, crushing and lack of representative fracture coating material. For example, there are indications of gouge (infilling) material in Feature A, but it has not been possible to obtain any such material from the studied feature for laboratory studies.

### **Matrix sorption coefficients**

Matrix sorption coefficients were determined for the host rock and for some altered wall rock and mylonite samples from Feature A, by applying both the batch sorption and the through-diffusion technique. In the batch experiments, crushed rock particles were contacted with synthetic groundwater and the distribution of the radioactive tracers between the solid and the aqueous phase was measured by monitoring the concentration decrease in the aqueous phase as a function of time.

Table 3b-9 shows the  $K_d$  values for each tracer, evaluated both from batch experiments and through-diffusion experiments. A number of factors contribute to the variability in  $K_d$ . For example, a varying amount of biotite, which has a high cation exchange capacity, causes variability in the measured  $K_d$  values in the mylonite and



altered diorite. The  $K_d$  values evaluated from through-diffusion experiments were generally lower compared to the batch experiments.

Earlier studies of  $K_d$  using batch techniques have shown a strong increase in  $K_d$  with decreasing particle size for granitic rock /Byegård et al., 1995/. In this work, the  $K_d$  values evaluated from diffusion experiments using the host rock gave the lowest  $K_d$  values, even though the host rock was found to be the most sorptive rock type in the batch experiments. Considering the increased disturbances in crushed rock, compared to the rock discs used in the through-diffusion experiments,  $K_d$  values obtained from diffusion experiments, or alternatively large particle size fractions, were considered to be the most representative for the *in situ* rock matrix, at least for time scales employed in the TRUE-1 experiments. The  $K_d$  values for the weakly sorbing Na and Sr determined using 2–4 mm size fractions were approximately five times higher than  $K_d$  values evaluated from through-diffusion experiments /Johansson et al., 1997/. This factor of five was later used for extrapolation of  $K_d$  values from batch experiments, with 2–4 mm particles, for other tracers that could not be studied by the through-diffusion technique.

Through-diffusion data has not been obtained for Rb, due to the short half-life and the relatively strong sorption. Furthermore, due to the strong sorption of Ba and Cs, the through-diffusion data obtained for these tracers were either very uncertain or in some cases not observed at all. In an earlier work /Andersson et al., 1997/ the described factor of five was applied for extrapolation of  $K_d$  values for Rb, Ba and Cs from batch experiments. By doing so,  $K_d$  values of  $4 \cdot 10^{-4}$  (Rb),  $2 \cdot 10^{-4}$  (Ba) and  $6 \cdot 10^{-3}$  (Cs) ( $\text{m}^3/\text{kg}$ ) were obtained. In a later work, /Johansson et al., 1998/ concentration profiles in through-diffusion rock specimens were analysed for Ba and Cs. By this technique  $K_d$  values of  $2 \cdot 10^{-4}$  ( $\text{m}^3/\text{kg}$ ) for Ba and  $8 \cdot 10^{-4}$  ( $\text{m}^3/\text{kg}$ ) for Cs were possible to obtain. In the process of selecting  $K_d$  values for this work, it was decided to use the  $K_d$  values that were evaluated from the concentration profiles for Cs and Ba. The  $K_d$  value for Rb was obtained by extrapolation of batch results and  $K_d$  values evaluated from through-diffusion experiments were used for Sr and Na. The selected  $K_d$  values in this work are presented with bold numbers in Table 3b-9.

Among the tracers, the most significant increase in sorption as a function of time in the batch experiments was observed for Cs /Byegård et al, 1998/, which is in agreement with the results of other authors /e.g. Comans et al., 1991/. However, since the selected  $K_d$  value for Cs is based on evaluation of the penetration profile from the diffusion experiment, which lasted for 16 months, it was not necessary to consider any time dependency in selecting a  $K_d$  value for Cs. The use of single  $K_d$  values for modeling purposes is, however, not obvious if it is shown that the sorption/desorption reaction is kinetically hindered, which is further discussed below.

**Table 3b-9. Laboratory sorption data. Figures in bold were later used for modeling.**

	Matrix sorption			Surface Sorption	Reversibility
Data description	Feature A crushed material  1–2 mm size, 9 days contact time.  Min. and max. values obtained from 2 mylonites, 2 altered diorites and 1 altered fine-grained granite <sup>1)</sup> .	Host rock crushed material  1–2 mm size, 9 days contact time. Åspö diorite <sup>1)</sup> .	Host rock Diffusion experiment  Na, Sr from through-diffusion <sup>2)</sup> .  Ba, Cs from penetration profiles <sup>3)</sup> .  Rb <sup>5)</sup> estimated from batch $K_d/5$ . Co assumed equal to Cs <sup>4)</sup> . These $K_d$ data were used for modeling.	Host rock crushed material  2–4 mm size, 1 day contact time, Åspö diorite <sup>1)</sup> .  $K_a = K_d/A_{geom}$	Feature A crushed material  1–2 mm size, 9 days contact time, 7 days desorption. Estimated slow or irreversible sorbed fraction of total sorbed amount <sup>1)</sup> . Min. and max. values for 2 mylonites, 2 altered diorites and 1 altered fine-grained granite. Average values are given within paren thesis.
Tracer	$K_d$ (m <sup>3</sup> /kg) min-max	$K_d$ (m <sup>3</sup> /kg)	$K_d$ (m <sup>3</sup> /kg)	$K_a$ (m)	Irreversibly-sorbed fraction (%)
<sup>22</sup> Na <sup>+</sup>	<3·10 <sup>-4</sup>	<3·10 <sup>-5</sup>	<b>1.4·10<sup>-6</sup></b>	<b>5·10<sup>-6</sup></b>	< 10
<sup>85</sup> Sr <sup>2+</sup>	<4·10 <sup>-4</sup>	<2·10 <sup>-4</sup>	<b>4.7·10<sup>-6</sup></b>	<b>2·10<sup>-5</sup></b>	< 10
<sup>86</sup> Rb <sup>+</sup>	5·10 <sup>-4</sup> - 2·10 <sup>-3</sup>	1.4·10 <sup>-3</sup>	<b>4·10<sup>-4</sup></b>	<b>1·10<sup>-3</sup></b>	8-59 (31)
<sup>133</sup> Ba <sup>2+</sup>	4·10 <sup>-4</sup> - 2·10 <sup>-3</sup>	1.2·10 <sup>-3</sup>	<b>2·10<sup>-4</sup></b>	<b>6·10<sup>-4</sup></b>	20-48 (35)
<sup>137</sup> Cs <sup>+</sup>	1·10 <sup>-3</sup> - 1·10 <sup>-2</sup>	1.4·10 <sup>-2</sup>	<b>8·10<sup>-4</sup></b>	<b>8·10<sup>-3</sup></b>	45-67 (56)
<sup>58</sup> Co	not measured	not measured	<b>8·10<sup>-4</sup></b>	<b>8·10<sup>-3</sup></b>	not measured

<sup>1)</sup>/Widstrand et al., 2000/, <sup>2)</sup>/Johansson et al., 1997/, <sup>3)</sup>/Johansson et al., 1998/, <sup>4)</sup>/Carbol and Engkvist, 1997; Suksi et al., 1987/, <sup>5)</sup>/Byegård et al., 1998/.

### **Surface sorption coefficients**

Surface distribution coefficients,  $K_a$ , were estimated from batch  $K_d$  of host rock obtained after 1 day of contact time assuming spherical geometric surface areas and sorption only onto outer surfaces. For the more sorbing Rb and Cs, sorption onto the surface of the rock discs used in the through-diffusion experiments was also evaluated as surface distribution coefficients,  $K_a$ , after 5 to 10 days of contact time. In this case the geometrical cross-sectional area of the rock surface exposed to the tracer solution was assigned as the area for sorption.

Both methods mentioned above for estimation of  $K_a$  are very rough approximations, assuming that no matrix diffusion occurred during the contact time with tracer solution. Sorption of Na, Sr and Ba was not strong enough to be detected on the rock surfaces in the diffusion experiments. The  $K_d$  values for these tracers were thus evaluated from the batch experiments with larger surface area available for sorption.

It should be noted that the surface distribution coefficient,  $K_d$ , for the natural fracture surface of the Feature A diffusion cell and other diffusion cells of host rock agreed within a factor of 2 with the surface sorption evaluated from the batch experiments for Rb and Cs.

### **Desorption studies**

Sorption reversibility was studied by replacing the groundwater containing the tracers in the batch experiments after a certain contact time, with groundwater without tracer and subsequent measurements of the desorbed tracer.

Na and Sr were almost totally reversibly sorbed, while Ba, Rb and in particular Cs showed a very slow desorption reaction that may be interpreted as irreversible sorption on Äspö materials, in the time perspective of relevance for the in-situ experiment, as shown in Table 3b-9. Limited reversibility of Rb, Ba and Cs has also been observed by others /e.g. Landström and Tullborg, 1995; Vandergraaf et al., 1997/. Co is believed to sorb with an inner-sphere surface complexation mechanism /Jakobsson and Albinsson, 1998; Cui and Eriksen, 1997/. In sorption/desorption experiments by Cui and Eriksen /1997/ on Stripa granite fracture filling material, the Co sorption was found to be more reversible than the Cs sorption. Thus, less influence of irreversible sorption of Co is expected even in this study.

For modelling purposes, the limited reversibility was neglected for Ba and Rb since the recovery was relatively high. It should be noted that the recoveries of Rb given in Table 3b-8 are associated with large uncertainties since the dynamic range in the measurements of the breakthrough curve is low (see Figure 3b-30). According to the laboratory experiments, Rb and Ba show limited reversibility. Irreversible losses may be time dependent and there is a time difference between the residence time of Cs and Rb/Ba in the field tests, while the time scale for sorption/desorption was the same for the three tracers in the laboratory experiments. This may explain the relatively low losses of Rb and Ba observed in the field test. For Cs, the average value of the reversibly sorbed fraction from the laboratory data was used in the modeling (Table 3b-9). Since no information about the reversibility of Co was available from the laboratory experiments, fully reversible sorption was used in the model test /Cui and Eriksen, 1997/.

### **Porosity**

Porosities were obtained from water saturation measurements, through-diffusion measurements of HTO and from impregnation with  $^{14}\text{C}$ -labelled methylmethacrylate (the  $^{14}\text{C}$ -PMMA method, /Hellmuth et al., 1994/.

The porosity of the host rock was approximately 0.4% obtained from through-diffusion experiments and the  $^{14}\text{C}$ -PMMA method /Johansson et al., 1998/. For fracture wall rock composed of altered diorite, a somewhat higher porosity (~1%) than for host rock is expected /Eliasson, 1993/. However, the porosity in altered and partly mylonitised material was found to be only 0.15%, due to the very dense and fine-grained mylonite /Byegård et al., 1998/. A few other samples of fracture wall rock from intersecting drill cores at the Feature A site have shown a porosity variation between 0.1 and 1.1% /Byegård et al., 2000/. Considering the variation in porosity of

different wall rock materials, a total matrix porosity of 0.4% was adopted in the modeling.

The transport porosity,  $\phi_m$  (conducting part of the porosity), is a poorly known parameter. The ratio of transport to total porosity in different granites was estimated by Bradbury and Green /1985/ to be 0.05 to 0.4 and by Valkiainen et al. /1992/ to be 0.6. In this work a transport porosity of half the total porosity, 0.2%, was used in the modeling.

Measurements of porosities in 2–5 cm fragments obtained from other fractures at Äspö varies between 0.3% (mylonites) to 1.5 % (altered diorite) /Tullborg, 1999/. The porosity of possible gouge material in Feature A is not known, therefore it was included in the estimated parameters in the model.

### **Diffusivity**

The effective diffusivity was measured using through-diffusion experiments, in which a rock disc separates two water containers. Tracers are added to one container and allowed to diffuse to the other container through the rock disc. By monitoring the concentration increase on the low concentration side, the effective diffusivity,  $D_e$ , and matrix porosity,  $\epsilon$ , can be evaluated for non-reactive tracers. The sorption coefficient,  $K_d$ , can be evaluated for a sorbing tracer if a non-reactive tracer is used simultaneously according to, e.g., Skagius and Neretnieks /1986/.

Studies of through-diffusion in Äspö diorite indicated that the effective diffusivity decreased with increasing sample length between 1 and 4 cm, and that effective diffusivity was positively correlated to the porosity /Johansson et al., 1997/. It was also found that the formation factor,  $F$  ( $F = D_e/D_w$ ), agreed within a factor of 2 between sorbing tracers and HTO. The mean value of the effective diffusivity obtained in 1 and 2 cm samples of Äspö diorite was  $1.2 \pm 0.3 \times 10^{-13} \text{ m}^2/\text{s}$ .

Through-diffusion in a ~18-mm-thick sample of altered and partly-mylonitised diorite (taken from the intersection of a borehole with Feature A) was also studied /Widestrand et al., 2000/. Both sides of the nearly parallel surfaces had been in contact with groundwater. The effective diffusivity of HTO,  $4 \times 10^{-14} \text{ m}^2/\text{s}$ , was approximately a factor 3 lower than obtained for the Äspö diorite. This can be explained by the very dense and fine-grained mylonite bands found perpendicular to the direction of diffusion in the sample. Thus, for the mylonitic sections of the feature wall rock, this lower diffusivity is a reasonable estimate.

Regarding modeling of the experiments in Feature A, a somewhat higher porosity (see 2.3.4) is expected for the unknown area of exposed wall rock composed of altered diorite, which would enhance the effective diffusivity /Eliasson, 1993/. A complicating factor in choosing a representative diffusivity is that diffusivities have been observed to decrease with increasing sample length /Johansson et al., 1997; Skagius, 1986; Valkiainen, 1992/. For the short time that the rock surfaces were exposed to tracers in the experiments, short penetration depths were expected. To compensate for enhancing effects due to altered material and short penetration depths, an effective matrix diffusivity for HTO of  $1 \times 10^{-13} \text{ m}^2/\text{s}$  was adopted as an estimate to be used in the modeling. Thus, a formation factor,  $F$ , of  $4.5 \times 10^{-5}$  was obtained. Using this value of the formation factor, effective diffusivities for the sorbing tracers were calculated using the aqueous diffusivities ( $D_w$ ) obtained from Mills and Lobo /1989/. The

aqueous diffusivity of less charged Co complexes (e.g.,  $\text{CoCl}^+$ ,  $\text{CoSO}_4$ ) will be enhanced compared to the diffusivity of  $\text{Co}^{2+}$ , since diffusivity increases with decreasing ionic potential /Li and Gregory, 1974/. However, the diffusivity and exact amount of Co complexes is not known, therefore the Co diffusivity was included as an estimated parameter in the modeling.

Finegrained fault? gouge material may have a higher porosity and thus a higher effective diffusivity than the host rock. Due to the absence of material for laboratory measurements, mass transfer in gouge material was included as estimated parameters in the model.

### 3 Conceptual and Mathematical Model

#### **Conceptual model**

The rock fracture is conceptualised as being composed of a mobile zone (where advection occurs) and two types of immobile zones. The immobile zones are (1) the rock matrix and (2) stagnant zones within the fracture plane, which include immobile water in the fracture and within the gouge. Since diffusion into immobile water and gouge are modeled with a single set of parameters, a distinction between the two can only be made from an interpretation of the modeling results. Sorption (assumed to be linear, i.e., that sorbed concentration is linearly dependent on aqueous concentration) occurs on the fracture surfaces and within the matrix and gouge.

#### **Mathematical model**

The mass balance equation for the fracture is

$$\frac{\partial c_f}{\partial t} = \frac{\alpha_L v_x}{R_a} \frac{\partial^2 c_f}{\partial x^2} - \frac{v_x}{R_a} \frac{\partial c_f}{\partial x} - \frac{1}{b_f R_a} J_m \Big|_{z=0} - \Gamma_s(t) \quad (1)$$

where  $c_f$  [ $\text{ML}^{-3}$ ] is the aqueous concentration in the fracture;  $\Gamma_s(t)$  [ $\text{ML}^{-3}\text{T}^{-1}$ ] is a time-varying source-sink of mass due to diffusion and sorption within stagnant zones along the fracture;  $R_a$  [1] is the surface retardation factor in the fracture;  $\alpha_L$  [L] is the longitudinal dispersivity;  $b_f$  [L] is the fracture half-aperture;  $v_x$  [ $\text{LT}^{-1}$ ] is the velocity of water in the fracture; and  $J_m|_{z=0}$  [ $\text{MT}^{-1}\text{L}^{-2}$ ] is the mass flux across the fracture/matrix interface.

The model assumes a constant velocity toward the pumping well along a single flow path. One alternative to constant velocity would be radial flow. Due to channeling effects, however, it is not clear that this assumption would be superior to constant velocity. Another alternative would be to assume some arbitrary number of flow paths. However, the velocity along these flow paths would have to be estimated, and therefore would add parameters to our model that may not be defensible. Therefore, we have remained with the simplest assumption of constant velocity along a single pathway. In addition, these are reasonable assumptions for this study because (1) we are primarily interested in the mass transfer behaviour of the tracers and not dispersion, meaning that the peak arrival time and late-time behaviour of the breakthrough

curve (BTC) is most important, and not the spread about the peak arrival time; and (2) since no overpressure was added to the injection section the solute is expected to follow a single flow path to the pumping well.

The upstream and downstream boundary conditions for the transport equation are

$$c_f - \alpha_L \frac{\partial c_f}{\partial x} = c_{inj}(t) \quad \text{at } x = 0 \quad (2a)$$

$$\frac{\partial c_f}{\partial x} = 0 \quad \text{at } x = L \quad (2b)$$

where  $c_{inj}(t)$  [ $\text{ML}^{-3}$ ] is the input concentration and  $L$  [L] is the user-defined system length. The initial condition for the system is zero concentration everywhere.

The flux across the fracture/matrix interface is

$$J_m|_{z=0} = -\phi_m D_{p,m} \frac{\partial c_m}{\partial z}|_{z=0} \quad (3)$$

where  $c_m$  [ $\text{ML}^{-3}$ ] is the concentration in the rock matrix;  $\phi_m$  [1] is the transport porosity of the rock matrix; and  $D_{p,m}$  [ $\text{L}^2\text{T}^{-1}$ ] is the pore diffusivity of the matrix. The derivative in eqn. (3) is obtained by solving the diffusion equation for the rock matrix:

$$\frac{\partial c_m}{\partial t} = \frac{D_{p,m}}{R_m} \frac{\partial^2 c_m}{\partial z^2} \quad (4)$$

with the boundary conditions  $c_m = c_f$  at  $z = 0$  and  $c_m(z \rightarrow \infty) = 0$ .  $R_m$  [1] is the retardation factor of all internal surfaces and  $z$  [L] is the coordinate into the matrix perpendicular to the fracture plane.

Single-rate mass transfer is modeled by substituting the following into eqn. (1):

$$\Gamma_s(t) = \frac{\beta_{tot}}{b_s} \int_0^{b_s} \frac{\partial c_s}{\partial t} dz_s \quad (5)$$

where  $c_s$  [ $\text{ML}^{-3}$ ] is the concentration in stagnant zones and gouge material and  $b_s$  [L] is the effective thickness of the stagnant zones and gouge. The parameter  $\beta_{tot}$  [1] is the capacity coefficient, defined here as the ratio of mass in stagnant zones (i.e., not including the matrix) to mass in the fracture when equilibrium conditions are obtained:

$$\beta_{tot} = \frac{R_m}{R_a} \beta_n; \quad \beta_n = \frac{b_s \phi_s}{b_f} \quad (6)$$

where  $\beta_n$  [1] is the capacity coefficient for a non-sorbing tracer; and  $\phi_s$  [1] is the porosity of the stagnant zone and gouge material. In the case where the stagnant zones are within the fracture plane, the value of  $b_f$  is replaced in (6) by the half-width of the

flow path ( $b_w$ ),  $b_s$  is interpreted as the thickness of the stagnant zone on each side of the flow path, and  $\phi_s$  is the fraction of the flow path that is adjacent to a stagnant zone. The time derivative in Equation (5) is calculated using the diffusion equation for the stagnant zone:

$$\frac{\partial c_s}{\partial t} = \frac{D_{p,s}}{R_m} \frac{\partial^2 c_s}{\partial z_s^2} \quad (7)$$

with the boundary conditions  $c_s = c_f$  at  $z_s = 0$  and  $\partial c_s / \partial z_s = 0$  at  $z_s = b_s$ . The variable  $D_{p,s}$  [ $L^2T^{-1}$ ] is the pore diffusivity in the stagnant zone.

The retardation factors for sorption on internal surfaces,  $R_m$ , and fracture surface sorption,  $R_a$ , are defined as

$$R_m = 1 + \frac{K_d \rho}{\phi_{m,tot}} \quad (8)$$

$$R_a = 1 + \frac{K_a}{b_f} \quad (9)$$

where  $\rho$  [ $ML^{-3}$ ] is the bulk density;  $\phi_{m,tot}$  [1] is the total porosity of the rock matrix;  $K_d$  [ $L^3M^{-1}$ ] is the sorption distribution coefficient for all internal surfaces; and  $K_a$  [ $L^{-1}$ ] is the surface sorption coefficient for fracture surfaces. Sorption is assumed to be linear and reversible. Note that the same  $K_d$  value is applied both to rock matrix and gouge material, hence the retardation factor  $R_m$  is used for both matrix and gouge.

Due to the converging flow field, concentrations are diluted at the pumping well by a dilution factor,  $f_{dil}$  [1]. This factor is the ratio of the pumping rate  $Q_p$  [ $L^3T^{-1}$ ] to the injection rate  $Q_{inj}$  [ $L^3T^{-1}$ ]:

$$f_{dil} = \frac{Q_p}{Q_{inj}} \quad (10)$$

Very slow desorption reactions, that can be interpreted as irreversible sorption, were included in the model as an increased dilution factor,  $F_{dil}$ , defined as

$$F_{dil} = \frac{f_{dil}}{S_{rev}} \quad (11)$$

where  $S_{rev}$  is the reversibly sorbed fraction.

A modified version of STAMMT-L /Haggerty, 1998/ was used for solution of these equations. STAMMT-L is a FORTRAN 77 code that solves the advective-dispersive and mass transfer equations within a linear coordinate system, and is capable of handling any number of diffusion and linear sorption (equilibrium or nonequilibrium) processes.

### **Parameter determination and estimation**

The majority of parameters in the mathematical model were obtained directly from laboratory and field measurements (i.e., for 4 tracers, 22 parameters are required: of these, 18 were obtained from the lab and field). A set of only 4 transport parameters were estimated simultaneously from the entire suite of BTCs:  $\beta_n$ ,  $\mu = \ln(D_{p,s}/b_s^2)$ ,  $\alpha_L$  and  $v_x$ . Later, for comparison, we show results where sorption coefficients were also estimated.

Parameter estimation was performed using the modified Levenberg-Marquardt algorithm /Marquardt, 1963/ and a finite-difference Jacobian to solve the non-linear least-squares optimization problem, where the residual errors in simulated BTC concentration are minimized. The logarithms of the parameters were estimated, and the sensitivities of the model output were used to obtain an estimate of the parameter covariance using conventional techniques /Bard, 1974; Donaldson and Tryon, 1990/.

To compare the model error with the experimental data, we used the root mean squared error (RMSE) of the logarithms of concentration:

$$\text{RMSE} = \left[ \frac{\sum_{j=1}^{N_d} \left( \ln \frac{C_{s,j}}{C_{d,j}} \right)^2}{N_d - N_p} \right]^{1/2} \quad (12)$$

where  $C_{s,j}$  is the  $j$ :th simulated concentration,  $C_{d,j}$  is the  $j$ :th data value of concentration,  $N_d$  is the number of data points for all tracers and  $N_p$  is the number of parameters estimated.

## **4 Analysis of experimental BTCs**

In all cases, the evaluation procedure began with a calibration of the transport parameters, estimated simultaneously from the HTO, Na, Sr and Rb BTC data. In our first model, the parameters were fixed from field and laboratory data. Using this parameter suite, we ran forward simulation for three tracers with different sorption characteristics: Ba (STT-1) and Cs (STT-1) and Co (STT-1b). For comparison, a second model was developed where the sorption parameters for all tracers were estimated from the BTCs.

### **Model with minimum number of estimated parameters**

In our first model we estimated 4 transport parameters from the HTO, Na, Sr and Rb BTCs, while fixing the other 18 required parameters from independent laboratory and field measurements. Table 3b-10 shows the resulting parameter suite. Ba (STT-1 only) was excluded from the calibration to be used later for a test of the model. Effects of irreversible sorption were neglected for Rb and Ba, since relatively high recoveries were obtained for those tracers.



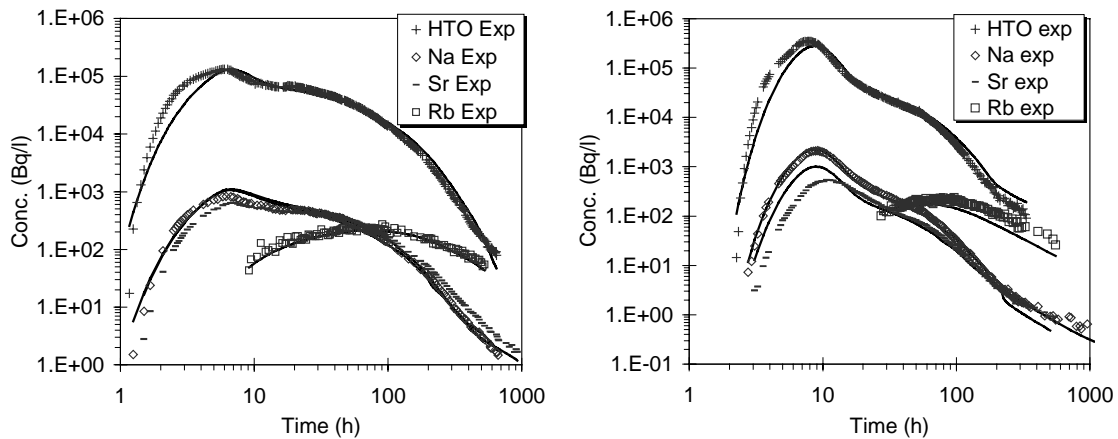


**Figure 3b-30.** Plot of single rate model (lines) and breakthrough data for STT-1 (left) and STT-1b (right) estimating  $\beta_n$ ,  $\mu$ ,  $\alpha_L$  and  $v_x$ . In the left plot the model curves for Na and Sr overlaps, showing only one curve for most of the time interval plotted.

Figure 3b-30 compares the single rate model to the experimental BTCs. The model BTCs reproduce the full range and shape of the curves reasonably well. In particular, peak times and late-time behavior (dominated by mass transfer effects) are well-represented, even though several parameters were measured in the laboratory. STT-1 data show a deviation at early times, with a narrower modelled peak than exhibited in the experimental data. Most likely, this is due to transport in two flow paths, which was indicated by the small second peak and later experiments with lower water velocity in the same geometry that gave two distinct peaks in the BTCs /Widstrand et al., 2000/ which causes a broadening of the whole BTC. Double pathways may also be indicated by the larger dispersion (see Table 3b-10) obtained for STT-1 compared with STT-1b. Some of the divergence around the peaks may be ascribed to the assumption of constant velocity towards the well in the model, whereas the velocity in reality certainly increases toward the well.

A multirate model e.g., /Haggerty and Gorelick, 1998/ was tested, but gave only small improvement in the model fits compared to the single rate model, and required one extra parameter. A model with no diffusion was also tested, resulting in very poor fits to the experimental BTC tails. The tails could not be fitted longer than to about half the total experimental time.

### **Model test with Ba, Cs and Co**

The model developed in Section 4.1 (i.e., 4 estimated parameters out of 22 total parameters) was tested by predicting the breakthrough of Ba and Cs in STT-1 and Co in STT-1b using laboratory sorption data. Before proceeding, it is important to emphasize that the sorption/desorption mechanisms of Cs and Co may be too divergent from a fast reversible ion exchange, so it is not expected that the model will predict transport of these tracers with a high accuracy.

For Cs the limited reversibility in the sorption was taken into account by dividing the dilution factor by the reversibly sorbed fraction obtained in the laboratory experiments (Table 3b-9). In the absence of laboratory reversibility data for Co, sorption was assumed fully reversible for the prediction. No aqueous diffusivities of the different possible complexes of Co were found in the literature. A literature value for

**Table 3b-10. Summary of modeling data.**

<b>Fixed parameters</b>						
<b>Aqueous diffusivity (<math>m^2/s</math>)<sup>1)</sup>:</b>			<b>Other fixed parameters were:</b>			
	$D_w$					
HTO	$2.24 \cdot 10^{-9}$	Ba <sup>2+</sup>	$0.85 \cdot 10^{-9}$	$\rho = 2740 \text{ kg/m}^3$ <sup>2)</sup>	$\phi_{m,tot} = 4 \cdot 10^{-3}$	
Na <sup>+</sup>	$1.33 \cdot 10^{-9}$	Cs <sup>+</sup>	$2.06 \cdot 10^{-9}$	$b_f = 7.5 \cdot 10^{-4} \text{ m}$ <sup>3)</sup>	$\phi_m = 2 \cdot 10^{-3}$	
Rb <sup>+</sup>	$2.07 \cdot 10^{-9}$	Co <sup>6)</sup>	$1.5 \cdot 10^{-9}$	$Q_p = 6.73 \cdot 10^{-6} \text{ m}^3/s$	$D_{\rho,m} = 5 \cdot 10^{-11} \text{ m}^2/s$	
Sr <sup>2+</sup>	$0.79 \cdot 10^{-9}$			$L_x \text{ (STT-1)} = 4.68 \text{ m}$	$L_x \text{ (STT-1b)} = 5.07 \text{ m}$	
				$f_{dil} \text{ (STT-1)} = 609$ <sup>4)</sup>	$f_{dil} \text{ (STT-1b)} = 437$ <sup>4)</sup>	
<b>STT-1</b>						
<b>Model parameters:</b>			<b>Laboratory sorption parameters:</b>		<b>Estimated sorption parameters:</b>	
		<b>Tracer</b>	<b><math>K_d</math> (<math>m^3/kg</math>)</b>	<b><math>K_a</math> (m)</b>	<b><math>K_d</math> (<math>m^3/kg</math>)</b>	<b><math>K_a</math> (m)</b>
$\beta_n$ (1)	* $2.7 \pm 0.1$	<sup>22</sup> Na <sup>+</sup>	$1.4 \cdot 10^{-6}$	$5 \cdot 10^{-6}$	* $(1.0 \pm 0.3) \cdot 10^{-6}$	* $(5.7 \pm 1.6) \cdot 10^{-5}$
$\mu$ (1/s)	* $-13.6 \pm 0.1$	<sup>85</sup> Sr <sup>2+</sup>	$4.7 \cdot 10^{-6}$	$2 \cdot 10^{-5}$	* $(2.9 \pm 0.3) \cdot 10^{-5}$	* $(6.5 \pm 2.2) \cdot 10^{-5}$
$\alpha_L$ (m)	* $1.0 \pm 0.1$	<sup>86</sup> Rb <sup>+</sup>	$4 \cdot 10^{-4}$	$1 \cdot 10^{-3}$	* $(3.5 \pm 0.3) \cdot 10^{-4}$	* $(9.6 \pm 0.7) \cdot 10^{-4}$
$v_x$ (m/s)	* $(2.5 \pm 0.8) \cdot 10^{-4}$					
RMSE (HTO, Na, Sr, Rb)	0.32				0.25	
Ba model test:					Ba estimation:	
RMSE (Ba)		<sup>133</sup> Ba <sup>2+</sup>	$2 \cdot 10^{-4}$	$6 \cdot 10^{-4}$	* $(2.8 \pm 0.1) \cdot 10^{-4}$	* $(1.4 \pm 0.3) \cdot 10^{-4}$
		0.17			0.09	
Cs model test:					Cs estimation:	
$F_{dil,Cs}$	1384 <sup>5)</sup>	<sup>137</sup> Cs <sup>+</sup>	$8 \cdot 10^{-4}$	$8 \cdot 10^{-3}$	* $(2.1 \pm 0.1) \cdot 10^{-3}$	* $(9.2 \pm 0.2) \cdot 10^{-3}$
RMSE (Cs)	0.78				$f_{dil,Cs} = *1920 \pm 10$	
					0.07	
<b>STT-1b</b>						
<b>Model parameters</b>			<b>Laboratory sorption parameters:</b>		<b>Estimated sorption parameters:</b>	
		<b>Tracer</b>	<b><math>K_d</math> (<math>m^3/kg</math>)</b>	<b><math>K_a</math> (m)</b>	<b><math>K_d</math> (<math>m^3/kg</math>)</b>	<b><math>K_a</math> (m)</b>
$\beta_n$ (1)	* $5.4 \pm 0.8$	<sup>22</sup> Na <sup>+</sup>	$1.4 \cdot 10^{-6}$	$5 \cdot 10^{-6}$	* $(2.2 \pm 0.3) \cdot 10^{-6}$	* $(2.0 \pm 1.0) \cdot 10^{-5}$
$\mu$ (1/s)	* $-15.6 \pm 0.3$	<sup>85</sup> Sr <sup>2+</sup>	$4.7 \cdot 10^{-6}$	$2 \cdot 10^{-5}$	* $(1.4 \pm 0.2) \cdot 10^{-5}$	* $(1.8 \pm 0.2) \cdot 10^{-4}$
$\alpha_L$ (m)	* $0.33 \pm 0.02$	<sup>86</sup> Rb <sup>+</sup>	$4 \cdot 10^{-4}$	$1 \cdot 10^{-3}$	* $(2.7 \pm 0.3) \cdot 10^{-4}$	* $(3.3 \pm 0.3) \cdot 10^{-3}$
$v_x$ (m/s)	* $(2.2 \pm 0.05) \cdot 10^{-4}$					
RMSE	0.40				0.31	
Co model test:					Co estimation:	
$F_{dil,Co}$	437		$8 \cdot 10^{-4}$	$8 \cdot 10^{-3}$	* $(2.5 \pm 0.1) \cdot 10^{-3}$	* $(6.8 \pm 0.2) \cdot 10^{-3}$
RMSE (Co)	1.36				$f_{dil,Co} = *670 \pm 10$	
					$D_w = * (2.1 \pm 0.05) \cdot 10^{-9}$	
					0.10	

\* Indicates that the data was obtained from parameter estimation. The estimated errors are given as one standard deviation.

References: <sup>1)</sup>/Mills and Lobo, 1989; <sup>2)</sup>/Stanfors et al., 1993; <sup>3)</sup>/Winberg et al., 2000; <sup>4)</sup> Average value for HTO, Na and Sr obtained from the ratio of the integrated concentration-time curves for the injection and the breakthrough data; <sup>5)</sup>  $f_{dil}$  divided by reversibly sorbed fraction; <sup>6)</sup> Average diffusivity of Co complexes was assumed to equal the diffusivity of  $CuCl_2$  /Leaist and Hao, 1994/.

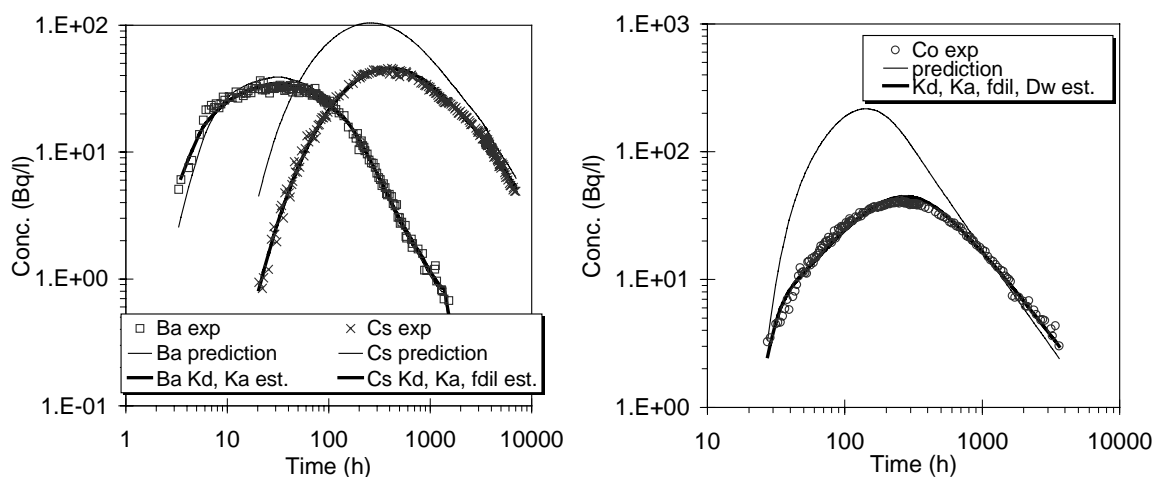


**Figure 3b-31.** Plot of prediction and estimation (see 4.3) of  $K_d$  and  $K_a$  values for Ba,  $K_a$ ,  $K_d$  and  $f_{dil}$  for Cs in STT-1 (left) and  $K_a$ ,  $K_d$ ,  $f_{dil}$  and  $D_w$  for Co in STT-1b (right).

the diffusivity of the uncharged complex  $\text{CuCl}_2$  was found to be  $1.5 \times 10^{-9} \text{ m}^2/\text{s}$  in 0.1 M NaCl, which is approximately twice as high as that of  $\text{Co}^{2+}$  /Leaist and Hao, 1994/. In lieu of more accurate estimates, this value was used.

The prediction for all tracers is shown in Figure 3b-31. Comparing with the experimental results, the prediction of Ba is very good, while the predictions of Cs and Co are poor.

### Model with estimated sorption coefficients

Sorption in laboratory samples may differ from sorption *in situ*, e.g. due to material disturbances in the laboratory experiments /Bradbury and Bayens, 1998/. Material disturbances may be either unintentional (e.g., stress release) or intentional (e.g., sample preparation or crushing). To investigate the magnitude of deviations between laboratory and field sorption data,  $K_a$  and  $K_d$  values for Na, Sr and Rb were estimated using the model discussed earlier in this section. It is important to note that this results in an increase in the number of estimated parameters from 4 to 10. The model fits are shown in Figure 3b-32 and the parameter estimates are listed in Table 3b-10.

As expected, improved fits are obtained, particularly for the Sr peaks, which showed the largest deviation from the fit with minimum number of estimated parameters. Of greater significance, however, is a comparison of the estimated *in situ* and lab values for  $K_d$  and  $K_a$ . For Sr, the estimated *in situ*  $K_d$  is 3 to 6 times higher than the lab  $K_d$ , while the estimated *in situ*  $K_a$  is 4 to 10 times higher than the lab  $K_a$ . For Na, the estimated *in situ* and lab  $K_d$  values are similar, while the estimated *in situ*  $K_a$  is 3 to 10 times higher than the lab  $K_a$ . For Rb, the estimated *in situ* and lab values of both  $K_d$  and  $K_a$  are similar. The difference in laboratory and field  $K_a$  data for Na and Sr is likely due to large uncertainties in the laboratory experiments due to the experimental difficulties of measuring the very small amounts of sorbed tracer.

Subsequently, the sorption coefficients for Ba, Cs and Co, and the dilution factor for Cs and Co were also estimated from the BTCs. The models resulting from these estimations are plotted together with the predictions in Figure 3b-31. The water

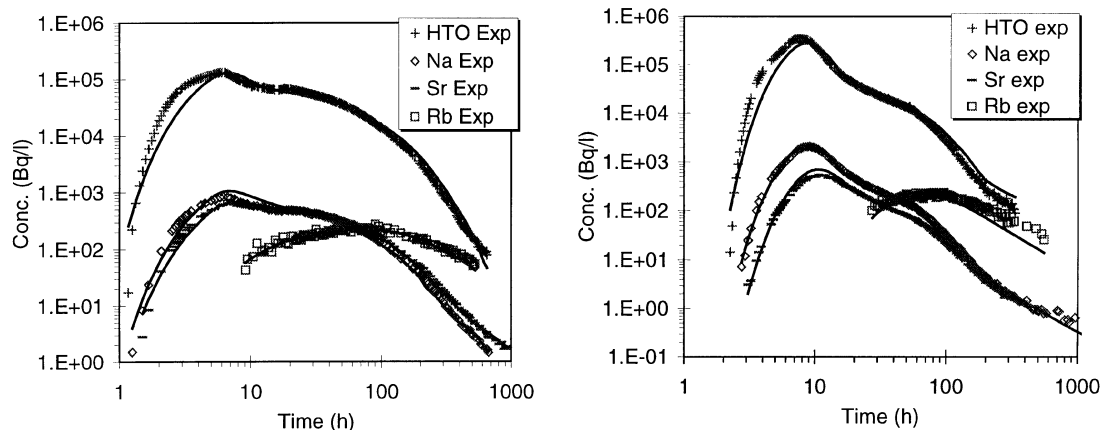


**Figure 3b-32.** Plot of single rate model (lines) and breakthrough data for STT-1 (left) and STT-1b (right) estimating  $K_a$  and  $K_d$  values for Na, Sr and Rb.

diffusivity for Co was also included in the Co estimation, since it is only approximately known.

For Cs, the estimated dilution factor corresponds to a 32% reversibly sorbed fraction. The  $K_a$  values correspond well for Cs, but the estimated  $K_d$  is about 3 times higher than laboratory data.

For Co, the estimated  $K_d$  is about 3 times larger than the estimated lab value, while the  $K_a$  values correspond well. The estimated  $D_w$  for Co is higher than the adopted value in the prediction (based on  $\text{CuCl}_2$ ). The higher  $D_w$  for Co is needed primarily to fit the tail of the BTC. The dilution factor for Co corresponds to a reversible sorption fraction of 65%, indicating that slow sorption/desorption kinetics may be of importance for parts of the sorbed Co.

## 5 Discussion

With the exception of the weakly sorbing Na and Sr, the selected laboratory sorption data and the extracted field parameter values agree within a factor of 3. The  $K_d$  data obtained from diffusion measurements are slightly lower than the estimated field data, while the  $K_d$  data obtained from experiments using crushed host rock material are slightly higher. If the diffusion experiments underestimate  $K_d$  and the crushed material overestimates  $K_d$ , the reason may be that the sorption took place in material within the fracture that was intermediate in surface area compared to 1–2 mm crushed particles used in the batch experiments or 1–2 cm thick rock discs used in the through-diffusion experiments. However, the minimum  $K_d$  values obtained in batch experiments with crushed Feature A material correspond well to the estimated field  $K_d$  data.

It is obvious that selection of geological material and experimental techniques for laboratory investigations is a difficult task. Large amounts of host rock are usually available, whereas site specific geological material from the fracture to be used in an *in situ* experiment is very limited. The majority of the laboratory experiments in this study, both as batch sorption experiments and diffusion experiments, have been done with host rock. Only small samples obtained from drill cores intersecting the fracture plane, used for the *in situ* experiments, at a few locations were available for laboratory experiments. This gives large uncertainties regarding mineralogical composition and distribution as

well as physical properties such as porosity, porosity distribution and foliation of the site-specific rock samples. The available amount and physical form of the geological material will to some extent determine the possible experimental techniques for the laboratory studies. In order to obtain some information about the sorption behavior the so-called batch technique was applied. By working with crushed rock material it was possible to get some information about the sorption and desorption behavior within a realistic time frame. Diffusivities for the different tracers together with the matrix porosities were determined for cm-sized host rock samples by the through-diffusion technique. These rock samples were also subject to determination of the matrix porosity by other techniques. Laboratory experiments with representative rock samples from the actual fracture to be used in the *in situ* experiment would be of most relevance to get input data for modeling. Practical aspects such as the available amount of geological material, the time perspective of the laboratory experiments and number of experiments will, however, give certain limitations to what is possible to be done. It is possible that the actual fracture used for the in-situ experiment will be excavated later on.

Summing up the comparison of laboratory and field sorption data, the overall agreement of different sorption data implies that laboratory sorption data obtained using large (mm-sized) particle sizes or diffusion experiments can be used reasonably well for predictive purposes for ion-exchangeable tracers. Consideration of limited sorption reversibility was necessary in the modeling of Cs and Co. In this work, the very slow desorption reactions of Cs (e.g. due to sorption onto high affinity mineral sites /see e.g. Comans et al., 1991 or Poinssot et al., 1999/ and possible limitation in reversibility of the Co sorption were treated as an irreversible loss of tracer and modeled by a simple enhanced dilution factor. Since the effect of sorption/desorption kinetics was neglected, one can not expect a specific laboratory obtained reversibility factor to be applicable to a field experiment; thus the poor predictions of Cs and Co were not surprising. Co complexation in the aqueous phase was indicated by the increased water diffusivity needed for Co in order to fit the tail of the BTC.

In addition to the sorption parameters, the diffusion and capacity coefficients merit discussion. The capacity coefficient for a non-sorbing tracer,  $\beta_n$ , is the ratio of the volume of the stagnant water, other than rock matrix, to the volume of the mobile water in the fracture. Thus, according to Table 3b-10, the volume of stagnant zones is 2–6 times larger than the volume of mobile water in the fracture. Our explanation for this large ratio is that the stagnant zones consist of non-flowing water within the fracture plane and that the water flow is channelized, with channel widths of a few centimetres. The depth,  $b_s$ , of the stagnant zones can be calculated from the diffusion rate,  $\mu = \ln(D_{p,s}/b_s^2)$ . If the diffusion occurs in gouge material, then a  $D_{p,s}$  of  $2.5 \cdot 10^{-11} \text{ m}^2/\text{s}$  (approximate value from the laboratory experiments with rock material) requires the stagnant zone to have a depth of a few mm to 1 cm. A very high porosity of the gouge material (calculated from Equation 6) is needed to accommodate enough volume (30 to 40%), which seems unrealistic. Diffusion into stagnant water would have a  $D_{p,s}$  of about  $2 \cdot 10^{-9} \text{ m}^2/\text{s}$ , which gives a thickness to the stagnant zone of a few cm to 1 dm. Then, for a 1 to 2 cm wide flow path, about 20 to 60% of the length of the flow path (Equation 6) needs to have adjacent stagnant zones of a few cm to 1 dm depth within the fracture plane. A flow path wider than 3 to 4 cm would not be possible, since then more than 100% of the flow path length would need to have adjacent stagnant zones. Several studies of fracture flow in granites have found that the flow is highly channelled /Abelin et al., 1994; Birgersson et al., 1993; Tsang, 1998/. Abelin et al. /1994/ reported channel widths in the order of mm to 1 dm based on photographs of a fracture trace in the Stripa mine.

An attempt was made to model the data with only matrix diffusion and no gouge or stagnant zones diffusion, i.e. setting the capacity coefficient  $\beta_n$  to zero. When fitting the matrix pore diffusivity alone, values near that of pure water diffusivity were required, which is very unlikely for the rock matrix. This indication of enhanced diffusion, in our interpretation, can only be attributed to zones of stagnant water within the fracture plane. Most likely, diffusion is occurring in a thin zone in the wall rock of the fracture and possibly within gouge material in the fracture plane. However, the amount of diffusion into the low-diffusivity rock matrix (i.e., Äspö diorite) is likely very small over the timescale of these experiments.

Our attempt to use a multirate model (i.e., with a distribution of diffusivities and block sizes) proved to be unsupportable for the available BTCs and the timescales of this study. Although it is reasonable that a range of diffusivities and block sizes do, indeed, exist within fractures and fracture zones at the Äspö HRL, they were not observed in this experiment. Even though such a distribution may be present within the fracture examined, due to the very small diffusivities in these rocks, longer experimental time is needed to observe them. Within our analysis, different diffusion rates in different materials can therefore not be distinguished. More exact information of the amount and characteristics of possible gouge material and matrix properties of the wall rock along the flow path of Feature A is needed before any conclusive comparisons between laboratory and *in situ* derived diffusion and porosity data can be made.

## 6 Conclusions

The BTCs for HTO, Na, Sr, Rb, Ba, Cs and Co tracers in two field experiments were modeled successfully using laboratory sorption data and a common set of 4 tracer independent advection, dispersion and mass transfer related parameters that were estimated simultaneously. By using a simultaneous estimation, a consistent set of data could be obtained.

Parameter estimation of surface and matrix sorption distribution coefficients improved the model fits and showed a good agreement with experimentally obtained sorption data using mm-sized crushed particle fractions or diffusion experiments. Consequently, carefully obtained laboratory sorption data can be used for predictions of field tracer tests over the studied timescales.

Limited sorption reversibility was necessary to include in the modeling of Cs and Co. Thus, for elements with non- or slowly reversible sorption mechanisms, a simple reversible sorption model using  $K_d$  values can not be used to reproduce the field data correctly. An enhanced water diffusivity for Co relative to  $\text{Co}^{2+}$  was needed for the modeling of the Co BTC. The enhanced water diffusivity was interpreted as being caused by formation of Co complexes in the groundwater.

The tails of the BTCs could not be modelled using laboratory obtained diffusivities and diffusion into the wall rock alone. Instead, a large capacity of diffusion into stagnant zones of water within the fracture plane was necessary to explain the observed tailing in the breakthrough curves. The flow path was interpreted as being channelized, with a channel width of a few centimeters. More exact information on the properties of various rock matrices along the flow path is needed before any comparisons between laboratory and *in situ* derived diffusivities can be made.

## Acknowledgements

SKB, for funding CTH, and partial funding to Haggerty.

## Notations

$b_f$	fracture half-aperture [L]
$b_s$	effective thickness of the immobile zone [L]
$b_w$	half-width of flow path [L]
$C_{d,j}$	the $j$ :th data value of concentration,
$c_f$	aqueous concentration in the fracture [ $\text{ML}^{-3}$ ]
$c_s$	concentration in immobile water other than the rock matrix water [ $\text{ML}^{-3}$ ].
$c_{inj}(t)$	time-varying input concentration [ $\text{ML}^{-3}$ ]
$c_m$	aqueous concentration in the rock matrix [ $\text{ML}^{-3}$ ]
$C_{s,j}$	the $j$ :th simulated concentration
$D_{p,m}$	pore diffusivity in the rock matrix [ $\text{L}^2\text{T}^{-1}$ ]
$D_{p,s}$	pore diffusivity in stagnant zones and gouge [ $\text{L}^2\text{T}^{-1}$ ]
$f_{dil}$	dilution factor for dilution in the pumping bore hole [1].
$K_a$	surface sorption coefficient for fracture surfaces [ $\text{L}^{-1}$ ]
$K_d$	mass related sorption distribution coefficient in rock matrix and gouge [ $\text{L}^3\text{M}^{-1}$ ]
$L$	length of the system [L]
$N_d$	number of data points for all tracers
$N_p$	number of parameters estimated
$Q_{inj}$	injection flow rate [ $\text{L}^3\text{T}^{-1}$ ]
$Q_p$	pumping flow rate [ $\text{L}^3\text{T}^{-1}$ ]
$R_a$	surface retardation factor [1]
$R_m$	retardation factor for sorption on internal surfaces in rock matrix and gouge [1]
$S_{rev}$	reversibly sorbed fraction
$v_x$	velocity of the mobile zone [ $\text{LT}^{-1}$ ].
$z$	coordinate into the matrix [L]
$\alpha_L$	longitudinal dispersivity [L]
$\beta_n$	capacity coefficient for a non-sorbing tracer, equal to the ratio of the volume of the immobile zone to the volume of the mobile zone [1]
$\beta_{tot}$	capacity coefficient, defined as the ratio of mass in the immobile zone to mass in the mobile zone at equilibrium [1]

$\phi_s$	porosity of the stagnant zones and gouge [1]
$\phi_m$	transport porosity of the rock matrix [1]
$\phi_{m,tot}$	total porosity of the rock matrix [1]
$\Gamma_s(t)$	time-varying source or sink of mass in gouge and stagnant zones due to rate-limited mass transfer [ $ML^{-3}T^{-1}$ ]
$\mu$	natural logarithm of the mean diffusion rate [ $T^{-1}$ ]
$\rho$	bulk rock density [ $ML^{-3}$ ]

## References

**Andersson P, Byegård J, Cvetkovic V, Johansson H, Nordqvist R, Selroos J-O, Winberg A, 1997.** Experimental plan for tests with sorbing tracers at the TRUE-1 site. TRUE 1<sup>st</sup> stage tracer test programme. Äspö Hard Rock Laboratory PR HRL-97-07, Swedish Nuclear Fuel and Waste Management Company.

**Abelin H, Birgersson L, Widén H, Ågren T, Moreno L, Neretnieks I, 1994.** Channeling Experiments in Crystalline Fractured Rocks. *Journal of Contaminant Hydrology*, 15(3): 129–158.

**Bard Y, 1974.** Nonlinear parameter estimation. Academic Press, San Fransisco, CA.

**Birgersson L, Moreno L, Neretnieks I, Widén H, Ågren T, 1993.** A tracer migration experiment in a small fracture zone in granite. *Water Resources Research*, 29(12): 3867–3878.

**Birgersson L, Widén H, Ågren T, Neretnieks I, 1992.** Tracer migration experiments in the Stripa mine 1980–1991. SKB STRIPA Technical Report TR 92-25, Swedish Nuclear Fuel and Waste Management Company.

**Bond K, Moreton A D, Heath T G, 1992.** Hatches 5.0 The HARWELL/NIREX Database, Harwell Laboratory, Oxfordshire OX11, ORA, UK.

**Bradbury M H, Green A, 1985.** Measurement of important parameters determining aqueous phase diffusion rates through crystalline rock matrices. *J. Hydrol.*, 82(1–2): 39–55.



**Bradbury M H, Bayens B, 1998.** N<sub>2</sub>-BET surface area measurements on crushed and intact minerals and rocks: a proposal for estimating sorption transfer factors. Nuclear Technology, 122: 250–253.

**Byegård J, Skålberg M, Widestrand H, 2000.** To be published.

**Byegård J, Johansson H, Skålberg M, 1998.** The interaction of sorbing and non-sorbing tracers with different Äspö rock types. SKB TR 98-18, Swedish Nuclear Fuel and Waste Management Company.

**Byegård J, Skarnemark G, Skålberg M, 1991.** Radioactive tracer study performed in a dipole geometry in a highly conductive fracture zone. Mat. Res. Soc. Symp. Proc., 212: 677–684.

**Byegård J, Skarnemark G, Skålberg M, 1995.** The use of some ion-exchange sorbing tracer cations in *in-situ* experiments in high saline groundwaters. Mat. Res. Soc. Symp. Proc., 353: 1077–1084.

**Carbol P, Engkvist I, 1997.** Compilation of radionuclide sorption coefficients for performance assessment. SKB R 97-13, Swedish Nuclear Fuel and Waste Management Company.

**Comans R N J, Haller M, DePreter P, 1991.** Sorption of Cesium on Illite – Non-equilibrium Behaviour and Reversibility. Geochimica et Cosmochimica Acta, 55(2): 433–440.

**Cui D, Eriksen T D, 1997.** On the sorption of Co and Cs on Stripa granite fracture-filling material. Radiochi. Acta 79, 29.

**D'Alessandro M, Mousty F, Bidoglio G, Guimerà J, Benet I, Sánchez-Vila X, García Gutiérrez M, Yllera De Llano A, 1997.** Field tracer experiment in a low permeability fractured medium: results from El Berrocal site. Journal of Contaminant Hydrology, 26(1–4): 189–201.

**Donaldson J R, Tryon P V, 1990.** Nonlinear least squares regression using STARPACK: The standards time series and regression package. Natl. Bureau of Standards, Boulder, CO.

**Eliasson T, 1993.** Mineralogy, geochemistry and petrophysics of red coloured granite adjacent to fractures. SKB TR 93-06, Swedish Nuclear Fuel and Waste Management Company.

**Gustafsson E, Klockars C-E, 1981.** Studies of groundwater transport in fractured crystalline rock under controlled conditions using non-radioactive tracers. SKBF/KBS TR 81-07, Swedish Nuclear Fuel and Waste Management Company.

**Hadermann J, Heer W, 1996.** The Grimsel (Switzerland) migration experiment: integrating field experiments, laboratory investigations and modelling. Journal of Contaminant Hydrology, 21: 87–100.

**Haggerty R, 1998.** STAMMT-L Solute transport and multirate mass transfer – Linear coordinates Version 1.0, Department of Geosciences, Oregon State University, Oregon, USA.

**Haggerty R, Fleming S W, Meigs L C, McKenna S A, 1998.** Tracer tests in a fractured dolomite, 2., Analysis of mass transfer in single-well injection-withdrawal tests. Water Resources Research, in review.

**Haggerty R, Gorelick S M, 1998.** Modeling mass transfer processes in soil columns with pore-scale heterogeneity. Soil Sci. Soc. Am. J., 62(1): 62–74.

**Heer W, Hadermann J, 1994.** Grimsel test site: Modelling radionuclide migration field experiments. Nagra Technical Report 94-18, National Cooperative for the Disposal of Radioactive Waste, Wettingen, Switzerland.

**Hellmuth K-H, Lukkarinen S, Siitari-Kauppi M, 1994.** Rock matrix studies with carbon-14-polymethylmethacrylate (PMMA); method development and applications. Isotopenpraxis Environ. Health Stud., 30: 47–60.

**Himmelsbach T, Hotzl H, Maloszewski P, 1998.** Solute transport processes in a highly permeable fault zone of Lindau fractured rock test site (Germany). Ground Water, 36(5): 792–800.

**Jakobsson A-M, Albinsson Y, 1998.** Sorption of  $\text{NpO}_2^+$  and  $\text{Co}^{2+}$  onto  $\text{TiO}_2$ . Radiochimica Acta, 82: 257–262.

**Johansson H, Byegard J, Skarnemark G, Skalberg M, 1997.** Matrix diffusion of some alkali- and alkaline earth-metals in granitic rock. Mater. Res. Soc. Symp. Proc., 465: 871–878.

**Johansson H, Siitari-Kauppi M, Skålberg M, Tullborg E-L, 1998.** Diffusion pathways in crystalline rock – examples from Äspö-diorite and fine-grained granite. Journal of Contaminant Hydrology, 35: 41–53.

**Landström O, Klockars C E, Persson O, Andersson K, Torstenfelt B, Allard B, Larsson S Å, Tullborg E-L, 1982.** A comparison of *in-situ* radionuclide migration studies in the Studsvik area and laboratory measurements. In: W. Lutze (Editor), Scientific Basis for Nuclear Waste Management – V. Elsevier Science Publishing Co.

**Landström O, Tullborg E-L, 1995.** Interactions of trace elements with fracture filling minerals from the Äspö Hard Rock Laboratory. SKB TR 95-13, Swedish Nuclear Fuel and Waste Management Company.

**Leaist D, Hao L, 1994.** Tracer diffusion of some metal ions and metal-EDTA complexes in aqueous sodium chloride solutions. J. Chem. Soc. Faraday Trans., 90(1): 133–136.

**Li Y-H, Gregory S, 1974.** Diffusion of ions in sea water and in deep sea sediments. Geochimica et Cosmochimica Acta, 38: 703–714.

**Marquardt D W, 1963.** An algorithm for least-squares estimation of nonlinear parameters. SIAM J. Indust. Appl. Math., 11(2): 431–441.

- Mills R, Lobo V M M, 1989.** Self-diffusion in electrolyte solutions – a critical examination of data compiled from the literature. Elsevier, Amsterdam.
- Neretnieks I, 1980.** Diffusion in the rock matrix; an important factor in radionuclide retardation? *Journal of Geophysical Research*, 85(8): 4379–4397.
- Nilsson A-C, 1997.** Results of the analyses of groundwater sampled in the TRUE-1 site. SKB Technical Note TN-97-08t, Swedish Nuclear Fuel and Waste Management Company.
- Parkhurst D L, Thorstenson D C, Plummer L N, 1980.** PHREEQE, A Computer Program for Geochemical Calculations. U.S. Geological Survey Report WRI-80-96.
- Poinssot C, Bayens B, Bradbury M H, 1999.** Experimental studies of Cs, Sr, Ni and Eu sorption on Na-illite and the modelling of Cs sorption. PSI Bericht 99-06, PSI, Villigen, Switzerland.
- Skagius A-C, 1986.** Diffusion of dissolved species in the matrix of some Swedish crystalline rocks. Ph.D. Thesis, Royal Institute of Technology, Stockholm.
- Skagius K, Neretnieks I, 1986.** Porosities and diffusivities of some nonsorbing species in crystalline rocks. *Water Resources Research*, 22(3): 389–398.
- Stanfors R, Liedholm M, Munier R, Olsson P, Stille H, 1993.** Geological – structural evaluation of data from section 1475–2265 m. Äspö Hard Rock Laboratory PR 25-93-05, Swedish Nuclear Fuel and Waste Management Company.
- Suksi S, Kaemaeraeinen E L, Siitari-Kauppi M, Lindberg A, 1987.** Sorption and diffusion of cobalt, nickel, strontium, iodine, cesium and americium in natural fissure surfaces and drill core cups studied by autoradiography, 3. YJT Report 87-17, Voimayhtioeiden Ydinjätetoimikunta, Helsinki.
- Tsang C F N I, 1998.** Flow channeling in heterogeneous fractured rocks. *Reviews of Geophysics*, 36(2): 275–298.
- Tullborg E-L, 1999.** Personal communication.
- Valkiainen M, 1992.** Diffusion in the rock matrix – a review of laboratory tests and field studies. YJT Report 92-04, Voimayhtioeiden Ydinjätetoimikunta, Helsinki.
- Valkiainen M, Uusheimo K, Olin M, Muurinen A, 1992.** Diffusivity and porosity in rock matrix related to the ionic strength in the solution. *Mater. Res. Soc. Symp. Proc.*, 257: 675–82.
- Vandergraaf T T, Drew D J, Archambault D, Ticknor K V, 1997.** Transport of radionuclides in natural fractures: some aspects of laboratory migration experiments. *Journal of Contaminant Hydrology*, 26(1–4): 83–95.
- Widestrand H, Andersson P, Byegård J, Skarnemark G, Skålberg M, Wass E, 2000.** *In-situ* migration experiments at Äspö HRL, Sweden: results of radioactive tracer studies in a single fracture, submitted to *J. of Radioanalytical and Nuclear Chemistry*.

**Winberg A, Andersson P, Hermanson J, Byegård J, Cvetkovic V, Birgersson L, 2000.** Äspö Hard Rock Laboratory. Final report of the first stage of the Tracer Retention Understanding Experiments. SKB TR-00-07, Swedish Nuclear Fuel and Waste Management Co.

**Winberg A (ed.), 1996.** First TRUE Stage – Tracer Retention and Understanding Experiments. Descriptive structural-hydraulic models on block and detailed scales of the TRUE-1 site. SKB ICR 96-04, Swedish Nuclear Fuel and Waste Management Company.

# Evaluation of TRUE–1 tests with sorbing tracers using CHAN3D

Luis Moreno,  
Chemical Engineering and Technology, Royal Institute of Technology,  
Stockholm, Sweden

## Abstract

Three tracer tests (STT1a, STT1b and STT2) with sorbing species performed as a part of the TRUE-1 experiments are studied. The tests were carried out in a radially converging flow geometry with a travel distance of about 5 m. The injected sorbing tracers were:  $\text{Na}^+$ ,  $\text{Sr}^{2+}$ ,  $\text{Ca}^{2+}$ ,  $\text{Ba}^{2+}$ ,  $\text{Cs}^+$ ,  $\text{Co}^{2+}$ ,  $\text{Rb}^+$ . The sorption properties of the tracer cover a wide interval. The tracer tests were modelled using the Channel Network Model, which assumes that fluid flow and solute transport take place through a network of channels. It includes solute transport by advection, diffusion into the rock matrix, and sorption within the matrix and onto the channel surface. Sorption and diffusion data were obtained from laboratory measurements carried out over generic Äspö material. Some measurements were made using material from the Feature A. Large differences are found between the experimental and the predicted breakthrough curves. The predicted times are much shorter than the experimental ones. An attempt is made to explain these differences using various possible retardation mechanisms. Finally, it is concluded that several mechanisms must act simultaneously in order to explain the large differences.

## 1 Introduction and background

As a part of the TRUE-1 experiments, three tracer tests (STT1a, STT1b and STT2) with sorbing species were performed. Blind predictions were carried out for the three tracer tests. Previous to these tests, several tests with non-sorbing tracers were carried out in the same site. Some of these tests were used to calibrate the site model.

The overall objectives of the TRUE project are /Winberg, 2000/; to develop the understanding of radionuclide migration in fractured rock; to evaluate the conceptual models and data collection; and to provide in-situ data on radionuclide migration and retention. Tracer tests at different experimental scales are included in the TRUE project. The first stage (TRUE-1) comprises tracer tests on a detailed scale using conservative and sorbing tracers in a simple geometry.

The aim of this paper is to present the predictive modelling results of the tracer tests with sorbing tracers and to compare the results with the experimental values. The differences are analysed and discussed. The simulations were made by using the code CHAN3D /Gylling et al., 1999/, which is based in the Channel Network Model developed by Moreno and Neretnieks /1993/.

## 2 Channel Network Model

The simulations were made by using the code CHAN3D /Gylling et al., 1999/. The model takes into account the uneven flow distribution observed in fractured rock and includes retarding physical processes like matrix diffusion and sorption within the matrix. Sorption onto the fracture/channel surfaces is also included. Data can be obtained from borehole transmissivity measurements and observations on fracture widths.

Each member of the network is assigned a hydraulic conductance. This is the only entity needed to calculate the flow, if the pressure field is known. If the residence time for non-interacting solutes is to be calculated, then the volume of the channel members is needed as well. If sorption onto the fracture surface or diffusion into the matrix will be included in the model, the flow-wetted surface area must also be included. Some properties of the rock are also needed, such as rock matrix porosity, diffusivity, and sorption constants. In present simulations, it is assumed that the conductances of the channel members are log-normally distributed and not correlated in space. The channel volume was estimated by assuming that the conductance of the channels is proportional to the cube of the channel aperture.

The solute transport is simulated by using a particle-following technique /Moreno et al., 1988/. Many particles are introduced, one at a time, into the known flow field at one or more locations. Particles arriving at an intersection are distributed in the outlet channel members with a probability proportional to their flow rates. The residence time of an individual particle along the whole path is determined as the sum of residence times in every channel member that the particle has traversed. The residence time distribution is then obtained from the residence times of a multitude of individual particle runs.

In the flow model the tunnel with the niche (see Figure 3b-33), all the boreholes, the Feature A and the Feature B planes were included. Feature A was extended to the boundaries whereas Feature B fractures were treated as confined fracture planes. As the boundary conditions, a predetermined hydraulic head was used on the top, on the bottom, and on the right-hand side of the rock control volume. No flow was assumed on the sides perpendicular to the tunnel. The hydraulic head in the tunnel was taken to be the boundary condition on the left-hand side, and for the other region on this side, a no flow condition was assumed. The withdrawal flow rate in the location where the tracers were collected was also included in the boundary conditions. The conductance of the channels that connect the rock with the tunnel and the niche was reduced by a constant factor to simulate the skin effect. The size of the modelled rock volume was 30×30×40 metres in the longitudinal direction to the tunnel, the horizontal direction, and the vertical direction respectively. In the model, the channel length was 0.7 m and therefore the number of channels in the network was 320 000. The mean transmissivity values for the different features were assigned from the experimental data.

No hydrodynamic dispersion is assumed in the channels. Different velocities in different channels in the network cause the dispersion of the solute. The volume of the channels is determined by matching the volume of the channels with the desired flow porosity. The specific flow wetted surface was estimated to be  $2.0 \text{ m}^2/\text{m}^3$ . For a species that does not interact with the rock, the residence time in one channel is given by the volume of the channel divided by the water flow rate in it. For a species that is sorbed onto the channel surfaces, the residence time is increased by a factor  $R_a$  that is given by

$$R_a = 1 + \frac{K_a}{2\delta} \quad (1)$$

where  $K_a$  is the surface sorption constant (m) and  $\delta$  the fracture aperture (m). For a species that diffuses into the rock matrix a varying residence time is obtained. This is longer than the residence time for a species that does not diffuse into the rock matrix.

For a flat channel from which the diffusion is perpendicular to the channel surface, a simple analytical solution is available for the RTD for matrix-interacting species. The cumulative curve, F, for the residence times is obtained as:

$$F = \operatorname{erfc} \left[ \frac{\left( K_d D_e \rho_p \right)^{0.5} \cdot L \cdot W}{(t - t_w)^{0.5} \cdot Q} \right] \quad (2)$$

Equation (2) applies for times greater than the water-plug-flow residence time /Carslaw and Jaeger, 1959/. Otherwise, the function is zero. Here,  $K_d$  is the sorption coefficient,  $D_e$  is the effective diffusivity,  $\rho_p$  is the density of the porous rock, LW is half the flow-wetted surface and Q is the flow rate in the channel. Equation (2) accounts for advection in the channel, diffusion into the rock matrix, and sorption on the micro fracture surfaces. It is not applicable for long contact times if the distances between fractures are short compared to the penetration depth into the matrix. The residence time for each particle in a channel member is determined by using the technique proposed by Yamashita and Kimura /1990/. Where uniformly distributed, random numbers in the interval [0,1] are chosen for F and the residence time for the particle is then calculated by solving for t in Equation (2).

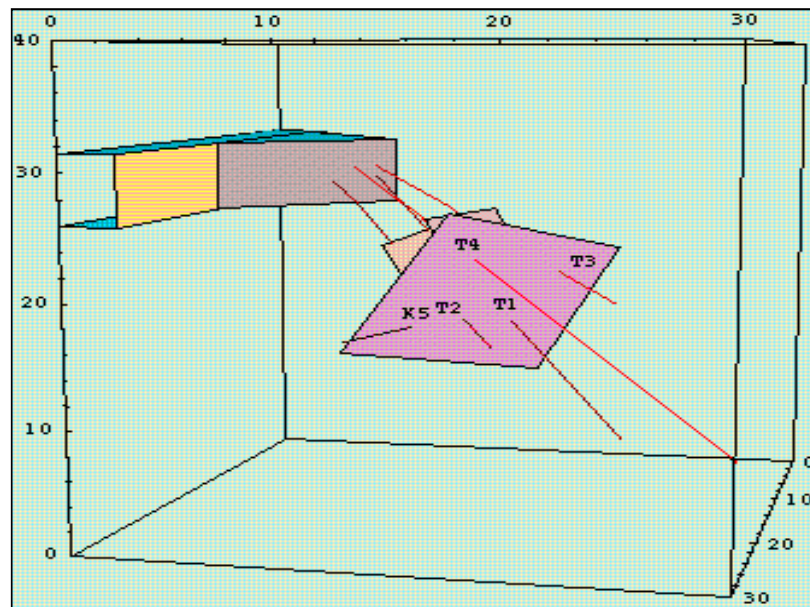


**Figure 3b-33.** Feature A, the boreholes, the tunnel, and the niche. Behind feature A some of the feature B planes may be seen. The intersection of the boreholes KXTT1, KXTT2, KXTT3, KXTT4 and KA3005A with the Feature A are labelled as T1, T2, T3, T4 and K5, respectively.

### 3 Experiments

This paper includes analysis of three sets of tracer tests with sorbing species. Preliminary tracer tests with non-sorbing species were carried to recalibrate the model, to test eventual changes in the hydraulic conditions or refine the experimental design. The first set of tracer tests (STT1a) with sorbing tracers was performed with injection at borehole KXTT4:R3 and extraction at borehole KXTT3:R2. Due to the low recovery of Caesium, the collection of tracers was maintained for a longer time. It was then decided to perform an additional experiment (STT1b) with sorbing tracers injected at borehole KXTT1:R2 and with extraction at the same section used for the test STT1a (i.e. borehole KXTT3:R2). Finally a tracer test with sorbing species was done using a smaller extraction flow rate (0.2 l/min). The tests STT1 were carried out with a extraction flow rate of 0.4 l/min. The tracer tests included in this report are listed in Table 3b-11.

**Table 3b-11. Summary of the tracer tests with sorbing species discussed in this report. Preliminary tests are also shown.**

	STT1a	STT1b	STT2
Injection section	KXTT4-R3	KXTT1-R2	KXTT4-R3
Extraction section	KXTT3-R2	KXTT3-R2	KXTT3-R2
Extraction flow rate, l/min	0.400	0.400	0.200
Preliminary tests	PD5, DP6, RC2 PDT1, PDT2, PDT3	PDT4	–

These tests were performed using a radially converging geometry; i.e. water was not injected at the “injection” section. The tracer was introduced into the fracture only by the natural water flow. Therefore, the injection was a decaying pulse injection where the tracer solution is diluted by the natural groundwater flow through the packed-off borehole section. The tracers injected in these tracer tests are listed in Table 3b-12. All the concentration values are corrected for radioactive decay. For sake of illustration, the concentration in the injection borehole as a function of time for the STT1b experiment is shown in Figure 3b-34.

#### **Laboratory experiments**

Diffusion and sorption data were determined in laboratory experiments. They were carried out using generic Äspö material. The data used in the predictive simulations is shown in Table 3b-13. Other data are also used in this report, but they will be presented and discussed later.



**Table 3b-13. Tracer injected in the tests.**

Tests	STT1a	STT1b	STT2
Non-sorbing species	Uranin HTO	Uranin HTO	Uranin HTO
Sorbing species	Na <sup>+</sup> Sr <sup>+2</sup> Rb <sup>+</sup> Ca <sup>+2</sup> Ba <sup>+2</sup> Cs <sup>+</sup>	Na <sup>+</sup> Sr <sup>+2</sup> Rb <sup>+</sup> Co <sup>+2</sup> K <sup>+</sup>	Br <sup>-</sup> Na <sup>+</sup> Sr <sup>+2</sup> Rb <sup>+</sup> Ca <sup>+2</sup> Ba <sup>+2</sup> Cs <sup>+</sup>

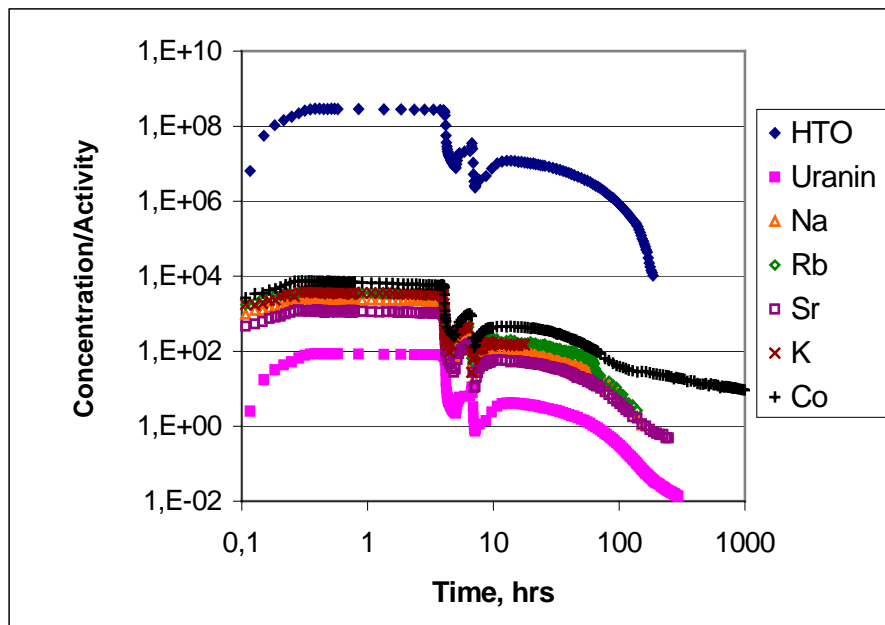


**Figure 3b-34.** Tracer concentration at the injection borehole as a function of time for the STT1b experiment. Concentration of Uranine is in ppm and activity in Bq/kg for the other tracers.

**Table 3b-12. Sorption constant and effective diffusivity for tracers used in these tests.**

Species	$K_d$ , m <sup>3</sup> /kg	$D_e$ , m <sup>2</sup> /s	$K_a$ , m	Radionuclide
Uranin	–	$1.2 \times 10^{-13}$	–	
HTO	–	$1.2 \times 10^{-13}$	–	H-3
Br <sup>-</sup>	–		–	Br-82
Na <sup>+</sup>	$1.4 \times 10^{-6}$	$6.7 \times 10^{-14}$	$7.0 \times 10^{-7}$	Na-22
Sr <sup>+2</sup>	$4.7 \times 10^{-6}$	$4.0 \times 10^{-14}$	$5.0 \times 10^{-4}$	Sr-85
Rb <sup>+</sup>	$4.0 \times 10^{-4}$	$1.0 \times 10^{-13}$	$8.0 \times 10^{-6}$	Rb-86
Ca <sup>+2</sup>	$5.2 \times 10^{-6}$	$4.0 \times 10^{-14}$		Ca-47
Ba <sup>+2</sup>	$2.0 \times 10^{-4}$	$4.2 \times 10^{-14}$		Ba-133
Co <sup>+2</sup>	$3.2 \times 10^{-6}$	$4.0 \times 10^{-14}$	$4.0 \times 10^{-5}$	Co-58
K <sup>+</sup>	$2.0 \times 10^{-4}$	$1.0 \times 10^{-13}$	$5.6 \times 10^{-4}$	K-42
Cs <sup>+</sup>	$6.0 \times 10^{-3}$	$1.0 \times 10^{-13}$		Cs-137

## 4 Results

The breakthrough curves were re-calculated in order to eliminate possible calibration errors. No other modifications are introduced. Surface sorption is not included in these calculations, it is added later in the discussion.

### ***Evaluation of the STT1a Sorbing Tracer Tests***

Figure 3b-35 shows the times for 50% of the injected tracer. The figures show the values for the 5%, 50% (median) and 95% percentiles for the set of simulations done. 50 realisations were carried out in each case.

### ***Evaluation of the STT1b Sorbing Tracer Tests***

Figure 3b-36 show the results for 50% of the injected tracer. Values for the 5%, 50% (median) and 95% percentiles for the set of simulations done are also shown. 50 realisations were carried out.

### ***Evaluation of the STT2 Sorbing Tracer Tests***

Figure 3b-37 show the results for 50% of the injected tracer. Values for the 5, 50 (median) and 95% percentiles for the set of prediction done are also shown. 50 realisations were carried out.

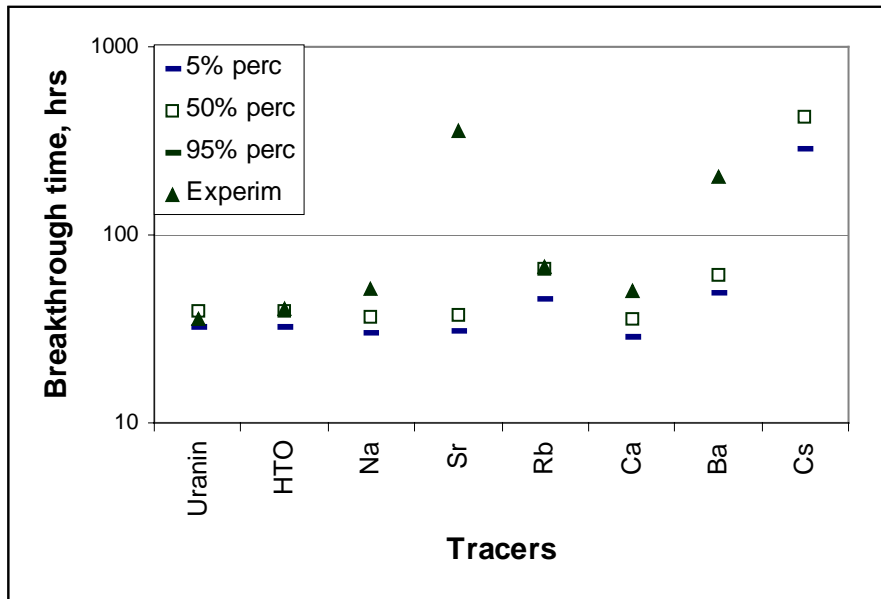


**Figure 3b-35.** Breakthrough times for 50% of the injected tracer. The figure shows 5%, 50% and 95% percentile levels for the simulated results. The experimental results are also shown.

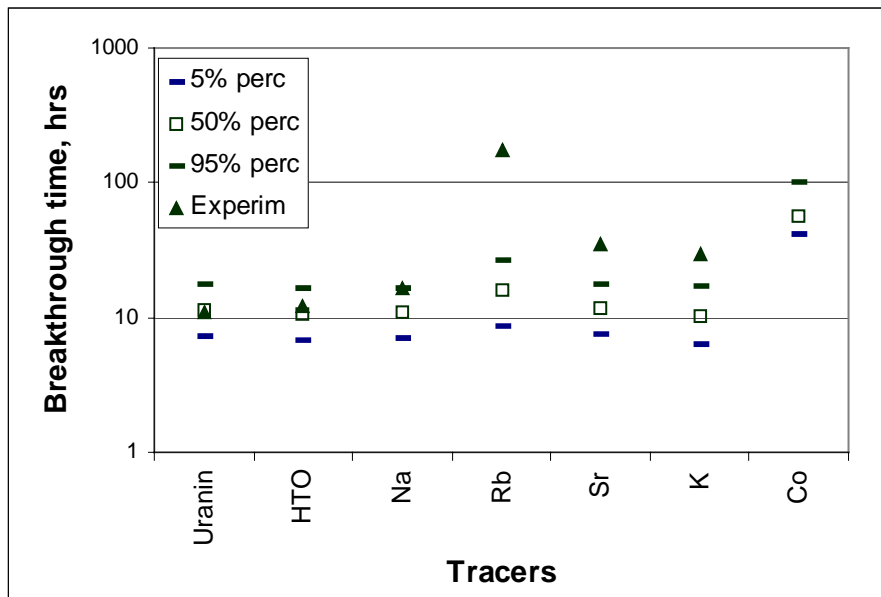


**Figure 3b-36.** Breakthrough times for 50% of the injected tracer. The figure shows 5%, 50% and 95% percentile levels for the simulated results. The experimental results are also shown.

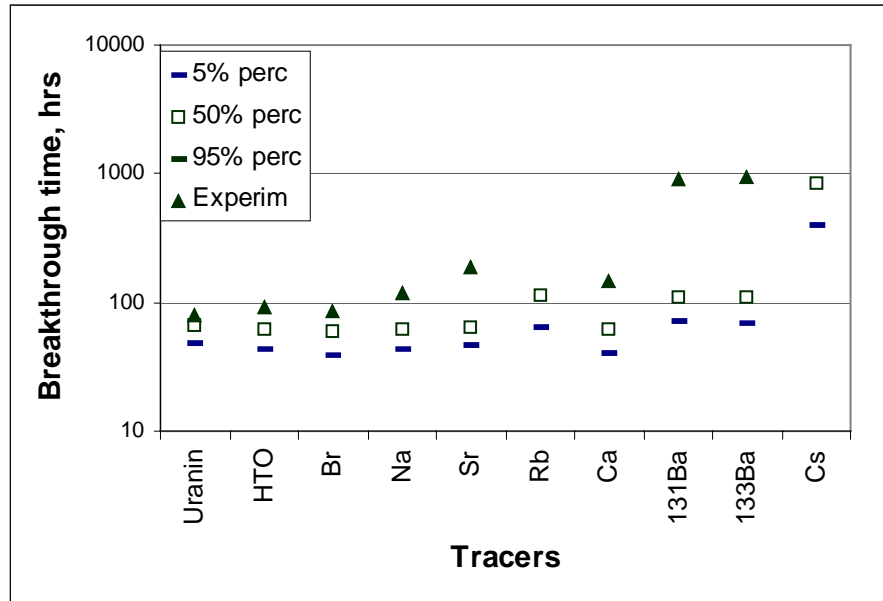


**Figure 3b-37.** Breakthrough times for 50% of the injected tracer. The figure shows 5%, 50% and 95% percentile levels for the simulated results. The experimental results are also shown.

## 5 Discussion and conclusions

In the simulations reported, it is found that the predicted residence times for the sorbing tracer are shorter than the experimental ones. As shown in Equation (2), the retardation caused by the sorption within the matrix is determined by the following term

$$G = \cdot (K_d D_e \rho_p)^{0.5} \cdot \frac{L \cdot W}{Q} \quad (3)$$

According to the results,  $G$  should be about 30 times larger in order to match the experiments. This means that the sorption or diffusion would be about 900 times higher. The same effect could be observed if the water flow rate in the fractures/channels is lowered by a factor of 30. It is most probable that several factors are acting simultaneously. For example, the diffusion and sorption are higher, the tracers are transported through pathways with smaller flow rates and they are sorbed on the fracture surface, filling material, rock fragments. A discussion of these processes follows.

### **Impact of greater diffusion and sorption**

Weathering of the rock adjacent to the fracture can increase the porosity of this region and increase its diffusivity. The duration of these tracer tests is quite short, meaning that only the rock close to the fracture is involved in diffusion/sorption. Values of porosity in the 0.02–0.03 range are estimated for the part of the altered rim zone which is accessible for the tracers over the time scales of the in-situ experiments /Winberg et al., 2000/. An increase in the porosity by a factor of 10 may increase the formation factor by a factor of between 10–20. This means diffusivity 10–20 times larger than the value used for the rock mass.

The data used in the blind predictions are shown in Table 3b-13. At the present, new site-specific data have been available /Byegård et al., 1998/. Äspö diorite and Fine-grained granite were used in batch experiments. Material from the Feature A included mylonite, altered Äspö diorite and altered fine-grained granite.

The times for experiments were however too short. Sorption constants determined under these conditions may be much lower than the actual value, since equilibrium is far from being reached. Therefore, the obtained sorption constants will be corrected. In the calculations, it is assumed that the particles are spherical and the diffusion coefficient is taken from Byegård et al. /1998/. The new values for the sorption constant of the Äspö diorite are in the interval 0.3 – 1.1 m<sup>3</sup>/kg, for Fine-grained granite they were about 0.07 m<sup>3</sup>/kg. For material from Feature A, the values are in the interval, 0.01 to 0.60 m<sup>3</sup>/kg.

In order to address the impact of a higher sorption on the breakthrough times, a value of 0.40 m<sup>3</sup>/kg is chosen for the sorption constant of caesium. Similar analyses are applied to the other species. A summary of these data is given in Table 3b-14. The breakthrough times for both cases, with and without sorption on the fracture surface, are shown in Figure 3b-38. They show that, even if a larger value for the sorption constant is chosen, the experimental breakthrough times are not obtained for Sr, Ba and Cs.

**Table 3b-14. Values experimentally determined for material from Feature A /Byegård et al., 1998/ and estimated values.**

Species	K <sub>d</sub> used in predictions m <sup>3</sup> /kg	New K <sub>d</sub> data m <sup>3</sup> /kg	“Large” K <sub>d</sub> m <sup>3</sup> /kg
Na <sup>+</sup>	1.4×10 <sup>-6</sup>	< 0.10-0.20×10 <sup>-3</sup>	0.03×10 <sup>-3</sup>
Sr <sup>+2</sup>	4.7×10 <sup>-6</sup>	< 0.10-0.40×10 <sup>-3</sup>	0.10×10 <sup>-3</sup>
Rb <sup>+</sup>	0.4×10 <sup>-3</sup>	0.9-2.0×10 <sup>-3</sup>	8×10 <sup>-3</sup>
Ca <sup>+2</sup>	5.2×10 <sup>-6</sup>	< 0.7×10 <sup>-3</sup>	0.05×10 <sup>-3</sup>
Ba <sup>+2</sup>	0.2×10 <sup>-3</sup>	0.4-1.8×10 <sup>-3</sup>	5×10 <sup>-3</sup>
Cs <sup>+</sup>	6.0×10 <sup>-3</sup>	1-11×10 <sup>-3</sup>	400×10 <sup>-3</sup>

### ***Impact of an uneven flow distribution***

The hydraulic characteristics of Feature A are quite heterogeneous. The transmissivities at the locations where the boreholes meet the fracture are in the interval 5.9E-9 to 2.1E-7, a ratio of about 35 between the largest and the lowest values. The transmissivities and the drawdowns measured in the STT1b tracer test are shown in Table 3b-15. A schematic picture of the location of the different sections at the Feature A is shown in Figure 3b-39. In these tracer tests, the section KXTT3-R2 was used as extraction section and the tracers were injected at sections KXTT4-R3 and KXTT1-R2. The section KXTT3-R2 is hydraulically well connected with section KXTT2-R2. However, the connections with the sections KXTT1-R2 and KXTT4-R3 are not good. Based in this and the irregular drawdowns, an uneven flow distribution in Feature A may be expected.

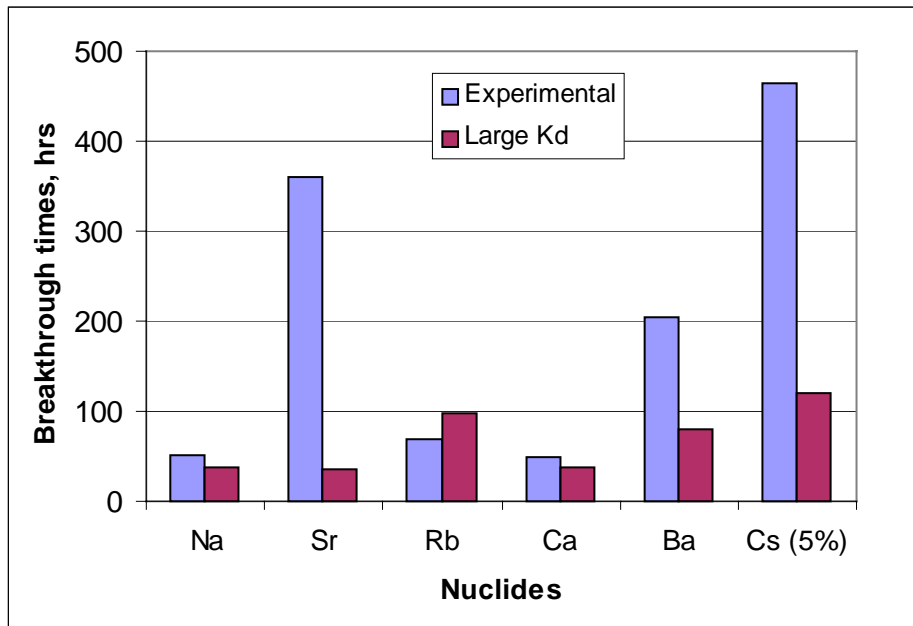


**Figure 3b-38.** Simulated breakthrough times obtained using a large value for the sorption constants. The times correspond to 50% of the injected tracer are used, except for Cs, where 5% is used. STT1a tracer test.

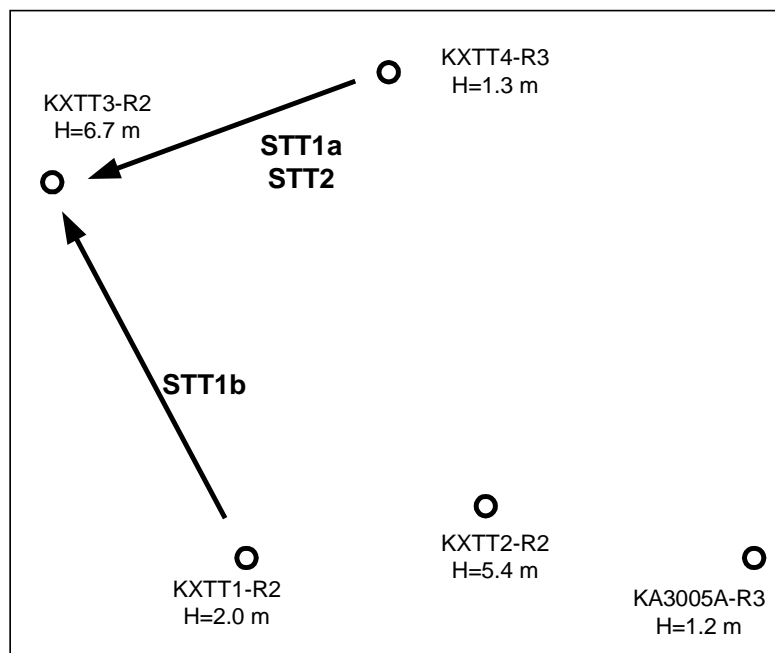


**Figure 3b-39.** Schematic picture showing the locations of the borehole sections at Feature A.

**Table 3b-15. Hydraulic data for Feature A.**

Borehole	KXTT1	KXTT2	KXTT3	KXTT4	KA3005
Transmissivity, m <sup>2</sup> /s	8.3E-9	5.9E-9	2.1E-7	1.8E-8	2.7E-8
Drawdown, m	2.0	5.4	6.7	1.3	1.2

Moreover, the water residence times of these tests are about 10 hours. Considering a distance between injection and extraction hole of about 5 metres and an extraction flow rate of 0.4 l/min, the mean fracture aperture required to fit the travel time is

$$\delta_m \approx 3.0 \text{ mm}$$

It is very improbable that such a large fracture aperture exists over an extent of 10 m. The most probable situation is an uneven flow distribution with a small fraction of water flowing through the injection sections. In order to match the experimental breakthrough times the flow in the injection zones would be reduced by a factor of 30.

### ***Sorption in the fracture***

In many situations, the fractures are not clean. In addition to the coating material, other material may be found in the fracture plane, small rock fragments, fault gouge and filling material (e.g., clays). The tracer transported in the fracture may then be sorbed onto these materials. A large surface sorption may be due to a larger available surface for sorption; e.g. sorption on gouge, sorption on filling material or the existence of several parallel fractures.

The sorption on the fracture surface or on filling material is usually a fast reaction and for many situations may be considered to be instantaneous. In this case, the shape of the breakthrough curve is kept constant. It is only translated in the direction of longer times (see Figure 3b-40). Figure 3b-40 shows breakthrough curves for the caesium tracer in STT1a when the effect of surface sorption has been increased 10 and 20 times. Therefore, surface sorption (instantaneous) can not explain the larger retardation observed in the tracer tests. In order to explain the longer breakthrough times by sorption onto these materials, slow kinetics is required. A similar effect may be found if the sorption occurs within particles with a size larger than a few millimetres.

### ***Diffusion into the stagnant water***

Since the injection is carried out without over-pressure, it is expected that the tracer transport from the injection to the extraction hole takes place through one or a few paths. In addition to diffusion into the rock matrix, the tracer in the fracture may diffuse into the stagnant water in the fracture plane. This effect is important for narrow paths and large fracture apertures. Neretnieks /2000/ showed that if the tracer is transport by several channels a significant retardation is obtained.

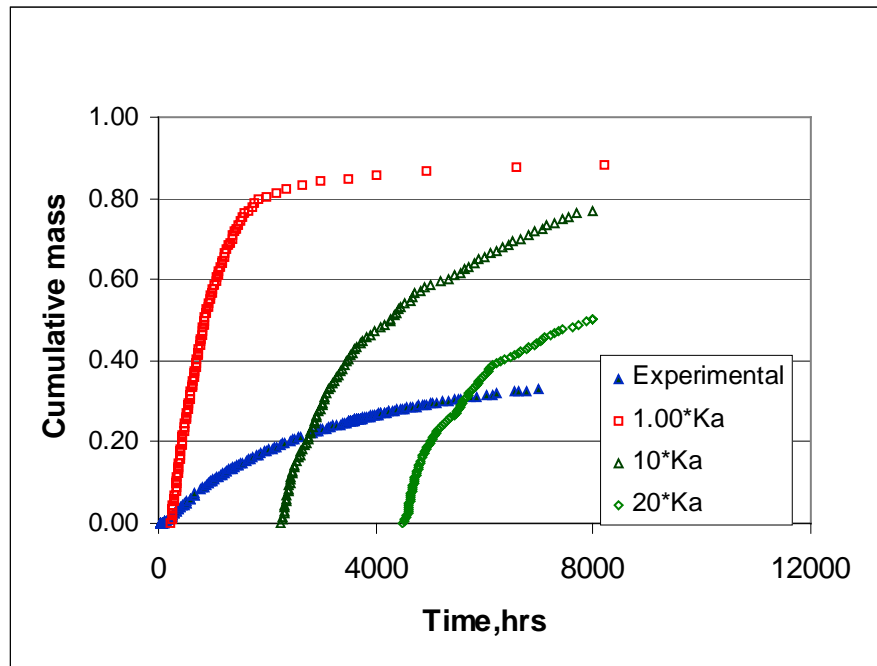


Figure 3b-40. Cumulative mass for increasing surface sorption..

### Impact of surface sorption

In the simulations shown above, surface sorption was not included. To test the impact of surface sorption, simulations were performed for sorption within the matrix and on the fracture surface acting separately and for both mechanisms acting simultaneously. The results are for the tracer test STT1b and are shown in Figure 3b-41.

For sodium, the simulated breakthrough times are very similar to the values obtained for non-sorbing species due to its very small sorption. For rubidium the simulated breakthrough times are very short if compared with the experimental values. Surface sorption is important in this case, but it is not enough to explain the experimental retardation.

For strontium and potassium the experimental breakthrough times are about three times longer than the modelled times. Finally for cobalt the breakthrough times are very long, 29% of the tracer is recovered after 3 600 hours. For this reason the arrival times for the 5% of the tracer are compared. The simulated breakthrough times are very short if compared with the experimental ones.

### Conclusions

It is concluded that the longer experimental times may be caused by several factors acting simultaneously:

- Higher diffusion/sorption in the rock close to the fracture. New data /Byegård et al., 1998/ show higher sorption is higher than the values initially obtained.



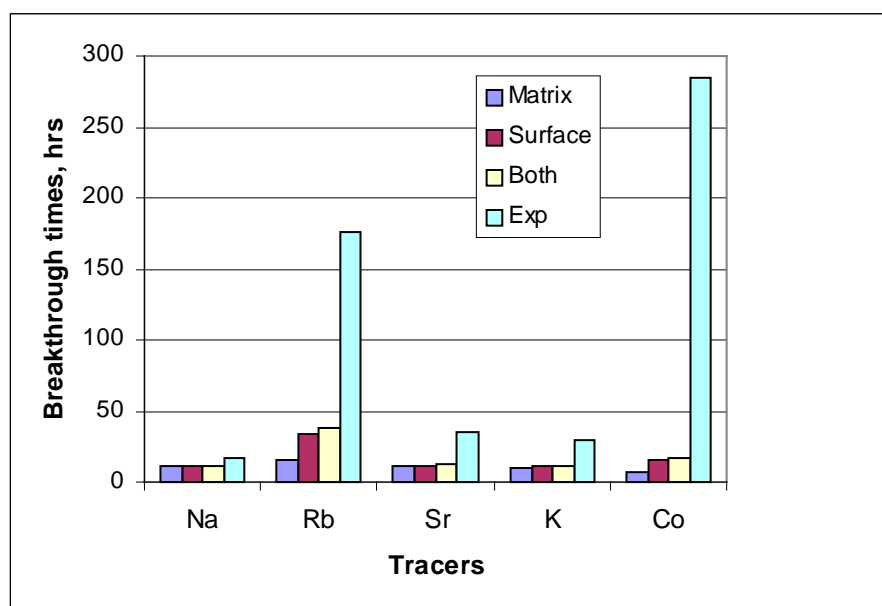


**Figure 3b-41.** Breakthrough times for 50% of injected tracer,  $T_{50}$ . The staples show the simulation results for sorption within the matrix, surface sorption and simulation including both mechanisms.

- Tracer are transported by a smaller water flow rate. This is supported by the drawdowns, hydraulic connections and the large fracture aperture needed to fit residence time.
- Sorption in the fracture surface, filling material, or fault gouge. Some kinetic effect or diffusion resistances are needed to match the breakthrough curves.
- Diffusion into stagnant water may be important if the transport paths are narrow and the fracture aperture large.

## References

**Andersson P, Byegård J, Cvetkovic V, Johansson H, Nordqvist R, Selroos J, Winberg A, 1997.** Experimental plan for tests with sorbing tracers at the TRUE-1 site. Äspö Hard Rock Laboratory PR HRL-97-07, Swedish Nuclear Fuel and Waste Management Co.

**Byegård J, Skarnemark G, Skålberg M, 1995.** The use of some ion-exchange sorbing tracer cations in in-situ experiments in high-saline groundwaters. Mat. Res. Soc. Symp. Proc., vol. 353, pp. 1077–1084.

**Byegård J, Johansson H, Skålberg M, Tullborg E, 1998.** The interaction of sorbing and non-sorbing tracers with different Äspö rock types. Sorption and diffusion experiments in the laboratory scale. SKB TR-98-18, Swedish Nuclear Fuel and Waste Management Co.

**Carslaw H S, Jaeger J C, 1959.** Conduction of Heat in Solids, 2nd Edition, Oxford University Press, pp 396.

- Gylling B, Birgersson L, Moreno L, Neretnieks I, 1998.** Analysis of a long-term pumping and tracer test using the Channel Network Model, *Journal of Contaminant Hydrology*, Vol 32, 203–222.
- Gylling B, Moreno L, Neretnieks I, 1999.** The Channel Network Model – A tool for transport simulation in fractured media, *Groundwater*, 37 (3), 367–375.
- Moreno L, Tsang Y W, Tsang C F, Hale F V, Neretnieks I, 1988.** Flow and tracer transport in a single fracture: A stochastic model and its relation to some field observations, *Water Resources Research*, 24(12), 2033–2048.
- Moreno L, Neretnieks I, 1993.** Fluid flow and solute transport in a network of channels, *Journal of Contaminant Hydrology*, Vol 14, 163–192.
- Moreno L, Gylling B, Neretnieks I, 1997.** Solute transport in fractured media – The important mechanisms for performance assessment, *Journal of Contaminant Hydrology*, 25, pp. 283–298.
- Neretnieks I, 2000.** Revisiting the Advection-Dispersion model. Testing an alternative, Submitted for publication.
- Robinson P C, 1984.** Connectivity, flow and transport in network models of fractured media, Ph. D. Thesis, St. Catherine's College, Oxford University, Ref. TP 1072.
- Winberg A, Andersson P, Hermanson J, Byegård J, Cvetkovic V, Birgersson L, 2000.** Hard Rock Laboratory 2000 : Final report of the first stage of the tracer retention understanding experiments. SKB TR-00-07, Swedish Nuclear Fuel and Waste Management Co.
- Yamashita R, Kimura H, 1990.** Particle-tracking technique for nuclide decay chain transport in fractured porous media, *Journal of Nuclear Science and Technology*, 27, pp 1041–1049.

# Revisiting the Advection-Dispersion model – Testing an alternative

*Ivars Neretnieks,  
Department of Chemical Engineering and Technology,  
Royal Institute of Technology, Stockholm, Sweden*

## Abstract

Some of the basic assumptions of the Advection-Dispersion model, AD-model, are revisited. That model assumes a continuous mixing along the flowpath similar to Fickian diffusion. This implies that there is a constant dispersion length irrespective of observation distance. This is contrary to most field observations. The properties of an alternative model based on the assumption that individual water packages can retain their identity over long distances are investigated. The latter model is called the Multi-Channel model, MChM. Inherent in the latter model is that if the waters in the different pathways are collected and mixed, the “dispersion length” is proportional to observation distance.

Using diffusion theory it is investigated over which distances or contact times, adjacent water packages will keep their identity. It is found that for a contact time of 10 hours, two streams, each wider than 6 mm, that flow side by side, will not have lost their identity. For 1000 hours contact time the minimum width is 6 cm.

The MChM and AD-models were found to have very similar Residence Time Distributions, RTD, for Peclet numbers larger than 3. A generalised relation between flowrate and residence time is developed, including the so-called cubic law and constant aperture assumptions. Using the generalised relation, surprisingly it is found that for a system that has the same average flow volume and average flowrate the form of the RTD curves are the same irrespective of the form of the relation.

Both models are also compared for a system where there is strong interaction of the solute with the rock matrix. In this case it is assumed that the solute can diffuse into and out of the fracture walls and also to sorb on the micro-fractures of the matrix. The so-called Flow Wetted Surface, FWS, between the flowing water in the fracture and the rock is a key entity in such systems. It is found that the AD-model predicts much later arrivals and lower concentrations than does the MCh-model for strongly sorbing solutes.

The conditions are explored for when in-filling particles in the fracture will not be equilibrated but will act as if there was seemingly a much larger FWS. It is found that for strongly sorbing tracers, relatively small particles can act in this way for systems and conditions that are typical of many tracer tests.

Conditions for when uptake into stagnant zones of water in the fracture itself could be important are also explored. It is found that this mechanism can be quite important in fractures with large apertures.

The assumption that the tracer residence time found by cautiously injecting a small stream of traced water represents the residence time in the whole fracture is explored. It is found that the traced stream can potentially sample a much larger fraction of the fracture than the ratio between the traced flowrate and the total pumped flowrate. In some recent field experiments the visually observed fracture apertures indicate that this may well be the case and possibly a more than two times larger fraction of the fracture is sampled than the flow rate ratio would indicate. This of course has an impact on the Flow Wetted Surface the traced stream contacts.

The MCh-model was used to simulate some recent tracer tests in what has been proposed to be a “single” fracture at the ÄSPÖ Hard rock laboratory in Sweden. Non-sorbing tracers, HTO and Uranin were used to determine the mean residence time and its variance. Laboratory data on diffusion and sorption properties were used to “predict” the RTD of the sorbing tracers. It was found that if all the flow occurs in a single fracture, diffusion into stagnant zones of water in the fracture could be 10 to 300 times larger than the uptake into the rock matrix in these experiments. This was also found to give good agreement with the experiments for the non-sorbing and weakly sorbing tracers. For the strongly sorbing tracers it was necessary to invoke a 2–6 times stronger interaction with the material in the stagnant zones than expected. Some reasons for such behaviour are explored.

The transmissivity variance found from the five bore-holes intersecting the fracture where the tracer experiments were made were used to determine the exponent in the generalised relation between aperture and flowrate. The equivalent to the exponent 3 in the cubic law was found to be 1.3–1.6.

It is found that if all the flow takes place in a single fracture its aperture would have to be nearly 3 mm, averaged over the whole feature A. This casts considerable doubt on the assumption that the pumped flow has been collected from a 2-dimensional feature.

## 1 Introduction

It has been increasingly recognised that dispersion is not always Fickian. Compilations of dispersion data show that over a very large range of observation distances, the dispersion length increases with distance. /Lallemand-Barres and Peaudecerf, 1978; Matheron and Marsily, 1980; Neretnieks I, 1981; 1983; 1993; Gelhar et al., 1985/.

It is, however, common practice to use the Advection-Dispersion (AD) equation, with a constant dispersion length, to analyse, simulate, and predict tracer transport in the geosphere. For a given distance the Advection-Dispersion, the Channeling, the Channel Network and probably several other models can be made to adequately describe a tracer breakthrough curve. In the AD-model a constant dispersion length is then typically used. This has some strange consequences. Assume that a dispersion length  $a$  is chosen when simulating the tracer breakthrough curve at distance  $L$  along the flowpath. The commonly used analytical solutions have been obtained based on the assumption that  $a$  is constant all along the path. With the same solution the tracer breakthrough curve also at, say a distance  $L/10$  along the flow path could be predicted. This, however, is in violation of the observations that at distance  $L/10$  the dispersion length is  $a/10$ . A different breakthrough curve, would then be predicted if  $a/10$  was to be used to make

predictions for the distance  $L/10$ . It may thus be concluded that the common analytical solution(s) based on a constant  $a$  cannot give a correct representation of the transport along all the flowpath.

Consider an alternative approach. Assume that  $a$  increases with distance from the point where the tracer is injected. This is readily incorporated in numerical schemes that solve the Advection-Dispersion equation. Some difficulties arise, however. To begin with the  $a$ -value(s) to use cannot be taken from the literature because these were evaluated using the equations which are based on  $a$  being independent of distance. This is probably a minor problem because data can be re-evaluated or a relation can probably be found by which the old  $a$ 's can be transformed into the new, distance dependent,  $a$ 's.

Using simulations with the distance dependent  $a$ 's for reacting tracers gives strange effects. Consider a case where a solute that enters at point A reacts with the solute which enters at point B, somewhere downstream. Should different  $a$ 's be used for the two solutes in the same point because solute 1 has travelled the distance  $L_1$  and solute 2 has travelled  $L_2$ ? What value of  $a$  should the reaction product have in a point along the flowpath? Another difficulty which has been encountered is when a solute flows through a porous medium, reacts with a stationary component to form a product P, which then is transported onward. Not only is it indeterminate what  $a$  to choose for P, and how to vary  $a$  along the path, but also if P should be allowed to move "upstream" by Fickian dispersion/diffusion. For a constant  $a$ , if there is no P at the "inlet" to the flowpath and the Peclet number  $L/a$  is small, which means that dispersive transport is important compared to advective transport, P would disperse upstream. This is mostly not the case.

The problems seem to become more pronounced when multiple solute transport and reactions are involved. Then it is very unclear what assumptions are reasonable regarding  $a$ . All programs (codes), known to the author, which couple transport and chemical reaction inherently use the assumptions that  $a$  is constant, independent of distance although some codes can mimic a time or distance dependent  $a$ .

The AD model must be used with caution and afterthought, if at all. Alternative models which challenge the basic assumptions of the AD model and which satisfactorily handle the above issues must be developed.

There are known geometrical structures that have the property that the residence time distribution will give a dispersion length that increases with distance observation distance. Systems with independent pathways /Neretnieks I, 1981; 1983/ have been used to model the transport of non-reactive and reactive solutes. Systems with self-similar structures have also been shown to have the desired property, /Schweich, 1993/. They have so far been sparingly studied for flow and transport in fractured media but there are observations that fractures have self- similar properties /Turcotte, 1997/.

## 2 Channelling model

In the channelling model that is presented below it is assumed that flowpaths keep their identity along all the flow path. They mix only when collected together in e.g. a well. Some properties of the model have been explored previously /Neretnieks I, 1983;

Chesnut, 1994/. The model has also been used to analyse laboratory /Neretnieks et al., 1982; Moreno et al., 1985/ as well as field experiments /Abelin et al., 1991a; 1991b; Chesnut, 1994/.

For this type of channelling model to be reasonably applicable the mixing by diffusion between two adjacent channels should be small. Diffusional mixing can be estimated to barely mix two channels if their widths are larger than  $2.2(D_w t)^{0.5}$ , where  $D_w$  is the diffusivity in water and  $t$  is the contact time /Carslaw and Jaeger, 1959/. For a contact time of 10 (1000) hours, channels larger than 6 (60) mm will essentially retain their identity. In many field experiments it can be expected that this condition is fulfilled.

In a system with a multitude of independent channels with a flowrate distribution  $f(q)$  where each channel will have an effluent concentration that varies in time  $c(q,t)$ , the effluent concentration from the system when waters from all channels are mixed is

$$\frac{c}{c_o} = \frac{1}{\bar{q}} \int_0^{\infty} f[q]c[q,t]q dq \quad (1)$$

In the application of the model in this paper a log-normal distribution is used for  $f[q]$  and a previously developed model for flow in a single channel where the solute is subject to matrix diffusion and diffusion into stagnant zones of water is used for  $c[q,t]$  /Neretnieks I, 1980/. The solute can also sorb in the matrix and in in-fill in the channels as well as in the stagnant zones /Neretnieks I, 1980; Neretnieks and Rasmuson, 1984/. For a Heaviside pulse input it is

$$c(q,t) = \frac{MG}{q^2 \sqrt{\pi}} \frac{e^{-\frac{G^2}{q^2(t-R_a t_w)}}}{(t-R_a t_w)^{3/2}} \quad (2)$$

$$G = \int_0^L (Wz \epsilon_p \sqrt{D_p R} + \delta z \epsilon_{sw} \sqrt{D_{sw} R_{sw}}) dz \quad (3)$$

$G$  accounts for matrix diffusion and sorption in the matrix over the Flow Wetted Surface  $LW$  (first term) and diffusion and sorption in the stagnant zones adjacent to the flowing channel (second term). The  $R$ 's are the retardation factors in the matrix and the in-fill in the flowing channel ( $a$ ) and in the in-fill in the stagnant zones ( $SW$ ). It will be found that the latter effect can dominate over the matrix diffusion.

There remains to define a relation between the flowrate in a channel and the velocity or residence time in order to use the model. In this paper a generalised model is used, that includes the so-called cubic law as one special case but also the cases of constant channel aperture and channels with in-fill that determine the pressure drop. For a log-normal flowrate distribution and with  $q=k\delta^n$  the relation between residence time and flowrate in a channel is  $n$  is 3 for the cubic law,  $n=0$  for constant aperture channels and  $n \rightarrow \infty$  for a channel in-filled with small particles. Surprisingly, for a system with a given mean residence time and variance in residence time (first and second moments equal), the residence time distribution in the system was found to be independent of  $n$ .

$$t_w = \frac{1}{R_a} \left( q \left( Ve^{-\frac{\mu}{n} - \frac{\sigma^2}{2n^2}} \right)^{-\frac{n}{-1+n}} \right)^{\frac{1-n}{n}} \quad (4)$$

Equations (1)–(4) define the MCh-model as it was used to interpret some recent field experiments.

### 3 Field experiments and interpretation

These tests were performed in deep lying rocks. A wealth of background information and results from supporting laboratory investigations is available. The tests are described in detail in /Winberg et al., 2000/. Laboratory and other background data are reported in /Byegård et al., 1998/.

The tests were performed in a well-characterised fracture in the Äspö hard rock laboratory. The fracture, feature A, is located more than ten meters from a drift at about 400 m below the ground. Five boreholes intersect feature A. Cores were investigated and the holes were inspected using a high-resolution bore hole camera. The feature consists of one or a few open fractures. The open parts of the fracture probably contained some in-fill but this has been washed away during drilling. The visible aperture is less than one mm.

The boreholes were used to characterise the feature hydraulically and for injecting tracers and for recovering them by pumping in one hole. Converging and dipole tests were made. The converging tests had full recovery of the non-sorbing tracers.

In the tests a mixture of non-sorbing and sorbing tracers was injected during 4 hours in a packed off section. Water passing this section carried the tracer into the fracture. The collection took place in another borehole about 5 m distant where the pumping rate was 24 litres per hour. This ensured essentially a converging flow field. After the injection the injection section was cleaned of tracer by exchanging the water. However, there were still tracers in and adjacent to the injection section. The remaining tracers were also slowly entering into the flow field by the water passing the injection section. The concentration in the injection section was monitored. The total mass of injected tracer is determined by assuming that the injection flowrate is constant over time and that the total mass injected is the integral of the product of the concentration in the injection section and the average injection flowrate. The injection flowrate was about 0.2% of the pumping flowrate. Non-sorbing (HTO and Uranin), weakly sorbing (Ca, Na and Sr) as well as strongly sorbing tracers (Ba, Cs and Rb) were used.

The non-sorbing tracer breakthrough curves were used to assess the water residence time and variance. These were found to be 8 hours and to have a variance corresponding to a Peclet number of 3. The flow aperture was found to be about 3 mm. These values were used for all other tracers. Laboratory data on matrix diffusion and sorption properties were used in predictive simulations of the sorbing tracers. These simulations consistently showed a much to low tracer interaction along the flowpath than the

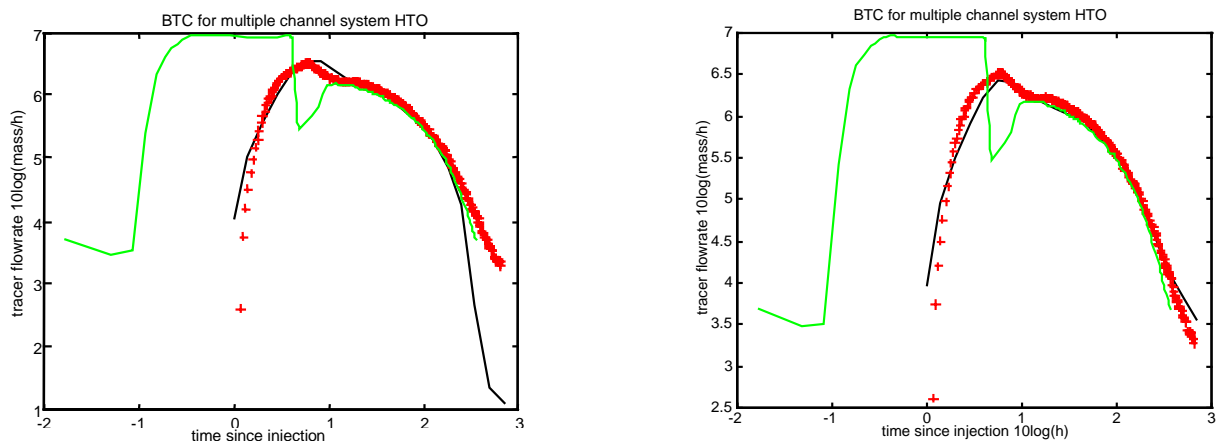
experimental results. If only matrix diffusion and sorption are assumed to be the dominating mechanisms for solute interaction, a FWS 30–40 times larger or a porosity, sorption coefficient or pore diffusivity 1000 times larger than thought would be needed to obtain agreement between field and simulated Break Through Curves (BTC). Very similar results are obtained when the AD-model is used instead of the MCh-model.

If account is also taken of diffusion into stagnant zones adjacent to the flowpaths, the non-sorbing tracer results agree fairly well when diffusion into one or two pathways in contact with stagnant water are invoked. Then there is no need to invoke any increase in the transport parameters for matrix diffusion.

For the sorbing tracers diffusion into the stagnant zones must be accompanied by sorption onto in-fill there to account for the observed effects. Even so, more than one flowing pathway in contact with stagnant zones must be invoked. Typically 1–2 pathways are needed for the non-sorbing, 2–4 for the weakly sorbing and 4–6 for the strongly sorbing if an in-fill porosity of 0.5 is assumed. This is shown in Figures 3b-42–3b-45.

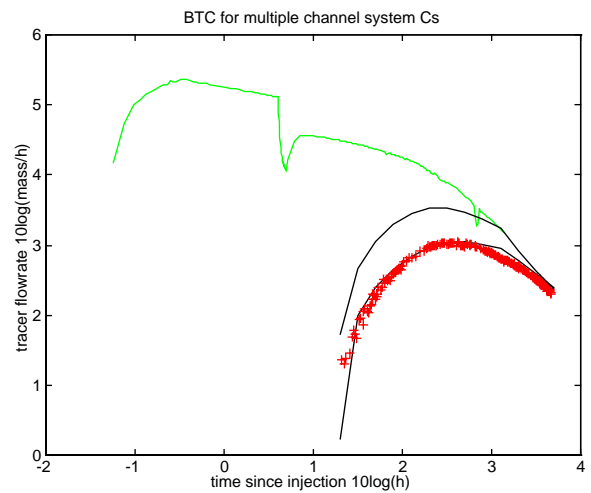
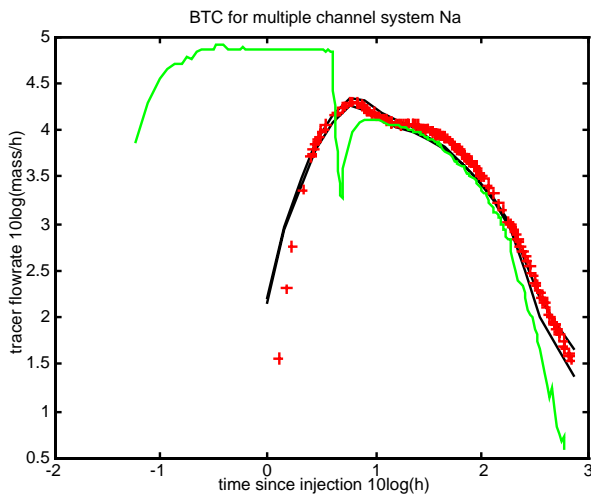
Several other reasons that might cause large interaction along the flowpath were also investigated. One is the rate of sorption in in-fill particles in the flowpath. For highly sorbing solutes even small particles may not have equilibrated over typical times, days to weeks, used in laboratory measurements. An analysis of the laboratory sorption data /Byegård et al., 1998/ showed that even the smallest particles used in the sorption experiments would not have had time to equilibrate to more than about 1/3 for the strongly sorbing tracer Cs. However, such an underestimate is far from sufficient to explain the discrepancy of about a factor 1000.

Another possible reason for underestimating the interaction is caused by the injection procedure. The very small injected flowrate, about 0.2% of the total flowrate, would ideally be in contact with the same proportion of the total surface of the flowpath that the pumping flowrate contacts. However, because the width of the injection flowrate is about the same as the diameter of the injection borehole, the injection stream will spread out to at least twice the width, probably much more. This would have two effects.



**Figures 3b-42 and 3b-43.** HTO. Input curve (grey) and BTC. Flowrate of tracer Log Bq/h versus log time. Experiments “+”. Black lines, simulated curves. Only Matrix Diffusion, left Figure 3b-42. Also diffusion into stagnant zones with 2 pathways, right Figure 3b-43.





**Figures 3b-44 and 3b-45.** Input curve (grey) and BTC. Flowrate of tracer Log Bq/h versus log time. Experiments +. Fitted curves, black lines. Left figure Na with 2 and 4 pathways. Right figure Cs with 2 and 6 pathways, lower curve.

The stream would be in contact with a larger FWS and would thus have a proportionally larger interaction with the matrix than what the basic model assumes. It is not conceivable that this effect would be as large as the needed increase of 30–40 in the FWS needed.

The other effect is that a larger number of separated pathways could form in the heterogeneous fracture. This would give the desired multiple paths needed for a larger contact with stagnant water zones.

## 4 Discussion and conclusions

Waters even in rather narrow channels can keep their identity over long distances and travel times. This implies that there may be little mixing along the pathways. This is contrary to the basic assumptions underlying the AD-model.

The simple concept of the MCh-model, has been used to study the impact of some processes that affect the residence time distribution of tracers. Surprisingly it was found the relation between the flowrate and the residence time in the channels did not affect the overall form of the RTD. This was found to apply for non-interacting as well as for strongly sorbing tracers.

Diffusion into the stagnant water zones with fault gouge in the fracture can contribute considerably to the diffusional withdrawal of tracer from the flowing water. This mechanism is identical from the mathematical point of view to the uptake into the rock matrix. In fractures with large apertures it can totally dominate over the matrix uptake.

The above mentioned effects were found to be noticeable and even prominent in a set of field experiments that were analysed. The flowpaths were then assumed to all be in a single fracture. The BTC's could not be interpreted using only matrix diffusion as the interacting mechanism. Uptake into the stagnant zones totally dominated the solute behaviour. This effect could well account for the behaviour of the non-sorbing and weakly sorbing tracers. For the strongly sorbing tracers it had the same effect as if they had access to two to six times as many pathways as the non-sorbing.

Such behaviour is expected if there were several pathways that the traced water follows. If the pathways are close to each other, non-sorbing tracers could mix by diffusion between the pathways, whereas sorbing tracers could be retarded in their sideways diffusion in the in-fill. The sorbing tracer pathways would then keep their identity.

The value of the exponent  $n$  in the generalised relation  $q=k\delta^n$  was estimated from data on the measured transmissivities assuming that the flowrate distribution follows that of the transmissivity distribution. The transmissivities in five boreholes were evaluated using different techniques. The exponent  $n$  was found to be 1.3–1.6. For the cubic law case it would be 3.

The present analysis gives some circumstantial evidence that stagnant zones may play an important role. However, there is a definite need to actually find field evidence that multiple paths form as well as evidence for the presence of sorbing in-fill in the stagnant zones.

It is found that if all the flow takes place in a single fracture its aperture would have to be nearly 3 mm, averaged over the whole feature A. Such large fracture apertures extending over large areas, more than 70 m<sup>2</sup>, are not known to exist. This casts considerable doubt on the assumption that the pumped flow has been collected from a 2-dimensional feature. As there is evidence that there is a multitude of fractures in the region and that these are connected in 3-dimensional space alternative interpretations should be attempted.

A simple scoping calculation shows that if the flow takes place in a 3-dimensional network of channels instead of being limited to a single fracture, a fracture spacing of about 1 m is sufficient to supply sufficient FWS for tracer uptake into the rock matrix to agree with the experimental break through curves. Then no uptake into stagnant zones or other diffusion enhancement is needed to predict the observed break through curves. A much more reasonable fracture aperture of about 0.1 mm is also obtained for this case.

## Notations

$c$	Concentration
$c_o$	Concentration at inlet
$D_p$	Pore diffusion coefficient
$D_w$	Diffusion coefficient in water
$G$	Materials and flow path property group (Equation 3)
$L$	Length of flowpath
$M$	Tracer mass injected
$N$	Exponent in generalised flowrate-aperture: relation $q=k\delta^n$

$q$	Flowrate
$R$	Retardation coefficient for rock matrix
$R_a$	Retardation coefficient for in-fill in flowpath
$R_{sw}$	Retardation coefficient for in-fill in stagnant zone
$t$	Time
$t_w$	Residence time of water in flowpath
$V$	Flowpath volume
$W$	Width of flowpath
$z$	Distance along flowpath
$\alpha$	Dispersion length
$\delta$	channel aperture
$\epsilon_p$	Porosity of rock matrix
$\epsilon_{sw}$	Porosity in stagnant zones
$m$	Log mean flowrate
$\sigma$	Standard deviation of log flowrates

## Acknowledgements

The support of the Swedish Nuclear Fuel and Management Co, SKB is gratefully acknowledged. Discussions with many of those involved in the tracer experiments notably, Olle Olsson, Anders Winberg, Peter Andersson, Johan Byegård, Vladimir Cvetkovic, Lars Birgersson and Luis Moreno have greatly contributed to the forming of this report. The work was performed at Oxford University, where the author enjoyed the Christensen Fellowship at St. Catherine's College during Michaelmas term 1999.

## References

- Abelin H, Birgersson L, Gidlund J, Neretnieks I, 1991a.** A Large Scale Flow and Tracer Experiment in Granite I. Experimental Design and Flow Distribution. *Water Resources Research*, 27, p 3107–3117.
- Abelin H, Birgersson L, Moreno L, Widén H, Ågren T, Neretnieks I, 1991b.** A Large Scale Flow and Tracer Experiment in Granite II. Results and interpretation. *Water Resources Research*, 27, p 3119–3135.
- Byegård J, Johansson H, Skålberg M, Tullborg E-L, 1998.** The interaction of sorbing and non-sorbing tracers with different Äspö rock types. Sorption and diffusion experiments in the laboratory scale. SKB TR 98-18, Swedish Nuclear Fuel and Waste Management Co.
- Carslaw H S, Jaeger J C, 1959.** Conduction of heat in solids, 2nd ed. Oxford University Press.
- Chesnut D A, 1994.** Dispersivity in heterogeneous media. Lawrence Livermore National Laboratory, UCRL-JC-114790 January 1994. daches@earthlink.net.

- Gelhar L W, Mantoglou A, Welty C, Rehfeldt K R, 1985.** A review of field scale physical solute transport processes in saturated and unsaturated media, EPRI EA-4190S.
- Lallemand-Barres A, Peaudecerf P, 1978.** Recherche des relations entre la valeur de la dispersivité macroscopique d'un milieu aquifère, ses autres caractéristiques et les conditions de mesure, Bull. BRGM (2) III, 4, 277.
- Matheron G, de Marsily G, 1980.** "Is transport in porous media always diffusive? A counterexample". Water Resources Res. 6, p. 90.
- Moreno L, Neretnieks I, Eriksen T, 1985.** Analysis of some laboratory tracer runs in natural fissures, Water Resources Res. 21, p 951–958.
- Neretnieks I, 1980.** Diffusion in the rock matrix: An important factor in radionuclide retardation? J. Geophys. Res. 85, p 4379–4397.
- Neretnieks I, 1981.** Prediction of radionuclide migration in the geosphere. – Is the porous flow model adequate? International symposium on migration in the terrestrial environment of long-lived radionuclides from the nuclear fuel cycle; IAEA symposium, Knoxville, Tennessee, USA, July 1981, IAEA – SM – 257/49, p 635–657.
- Neretnieks I, 1983.** A note on fracture flow mechanisms in the ground, Water Resources Res. 19, p. 364–370.
- Neretnieks I, 1993.** Solute Transport in Fractured Rock – Applications to Radioactive Waste Repositories. Chapter 3 . Ed Bear J., de Marsily G., Tsang C-F. Academic Press p 39–127.
- Neretnieks I, Eriksen T, Tähtinen P, 1982.** Tracer movement in a single fissure in granitic rock: Some experimental results and their interpretation. Water Resources Res. 18, p 849.
- Neretnieks I, Rasmuson A, 1984.** An approach to modelling radionuclide migration in a medium with strongly varying velocity and block sizes along the flowpath. Water Resources Res., p 1823–1836. 1984
- Schweich D, 1993.** Transport of linearly reactive solutes in porous media. Basic models and concepts. In Migration and fate of pollutants in soils and subsoils. Ed. Petruzzelli D. and Helfferich F.G. NATO ASI series, Vol G 32. p 221–245, Springer Verlag.
- Turcotte D L, 1997.** Fractals and Chaos in Geology and Geophysics, Cambridge University Press, 2nd Ed.
- Winberg A, Andersson P, Hermanson J, Byegård J, Cvetkovic V, Birgersson L, 2000.** Final report of the first stage of the tracer retention understanding experiments. Äspö Hard Rock Laboratory, SKB TR-00-07, Swedish Nuclear Fuel and Waste Management Co.

# **Session 3c**

## **Related studies**

# Contents

	Page
<b>Session 3c Related studies</b>	
The Moderately Fractured Rock experiment: Background and overview	137
Anisotropy, reversibility and scale dependence of transport properties in single fracture and fractured zone – Non-sorbing tracer experiment at the Kamaishi mine	151
The TRUE Block Scale experiment – A status report	165

# The Moderately Fractured Rock Experiment: Background and overview

*M R Jensen,  
Ontario Power Generation*

## Abstract

The Moderately Fractured Rock (MFR) experiment is conducted at Atomic Energy of Canada Limited's Underground Research Laboratory (URL) as part of Ontario Power Generation's Deep Geologic Repository Technology Program. The MFR experiment was initiated in the mid-1990's with the purpose of advancing the understanding of mass transport in MFR (fractures  $1-5 \text{ m}^{-1}$ ,  $k \approx 10^{-15} \text{ m}^2$ ) in which groundwater flow and solute migration occurs through a network of interconnected fractures. The experimental program has involved a series of multi-well forced gradient tracer tests at scales of 10–50 m within a  $\approx 100,000 \text{ m}^3$  volume of MFR accessed from the 240 m level of the URL. The tracer tests conducted with non-reactive, reactive and colloidal tracers have served to explore the applicability of continuum models for prediction of groundwater flow and mass transport. Recently, a Modeling Task Force was created to re-examine tracer test experimental methodologies, MFR flow and transport conceptual models and provide a broader forum in which to apply alternative dual-permeability, discrete fracture and hybrid mathematical codes for flow system analysis. This paper provides a description of the MFR experiment, preliminary research findings and plans for the future.

## 1 Introduction

The prediction of mass transport in fractured crystalline rock settings is complicated by the spatial variability of physical and chemical properties within the flow domain. As a consequence, the development of a technically defensible Safety Assessment (SA) requires that confidence in methods used to characterise and predict geosphere barrier performance be demonstrated. It is within this context that the Moderately Fractured Rock (MFR) Experiment was undertaken at Atomic Energy of Canada Limited's (AECL) Underground Research Laboratory (URL) (Figure 3c-1). The primary purpose of the MFR experiment is to demonstrate predictive numerical modeling capabilities and assess the validity of the Equivalent Porous Media (EPM) approximation for flow and mass transport in porous-fractured media. Further, the experiment is used to illustrate the derivation and uncertainty in effective geosphere transport properties, a critical issue associated with justification of parameter input to simplified SA models.

The MFR experiment was initiated in 1993 and is comprised of two stages: i) MFR groundwater flow domain characterisation; and ii) non-reactive/re-active/colloid tracer tests and numerical simulation. Stage I activities involved the excavation of drifts to access the  $\approx 100,000 \text{ m}^3$  MFR test area and the drilling and instrumentation of 10 bores for

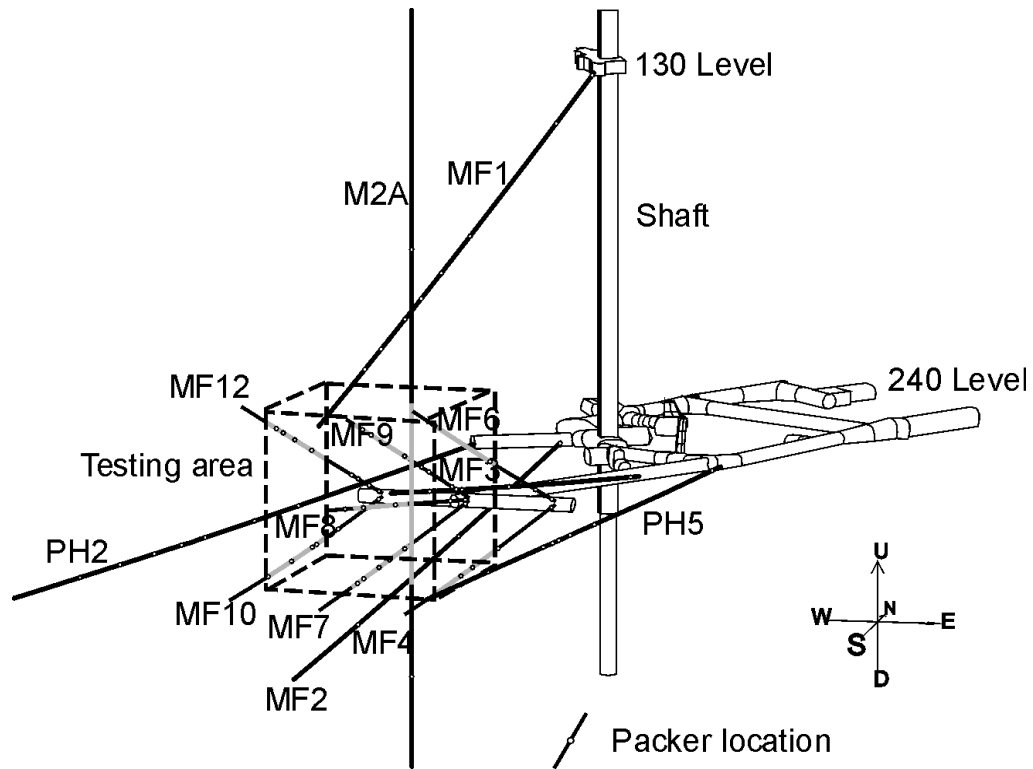


**Figure 3c-1.** Moderately Fractured Rock Experiment: Underground Research Laboratory flow domain and instrumented borehole network.

characterisation purposes. Characterisation activities were multi-disciplinary including the integration of geologic, geophysical, hydrogeochemical and hydrogeologic data into a conceptual flow system model (Frost et al., 1998). This conceptual understanding of the MFR flow domain has served to allow 3-dimensional numerical simulation of a series of forced gradient, multi-well tracer experiments. These experiments have furthered the understanding of the effect of flow system heterogeneity and anisotropy on advective-dispersive-diffusive transport in fracture networks. Recently, Ontario Power Generation (OPG) created a MFR Modeling Task Force to broaden the understanding of processes and mechanisms that influence mass transport in MFR, to re-examine tracer test methodologies to facilitate post-test analysis, and to allow application of alternative numerical models to simulate flow and transport in MFR. The Task Force and a series of renewed tracer experiments are a new initiative in the MFR experiment planned into 2003.

This paper provides an overview of the MFR experimental program. Abbreviated descriptions of key aspects in the program are described with cited references for readers requiring more detail. The focus of the paper is on the evolution of the MFR experiment that, in particular, has revealed the importance of integrated conceptual flow and transport model development. This recognition has led to an increased role for application of alternative numerical methods in the MFR program, and peer review in developing a common understanding of the process and mechanisms most influencing solute transport in complex interconnected fracture systems.



## 2 Moderately Fracture Rock Experiment: Stage I

### Flow domain characterisation

The characterisation of the MFR flow domain involved a multi-disciplinary approach over a 4-year period ending in late 1997. The period of characterisation involved excavation of the access drifts and a phased drilling program in which 10 (MF-series) well bores either intersecting or bounding the MFR flow domain where instrumented (Figure 3c-1). Characterisation activities included litho-structural mapping /Everitt et al., 1995/, fracture mineral characterisation /Ejeckham, 1997/, conventional and nuclear geophysical logs, single and cross-hole seismic and radar tomography surveys, hydro-geochemical sampling and multi- and single well hydraulic testing. These data were integrated into a conceptual model of the flow domain as described by Frost et al. /1998/.

The MFR flow domain is contained within a volume of 60 m x 50 m x 50 m on the URL 240 m level. A fence diagram depicting the 3-dimensional geometry of principal litho-structural features is shown in Figure 3c-2. The rock mass within the flow domain is comprised primarily of fractured leucocratic and gneissic granites. The key structural

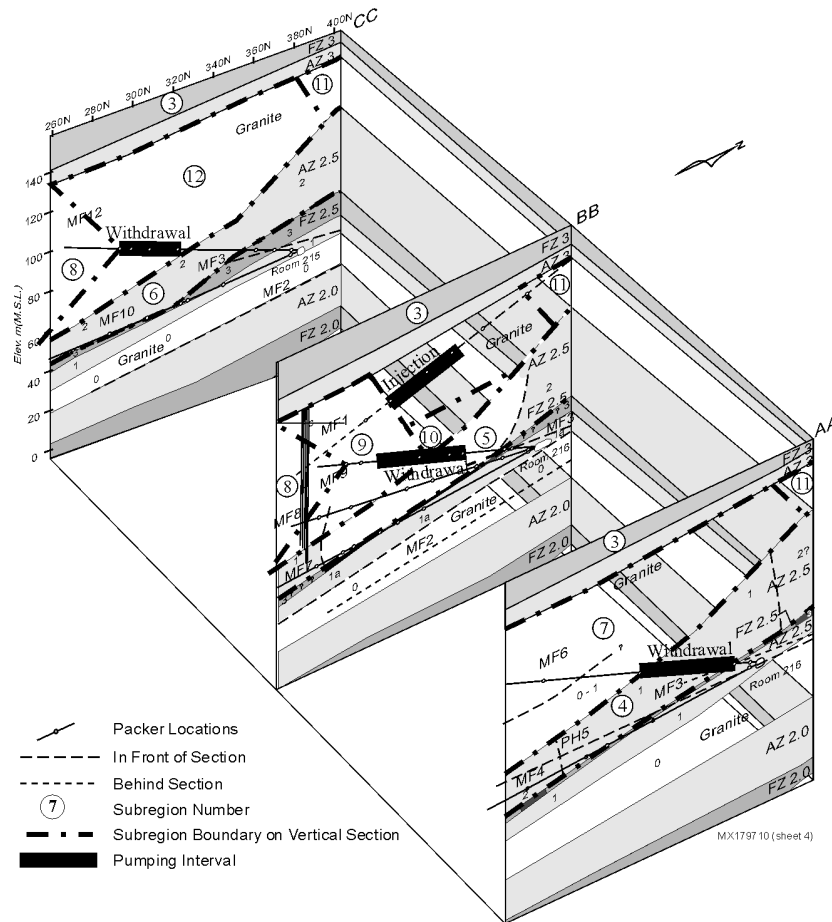


**Figure 3c-2.** Moderately Fractured Rock Experiment: Flow Domain Geometry – Litho- Structural Domains (Sub-region numbers denote numerical model domains).

feature is Fracture Zone (FZ) 2.5, a sub-horizontal thrust fault that transects the flow domain. Shear fractures within FZ 2.5 exhibit slickensides (point-loads) and dilatational gaps that infer a structural control and channeling of permeability within the FZ plane. Vertically, FZ 2.5 divides the flow domain into distinct fracture domains. Within the footwall (below), two subvertical fracture sets extending from the base of FZ 2.5 are evident (Fracture Domain C). Within the hanging wall (above), 3 sub-vertical fracture sets are distinguished (Fracture Domain B), which cross cut FZ 2.5. Examination of fracture mineral assemblages within the two fracture domains provides evidence of active and more prolonged groundwater-rock interaction within the hanging wall. This contention was found consistent with hydrogeochemical data.

As part of the MFR characterisation program, multi-level packer systems were installed into each of the MF-series bores. The packer string design was guided primarily by core log fracture frequency and measurements of wellhead water outflow recorded during drilling (i.e. indicates intersection with transmissive feature). A single hydraulic line accesses each interval to permit hydraulic testing and hydraulic head monitoring. Selected tracer injection and withdrawal intervals were equipped with two hydraulic lines to allow tracer circulation. These intervals were further fitted with volume reducers to minimize equipment tracer residence time and well bore mixing.

Hydraulic testing within the instrumented bores reveal, perhaps not surprisingly given moderate hydraulic diffusivities, that the MFR test area is hydraulically well connected. Single well response tests ( $n = 70$ ) yielded transmissivities ranging between  $3 \times 10^{-13}$  and  $1 \times 10^{-6} \text{ m}^2 \text{ sec}^{-1}$ , with those reported in the footwall typically less than  $1 \times 10^{-8} \text{ m}^2 \text{ sec}^{-1}$ .

Hydraulic heads within each of nearly 70 multi-level intervals to estimate hydraulic boundary conditions and gradients fields were initially monitored with 0–3500 kPa vibrating wire transducers attached to an Underground Data Acquisition System (UDAS). Later, manometer tubes connected to selected transmissive intervals were installed within the URL access shaft to improve the accuracy and precision of head measurements, a problematic issue in high pressure ( $\approx 2 \text{ MPa}$ ), low gradient flow systems. The use of manometer standpipes altered the understanding of gradients within the MFR flow field and, in particular, aided interpretation of hydraulic interference by URL drawdown. Further, this approach has permitted flow system boundary conditions to be defined more confidently.

Frost et al. /1998/ describes the conceptual flow model for the MFR domain. Development of the model focused, in part, on identifying regions within the flow domain favourable for tracer testing. Estimates of low transmissivities within the footwall implied the existence of large drawdowns in tracer experiments (scale 10–50 m) during reasonable periods of time and space. The heterogeneous and anisotropic nature of FZ 2.5 fracturing was determined to unnecessarily complicate tracer test analysis and interpretation and thus, was purposely avoided. As a consequence, the focus for the tracer experiments became the MFR hanging wall (Fracture Domain B) in which the fracture framework homogeneity and moderate permeabilities existed.

### 3 Moderately Fractured Rock experiment: Stage II

The following four sections provide a description of MFR Stage II activities. These activities have included the design and execution of 3 TT-series tracer experiments, pre- and post-test deterministic predictive modeling, geostatistical flow and transport analyses and more recently, creation of a MFR Modeling Task Force.

#### ***Tracer Test (TT-series) experiments***

A series of tracer test (TT) experiments involving non-reactive, reactive and colloidal tracers was initiated as part of MFR activities in mid-1998. Frost et al. /1998/ and, more recently, Vandergraaf et al. /2000/ provide details of the experimental design and analyses.

The TT-series experiments were conducted as multi-well steady state forced gradient non-recirculating tests. Specific tracer injection-withdrawal intervals were selected on the basis of the homogeneity of MFR conditions and fracture interconnectivity as determined through hydraulic testing. Individual test intervals were approximately 30–40 m in length with separation distances of 13 to 50 m. Interval test configurations varied with a single injection point and 1-3 withdrawal intervals. An example of a 4-interval test configuration used in test TT2 is shown in Figure 3c-2. Injection and withdrawal rates were typically set to a total accumulative rate of  $1 \text{ L min}^{-1}$  with resultant hydraulic gradients between injection-withdrawal intervals of unity or less. Tracer solutions were comprised of a mixture of alkali metals (LiBr, RbI), Lissamine FF and fluorescent latex colloids (0.19, 0.22 and  $0.56 \mu$ ). Ticknor and Vandergraaf /1998/ describe the results of batch sorption experiments with the alkali metals. Simultaneous tracer injections were a Dirac input with peak breakthroughs for unretarded species occurring at approximately 6 to 16 days. Tracer data collection ceased once i) background or analytical detection levels were approached; ii) further tracer recovery would not materially contribute to the total mass recovery; or iii) the potential to detect multiple peaks (i.e. tracer pathways) had diminished. This typically required 2 months.

Type normalized breakthrough curves are shown for tests TT2 and TT3 in Figures 3c-3 and 3c-4. The results reveal a skewed single peaked tracer breakthrough. In one example, TT3 (Figure 3c-4), evidence of a second ‘peak’ tracer arrival exists at approximately 20 days. Tracer breakthroughs were observed for Br, I, Li and Lissamine FF. Interestingly, batch sorption experiments had indicated that Li was selectively sorbed on illite-montmorillonite and that its retardation may indicate the presence of clays along fracture pathways. Although mass loss is implied by the TT2 breakthrough (Figure 3c-3), the similarity with the conservative Br arrival suggests Li migration occurred without significant retardation. The strongly sorbed Rb was not observed at any withdrawal point. Perhaps more surprisingly, fluorescent colloids were not detected at any of the withdrawal intervals suggesting effective filtration with the fracture network. Mass recoveries for conservative ions did not exceed 30%. This, in part, is symptomatic of divergent flow fields developed during the experiments, which promotes tracer dispersal within large volumes of the flow domain. This aspect of the TT-series experiments is being re-examined to reaffirm experiment scale, tracer concentrations, test interval configurations and applicability of divergent or convergent flow fields to tracer testing. As part of this re-assessment, a specific focus will be placed on improving the tracer test design to facilitate post-test analysis and transport parameter derivation.

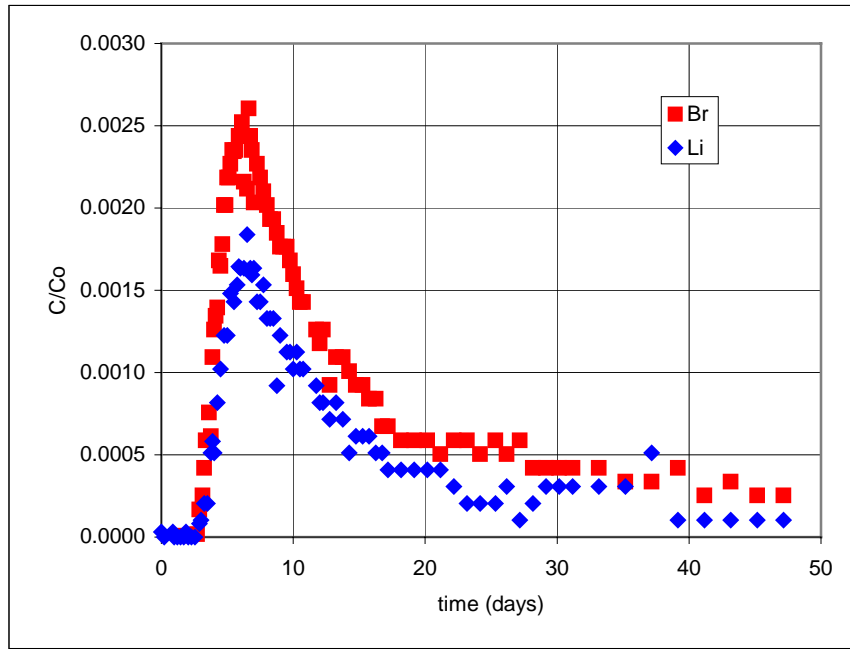


**Figure 3c-3.** Moderately Fractured Rock Experiment: Normalized breakthrough curve for Br and I at interval MF 9-3 in experiment TT2.

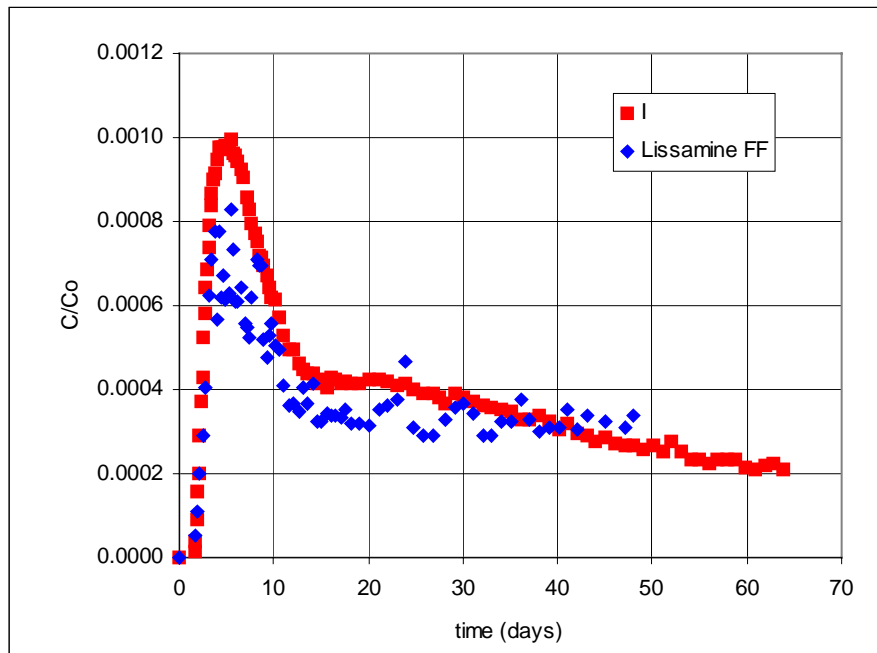


**Figure 3c-4.** Moderately Fractured Rock Experiment: Normalized breakthrough curve for I and Lissamine FF at interval MF 12-5 in experiment TT3.

### **Deterministic analysis**

Numerical simulation of flow and mass transport within the MFR flow domain was performed using the 3-dimensional finite element code MOTIF. The finite mesh was discretized through a volume of 360 m x 380 m x 200 m centered on the MFR flow domain using approximately 18,000 3-dimensional and ‘pipe’ elements (Figure 3c-5). Discretisation was conducted through matching the geometry of 17 fracture sub-regions and intersecting MF-series bores. Grid boundaries were made coincident with fracture zones, alteration zones or at distances assumed unaffected by MFR experimental activities (i.e. hydraulic perturbations). Refinement and calibration of the flow model was achieved through a manual iterative process in which differences between observed and predicted steady-state pump test drawdowns were minimized. Frost et al. /1998/ and Vandergraaf et al. /2000/ describe specific details of the flow model development and calibration.

In applying the calibrated MFR flow model to the TT-series experiments, pre-test predictions were conducted to aid tracer test design and yield ‘blind’ quantitative results for comparison with tracer experiments. Typical results illustrating the geometry and concentration distributions within an evolving tracer plume for multi-well experiment TT2 are shown in Figure 3c-6. As part of completing pre-test predictions, sensitivity analyses were also completed to assess the influence of topographic and density gradients on tracer breakthrough. Comparison of pre-test and observed breakthrough for conservative elements Br and I demonstrate the complex nature of mass transport in fracture networks and need for a carefully reasoned experimental design. While simulations of flow with the single continuum approach appear reasonable, estimates of advective-dispersive-diffusive (AD) transport are more uncertain. This recognition, in part, stems from the anisotropic and heterogeneous nature of the fracture network in which ‘accurate’ characterisation of porosity and permeability distributions is problematic. The non-uniqueness inherent in model derived geometries and parameter distributions should ideally be bound to best support Performance Assessment. Alternative and complementary modeling tools that may enable this are being pursued.

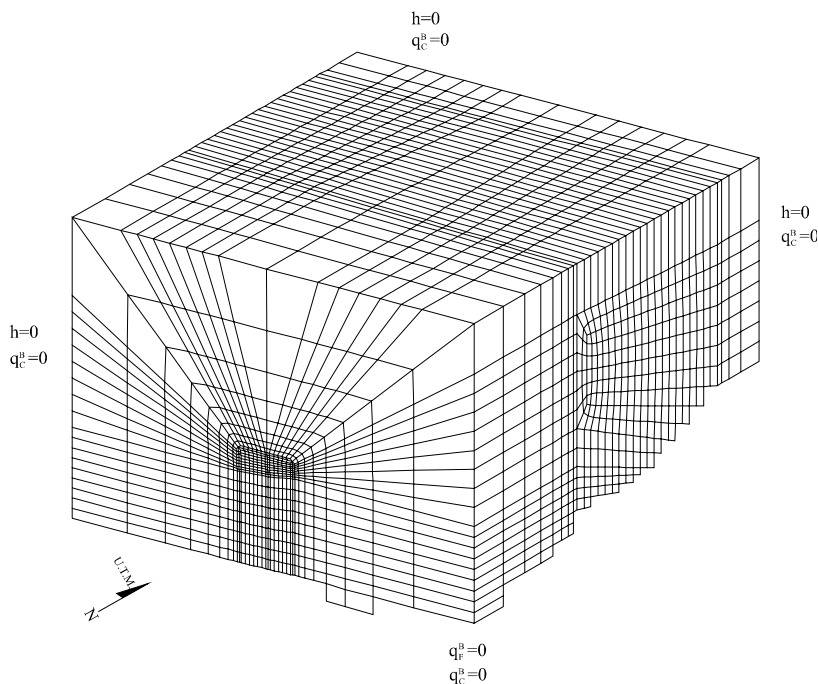


**Figure 3c-5.** Moderately Fracture Rock Experiment MOTIF Finite Element Mesh.

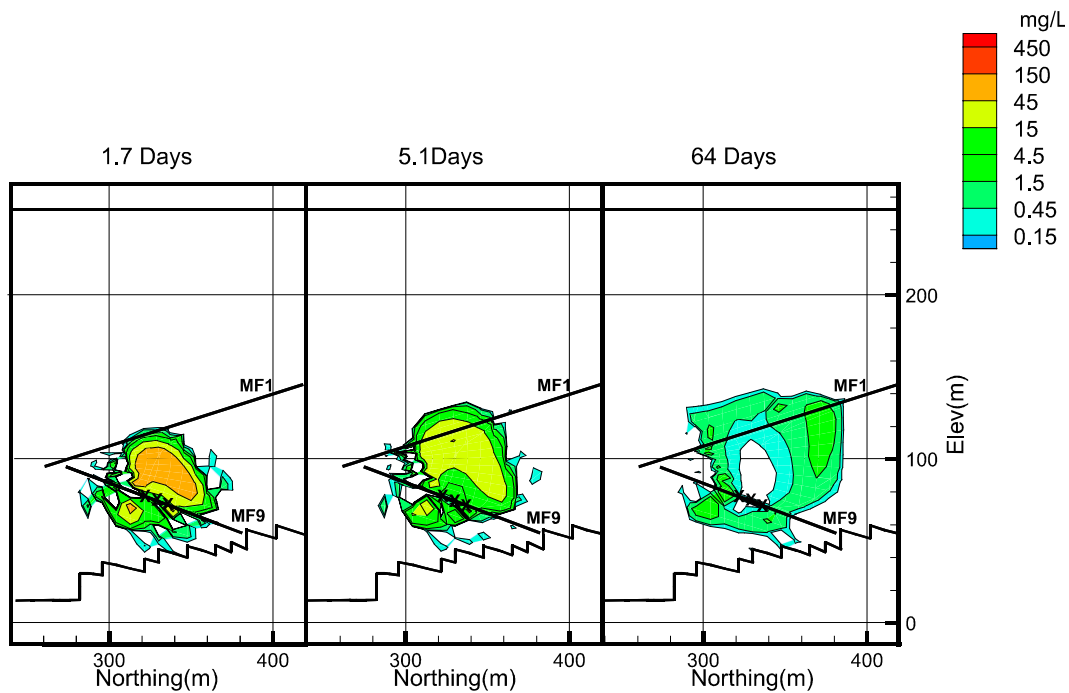


**Figure 3c-6.** Moderately Fractured Rock Experiment: predicted Iodide concentrations – Tracer Test (TT) 2.

### **Geostatistical analysis**

Numerical simulations of flow and transport within the MFR domain were coupled with a geostatistical analysis of the MFR permeability field to further investigate the effect of flow system geometry on advective-dispersive transport. As part of the analysis, several innovative approaches were developed and tested including; i) a method to circumvent a lack of common support in permeability data from packer testing; ii) the generation of stochastic permeability fields to a multi-stage non-regular cubic grid; and iii) a method of permeability up-scaling to finite-elements mesh of variable dimensions and geometry. A complete description of the geostatistical flow system analysis is provided by Chan et al. /2000/ and Chan et al. /2001/.

In summary, the geostatistical analysis adopted a P-field conditional simulation approach /Srivastava 1992; Froidevaux, 1993; Goovaerts, 1997/. Like other geostatistical procedures, P-field simulation generates realizations that honour three criteria: the available data, their histogram and their pattern of spatial variation. Each realization is generated by randomly sampling the local probability distributions that describe the range of possible values at each grid node. These local probability distributions are typically generated using an estimation procedure like indicator kriging that provides the entire probability distribution of the unknown value at a particular location rather than merely a single “best” estimate of the mean of that distribution. Stochastic realisations of the permeability field were determined for a non-regular flexible multi-stage grid (Figure 3c-7) ensuring that at least 5 points lie within each element. A logarithmic mean was then used to estimate and assign element permeabilities.

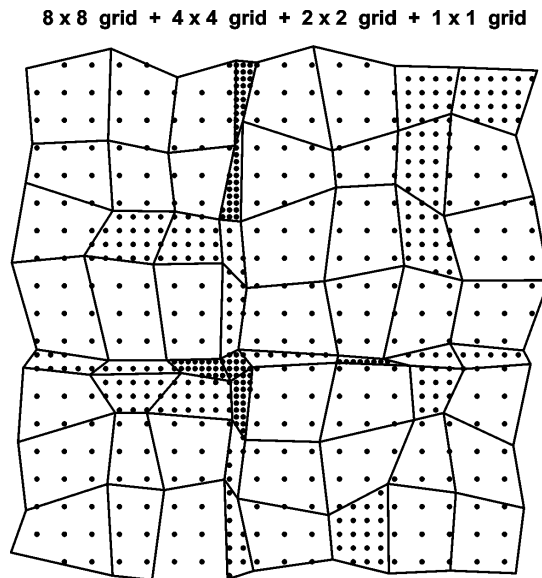


*Figure 3c-7. Non-regular grid (2-dimensions) used in multi-grid procedure.*

The approach above was used to develop 100 equally probable realisations of the MFR permeability field. The finite element code MOTIF was then used to perform simulations of flow and advective-dispersive transport. Simulations of flow were performed for each of the 100 permeability field realisations. Particle tracking was used to investigate the influence on advective transport through the release of 496 particles at a selected injection interval. Simulations of advective-dispersive solute transport were performed for 5<sup>th</sup>, 25<sup>th</sup>, 50<sup>th</sup>, 75<sup>th</sup> and 95<sup>th</sup> percentile cases determined by peak particle arrival times. An example of particle track and solute transport results for the 5<sup>th</sup> percentile case is shown in Figure 3c-8. Although stochastic AD realisation captured observed TT2 results, 4 of the 5 simulations reveal delayed peak concentrations and arrival times, as well as increased dispersion. Particle tracking results were characterized by further delay in the peak arrival time. Effective dispersivities estimated from particle tracking while variable were determined to be approximate 0.1 of the inter-well or transport distance. Further work is planned to investigate whether increased dispersion and decrease mean transport velocities may have resulted from insufficient field characterisation of MFR permeabilities.

The MFR Model Task Force (MTF) was created during the fall of 2000. The purpose of the MTF is three fold; i) to promote a broader understanding of the processes and mechanisms most influencing mass transport in MFR; ii) to re-examine experimental tracer test methodologies to facilitate post-test analyses (i.e. minimize or constrain non-uniqueness in derived parameters); and iii) to allow application of alternative dual-continuum, discrete fracture and hybrid numerical codes in simulation of flow and transport. In this role the MTF serves as a technical forum in which to test and reaffirm concepts of flow and transport in MFR.

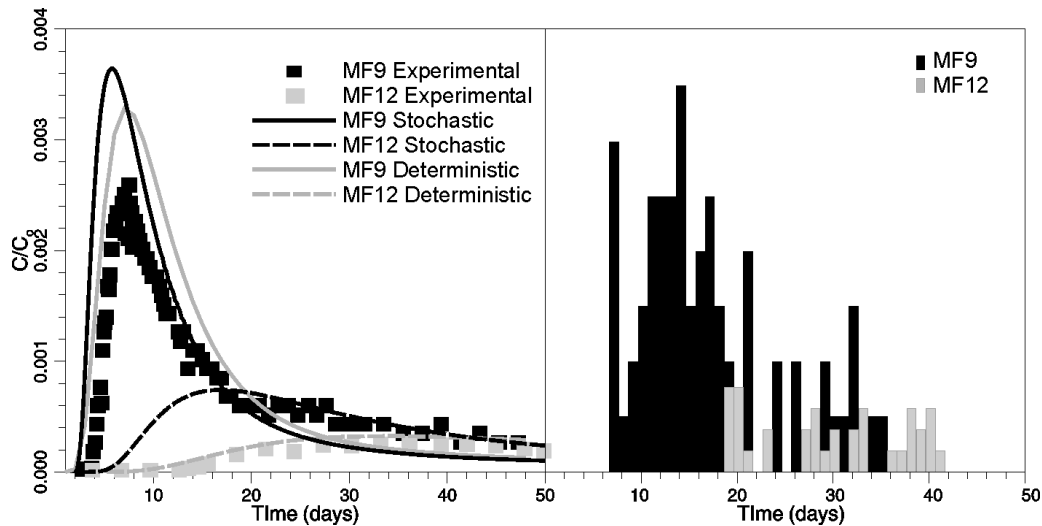


Figure 3c-8. Comparison of observed and predicted (geostatistical) breakthrough curves for I- in Tracer Test (TT) 2 (right – transport simulations; left – particle tracking).

### MFR Modeling Task Force

The MTF is comprised of three Canadian research groups, AECL, University of Waterloo and Université Laval. As a first step, the MTF is to re-examine the basis of the conceptual flow and transport model for the MFR domain. As part of this process a renewed characterisation program was initiated in early 2001, which among other activities involves the drilling of four new bores into the MFR test domain. These bores have been sited to improve knowledge of small-scale variability in MFR properties, as well as, to enable improved tracer test designs and well configurations. Other planned or associated activities include:

- A hydraulic testing program within the 14 MF-series bores to reassess MFR transmissivities, storativities, well bore influence, and flow dimensions (i.e. fracture geometry, interconnectivity);
- The application of VULCAN and Gocad visualisation software to aid integration and traceability of multi-disciplinary data used in development of flow and transport conceptual models;
- A new P-field geostatistical analysis of the MFR flow domain permeability field incorporating new hydraulic testing data;
- Aligned research and development with the In-situ Diffusion and Quarried Block experimental programs at the URL. These experiments are focused on improving the understanding of advective-dispersive-diffusive mass transport in the intact granitic rock and single fractures (scale – 1 m<sup>2</sup>).

Once a conceptual model has been reaffirmed, revised numerical simulation will be completed using control volume finite element codes such as FRAC3DVS /Therrien and Sudicky, 1996; Therrien et al., 2000; VanderKwaak, 1999/. Confidence building in assignment of spatial geometry and boundary conditions will be developed through calibration to both steady state and transient well interference data. Upon completion,



'blind' pre-test prediction of conservative tracer transport will be performed for a series of 5–10 tracer tests beginning in fall 2001. These tests, conducted at length scales of 5–50 m will include forced gradient convergent and injection-withdrawal configurations. The MTF is a 3-year initiative scheduled for completion in 2003.

#### **4 Summary and conclusions**

The Moderately Fractured Rock experiment is conducted within AECL's URL to advance the understanding of mass transport in fractured granitic rock. One objective of the experiment is to evaluate the applicability of the Equivalent Porous Media approximation for flow and solute transport within fractured-porous media. The experiment, initiated in 1993, is comprised of two stages; i) flow domain characterisation and conceptual flow/transport model development and ii) multi-well tracer test and numerical analysis. Stage 1 characterisation activities were completed in late 1997 /Frost et al. 1998/. These activities included a multi-disciplinary effort in which a 100,000 m<sup>3</sup> volume of MFR (1–5 fractures m<sup>-1</sup>, permeability  $\approx 10^{-15}$  m<sup>2</sup>) was identified and investigated from the URL 240 m level. As part of the MFR flow domain investigations, 10 bores were used to characterize litho-structural domains, hydraulic and hydrogeochemical properties and geophysical (cross-hole radar and seismic tomography). These data were used to develop a conceptual flow system model, which served as a basis to rationalize a 3-dimensional numerical analysis of the flow and solute transport. These analyses were performed using the AECL finite element code MOTIF /Frost et al., 1998/.

Tracer testing within the MFR area began in 1998. The experiments have been performed using non-sorbed (I, Br, Lissamine FF), sorbed (Rb, Li) and colloidal (0.19, 0.22 and 0.56 $\mu$  latex spheres) tracers in forced gradient 'dipole' type flow fields at scales of approximately 10 to 50 m. Breakthrough curves for non-sorbed ions, with one exception, were characteristically single peaked with long skewed tails that yielded mass balances of 30% or less. There was no evidence of colloid breakthrough suggesting effective fracture network filtering. Pre- and post-test 3-dimensional numerical simulations of tracer breakthrough were conducted using the finite-element code MOTIF. Representations of the flow domain permeability field, with values ranging between 10<sup>-14</sup> and 10<sup>-19</sup> m<sup>2</sup> were developed using deterministic and geostatistical techniques. Adequate matches to field data are obtained, but significant spatial permeability and porosity field variability is required, which complicates uniqueness of tracer test results and uncertainty in derived transport parameters.

Recent developments in the MFR experiment include the creation of a Modeling Task Force (MTF). The intent of the MTF is; i) to promote a broader understanding of the processes and mechanisms most influencing mass transport in MFR; ii) to re-examine experimental tracer test methodologies to facilitate post-test analyses; and iii) to allow application of alternative dual-continuum, discrete fracture and hybrid numerical codes in simulation of flow and transport. In this role, the MTF serves as a technical forum in which to test and reaffirm concepts of flow and transport in MFR. The MFR experiment will begin an anew set of tracer experiments in fall 2001. The MFR experiment is scheduled for completion in 2003.

## 5 Acknowledgements

The Moderately Fractured Rock experiment has evolved over a period of 8 years during which time many investigators have made valuable contributions. The experiment was initiated by C C Davison (AECL). Principal AECL investigators have included E Kozak, L H Frost and T T Vandergraaf. Flow system characterisation was achieved through the combined efforts of R Ejeckham, R A Everitt, M Gascoyne, G S Lohda, J D Ross, M H Sezu, K V Ticknor and P Vilks. Numerical simulations were completed by T Chan, N W Scheier and F Stanchell (AECL). Geostatistical analyses were completed by R M Srivastava (FSS Canada). Creation of the MFR Modeling Task Force has been accomplished with assistance from R Therrien (Université Laval) and J F Sykes and E A Sudicky (University of Waterloo).

## References

- Chan T, Stanchell F W, Srivastava R M, Scheier N W, Jensen M R, 2000.** Stochastic flow and transport simulations of a three-dimensional tracer test in moderately fractured plutonic rock. Proceedings 3<sup>rd</sup> – European Conference on Geostatistics for Environmental Applications, GeoENV 2000. Avignon, France. November 22–24, 2000.
- Chan T, Stanchell F W, Srivastava R M, Scheier N W, 2001.** Stochastic conditional flow and transport simulations of tracer test no. 2 (TT2) of the moderately fractured rock experiment at the underground research laboratory: a geostatistics case study. Prepared by Atomic Energy of Canada Limited for Ontario Power Generation. Ontario Power Generation, Nuclear Waste Management Division Report 06819-REP-01200-10039-R00. Toronto, Ontario.
- Ejeckham R B, 1997.** Report of the petrologic and mineralogic analysis of fracture surfaces for the moderately fractured rock experiment. Prepared by Atomic Energy of Canada Limited for Ontario Hydro. Ontario Hydro, Nuclear Waste Management Division Report 06819-REP-01200-0019-R00. Toronto, Ontario.
- Everitt R A, Chernis P J, Woodcock D R, 1995.** Compilation of fracture zones, litho-structural domains and alterations haloes from surface and sub-surface information for the underground research laboratory. Atomic Energy of Canada Limited Report TR-534. Pinawa, Manitoba.
- Froidevaux R, 1993.** Probability field simulation. Geostatistics Troia '92, Amilcar Soares (ed.), vol. 1, p. 73–84, Kluwer Academic Publishers, Dordrecht.
- Frost L H, Kozak E T, Everitt R A, Serzu M H, Lodha G S, Gascoyne M, Davison C C, 1998.** Transport properties in moderately fractured rock experiment stage 1: groundwater flow domain characterisation report. Prepared by Atomic Energy of Canada Limited for Ontario Hydro. Ontario Hydro, Nuclear Waste Management Division Report 06819-REP-01200-0021-R00. Toronto, Ontario.
- Goovaerts P, 1997.** Geostatistics for Natural Resources Evaluation, p. 405–409, Oxford University Press, New York.

**Srivastava R M, 1992.** Reservoir characterisation with probability field simulation, Proceedings: SPE Annual Conference and Exhibition, Washington, D.C., SPE Paper No. 24753, p. 927–938, Society of Petroleum Engineers. Dallas, Texas.

**Therrien R, McLaren R G, Sudicky E A, 2000.** User's Guide for NP 4.0, A preprocessor for FRAC3DVS: An efficient simulator for three-dimensional, saturated-unsaturated groundwater flow and chain-decay solute transport in porous or discretely-fractured porous formations, Groundwater Simulations Group.

**Therrien R, Sudicky E A, 1996.** Three-dimensional analysis of variably saturated flow and solute transport in discretely fractured porous media. *Journal of Contaminant Hydrology*, 23, 1–44.

**Ticknor K V, Vandergraaf T T, 1998.** Static batch sorption studies to assess the applicability of Li and Rb as chemically reactive tracers for the moderately fractured rock experiment. Prepared by Atomic Energy of Canada Limited for Ontario Hydro. Ontario Hydro, Nuclear Waste Management Division Report 06819-REP-01200-0041-R00. Toronto, Ontario.

**Vandergraaf T T, 2000.** Moderately fractured rock experiment stage II report: large and medium-scale migration experiments. Prepared by Atomic Energy of Canada Limited for Ontario Power Generation. Ontario Power Generation, Nuclear Waste Management Division. Technical Memorandum, 06819-03787.2-T25. Toronto. Ontario.

**VanderKwaak J E, 1999.** Numerical simulation of flow and chemical transport in integrated surface-subsurface hydrologic systems. Ph.D. Thesis, Department of Earth Sciences, University of Waterloo, Waterloo, Ontario, Canada.

For further information regarding the Moderately Fractured Rock Experiment or Ontario Power Generation's Deep Geologic Repository Technology Program contact M (Mark) R Jensen, 700 University Avenue. Toronto. Ontario M5G 1X6, Canada (Tel: 416-592-8672; Fax 416-592-7336; e-mail [mark.jensen@ontariopowergeneration.com](mailto:mark.jensen@ontariopowergeneration.com))

# **Anisotropy, reversibility and scale dependence of transport properties in single fracture and fractured zone – Non-sorbing tracer experiment at the Kamaishi mine**

*Atsushi Sawada, Masahiro Uchida*

*Japan Nuclear Cycle Development Institute, Tokai Works, 4-33, Tokai, Naka, Ibaraki, 319-1194, Japan*

*Michito Shimo, Hajime Yamamoto*

*Taisei Corporation, Technology Research Center, 344-1, Nase-cho, Totsuka-ku, Yokohama, 245-0051, Japan*

*Hiroyuki Takahara*

*Nittetsu Mining Co., Ltd., Yusen Building, 3-2, Marunouchi 2-chome, Chiyoda-ku, Tokyo 100, Japan*

*Thomas W Doe*

*Golder Associates Inc., 4104-148th Avenue, NE, Redmond, WA, 98052, USA*

## **Abstract**

A comprehensive set of the non-sorbing tracer experiments were run in the granodiorite of the Kamaishi mine located in the northern part of the main island of Japan-Honshu. A detailed geo-hydraulic investigation was carried out prior to performing the tracer migration experiments. The authors conducted a detailed but simple investigation in order to understand the spatial distribution of conductive fractures and the pressure field. Seven boreholes were drilled in the test area of which dimension is approximately 80 meters by 60 meters, revealing hydraulic compartmentalization and a heterogeneous distribution of conductive features. Central three boreholes which are approx. 2 to 4 meters apart form a triangle array. After identifying two hydraulically isolated fractures and one fractured zone, a comprehensive non-sorbing tracer experiments were conducted. Four different dipole fields were used to study the heterogeneity within a fracture. Firstly, anisotropy was studied using the central borehole array of three boreholes and changing injection/withdrawal wells. Secondly, dipole ratio was varied to study how prume spread could affect the result. Thirdly, reversibility was studied by switching injection/withdrawal wells. Lastly, scale dependency was studied by using outer boreholes. The tracer breakthrough curves were analyzed by using a streamline, analytical solution and numerical analysis of mass transport. Best-fit calculations of the experimental breakthrough curves were obtained by assigning apertures within the range of 1–10 times the square root of transmissivity and a dispersion length equal to 1/10 of the migration length. Different apertures and dispersion lengths were also interpreted in anisotropy case, reversibility case and scale dependency case. Fractured zone indicated an increased aperture and increased dispersivity.

# 1 Introduction

Performance assessment of a high-level waste repository in fractured rock requires a clear understanding the geometry, hydrology and mass transport properties of the natural fracture network /Ijiri et. al., 1998/. In a previous performance assessment (PA) report, the Power Reactor and Nuclear Fuel Development Corporation of Japan (PNC) used a simple homogeneous, one-dimensional parallel plate model which assumed a cubic relationship between fracture aperture and transmissivity /PNC, 1992/. This simple model assumes equivalent parameters, which are difficult to determine from the various field data. A major goal of the experimental work supporting PA is to develop more realistic flow models with a better understanding of *in-situ* conditions. Specifically, determining the existence, connectivity and spatial distribution of water-conducting fractures (flowing fractures) is critical for PA.

In crystalline, recently, a several *in-situ* experiments have focused on flow and transport in fracture networks /e.g. Uchida and Sawada, 1995; SKB, 1997; Frost et al., 1997/. Nuclide migration is explained by a combination of several phenomena, including advection, dispersion, adsorption onto the fracture surface or infilling, and diffusion and adsorption into the rock matrix /PNC, 1992/. Advection and dispersion are dominated by heterogeneity at the scale of the fracture network (several tens meter scale) and the heterogeneity of channels on single fractures (from several tens centimeter to several meter scale). Adsorption and diffusion are dominated by the micro-scale around the channel /Uchida et al., 1997/.

In this study, we focussed on transport at the fracture network scale and conducted a series of investigations of the conductive fracture network, and its hydraulic and transport properties. Once the fracture and hydraulic conditions at the test site were well-determined, two single fractures and a fracture zone were chosen for the mass transport portion of the study. That is; the experiments consist of the three major stages:

1. Geometrical and geological fracture system characterization.
2. Hydraulic characterization of the fracture system.
3. Dipole tracer tests.

Experimental activities employed to improve this understanding included:

- investigating the conductive fracture network at the borehole scale,
- obtaining geometric, hydraulic and mass transport properties of conductive fractures, and
- developing an approach to investigate the hydrogeology of fractured rock.

The experimental area is located on the 550 m level of the Kamaishi Mine at the northern end of the KD-90 drift, approximately 350 m below the surface. The study area is near the center of the Kurihashi granodiorite rock body (Figure 3c-9).

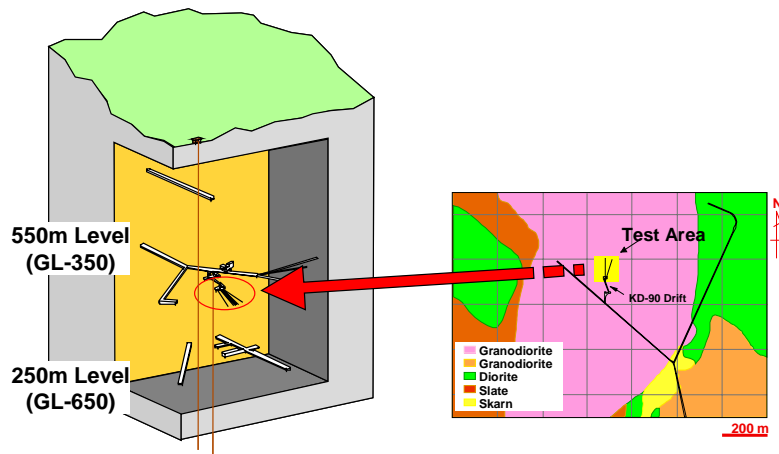


Figure 3c-9. Location and geological map at test area.

## 2 Geological and hydrological investigation

The main investigation of the hydraulic structure of the study area was conducted using 7 boreholes including existing KH-19 borehole as illustrated in Figure 3c-10, which were drilled in the following order: KH-20, KH-23, KH-21, KH-25, KH-22 and KH-24. Boreholes KH-20, 24 and 25 were drilled to make a triangular array in vertical cross section with about two meter spacing for the tracer migration experiments. During drilling of each new borehole, the flow rates and pressures in the new borehole were measured daily. At the same time, water pressures were monitored continuously in previously drilled boreholes.

The main purpose for flow and pressure monitoring was to detect conductive fractures in the new borehole and to identify their hydraulic connections to other boreholes. The intersection of a conductive fracture in the new borehole was often accompanied by an increase in outflow from borehole hole, an increase in the pressure readings when the new borehole was closed, at night, a drop in pressure in a monitoring interval of pre-existing hole, or all of these effects.

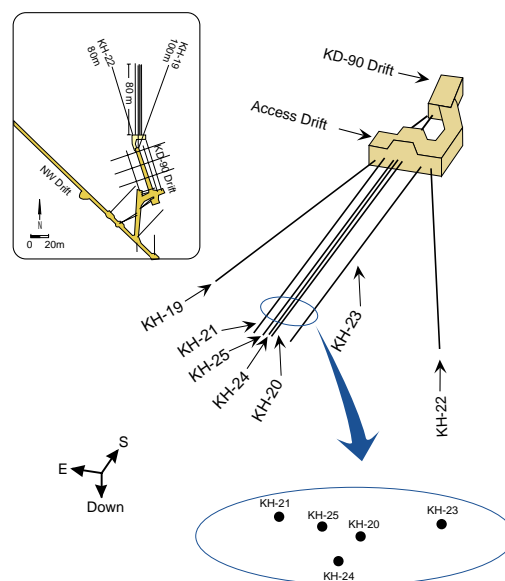
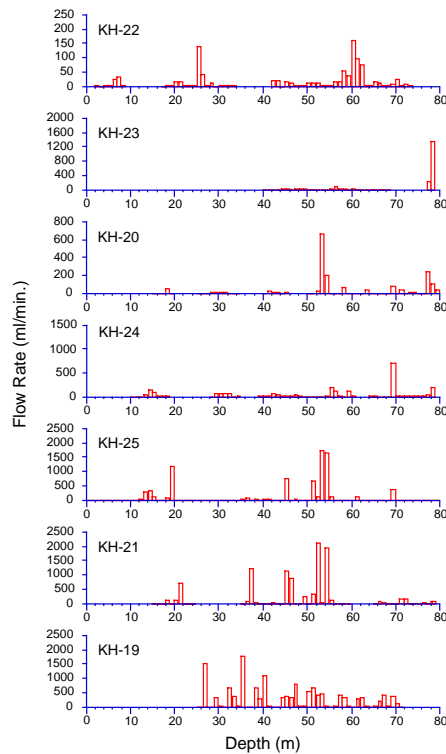


Figure 3c-10. Drifts and boreholes layout.



**Figure 3c-11.** Inflow distribution along each borehole by flow logging.

After completion of drilling, additional data was collected in each borehole through high-resolution television logging (BHTV) and core observation in order to map fractures, and flow logging using 1-m spaced double packers to measure the location and flow rate of groundwater into the hole. After completing the logs, multi-packer piezometers were prepared to isolate the major conducting zones, while providing access for measurements and water injection or withdrawal.

More than three thousand fractures were observed in the seven boreholes. The mean strike and dip of the fractures are about N70-80E and 70-80N, respectively. Conductive fractures identified by BHTV and core logging were characterized by a “orange” alteration halo or mineral infillings of chlorite, calcite, stilbite; and/or fine-grained dark green minerals.

The fractures located in high fracture density zones around 35m and 55m from access drift of KH-20, 24 and 25 boreholes tend to have the highest degree of alteration.

At each borehole, flow logging was conducted initially using a 5 m spaced packer system, followed by measurements using a 1 m system over those 5 m intervals that had measurable flow. This approach provided inflow data at a 1-m resolution. Figure 3c-11 shows the inflow distribution of each borehole. From West to East the borehole layout is KH-22, KH-23, KH-20, KH-24, KH-25, KH-21, and KH-19. From the flow logs, high inflow rate was observed in eastern part of the study area and decreased to the west.

An analysis of the transient pressure response observed existing boreholes during drilling new borehole indicate that some piezometer sections had similar patterns of responses to the drilling of new holes. The grouping of the similar patterns provides a strong indication that the flow system was compartmentalized; that is, the flow system

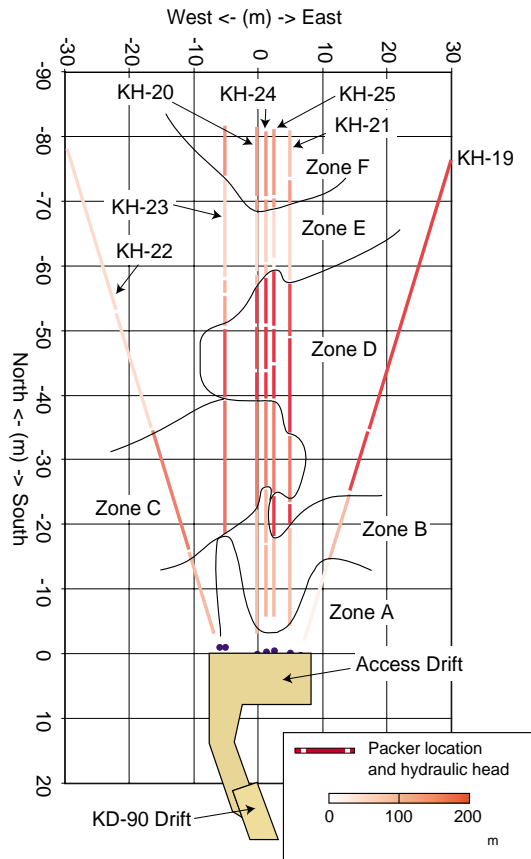


Figure 3c-12. Distribution of flow compartments.

consisted of conductive networks of fractures separated by less conductive regions. In the experimental area, six compartments were identified (Figure 3c-12). These were denoted compartment (or zones) A, B, C, D, E and F. In addition to the similar responses to drilling, each piezometer section within a compartment had similar pressure values. Each piezometer section responded relatively rapidly to pressure interferences within the compartment, but not to interferences from other compartments.

The groundwater flow system above the experiment area involves flow from shallow groundwater near the surface to the mine openings at depth. The hydraulic head in a given compartment reflects its connectivity to the hydraulic boundaries at shallow depth or to the mine. Compartments that are better connected to the surface have high hydraulic heads, while compartments that are better connected to the mine show effects of de-pressurization. The compartmentalization is most readily recognized when there is a large hydraulic gradient across the region of interest, such as in our experimental area. Previous studies at Kamaishi also encountered hydraulic compartments, however they went unrecognized because the compartments had similar low hydraulic heads due to connections to mine openings.

Figure 3c-13 shows the geologic map of fractures intersecting in the experimental area. The fractures in this map were extrapolated across holes based on their location, similarity of orientation, and similarity of other properties such as alteration or mineralization. The fractures exposed in the Kamaishi Mine’s underground workings are often very extensive and have trace lengths of several meters to tens of meters. The geologic map in Figure 3c-13 shows fracture connections across some of the compartment boundaries such as the C-zone’s boundary with the D-zone around the KH-21 and



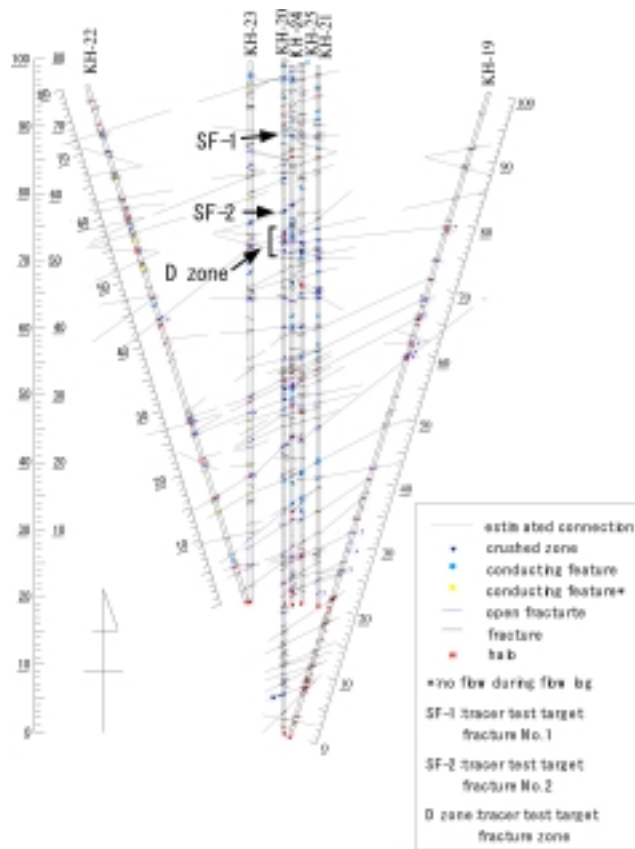


**Figure 3c-13.** Estimated conductive fracture distribution.

KH-25 boreholes. This inconsistency between the fracture and the hydraulic data suggests that fractures that are geologically continuous are not necessarily hydraulically continuous. The tracer migration test target fractures and fracture zones were selected by the following criteria :

- a single-fracture across KH-20, 24, 25 (center three )boreholes,
- a hydraulic connection among center three boreholes, and
- no other fractures within the 1m packer sections.

Based on these criteria, two fractures, called SF-1 in Zone F and SF-2 in Zone E, were selected. In addition to the single fractures, portions of the D-zone were targeted to provide test intervals in a more complex fracture zone. In order to confirm the hydraulic connectivity, and pressure interference, preliminary tracer migration tests were conducted between the center three boreholes. The preliminary tests involved injecting saline solutions in a packed off section of one hole, and logging the electrical conductivity of the water in adjacent open holes to determine the inflow points. These tests confirmed the connectivity of SF-1 between KH-20, 24 and 25 boreholes, and SF-2 between KH-20 and KH-24.

After all piezometers was replaced for tracer migration experiments, a set of pressure interference tests was run by withdrawing water from selected packer intervals in order to estimate hydraulic properties of tracer target fractures.

### 3 Non-sorbing tracer migration experiments

Each piezometer interval used a system of fixed-end packers with stiff extension tubes made by stainless-steel. The system had a constant outer diameter of 70-mm, largely filled the 76-mm boreholes, thus minimizing the water storage in the monitoring intervals. Up to ten zones were isolated in each borehole. Electrical conductivity and temperature sensors were used to measure tracer concentrations in the test zones. Flow and pressure measurement tubes provided independent access to each packer section. The pressure lines were instrumented with pressure transducers connected to a central data-acquisition system. At the borehole collar, a  $\text{Cl}^-$  ion-specific electrode provided real-time concentration data. Water samples were also collected for adsorption spectrophotometer analysis to confirm the tracer breakthrough (Figure 3c-14).  $\text{NaCl}$  (0.8 wt%) was used as the tracer. The tracer tests used dipole geometry consisting of injection at a source well and a higher withdrawal rate at the receiving well (Welty and Gelhar, 1989). The flow field was controlled by a constant rate pump at the injection hole and by a constant-rate valve at the withdrawal hole. The tracers were injected into a nearly steady flow field established by prior injection and withdrawal.

The tracer tests used a variety of source and receiver sections (Table 3c-1). For some source-receiver combinations, the dipole ratio (ratio of withdrawal to injection flow rate) was varied, and/or the injection and withdrawal zones were reversed. The selection of test sections and flow rates was designed to study anisotropy, reciprocity, and scale dependency. Fifteen tracer experiments were run successfully. The tracer recovery percentages were high ( $>80\%$ ) from the single fractures and were lower in the fracture zone tests (varying between 20% and 80%).

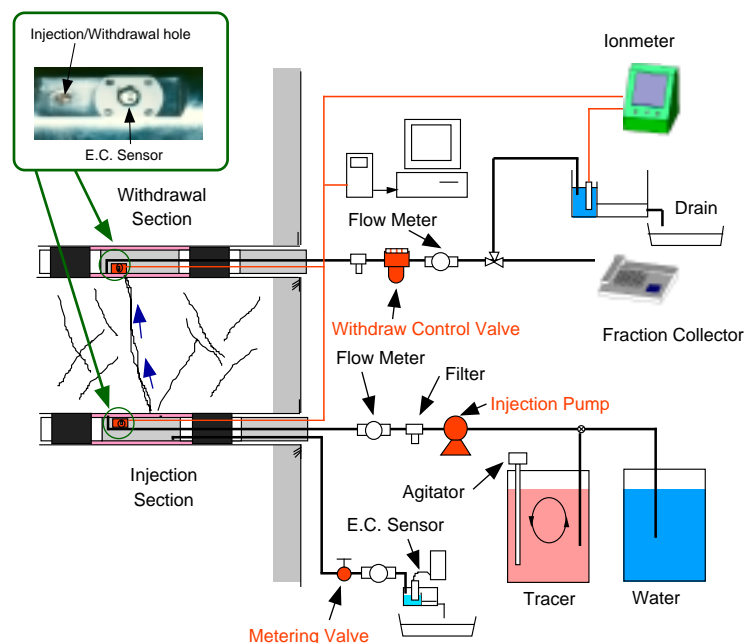
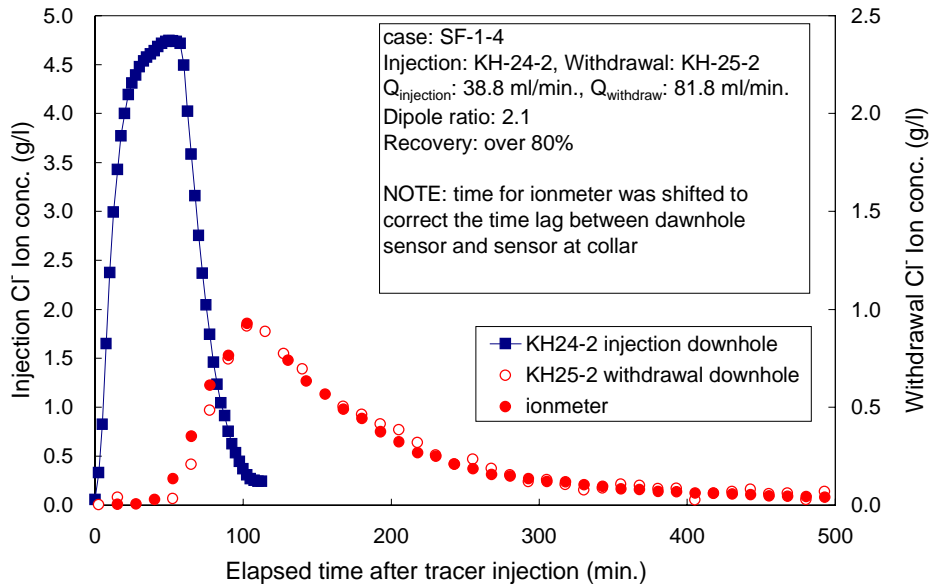


Figure 3c-14. Equipment for tracer tests.

**Table 3c-1. Tracer test cases.**

Target Fracture/Zone	Scale	Anisotropy	Reciprocity	Dipole ratio
<b>SF-1</b> 6 Cases (11) 	○	○	○	○
<b>SF-2</b> 3 Cases (6) 	—	—	—	△ different Flow rate
<b>D zone</b> 6 Cases (10) 	○	—	△	○

2 : Dipole ratio  
 (Withdrawal Flow rate)/(Injected Flow Rate)  
 ○ : good results  
 △ : lack of data  
 - : No activities



**Figure 3c-15. Tracer test results: an example conducted at SF-1 fracture.**

Figure 3c-15 shows an example of test results conducted on single fracture, SF-1, in which tracer was injected in KH-24 and recovered from KH-25. The mass recovery of the test was over 80%.

#### **4 Preliminary analysis of tracer test results**

This preliminary analysis assumed two-dimensional flow geometries, homogeneous properties, and an absence of boundary in order to simplify the analysis, although flow dimension analysis shows various geometry. Tracer tests were analyzed using analytical solutions of dipole streamlines /Heer and Hadermann, 1994/. Each streamline was discretized into stream tubes as illustrated in Figure 3c-16. Advection-dispersion equation was numerically solved by using Laplace Transform Galerkin (LTG) solution /Sudicky, 1990; Ijiri et al., 1998).

Transport aperture and longitudinal dispersion length were calculated by comparing tracer test breakthrough curves. For the single-fracture tracer breakthrough curves, the numerical analysis results were in good agreement with the experiment results. Figure 3c-17 shows an example of comparison results. However, for the fracture zone, it was difficult to fit the numerical results to the experiment results due to low recovery and different geometry between two-dimensional homogeneous model and three-dimensional fracture network in D-zone. For the single fractures, evaluated transport aperture ranges from 0.2 mm to 1 mm.

Because tracer tests require long times and are challenging to perform, it is attractive to find some method to relate transport aperture to more easily measured quantities such as transmissivity. Uchida et. al, 1995 suggest a square root relationship between transport aperture and transmissivity based on a pipe-bundle model of the fracture. This relationship was used to develop transport aperture data for numerical predictions of tracer tests. Figure 3c-18 compares transport aperture values with the transmissivity values for the same fracture. The transport aperture values are about one order of magnitude larger than apertures calculated from the flow rates using the cubic law and they range from 1 to 10 times square root of transmissivity. The spread in the data does not allow an unambiguous confirmation the square root relationship. The fitted longitudinal dispersion length varied from 0.2 m to 1.2 m for dipole spacings ranging from 2 m to 6 m, and suggest that dispersion coefficient has 1/10 of migration length relation (Figure 3c-19). Different aperture and dispersion length were also interpreted in anisotropy case (Figure 3c-20) and reversibility case (Figure 3c-21). Fractured zone indicated an increased aperture and increased dispersivity.

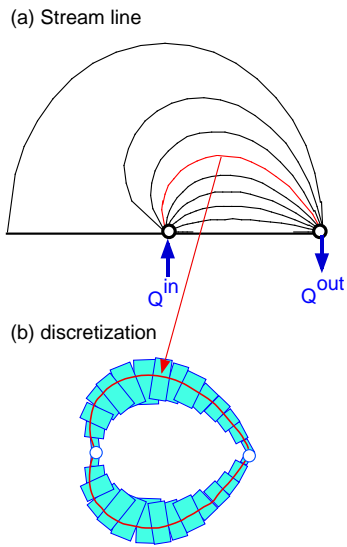


**Figure 3c-16.** Conceptual illustration of discretization of each streamline.

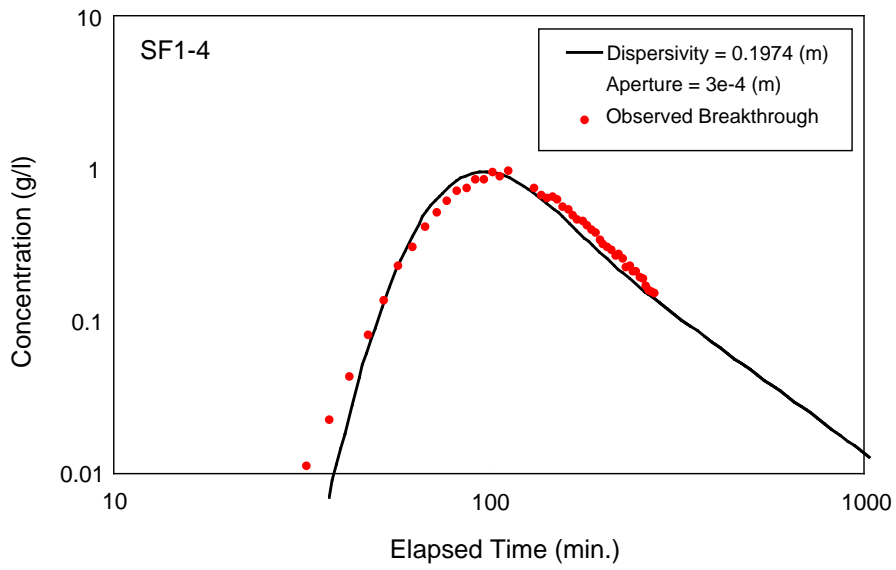


**Figure 3c-17.** Analyzed result of tracer breakthrough curve – the example of the SF-1-4 case.

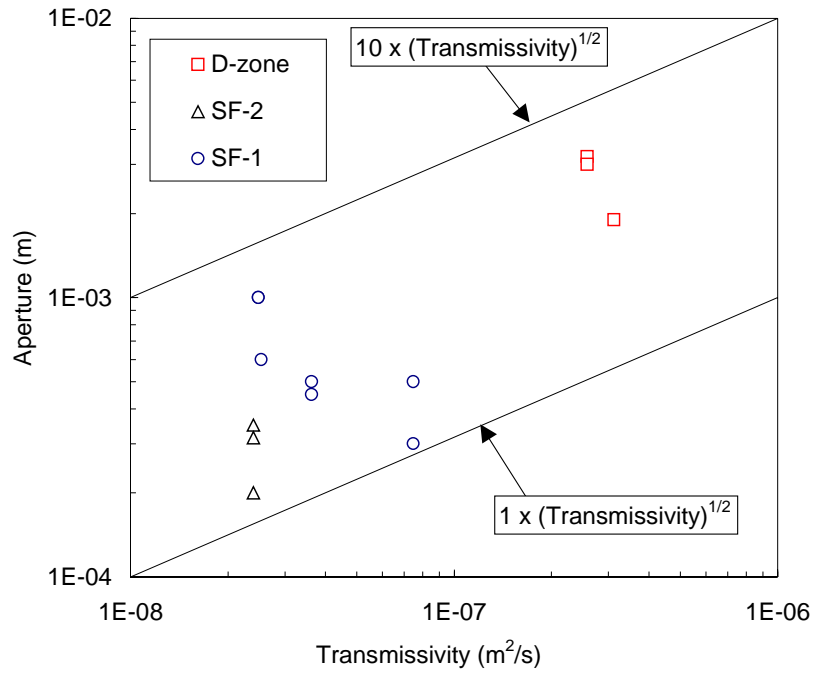


Figure 3c-18. The relation between analyzed aperture and transmissivity.

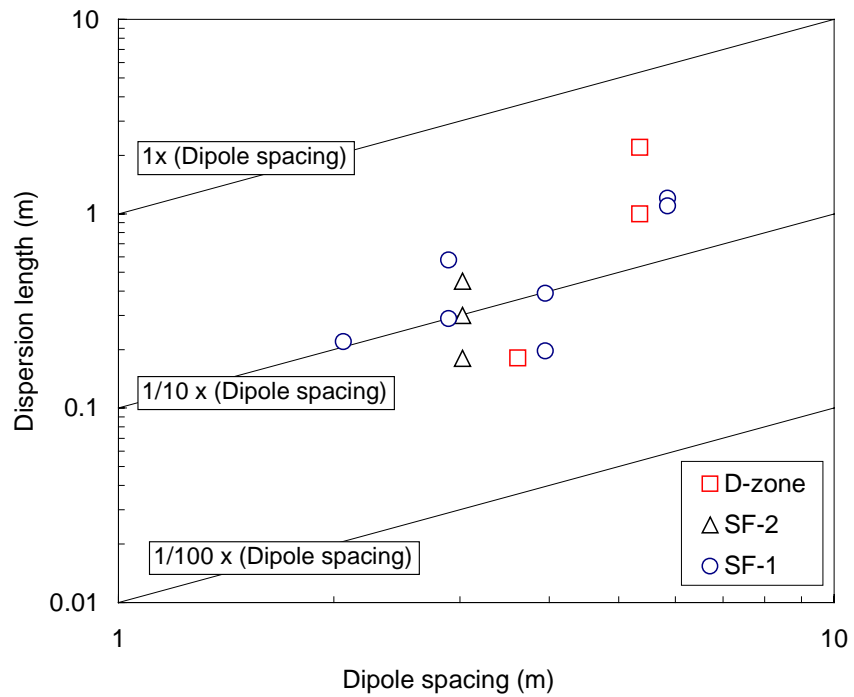


Figure 3c-19. The relation between analysed dispersion length and dipole spacing.

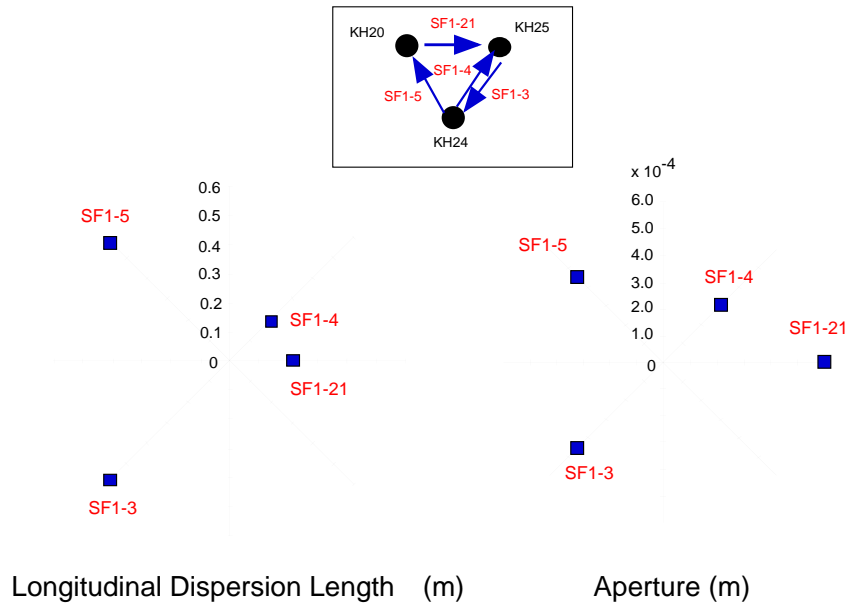


Figure 3c-20. Anisotropy of dispersion length and aperture.

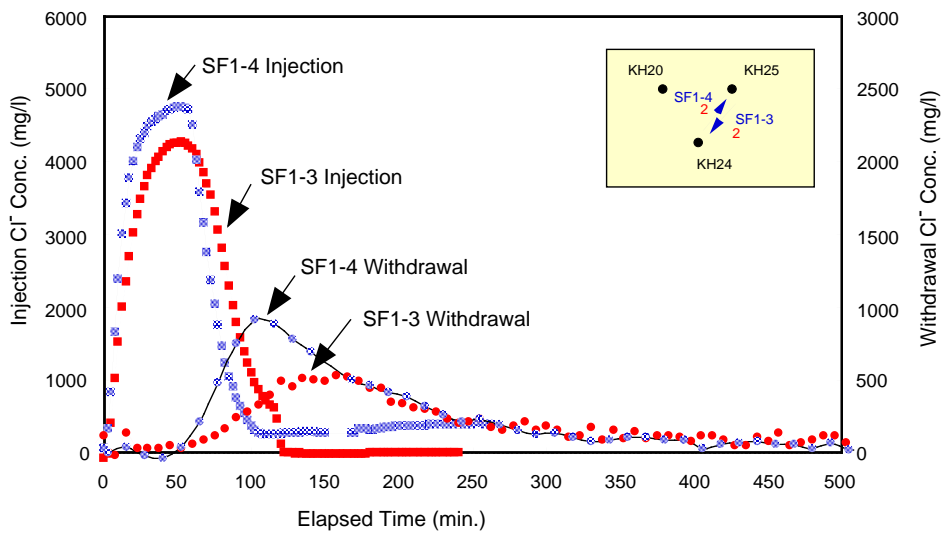


Figure 3c-21. Tracer reciprocity.

## 5 Conclusions and issues

The hydrologic investigations demonstrate clearly that variable connectivity of fracture networks can lead to compartmentalized flow systems. These compartments may be significant for understanding flow and transport in a repository site. The experimental program shows that complex geometries of fracture networks can be deduced by straightforward procedures, but careful monitoring of drilling and testing operations. Inadequate isolation of conducting features during experiment area development may short-circuit the flow system and make geometric assessment difficult or impossible. Once conducting features are identified, tracer tests can successfully provide information on transport properties. From the dipole tracer tests with varying combination of injection/withdrawal section and dipole ratio and the preliminary analyses, scale dependency of dispersion length, and anisotropy and reciprocity of transport properties were evaluated.

One goal of the experiment is to map the location and to identify the water conductive fractures. The flow logging approaches successfully identified conducting features to a 1 m resolution in the boreholes. However, given the high densities of fractures in core and television logs, it was not possible to clearly associate water conductivity with specific fractures, except in some cases where drilling responses could be precisely located. Furthermore, conductive fractures are heterogeneous internally, and a conductive fracture may not produce flow at all points of borehole penetration. Thus, while the larger scale geometries of compartment structure are clearly established, the location of individual conducting fractures has much uncertainty. It is possible the higher resolution flow logging could have provided better resolution. LaPointe et al. /1995/ studied the water conductive fracture identification by using neural network analysis with the complex fracture geological data at Äspö Hard Rock Laboratory. This approach has an advantage of taking into account both quantitative and qualitative data, and also analyzing non-linear relationship. In the future, with this kind of analysis, more high-resolution flow logging technique and packer tests will have to be developed.

## References

- Frost L, Davison C, Vandergraaf T, Scherer N, Kozak E, 1997.** Field tracer transport Experiments at the site of Canada's underground research laboratory, Field Tracer Experiments: Role in the prediction of radionuclide migration, Proceedings of GEOTRAP, the OECD/NEA Project on the Transport of Radionuclides in Geologic, Heterogeneous Media, pp. 131–144.
- Heer W, Hadermann J, 1994.** Modelling radionuclide migration field experiments, Paul Scherrer Institut Report 94-13.
- Ijiri Y, Sawada A, Hatanaka K, Webb E, Uchida U, Ishiguro K and Umeki H, 1998.** Strategy for Characterization and Radionuclide Migration Modelling in Block-Scale Geological Media, Proceedings of GEOTRAP, the OECD/NEA Project on the Transport of Radionuclides in Geologic, Heterogeneous Media, pp. 64–68.



**LaPointe P, Wallmann P, Follin S, 1995.** Estimation of effective block conductivities based on discrete network analyses using data from the Äspö site. SKB TR 95-15, Swedish Nuclear Fuel and Waste Management Co.

**PNC, 1992.** Research and development on geological disposal of high-level radioactive waste, First progress report, PNC TN1410 93-059.

**SKB, 1997.** Äspö Hard Rock Laboratory Annual Report 1996. SKB TR 97-08, Swedish Nuclear Fuel and Waste Management Co.

**Sudicky E A, 1990.** The Laplace Transform Galerkin Technique for Efficient Time-Continuous Solution of Solute Transport in Double-Porosity Media, *Geoderma*, 46, pp. 209–232.

**Uchida M, Doe T, Sawada A, Dershowitz W, Wallmann P, 1995.** Simulation of the LPT-2 large scale pumping and tracer test, Äspö Hard Rock Laboratory International Cooperation Report, ICR-95-09, Swedish Nuclear Fuel and Waste Management Co.

**Uchida M, Sawada A, 1995.** Discrete Fracture Network Modeling of Tracer Migration Experiments at Kamaishi Mine, *Mat. Res. Soc. Symp. Proc.*, vol.353, pp. 387–394.

**Uchida M, Umeki H, Yoshida H, 1997.** A tracer experiment at Kamaishi mine – as a part of an integrated approach to geosphere transport modelling – Field Tracer Experiments: Role in the prediction of radionuclide migration, *Proceedings of GEOTRAP, the OECD/NEA Project on the Transport of Radionuclides in Geologic, Heterogeneous Media*, pp. 191–201.

**Welty C, Gelhar L, 1989.** Evaluation of longitudinal dispersivity from tracer test data, MIT. Dept. of civil engineering report, R89-05.

# The TRUE Block Scale experiment – A status report

Anders Winberg  
Conterra AB, Sweden

## Abstract

One component in the Tracer Retention Understanding Experiments at the SKB Äspö Hard Rock Laboratory is the TRUE Block Scale experiment which focuses on the 10–100 m length scale. The objectives of TRUE Block Scale were to increase understanding and capability to predict transport and retention fracture networks. An iterative approach was adopted which included drilling, characterisation of five exploration boreholes. The results indicate that it is possible to build relatively robust hydrostructural models of a rock volume on a 300 m length scale, using a few and relatively unsophisticated characterisation techniques (registration of pressure responses, borehole TV (BIPS) and high resolution flow logging). It was found that the basic hydrostructural entities of the investigated rock block were identified using data from the first three boreholes. Tracer dilution tests proved to be an effective means to identify suitable tracer injection sections for any given sink. Subsequent experiments have successfully demonstrated the possibility to run well-controlled, quantitative experiments with radioactive sorbing tracers in interpreted single structures and networks of deterministic fractures/structures over length scales  $< 100\text{m}$ . A prerequisite for design, performance and associated model prediction and evaluation of the performed tests was a robust hydrostructural model. The breakthrough curves from performed tracer indicate that the longer and more complex source-sink set-ups show more profound indications of matrix diffusion, with near  $-3/2$  slopes in log-log plots. It is also noted, as in the case of TRUE-1, that diffusion effects are augmented for the more sorbing tracers. Numerical modelling of the TRUE Block Scale experiments was performed with a wide range of approaches/concepts. The results indicate successful outcome of model predictions in relation to experimental data on a length scale  $< 15\text{ m}$ . The correspondence between the predicted and the *in situ* results are not as good for the two longer flow paths, 35 and 100 m, respectively.

## 1 Introduction and background

For the Operating Phase of the SKB Äspö Hard Rock Laboratory (HRL), the Swedish Nuclear Fuel and Waste Management Company (SKB) initiated the Tracer Retention Understanding Experiments (TRUE) with the objective to improve the understanding of radionuclide transport and retention processes in fractured crystalline rock. Overall objectives included enhancement of confidence in models for transport of sorbing radionuclides in performance assessment (PA), and to show that pertinent transport data can be obtained from site characterisation or field experiments, and that laboratory results can be related to retention parameters obtained *in situ*. A basic drive from PA has been to obtain *in situ* data on transport and retention of sorbing radionuclides at different length scales. In addition, the address of multiple scales which is embedded in

TRUE is relevant for taking the step from experimental scales to site scale (100–1000 m). The first test cycle of the Tracer Retention Understanding Experiments, TRUE-1, which recently has been concluded (Winberg et al., 2000/ and which is the focus of the present international seminar, focused on transport and retention in an interpreted single fracture in the detailed scale (<10 m). This scale can be seen to represent the environment experienced by released radionuclides in the immediate vicinity of a deposition borehole. The block scale can be regarded as the natural extension where transport from the near canister environment to the connecting network of fractures and structures on the 10–100 m length scale is addressed. Hence, the multi-party TRUE Block Scale project was initiated in 1996. The project is expected to be concluded towards the end of 2001.

## **2 Specific objectives and performance**

In the TRUE Block Scale experiment /Winberg, 1997; Winberg ed., 2000/ the experiences from TRUE-1 have been transferred and tested on a larger length scale, and somewhat longer transport times. The specific objectives were to:

1. increase understanding and the ability to predict tracer transport in a fracture network,
2. assess the importance of tracer retention mechanisms (diffusion and sorption) in a fracture network,
3. assess the link between flow and transport data as a means for predicting transport phenomena.

The project is divided in five basic stages; Scoping, Preliminary Characterisation, Detailed Characterisation, Tracer Test and Evaluation /Reporting. After the series of characterisation and experimental stages /Winberg ed., 2000/, the TRUE Block Scale is presently in an evaluation and reporting stage and final reports are due early 2002.

## **3 Characterisation and hydrostructural models**

During the course of the basic characterisation of the TRUE Block Scale Rock volume (200x300x150m) a total of 5 boreholes have been drilled from two levels in the laboratory. The geometry of these boreholes are to a large extent restricted by the location and geometry of existing underground works. The characterisation strategy employed has been an iterative one. This implies that each new borehole position and geometry is the result of preceding borehole characterisation and core logging. The data have subsequently been used in the updating of the existing hydrostructural model and numerical model analysis based on the model. The results have subsequently formed the platform for decision as to the need for a new borehole and its geometry /Andersson et al., in prep I/. This approach differs from that employed during the First TRUE Stage where the complete borehole array of 4 boreholes was drilled in close sequence. Only temporary multi-packer systems were used to collect pressure responses in this case.

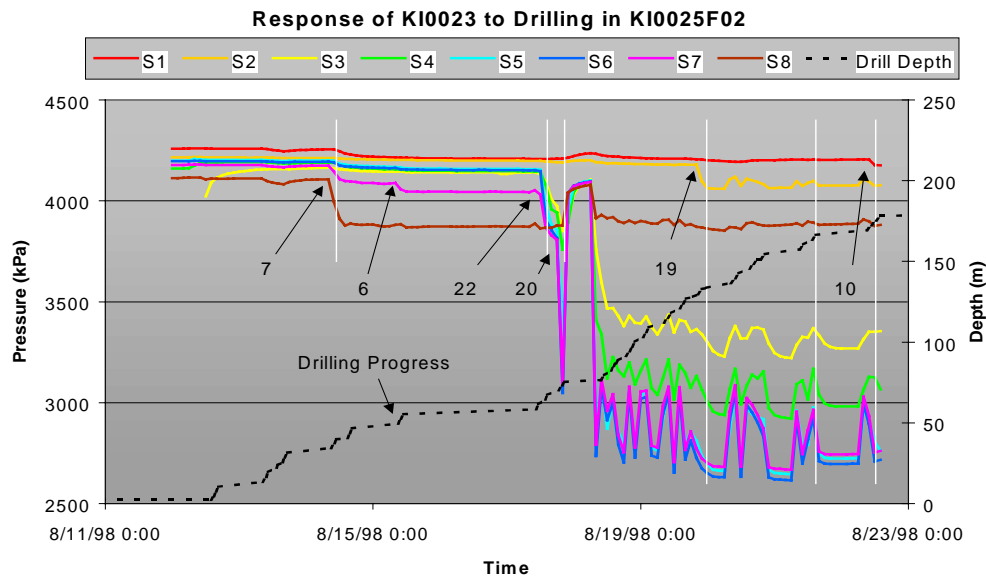


**Figure 3c-22.** Pressure responses in the packed off borehole KI0023B to drilling of borehole KI0025F02. Dashed line indicates drilling progress as a function of time.

Over the duration of the TRUE programme, successive refinements and modifications of the characterisation and experimental methodology have been made, but overall the important components in the basic characterisation remain the same. It was identified already during the First TRUE Stage that the basis for successfully designing, performing, and evaluating *in situ* tracer tests over the length scales considered is a sound and robust hydrostructural model complemented by a good hydraulic understanding of the studied system. In building the TRUE Block Scale hydrostructural models, the key elements have been integration of cross-hole pressure responses (collected during drilling and interference tests), cf. Figure 3c-22, and borehole TV imaging (BIPS), and results from high-resolution borehole flow-logging /Andersson et al., in prep./, cf. Figure 3c-23, the latter introduced during TRUE Block Scale. The most recent hydrostructural model is shown in Figure 3c-24 /Hermanson and Doe, 2000/. It has been identified that the important structures of the most recent hydrostructural model were identified during the first three boreholes. The additional two boreholes served to refine the model and to contribute additional source sections for tracer experiments. Fractures which could not be assigned to deterministic structures/fractures interpreted to extend between multiple boreholes were assigned to a stochastic background fracture population. The material properties, e.g. in terms of transmissivity, have been obtained through various types of single hole and cross-hole hydraulic tests /Winberg ed., 2000/. Hydraulic boundary conditions have been inferred either from larger scale numerical models or from measurements of hydraulic head in packed-off borehole sections.

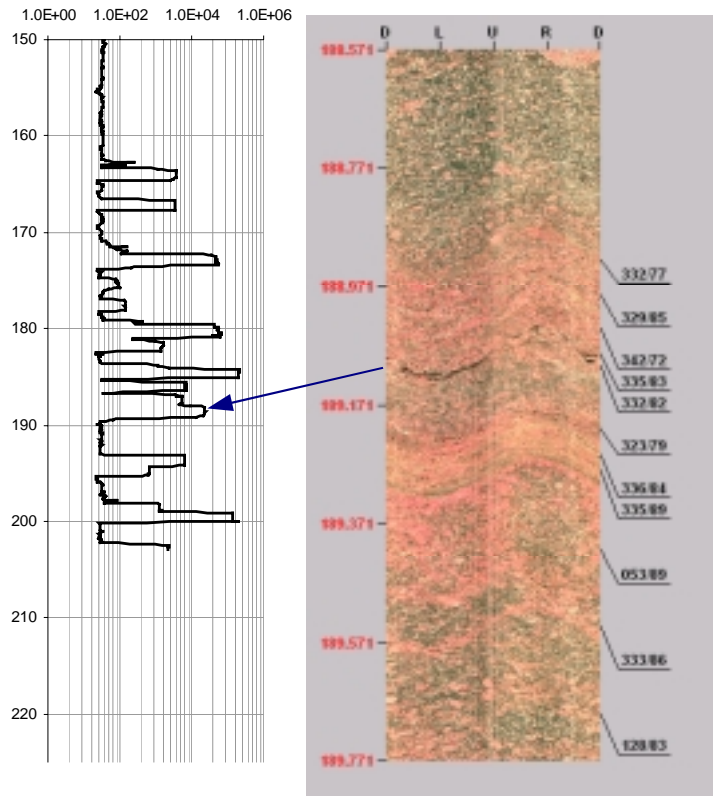


**Figure 2-3B** The last 75 m (150 – 225 m) of the POSIVA flow log of KI0025F02 with an example of a correlation with the BIPS image of a fault at 189 m depth.

**Figure3c-23.** Posiva flow log (left) and corresponding BIPS log. Note that the length scales of the two images are not the same.

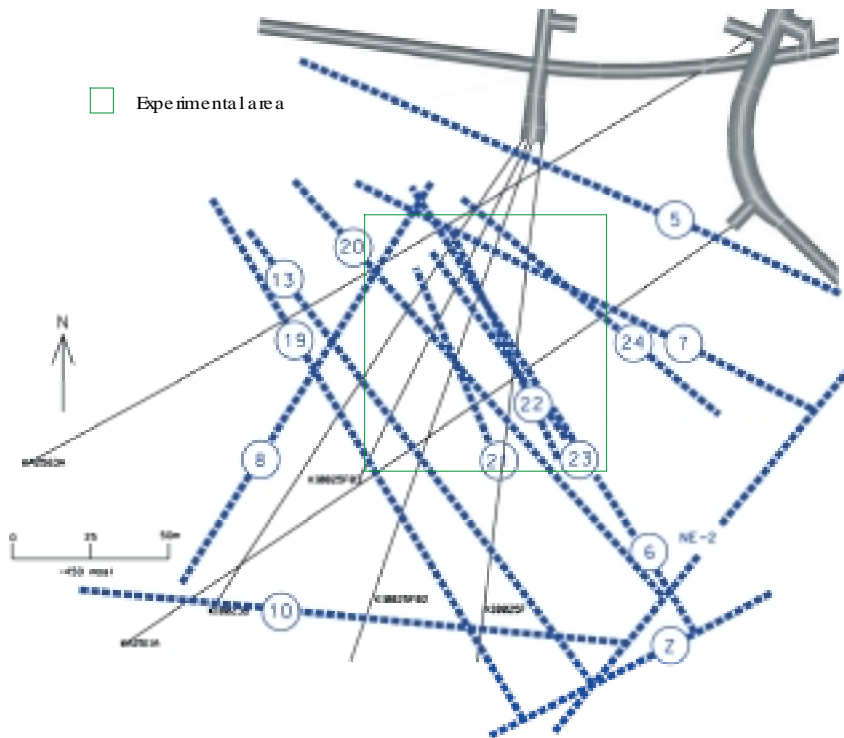


**Figure3c-24.** TRUE Block Scale hydrostructural model (March 2000).

## 4 Hypotheses to be tested

Before the onset of the tracer tests programme a number of questions were posed;

- Q1) "What is the conductive geometry of the defined target volume for tracer tests within the TRUE Block Scale rock volume? Does the most recent structural model reflect this geometry with sufficient accuracy to allow design and interpretation of the planned tracer tests?"
- Q2) "What are the properties of fractures and fracture zones that control transport in fracture networks?"
- Q3) "Is there a discriminating difference between breakthrough of sorbing tracers in a detailed scale single fracture, as opposed to that observed in a fracture network in the block scale?" Based on the defined questions a number of hypotheses were posed to be addressed by the *in situ* experiments;
- H1) "The major conducting structures of the target volume for tracer tests in the TRUE Block Scale rock volume trend northwest and are subvertical. Being subvertical, and subparallel, they do not form a conductive network in the designated target volume. For the purpose of testing fracture network flow and transport effects in the current borehole array, second-order NNW features are required to provide the necessary connectivity between the major conducting NW structures!"
- H2a) "Fracture intersections have distinctive properties and have a measurable influence on transport in fracture/feature networks. These distinctive properties may make the intersection a preferential conductor, a barrier, or a combination of both!"
- H2b) "In-plane heterogeneity and anisotropy have a measurable influence on transport of solutes in a block scale fracture network!"
- H3) "It is not possible to discriminate between breakthrough curves of sorbing tracers in a single fracture from those obtained in a network of fractures"!

It was identified that the available borehole array and its position in relation to the hydrostructural model only would allow partial address of the role of fracture intersection zones (FIZ). Success expectancy in relation to Hypothesis 2 should therefore be limited already at the onset of the *in situ* tests. It is however expected that comparison between breakthrough curves from source-sink pairs in individual structures with those collected in fracture networks will provide an indication on the role of the FIZs.

## 5 Tracer tests

Tracer tests in the block scale were conducted already as part of the Preliminary Characterisation stage and clearly showed the prospect of performing tracer tests in a network over a length scale of 15 m. This finding was further augmented during the Detailed Characterisation Stage when a series of four injections of conservative dye tracers were made over variable source-sink distances and complexity (in terms of

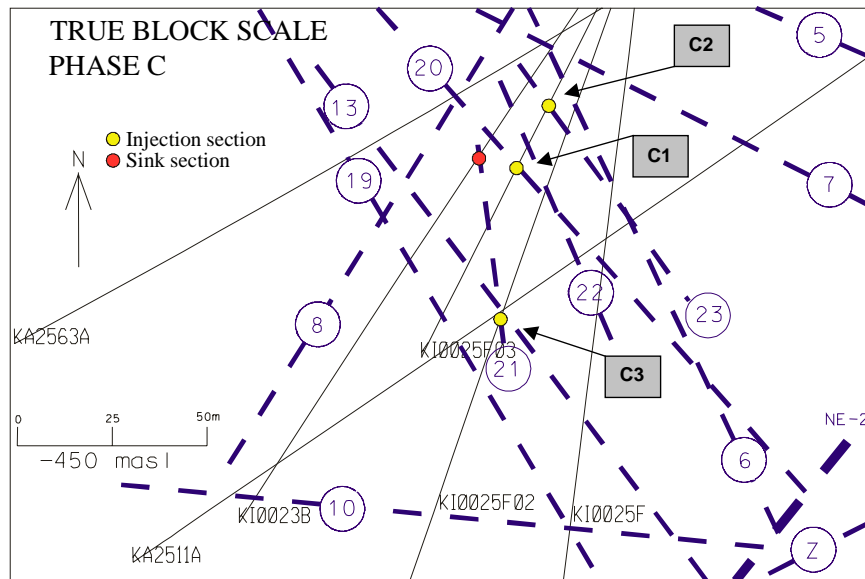


Figure 3c-25. Detail of Tracer Test area.

number of structures involved). The results of these tests clearly demonstrated feasibility to carry out tracer tests with high mass recovery in block scale fracture networks. A tracer test area was possible to delineate including Structures #20, #13 and #21–#23, cf. Figures 3c-24 and 3c-25, where Structure #20 constitutes the main conductive structure in the studied area.

With the available block scale and TRUE-1 results in hand the basic issues for the subsequent tracer tests were defined. These questions were used to pose hypotheses to be addressed by the tests, cf. Section 3. The Tracer Test Stage is divided into three defined phases; Phase A where the best suited sink location, section KI0023B:P6 (Structure #20), was selected and an elaborate programme of tracer dilution tests at ambient and pumped conditions were carried out /Andersson et al., 2000a/. The combined anomalies from pressure interference and tracer dilution tests were used to select the most suitable injection points for tracer. During Phase A the tracer tests were not driven to maximum mass recovery. Hence a Phase B /Andersson et al., 2000b/ was carried out with conservative tracers to identify those source-sink pairs which provided a recovery  $> 80\%$ , the latter defined as the lower limit for tests with radioactive sorbing tracers. Figure 3c-26 compiles breakthrough curves from tests performed with conservative tracers. It is evident from the figure that for longer transport times (longer distances, more complexity/heterogeneity) the late time log-log slope shows more distinct evidence of effects of matrix diffusion (slope  $\sim -3/2$ ). Phase B also included tests with dissolved He-3 gas employing two different flow rates. The results compared to a reference conservative dye tracer showed a marked retardation for the more diffusive He tracer compared to the conservative dye, interpreted as a manifestation of diffusion /Andersson et al., 2000b; Andersson et al., in prep. II/, cf. Figure 3c-27. Subsequently, a Phase C with four different tracer injections in three source-sink pairs were carried out at maximum possible flow rate, 2.1 l/min, in the selected sink section /Andersson et al., in prep./. The source sections employed and tracers used are listed in Table 3c-2. The location of the different sections are shown in plane view Figure 3c-25. A compilation of the *in situ* breakthrough curves from injections C1 and C4 are presented in Figure 3c-28.

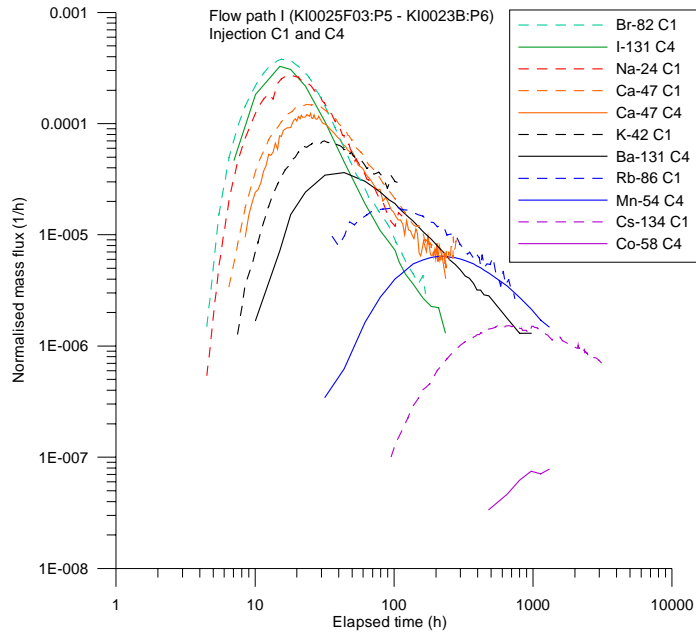


Figure 3c-26. Family of conservative breakthrough curves from different tracer test campaigns.

Table 3c-2. Performance of Phase C tracer tests (C1 through C-4) /Andersson et al., in prep./ The structural notation and interpretation refers to the March 2000 model /Hermanson and Doe, 2000/. Distances within brackets are calculated along the structures.

Test #	Source-Sink pairs	Structures	Flow geometry	Inj. Flow (ml/min)	Pump flow (ml/min)	Tracers used	Distance (m)
C-1	KI0025F03:P5 – KI0023B:P6	20, 21	Forced injection	45	1950	$^{82}\text{Br}^-$ , $^{24}\text{Na}^+$ , $^{42}\text{K}^+$ , $^{47}\text{Ca}^{2+}$ , $^{86}\text{Rb}^+$ , $^{134}\text{Cs}^+$ , Uranine	14 (16)
C-2	KI0025F03:P7 – KI0023B:P6	23, 20, 21	Forced injection	10	1950	$^{186}\text{ReO}_4^-$ , $^{47}\text{Ca}^{2+}$ , $^{131}\text{Ba}^{2+}$ , $^{137}\text{Cs}^+$ , Naphtionate	17 (97)
C-3	KI0025F02:P3 – KI0023B:P6	21	Passive injection	1.8	1950	HTO, $^{22}\text{Na}^+$ , $^{85}\text{Sr}^{2+}$ , $^{83}\text{Rb}^+$ , $^{133}\text{Ba}^{2+}$	33 (33)
C-4	KI0025F03:P5 – KI0023B:P6	20, 21	Forced injection	45	1950	$^{82}\text{Br}^-$ , $^{131}\text{I}^-$ , $^{47}\text{Ca}^{2+}$ , $^{131}\text{Ba}^{2+}$ , $^{54}\text{Mn}^{2+}$ , $^{57}\text{Co}^{2+}$ , $^{65}\text{Zn}^{2+}$	14 (16)



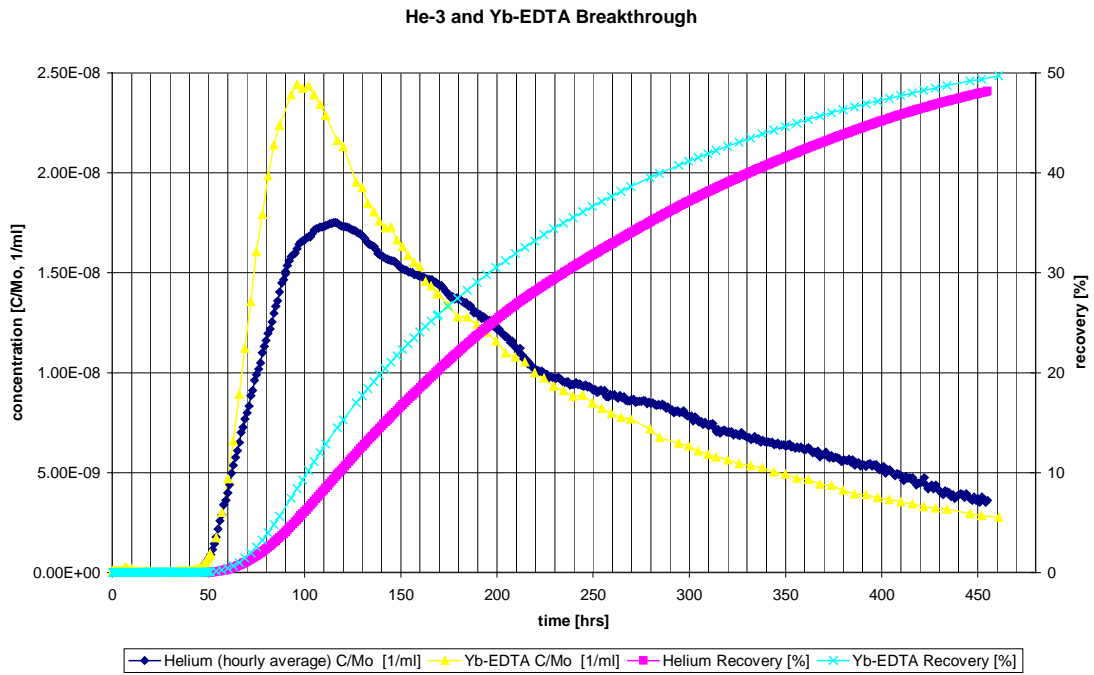


Figure 3c-27. He-3 and Yb-EDTA breakthrough curves (linear scales), Test B-2a.

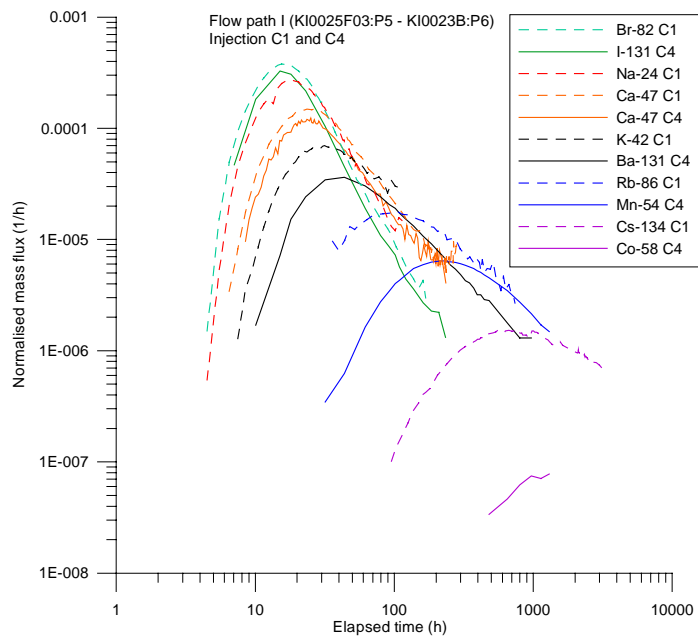


Figure 3c-28. Collection of breakthrough curves for radioactive sorbing tracers for injections C1 and C4 in source-sink pair I ( $L=16$  m).

## 6 Laboratory investigations

A comprehensive mineralogical and geochemical analysis programme has been carried out on geological material from the borehole intercepts with structures involved in the tracer tests. Structures # 20 and #22 are interpreted as major geological structures with cataclasite and mylonite and also include fault breccia. Calcite and pyrite have grown on fracture surfaces and on breccia pieces in these structures. Clay mineralogy combined with stable isotope analyses indicate that the fractures in the two structures are hydrothermal in origin and have been conductive during long periods of time, or during repeated events/periods.

No specific laboratory investigations in terms of batch sorption and through-diffusion experiments have been performed on site-specific material from the structures involved in the TRUE Block Scale tracer experiments. Instead results from generic and site-specific material from Feature A (TRUE-1) /Byegård et al., 1998; Byegård et al., 2001/ which resembles Structures #20 and #22 and have been imported and used. These data include sorption experiments conducted on different size fractions and, likewise, through-diffusion measurements made on variable sample thicknesses, 1–4 cm /Byegård et al., 1998/. In the case of TRUE Block Scale, where fault breccia has been collected from relevant structures,  $K_d$  values for breccia material fractions have been evaluated from cation-exchange capacities estimated from the mineralogy in combination with the ambient hydrogeochemistry /Andersson et al., in prep. I/. Additional laboratory work includes measurement of porosity and porosity distributions using water saturation and impregnation of rock samples with  $^{14}\text{C}$ -labelled polymethylmethacrylate ( $^{14}\text{C}$ -PMMA) /Siitari-Kauppi et al., 1998/.

## 7 Conceptual models of conductive fractures

Fractures at Äspö have typically been subject to variable amounts of tectonisation (indicated by the occurrence of cataclasites and/or mylonites) and variable degrees of chemical alteration (alteration of biotite to chlorite, saussuritisation of plagioclase, oxidation of magnetite to hematite, etc.). Almost all studied structures/fractures show alteration and tectonisation of the wall rock, and most intercepts follow mylonites.

Conceptual model development for fractures and their immediate surroundings has been concentrated to fractures exposed in tunnel openings and on the ground surface /Mazurek et al., 1997/, to the Feature A studied in TRUE-1 /Winberg et al., 2000/, and the structures involved in the tests with sorbing tracers in TRUE Block Scale /Andersson et al., in prep. I/. Some of the latter structures are comparable to Feature A, although they are slightly more complex, more transmissive, and wider. PMMA studies performed on Feature A material indicate a porosity of about 1–2% in the rim zone close to the fracture surface (locally the porosity is much higher) and a sharp gradient towards the interior where the porosity is about one order of magnitude lower some 1–2 cm from the surface of Feature A /Byegård et al., 2001/. A high porosity gradient and an increased pore connectivity near fracture surfaces may result in markedly increased

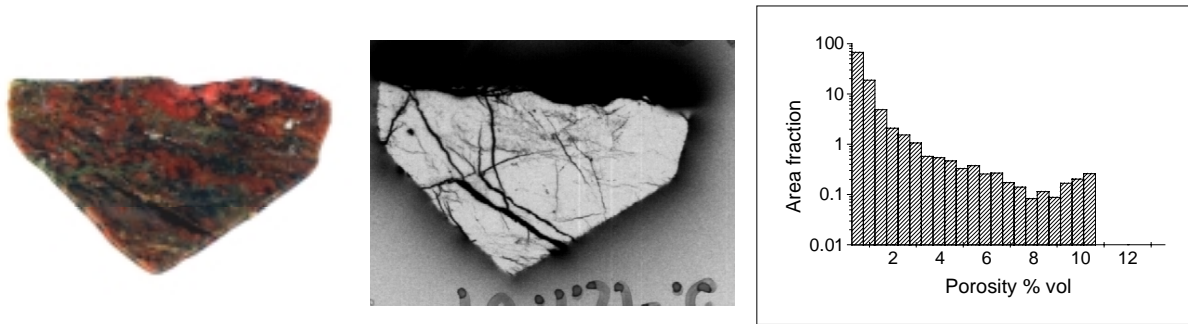


**Figure 3c-29. TRUE Block Scale:** Composite showing a cut surface of a cm sized PMMA impregnated fault breccia piece, the associated autoradiograph and the a histogram accounting for the area distribution of porosity. The total porosity assessed from the exposed surface is 0.8% /Andersson et al., in prep. I/.

diffusivity and sorption capacity compared to intact rock away from the fracture surfaces /Byegård et al., 2001/. Fault breccia has been recovered from some structures in the TRUE Block Scale studies. PMMA analyses performed on fault breccia pieces (1–3 cm) and fault breccia fragments (1–2 mm) show porosities in the order of 0.4–0.8% (with small areas with highs of about 10%), cf. Figure 3c-29, and 1.3–11%, respectively /Andersson et al., in prep. I/. In general, the porosity constitutes micro-fractures and porous mineral phases (secondary or altered minerals).

## 8 Numerical modelling

Although numerical modelling has been part of each update of the hydrostructural model it is only following the most recent model updates that numerical modelling has been employed more extensively, and employing different model concepts. The block scale tracer tests are presently subject to evaluation using five different model approaches which include stochastic continuum, discrete feature network, channel

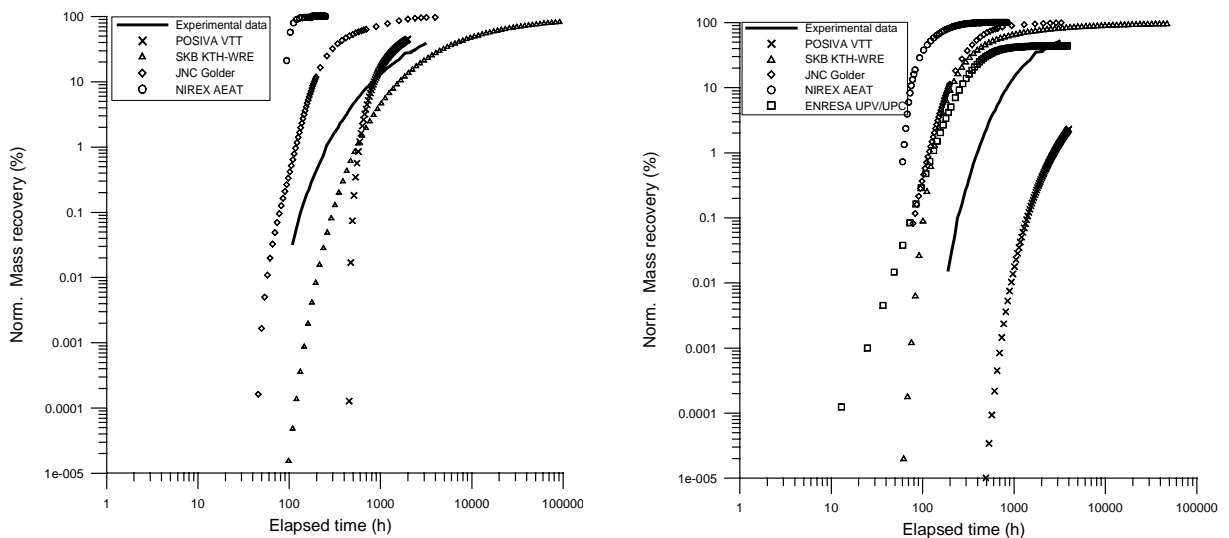


**Figure3c-30. TRUE Block Scale Phase C :** Comparison between predicted cumulative normalised mass recovery (%) and the corresponding experimental breakthrough. a) C1 (<sup>137</sup>Cs), b) C3 (<sup>86</sup>Sr), cf. Figure 3c-25.

network and two approaches which are more performance assessment-related; the LaSAR approach /Cvetkovic et al., 1999; Cvetkovic et al., 2000/ extended to the block scale and the so-called POSIVA approach /Hautojärvi and Taivassalo, 1994/. The ability to make reasonable predictions on a 15-m length scale was demonstrated when some of the models used in TRUE-1 were applied to the shortest (L=17 m) and least complex of the block scale source-sink pairs, cf. Figure 3c-30a. In the case of a longer (L=35 m) and more complex source-sink pair the models performed less well, cf. Figure 3c-30b.

## 9 Retention in the block scale

The results of the TRUE-1 *in situ* experiments /Winberg et al., 2000/ showed that radio-active sorbing tracers of the alkali and alkaline metal groups (for which ion exchange is the main sorption mechanism), Na, Ca, and Sr were transported only slightly retarded compared to the reference conservative tracers over transport distances of about 5 m, whereas Rb and Ba were moderately retarded, and Cs and Co were strongly retarded. A similar relative order of retention was also noted in the laboratory /Byegård et al., 1998/. In TRUE Block Scale, a similar pattern emerges for a single-structure flow path over a length scale of about 15 m (C1). However, no breakthroughs of  $^{83}\text{Rb}$  (C3) and  $^{137}\text{Cs}$  (C2), cf. Table 3c-2, have been observed after some six months of pumping for the two longer and more complex TRUE Block Scale flow paths, 35 and 100 m long, respectively, cf. Figure 3c-25. This in contrast to performed model predictions which overall project breakthrough for the two tracers. Continued sampling and employment of developed techniques to lower the measurement limit are expected to reveal whether the above observations in fact are true indications of a more pronounced retention on a larger scale. Possible explanations for the observed higher retention may arise from differences in mineralogy, more pronounced effects of fault breccia compared to conditions prevailing in Feature A at the TRUE-1 site, or a higher degree of heterogeneity.

## 10 Conclusions

The analysis of the characterisation data from the TRUE Block Scale rock volume has shown that it is possible to build relatively robust hydrostructural models of a rock volume on a 300 m length scale using a few and relatively unsophisticated characterisation techniques. These comprise registration of pressure responses collected during drilling and subsequent cross-hole interference tests, borehole TV (BIPS) and so-called POSIVA high resolution flow logging. It was found that the basic hydrostructural entities of the investigated rock block were identified using data from the first three boreholes. The additional two boreholes contributed additional geometrical refinement and identification of conductive structures of second order importance. Further refinement and parameterisation of the model have been achieved using various single hole and multiple hole cross-hole interference tests. The latter tests in many cases included tracer dilution tests. By comparing results of tracer dilution tests (in terms of flow rate) at pumped conditions with the corresponding values obtained at ambient conditions proved to be an effective means to identify suitable tracer injection sections for any given sink.

The TRUE Block Scale tracer experiments have successfully demonstrated the possibility to run well-controlled, quantitative experiments with radioactive sorbing tracers in interpreted single structures and networks of deterministic fractures/structures over length scales < 100m. Prerequisites for design, performance and associated model prediction and evaluation of the performed tests is a robust hydrostructural model of the investigated network of structures.

The breakthrough curves from performed tracer experiments with conservative tracers in short (spatially and temporally) single feature sink-source setups are essentially devoid of indications of effects of diffusion. In contrast, the longer and more complex source-sink set-ups show more profound indications, with near  $-3/2$  slopes in log-log plots. It is also noted, as in the case of TRUE-1, that diffusion effects are augmented for the more sorbing tracers.

Numerical modelling of the TRUE Block Scale experiments has been performed with a wide range of approaches/concepts ranging from analytical models, stochastic continuum, discrete fracture network and channel network models, to more performance assessment type model approaches. The results indicate successful outcome of model predictions in relation to experimental data on a length scale < 15 m. The correspondence between the predicted and the *in situ* results are not as good for the two longer flow paths, 35 and 100 m, respectively. The ongoing evaluation of the TRUE Block Scale experiments is expected to help assess the relative role of different retention processes and available pore spaces and increase the predictive capability on a 100 m length scale.

## 11 Acknowledgements

The collective contributions to the TRUE Block Scale Project from the field, analysis, and modelling crews of the SKB TRUE Project team, the Äspö Hard Rock Laboratory and colleagues in the TRUE Block Scale Technical Committee, field and analysis teams, are gratefully acknowledged.

The TRUE Block Scale work is funded jointly by ANDRA (France), Nirex (UK), JNC (Japan), ENRESA (Spain), Posiva (Finland) and SKB (Sweden).

## 12 References

**Andersson P, Ludvigsson J-E, Wass E, Holmqvist M, 2000a.** Interference tests, dilution tests and tracer tests (Phase A). Äspö Hard Rock Laboratory, International Progress Report IPR-00-28, Swedish Nuclear Fuel and Waste Management Co.

**Andersson P, Wass E, Homqvist M, Fierz T, 2000b.** Tracer tests, Phase B. Äspö Hard Rock Laboratory, International Progress report IPR-00-29, Swedish Nuclear Fuel and Waste Management Co.

- Andersson et al. in prep I.** TRUE Block Scale Project Final Report no. 1(4) – Characterisation and model development. SKB TR-XX-XX, Swedish Nuclear Fuel and Waste Management Co.
- Andersson et al. in prep. II.** TRUE Block Scale Project Final Report no. 2(4) – Tracer tests in the block scale. SKB TR-XX-XX, Swedish Nuclear Fuel and Waste Management Co.
- Andersson P, Byegård J, Holmqvist M, Skålberg M, Wass E, Widestrand H, in prep.** Tracer tests, Phase C. Äspö Hard Rock Laboratory, International Progress Report IPR-01-XX, Swedish Nuclear Fuel and Waste Management Co.
- Cvetkovic V, Selroos J-O, Cheng H, 1999.** Transport of reactive solute in single fractures. *J. Fluid Mech.*, Vol. 318, pp. 335–356.
- Cvetkovic V, Cheng H, Selroos J-O, 2000.** Evaluation of Tracer Retention Understanding Experiments (first stage) at Äspö. Äspö Hard Rock Laboratory, International Cooperation Report ICR-00-01, Swedish Nuclear Fuel and Waste Management Co.
- Byegård B, Johansson H, Skålberg M, Tullborg E L, 1998.** The interaction of sorbing and non-sorbing tracers with different Äspö rock types – Sorption and diffusion experiments in the laboratory scale. SKB TR-98-18, Swedish Nuclear Fuel and Waste Management Co.
- Byegård J, Widestrand H, Skålberg M, Tullborg E-L, Siitari-Kauppi M, 2001.** Complementary investigation of diffusivity, porosity and sorbtivity of Feature A site-specific material. Äspö Hard Rock Laboratory, International Cooperation Report ICR-01-04, Swedish Nuclear Fuel and Waste Management Co.
- Hermanson J, Doe T D, 2000.** March'00 structural and hydraulic model based on borehole data from KI0025F03. Äspö Hard Rock Laboratory, International Progress Report IPR-00-34, Swedish Nuclear Fuel and Waste Management Co.
- Hautojärvi A, Taivassalo V, 1994.** The INTRAVAL Project – Analysis of the Tracer Experiments at Finnsjön by the VTT/TVO Project Team. Report YJT-94-24, Nuclear Waste Commission of Finnish Power Companies, December 1994, Helsinki.
- Mazurek M, Bossart P, Eliasson T, 1997.** Classification and characterisation of water-conducting features at Äspö: Results of investigations on the outcrop scale. Äspö Hard Rock Laboratory, International Cooperation Report ICR-97-01, Swedish Nuclear Fuel and Waste Management Co.
- Siitari-Kauppi M, Flitsiyan E S, Klobes P, Meyer K, Hellmuth K-H, 1998.** Progress in physical rock matrix characterization; Structure of the pore space. In : I G McKinley and C McCombie (eds) : Scientific Basis for Nuclear Waste Management XXI, Mat. Res. Soc. Symp. Proc., Vol. 506, pp. 671–678.
- Winberg A, 1997.** Test plan for the TRUE Block Scale experiment. Äspö Hard Rock Laboratory, International Cooperation Report ICR 97-02, Swedish Nuclear Fuel and Waste Management Co.

**Winberg A, Andersson P, Hermanson J, Byegård J, Cvetkovic V, Birgersson L, 2000.** Final report of the first stage of the Tracer Retention Understanding Experiments. SKB TR-00-07, ISSN 1404-0344, Swedish Nuclear Fuel and Waste Management Co.

**Winberg A ed., 2000.** Final report of the detailed characterisation stage – Compilation of premises and outline of programme for tracer tests in the block scale. Äspö Hard Rock Laboratory, International Cooperation Report ICR-00-02, Swedish Nuclear Fuel and Waste Management Co.

# **Session 4**

**Understanding of retention  
processes in a single fracture**



# Contents

	Page
<b>Session 4 Understanding of retention processes in a single fracture</b>	
Radionuclide Retardation Project at GTS – An overview of lessons learned and ongoing experiments	181
Classification and characterisation of water-conducting features at Äspö	203

# Radionuclide Retardation Project at GTS – An overview of lessons learned and ongoing experiments

*A Möri*

*Geotechnical Institute Ltd, CH-3007 Bern, Switzerland*

## **Abstract**

The joint Nagra/JNC Radionuclide Migration Programme has now been ongoing for more than 15 years in Nagra's Grimsel Test Site (GTS). The main aim of the programme has been the direct testing of radionuclide transport models in as realistic a manner as possible. The understanding and modelling of both the processes and the structures influencing radionuclide transport/retardation in fractured granitic host rocks have matured as has the experimental technology, which has contributed to develop confidence in the applicability of the underlying research models in a repository performance assessment. In this paper, three in situ experiments which were carried out in a discrete granitic shear zone are briefly presented: The Migration Experiment (MI), the Excavation Experiment (EP) and the ongoing Colloid and Radionuclide Retardation Experiment (CRR). Each project expanded on the experimental experience and research results from the preceding experiment.

MI provided a sound data base of in situ tracer breakthrough curves which was used to derive relevant transport parameters by inverse modelling in order to enhance the capability for predictive modelling of tracer transport in a granitic shear zone. The Excavation Project (EP) then focussed on the excavation of the dipole flow field in order to describe the flow paths within the shear zone dipole and the retardation behaviour of sorbing radionuclides that are relevant to post-closure safety. The ongoing CRR experiment actually investigates the influence of bentonite colloids on the radionuclide transport behaviour through a fractured granitic host rock. Again, the experience in planning and handling of complex tracer field experiments gained in the preceding experiments will be availed.

The methodology adopted for the geological and hydrological characterisation of water-conducting features and the simplification of this characterisation for modelling purposes proved to be indeed effective on the modelling of radionuclide transport in a fractured rock.

## **1 Introduction**

The Grimsel Test Site (GTS) is an underground rock laboratory which has been operated since 1984 by the Swiss National Co-operative for the Disposal of Radioactive Waste (Nagra) in the crystalline rock of the Aare Massif. Organisations from Germany, France, Japan, Spain, Sweden, Taiwan, the USA and the Czech Republic, as well as the European Union, participate in different programmes at GTS. The partner organisations either work on Nagra projects or carry out their own experiments.

Over the last decade, a modelling approach to radionuclide transport in fractured crystalline rocks that integrates input from geological studies, hydrogeological data and geochemical data on the composition of the rock and groundwater was developed. This approach has been applied, for example, in the Kristallin-1 performance assessment (PA), that considered a repository for high-level waste sited in the crystalline basement of Northern Switzerland /Nagra, 1994/. Transport models represent always simplifications of reality insofar that:

- the processes that are incorporated and their representation in the model, and
- the geometry (structures in the rock) within which these processes operate.

In a PA, it is necessary to have confidence either that the simplifications have a negligible impact on the results or, if bounding estimates are acceptable, that the simplifications give rise to over-estimates of releases. It is also necessary to show that the parameters that are used are realistically (or at least conservatively) assigned. The direct testing of the results of a model, as used in PA, is impossible, due to the scales of space and time involved. Rather, confidence is developed through the consistency of the model assumptions, and associated databases, with a large number of diverse observations and experiments. Furthermore, the model should have the capability to make predictions, or at least bounding estimates, that can be tested, even if the scales differ from those relevant to PA. In the case of a geosphere transport model, testing needs to address /see Smith et al., 2000 for details/

- the adequacy of the catalogue of relevant processes incorporated in the model;
- the adequacy of data-collection techniques and the transferability of laboratory data to in situ conditions;
- the understanding and modelling of individual processes;
- the modelling of combined processes in the transport model.

The three presented experiments MI, EP and CRR are part of the above mentioned model development approach. Radionuclide selections as well as the definition of boundary conditions surrounding a repository have continuously adapted to the latest scenarios developed by the various experimental partners. The influence of the EBS (Engineered Barrier System) on ground water chemistry and radionuclide transport as well as the comparison with natural analogues become more and more important in the actual experiments.

## **2 Overview of Grimsel Test Site**

### ***Site characterisation and geological background***

The GTS is situated in the granitic rock of the Aare Massif at an altitude of 1730 m above sea-level with an overburden of about 450 meters. The main tunnel system, which is approximately 1 km long, was constructed in 1984 and further extended in 1996 and 1998 to accommodate new experiments. Most of the tunnels were drilled with a tunnel boring machine (diameter 3.5 m), while most of the caverns were excavated using standard drill and blast techniques. The horizontal access to the facility allows

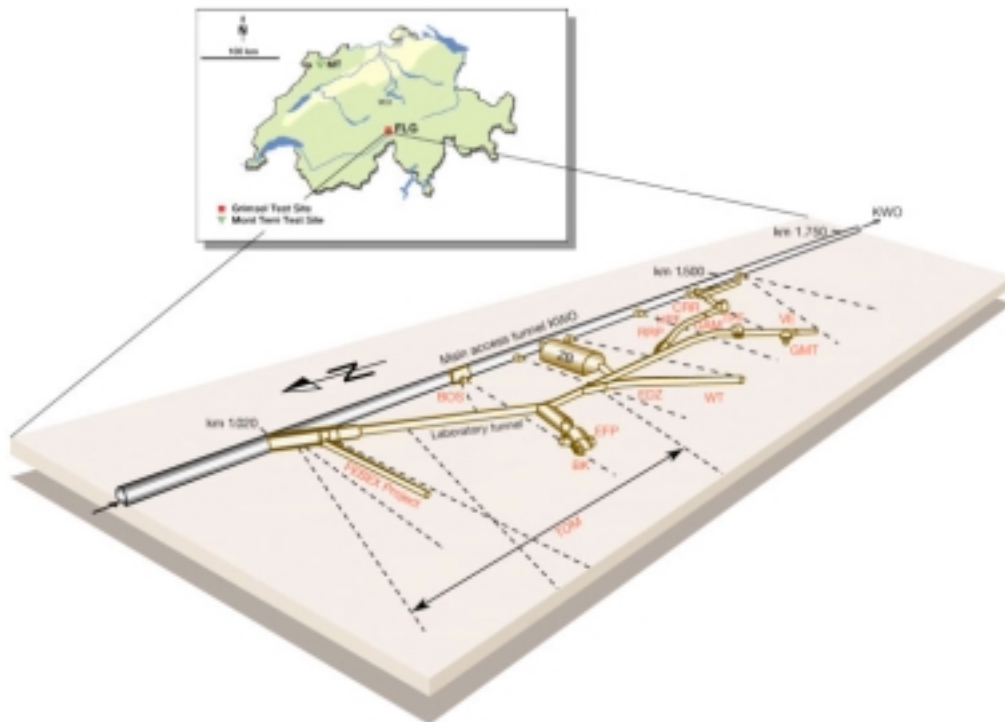


**Figure 4-1.** Geographic location and layout of the GTS.

easy transport of heavy experimental equipment and the layout of the tunnels allowed the establishment of a radiation controlled zone (IAEA type B/C) in 1990. The geographic location and schematic tunnel layout of the GTS are illustrated in Figure 4-1.

The granitic rock of the Aare Massif crystalline basement consists of a pre-Hercynian, metasedimentary envelope intruded by granitoids 320–280 Ma ago; this was followed by the intrusion of a series of lamprophyres and aplites. The whole complex underwent a “greenschist facies” metamorphism with a peak at  $19 \pm 3.9$  Ma ago. This ductile deformation stage is evidenced in NE-SW-orientated shear zones and mylonites. Reactivation of these structures took place during subsequent cooling and uplift and is mainly characterised by brittle deformation behaviour. All the main structural elements and the lamprophyre dykes dip sub-vertically. For radionuclide migration experiments in particular, deformation mechanisms and structures and their impact on the radionuclide transport properties of the shear zones (as the main water-conducting features) have been investigated in detail /Frick et al., 1992; Bossart et al., 1991/ and are summarised in Table 4-1. Basically, the southern part of the facility is characterised by the occurrence of single shear zones which form a set of sub-parallel striking fracture planes. This area is particularly suitable for experiments aimed at understanding transport processes of gas or radionuclides. In the northern part, a fracture network and more pronounced lamprophyres provide suitable locations for the development and testing of site characterisation tools, including geophysical investigations, as well as for the characterisation and definition of relevant parameters on a large scale.

**Table 4-1. Structural units, main deformation characteristics and resulting flow paths.**

Structural unit	Deformation	Flowpath	Porosity
Granitic matrix	<ul style="list-style-type: none"> <li>– ductile</li> <li>– weak cleavage</li> </ul>	<ul style="list-style-type: none"> <li>– grain boundary pores</li> <li>– solution pores</li> <li>– transgranular pores</li> </ul>	0.5–1.5%
Non-reactivated ductile shear zones and fractures	<ul style="list-style-type: none"> <li>– ductile</li> <li>– intense cleavage</li> <li>– quartz ribbons</li> <li>– stretching lineation</li> </ul>	<ul style="list-style-type: none"> <li>– sheet silicate pores</li> <li>– grain boundary pores</li> </ul>	< 0.1%
Reactivated ductile shear zones and fractures	<ul style="list-style-type: none"> <li>– brittle</li> <li>– creep structures</li> <li>– weak cohesion</li> </ul>	<ul style="list-style-type: none"> <li>– fault gouge porosity</li> </ul>	10–30%
Dykes	<ul style="list-style-type: none"> <li>– ductile, with brittle overprinting at contacts to granite</li> <li>– cleavage refraction</li> </ul>	<ul style="list-style-type: none"> <li>– grain boundary pores</li> <li>– sheet silicate pores</li> <li>– at contacts: fault gouge porosity</li> </ul>	ca 1%
Extension fractures	ductile to brittle	<ul style="list-style-type: none"> <li>– solution pores</li> <li>– grain boundary</li> </ul>	ca 5%

First indications of the general hydrogeological situation at the GTS were obtained from boreholes drilled prior to construction. Hydraulic pressures of up to 40 bar indicated that the overlying rock was fully saturated almost to the top of the Juchlistock, the overlying peak. At present, hydraulic pressures of up to 15 bar can be measured at most of the experimental sites at a distance of approximately 20 metres from the tunnel surface. The total water inflow to the GTS tunnel system is about 2 litres or more per minute and is concentrated in about 25% of the identified fractures. Almost all the water-bearing features appear to be associated with ductile structures, overprinted by subsequent brittle deformation. The hydrogeological characteristics of individual shear zones depend largely on the intensity of brittle deformation. General bulk hydraulic conductivity values of  $10^{-9}$  to  $10^{-10}$  m/s for shear zones and  $10^{-11}$  to  $10^{-12}$  m/s for the rock matrix are measured at GTS. It should be noted that the shear zones in particular show a large variability in their hydraulic properties.

### ***Experimental programme***

Since the start of operations at the GTS, a series of experimental programmes has been performed, covering geological, hydrogeological, geophysical, geochemical and engineering aspects of deep geological disposal. The results of the experiments are published in the Nagra Technical Report (NTB) series and provide a comprehensive database for planning and implementation of new, more complex investigations. For the most recent research phase, in particular, a systematic evaluation procedure has been applied to establish an experimental programme that is directly related to site selection and planned underground investigations at a repository site as well as to support the development of PA codes /McCombie et al., 1997/.

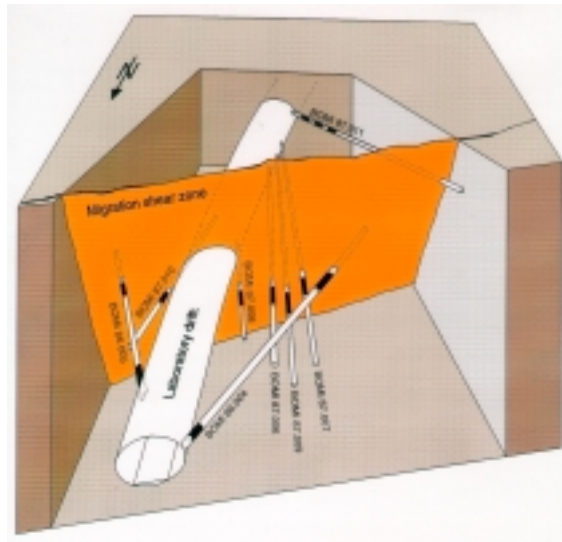


**Figure 4-2.** Block model of MI shear zone.

Work on transport modelling began at the GTS in 1985 with the hydrogeological characterisation of a water conducting shear zone in a granodioritic host rock, the MI zone (see Figure 4-2), and has continued with a large series of in situ tracer migration experiments, increasing in complexity from simple, non-sorbing tracers (fluorescein dye Uranine,  $^{82}\text{Br}$ ,  $^{123}\text{I}$ ,  $^3\text{He}$  and  $^3\text{H}$ ) through various weakly sorbing tracers ( $^{22}\text{Na}$ ,  $^{24}\text{Na}$ ,  $^{85}\text{Sr}$  and  $^{86}\text{Rb}$ ) to a long-term experiment with strongly sorbing  $^{137}\text{Cs}$  /Frick et al., 1992; Heer and Hadermann, 1996; Smith et al., 2000/. Most recently, chemically complex tracers ( $^{241}\text{Am}$ ,  $^{242}\text{Pu}$ ,  $^{237}\text{Np}$ ,  $^{99}\text{Tc}$ ,  $^{113}\text{Sn}$ ,  $^{75}\text{Se}$ ,  $^{234}\text{U}$ ,  $^{235}\text{U}$ ,  $^{237}\text{Np}$ ,  $^{60}\text{Co}$ ,  $^{152}\text{Eu}$  and stable Mo) have been utilised followed by the physical excavation of a part of the shear zone to recover these strongly retarded radionuclides /Alexander et al., 1996; 2000/.

In the ongoing Phase V (1997–2002), two experiments investigating radionuclide retardation in the geological barrier are being performed in the radiation-controlled zone of the GTS. Both the High-pH Plume in Fractured rock (HPF) and the Colloid and Radionuclide Retardation (CRR) experiments have similarities with the migration/excavation experiments /Heer and Hadermann, 1996; McKinley et al., 1988/, but now specifically address the retardation behaviour of safety-relevant nuclides in the presence of near-field colloids (CRR experiment) and the effect of high-pH leachates on the host rock and the retardation behaviour of radionuclides (HPF experiment). For both experiments, a single shear zone (in the case of CRR, the well characterised migration experiment (MI) zone) is used as the test field.

## 2 The Migration Experiment (MI)

As noted before, the MI experiment investigated the migration behaviour of a large series of non- to strongly-sorbing active tracers. Here the main findings will be summarised by a more detailed examination of the tracer breakthrough of the weakly sorbing tracer  $^{85}\text{Sr}$  and the strongly sorbing  $^{137}\text{Cs}$  and subsequent conclusions for predictive modelling of in situ tracer experiments.

## **Objectives**

Tracer migration experiments in the migration shear zone have been performed and modelled as a joint undertaking of Nagra (Swiss National Co-operative for the Disposal of Radioactive Waste) and JNC (Japan Nuclear Cycle Development Institute), with the support of PSI (Paul Scherrer Institute, Switzerland). The aims of the investigations were:

- to improve understanding of radionuclide transport through fractured crystalline rock;
- to develop and test transport models that describe the experimental system and allow predictive modelling and that may also provide a basis for geosphere performance assessment modelling;
- to compare laboratory results with in-situ results (with regard to the different conditions).

## **Experimental layout**

The central component of MI is a series of radiotracer-transport tests which were supported by a range of field and laboratory investigations and modelling studies aimed at understanding and, ultimately, predicting the radionuclide migration in the geosphere. The general proceeding of the MI experiment is shown in Figure 4-3. The in situ tests were performed in different dipoles within a single, approximately planar, shear zone that was selected on the basis of criteria given in Frick et al. /1992/. The layout of the dipoles is shown in Figure 4-4.

The following methodology was adopted when applying the PSI transport model to the migration experiments:

### *Step 1: Inverse modelling:*

For a suitable experimental flow field, the model was fitted to the experimental breakthrough curves for non-sorbing and sorbing tracers.

### *Step 2: Consistency of derived parameter values:*

Transport parameter combinations were derived from the tracer breakthrough curve fits. Since the number of individual physico-chemical parameters exceeds the number of parameter combinations that can be fitted, additional information (e.g. from independent observations and experiments) is required in order to obtain these individual parameters. Consistency of derived parameters with all available information was sought and, where necessary, the details of the model concept were modified.

### *Step 3: Predictive (or blind) modelling:*

The model was calibrated using parameters that were expected to be independent of the experimental flow field in a given shear zone. Predictions were then made, using the calibrated model, of the experimental breakthrough curves for a different flow field or different tracers, in which the various processes are expected to be weighted differently.

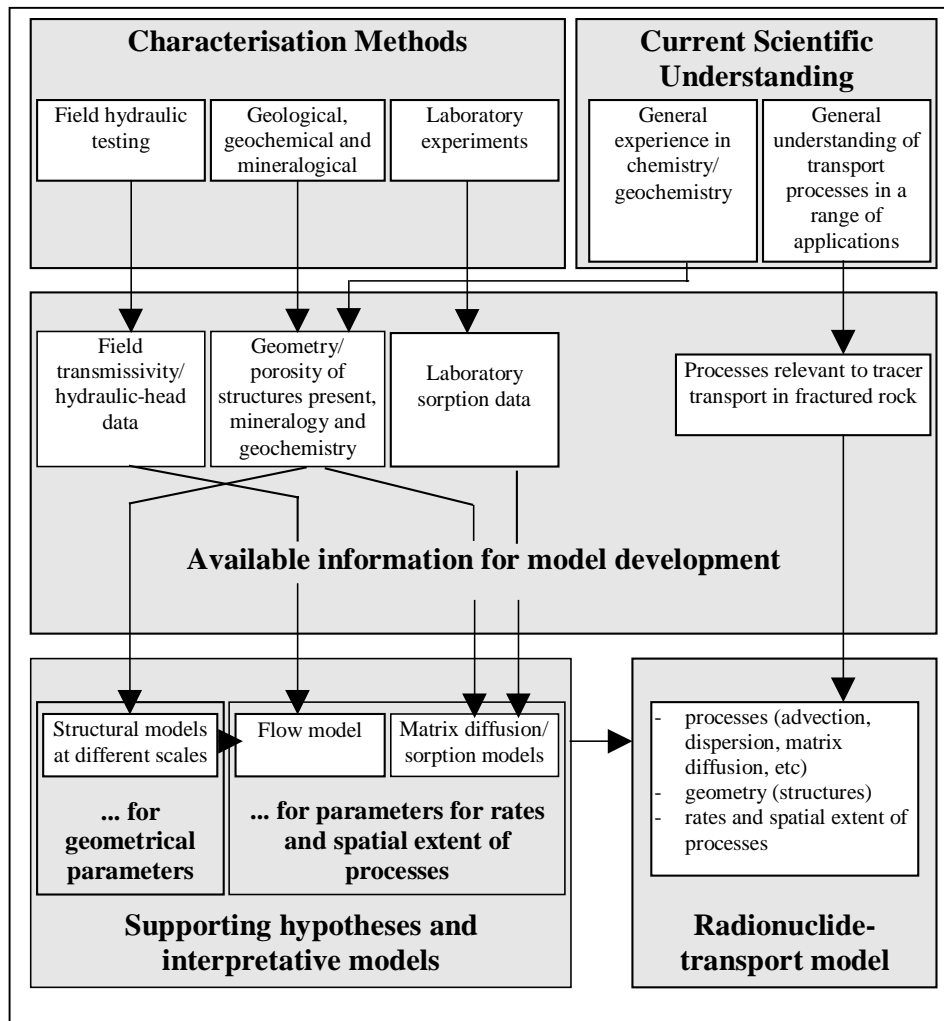


**Figure 4-3.** The use of supporting hypotheses and interpretative models to interpret field and laboratory data in terms of input parameters of a transport model /from Smith et al., 2000/.

Inverse modelling (step 1) and derivation of the relevant transport parameters (step 2) was carried out with the  $^{85}\text{Sr}$  and  $^{137}\text{Cs}$  tracer breakthrough data from the 4.9 m dipole (see Figure 4-4). The expected tracer breakthrough curves for  $^{85}\text{Sr}$  and  $^{137}\text{Cs}$  in the 1.7 m dipole were then predicted /for details see Heer and Hadermann, 1996/. In the final experiment of the MI project (not presented here),  $^{137}\text{Cs}$  was injected into the 14 m dipole (see Figure 4-4) and this work is discussed in Heer /2000/.

### **Conceptual model**

A conceptual model of the flow path and the related transport processes within the investigated MI shear zone was derived from both structural geological investigations on resin impregnated shear zone samples and a series of laboratory investigations. The laboratory work mainly focussed on the mineralogy and porosity distribution within the shear zone and on the characterisation of the cohesionless fraction (e.g. fault gouge and breccia) between the shear zone walls. A simplified picture of the complex reality of the internal build up of a granitic shear zone is shown in Figure 4-5 (upper part). This simplified reality and the derived laboratory parameters were then transferred into a conceptual model for tracer transport in a shear zone. The resulting transport model



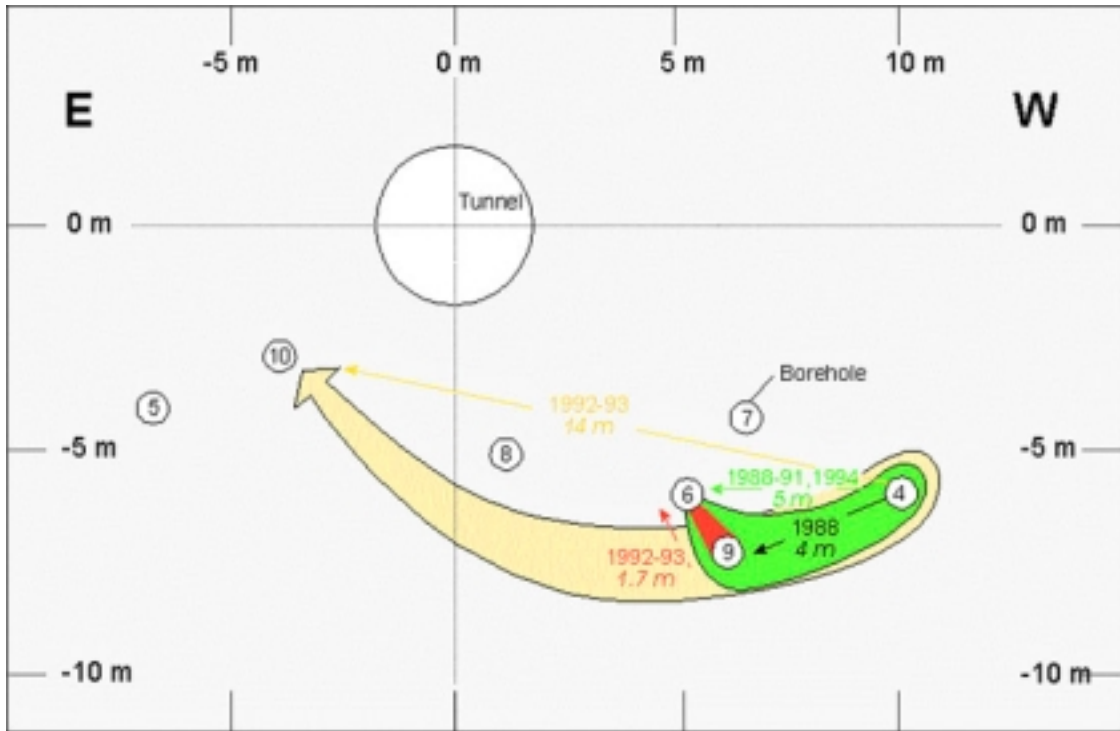


Figure 4-4. Dipole configuration of MI experiments.

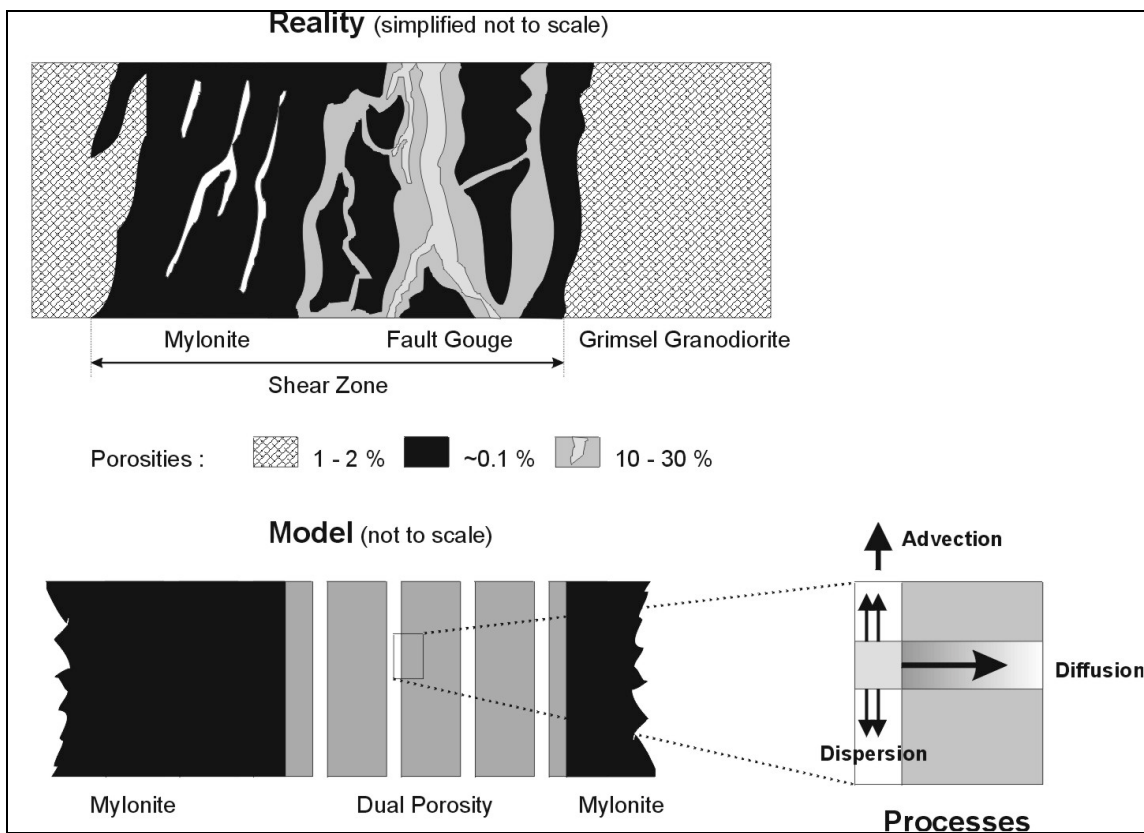


Figure 4-5. Dual porosity concept for transport modelling.

follows a dual porosity concept with open channels which take up advection and dispersion and with fault gouge which is accessible for matrix diffusion.

### Main findings

Figure 4-6 shows the breakthrough curves for  $^{85}\text{Sr}$  and  $^{137}\text{Cs}$  in the 4.9 m flow field. The graphs contain the experimental data (dots) collected at the outlet borehole as well as the modelled breakthrough curves with different modelling approaches. The black solid lines represent the final model fit curve to the measured breakthrough curves of  $^{85}\text{Sr}$  and  $^{137}\text{Cs}$ .

For the non-sorbing dye Uranine, position and shape of the peak were, to a large extent, governed by advection and dispersion. The pronounced tailing, that approaches the  $t^{-3/2}$  asymptote, was taken as an experimental indication of the occurrence of matrix diffusion /Heer and Hadermann, 1996/ and the presence of a “tail-end perturbation” suggested that the depth of the diffusion-accessible porosity is limited. For the sorbing tracers  $^{85}\text{Sr}$  and  $^{137}\text{Cs}$ , however, an increased influence of matrix diffusion with increasing sorption strength is observed, broad peaks without “tail end perturbations” within the duration of the experiments (see Figure 4-6). For  $^{137}\text{Cs}$ , especially noteworthy is the large peak height reduction (by a factor of 7,000) and delay (by a factor of 1,000) with respect to Uranine.

The predicted breakthrough curves for  $^{85}\text{Sr}$  and  $^{137}\text{Cs}$  for the shorter 1.7 m flow field are shown in Figure 4-7 where the model predictions are compared to the experimental data. Whereas the non-sorbing Uranine showed excellent agreement between the predictions and the field measurements of the breakthrough peaks, the strongly reduced breakthrough time with respect to the 4.9 m dipole flow field for  $^{85}\text{Sr}$  is less well predicted, but still tends to support the concept of advection through narrow, open channels. For  $^{137}\text{Cs}$ , the model does not predict the fast breakthrough, but only the final tail. An additional calculation with a lower sorption coefficient (dot-dashed line) fails to describe the overall shape of the experimental breakthrough curve, indicating that sorption kinetics, irrelevant for the larger time scales characterising the 4.9 m dipole, is the most obvious candidate for refining the model.

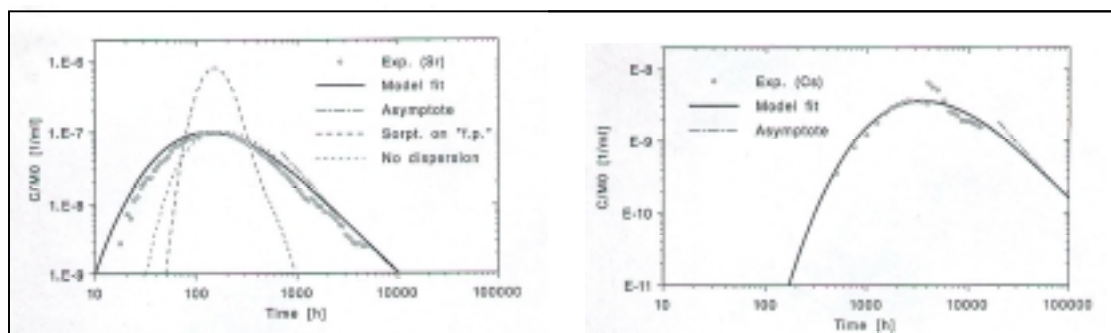


Figure 4-6. Breakthrough curves for  $^{85}\text{Sr}$  and  $^{137}\text{Cs}$  in the 4.9 m flow field (inverse modelling).

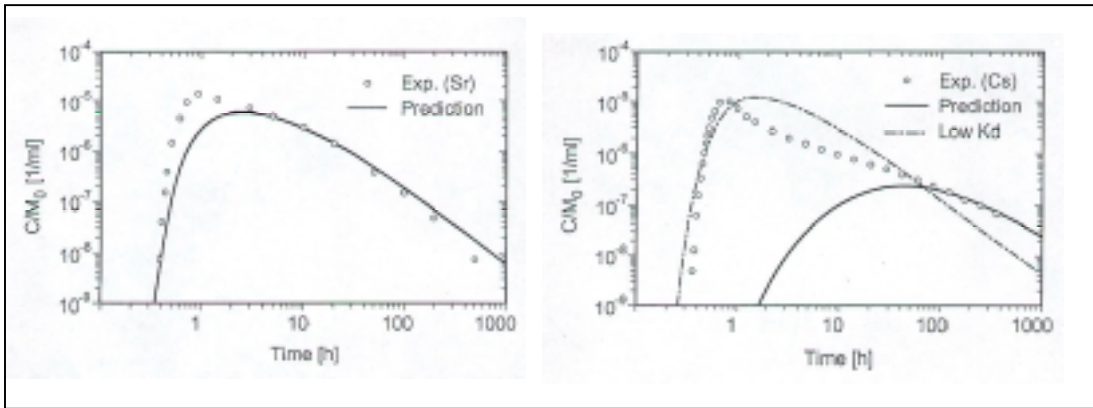


Figure 4-7. Breakthrough curves for  $^{85}\text{Sr}$  and  $^{137}\text{Cs}$  in the 1.7 m flow field (predictive modelling).

MI also showed, that physical parameters, such as flow porosity, dispersion length and diffusion coefficient, derived effectively through model testing, are consistent with values from independent field observations so supporting the underlying model concepts. In addition, and potentially more importantly, there is a good agreement between values for the radionuclide distribution coefficients ( $K_d$ ), obtained by different laboratory and field techniques (see Table 4-2). In particular, for radionuclides that sorb rapidly and exhibit a reversible cation exchange on the rock, the results of laboratory experiments can be extrapolated reasonably well to in situ conditions, provided sufficient care is exercised in selecting and preparing the rock samples so as to ensure that they properly reflect the geological character of the site.

Table 4-2.  $K_d$  values derived from breakthrough modelling compared to laboratory data.

Nuclide	$K_d$ ( $\text{m}^3 / \text{kg}$ )	
	Field data	Laboratory data
$^{85}\text{Sr}$	$2.1 \cdot 10^{-2}$	$1.3 \cdot 10^{-2}$
$^{137}\text{Cs}$	$2.9 \cdot 10^{-1}$	$1.6 \cdot 10^0$

### 3 The Excavation Experiment (EP)

The Excavation Experiment constitutes part of the Radionuclide Retardation Project (RRP) which expands on the MI experiment. Similar to MI, tracer breakthrough curves were recorded in the field, but were then followed by excavation of the whole flow field and subsequent core analyses.

#### Objectives

EP focussed on the structure of the shear zone and on the behaviour of radionuclides that are relevant to repository post-closure safety, but are so strongly retarded by interaction with the shear-zone rock that they are not expected to pass completely through the dipole flow field in experimentally reasonable times. The aims of EP were

- to elaborate an in situ injection technique for strongly sorbing tracers in a URL (Underground Rock Laboratory);
- to develop an in situ conservation technique of the shear zone and the potentially sorbed radionuclides and to find an appropriate excavation technique;
- to examine directly the sites of in situ radionuclide retardation and to obtain a better understanding of the in-situ flow system (channels, matrix porosity etc).

### **Experimental layout**

Before the in situ experiment was started, a large laboratory programme was carried out in order to determine sorption properties of the different nuclides, to develop the resin for shear zone impregnation and to select the appropriate analysis techniques for solid phase analysis of the nuclides sorbed on the shear zone (i.e. autoradiography, total dissolution analysis, secondary ion mass spectrometry and nuclear microprobe analysis). The tracer cocktail for the in situ experiment was kept in glass ampoules and the injection borehole was packed off by a triple packer system. The down hole equipment was constructed such that the glass ampoules could be introduced into the packed off shear zone interval without removing the injection system. The composition of the cocktail is shown in Table 4-3. Breakthrough curves of the  $\gamma$ -emitting nuclides were measured on-line by using an Intrinsic Ge detector whereas the  $\alpha$ -emitters were analysed off-line in the GTS tunnels with Si surface barrier  $\alpha$ -detectors /see Eikenberg et al., 1998 for details/.

**Table 4-3. Radioisotopes used in EP with the activity injected into the 1,7 m dipole.**

<b>Nuclide</b>	<b>Half-life</b>	<b>Decay mode</b>	<b>Injected activity (Bq)</b>
<sup>60</sup> Co	5.26 y	$\beta^-$ , $\gamma$	$2.03 (60.05) \cdot 10^6$
<sup>75</sup> Se	120.4 d	ec, $\gamma$	$1.08 (60.08) \cdot 10^7$
<sup>113</sup> Sn	115.1 d	ec, $\gamma$	$1.93 (60.10) \cdot 10^6$
<sup>152</sup> Eu	13.3 y	ec, $\beta^+$ , $\gamma$	$2.96 (60.10) \cdot 10^5$
<sup>234</sup> U	$2.5 \cdot 10^5$ y	$\alpha$ , ( $\gamma$ )	$5.74 (60.37) \cdot 10^5$
<sup>235</sup> U	$7.0 \cdot 10^8$ y	$\alpha$ , $\gamma$	$1.54 (60.10) \cdot 10^4$
<sup>233</sup> Pa	27.0 d	$\beta$ , $\gamma$	$5.80 (60.40) \cdot 10^{5(c)}$
<sup>237</sup> Np	$2.1 \cdot 10^6$ y	$\alpha$ , $\gamma$	$5.80 (60.60) \cdot 10^5$

After the injection phase, the 1.7 m long dipole flow field was impregnated with a fluorescein epoxy resin in order to stabilise the whole shear zone prior to the recovery of the radionuclide doped part of the shear zone. The flow field was excavated by means of two overcoring boreholes with an outer diameter of 380 mm (see Figure 4-8). The active cores were removed and kept in the plastic liner from the triple core drilling system and subdivided into core sections of about 0.5 m length. The core sections were then sawn into slabs of 3 to 5 cm thickness for “post-mortem” analysis. These analyses consisted of a structural geological characterisation of the shear zone and a three-dimensional model of the flow paths within the dipole as well as a determination of the distribution of injected radionuclides within the flow field /see Alexander et al., 1996, 2000 for details/.

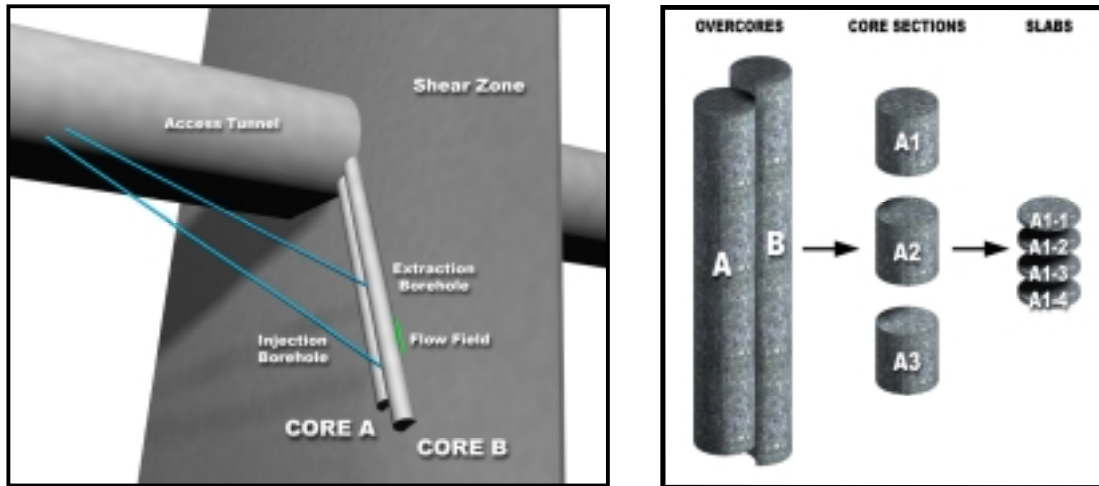


**Figure 4-8** Overcoring of dipole flow field (left) and sawing of slabs (right).

### **Main findings**

The methods applied in this technically challenging experiment were successful. 90% of the flow field containing almost 100% of the retarded radionuclides could be excavated owing to the resin impregnation of the shear zone and the applied triple-barrel drilling technique. The slabs revealed a sound data base for the characterisation of the flow path within the shear zone.

The experimental shear zone was known to be highly heterogeneous /Bossart et al., 1991/, but the degree to which channels in the water conducting features controlled radionuclide migration was nevertheless surprising and this would be worth considering further in any future in situ tests of transport codes (see Figure 4-9). Dead-end channels, short-cuts between adjacent channels and merging and bifurcating of migration pathways characterised radionuclide flow on the metre and centimetre scale.

Interestingly, not all the seemingly open channels were involved in radionuclide transport.

The breccia components for the adjacent wall rock (mylonite and less deformed granodiorite) were generally supported by fault gouge which was also impregnated with the fluorescein resin. This accessibility of the fault gouge for fluids was reflected also in the preferential distribution of sorbed radionuclides on fault gouge /for details see Berry et al., 2000; Möri and van Dorp, 2000a; Ota et al., 2000/.

Matrix diffusion played a significant role in radionuclide retardation although most material was not trapped in the rock matrix *sensu stricto*, rather in the highly porous fault gouge present in the system. This has serious implications for repository site characterisation drilling techniques: unless double-, or better still, triple-barrel core recovery technology is used, such fault gouges are frequently lost from deep boreholes and there will, therefore, be a tendency to under-estimate potential geosphere retardation (never mind the impact on the hydrogeological assessment of the site).

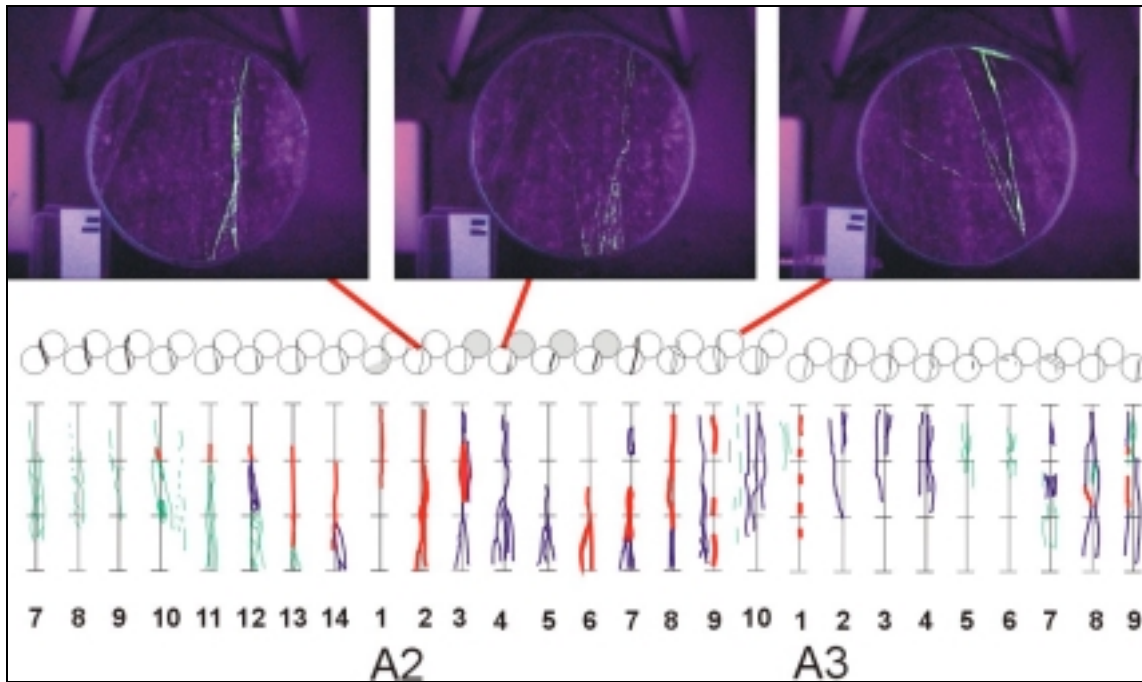


**Figure 4-9.** Evolution of impregnated flow paths along overcore “A” (flow direction was normal to the slab surfaces). Above: slab surfaces with impregnated flow path’s under UV light, below: development of flow path’s along flow field, red, blue and green lines indicate impregnated parts of the shear zone mapped from slab surfaces.

The spatial distribution of radionuclides along the flow path revealed element-specific concentration profiles. Figure 4-10 shows the element distribution of  $^{237}\text{Np}$  between the injection and the extraction borehole. The element concentrations were derived from total dissolution data from samples which were selected from active areas located by autoradiography imaging of the slab surfaces. The mass balance revealed that about 75% of the injected  $^{237}\text{Np}$  remained in the shear zone, with mostly sorbed around the injection borehole.

The basic modelling approach employed in MI was shown to reasonably predict the spatial distribution of the strongly sorbing radionuclides along the experimental flow path (namely in the vicinity of the injection borehole and at a short distance along the flow path). Again, this demonstrates, at least qualitatively, that laboratory derived  $K_d$  values may be used with care in transport modelling if the laboratory system can be set up to mimic the in situ conditions appropriately. Of course, this was not the case for all radionuclides:  $^{75}\text{Se}$ , although injected into the flow path in reducing form (selinite), appeared to behave as a non-sorbing tracer (i.e. as selenate). Unlike the case for  $^{137}\text{Cs}$  in the MI experiment (above), where kinetics was shown to be the problem, here it seems more likely that equipment problems allowed oxidation of the  $^{75}\text{Se}$  (but this is still under investigation).



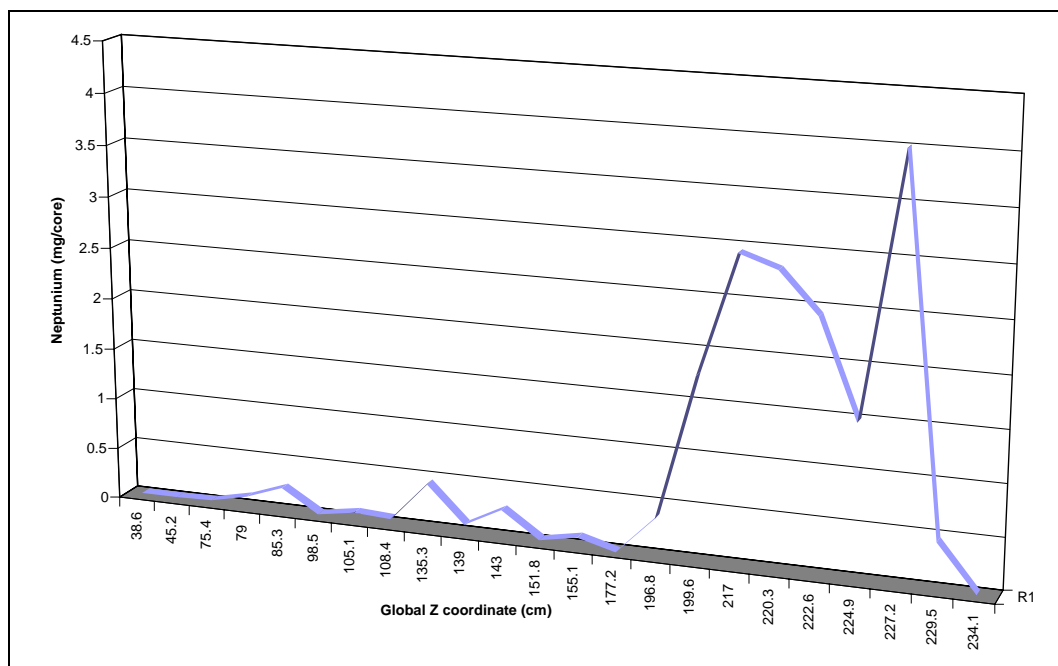


**Figure 4-10.** Distribution of  $^{237}\text{Np}$  between the injection borehole at 229.5 cm and the outlet borehole at 45.2 cm.

#### 4 The Colloid and Radionuclide Retardation project (CRR)

In most HLW (high-level radioactive waste) repository designs, the waste is packaged in a massive metal canister (e.g. steel, in the Swiss design) which is surrounded by a large volume of bentonite backfill. The canister will slowly degrade and eventually fail, releasing small quantities of radionuclides, most of which are expected to decay within the bentonite. However, it is conceivable that erosion of the bentonite at the bentonite/host rock interface (see Figure 4-11) could produce colloids, as noted in a memo of March 1989 from HSK, the Swiss Federal Office of Reactor Safety, which stated that “... the generation of colloids at the boundary of the bentonite package cannot be excluded...”. The full consequences of this scenario are unclear but, as HSK note further (*op cit*) “... colloid facilitated transport of strongly sorbing radionuclides at the near field / far field boundary remains very much an open question...”. As one of the major roles of the research programmes carried out in URLs is to address such open questions in the repository PA, it was decided to examine bentonite colloid facilitated transport of radionuclides in the far-field in GTS Phase V by means of the CRR (colloid and radionuclide retardation) project (which is based on the experience gained in MI and EP). Due to the complexity of the field experiment, CRR was divided into two phases: a first phase of detailed laboratory experiments (with associated modelling), followed by a second, still ongoing, phase of additional preparational field experiments and the final in situ experiment.

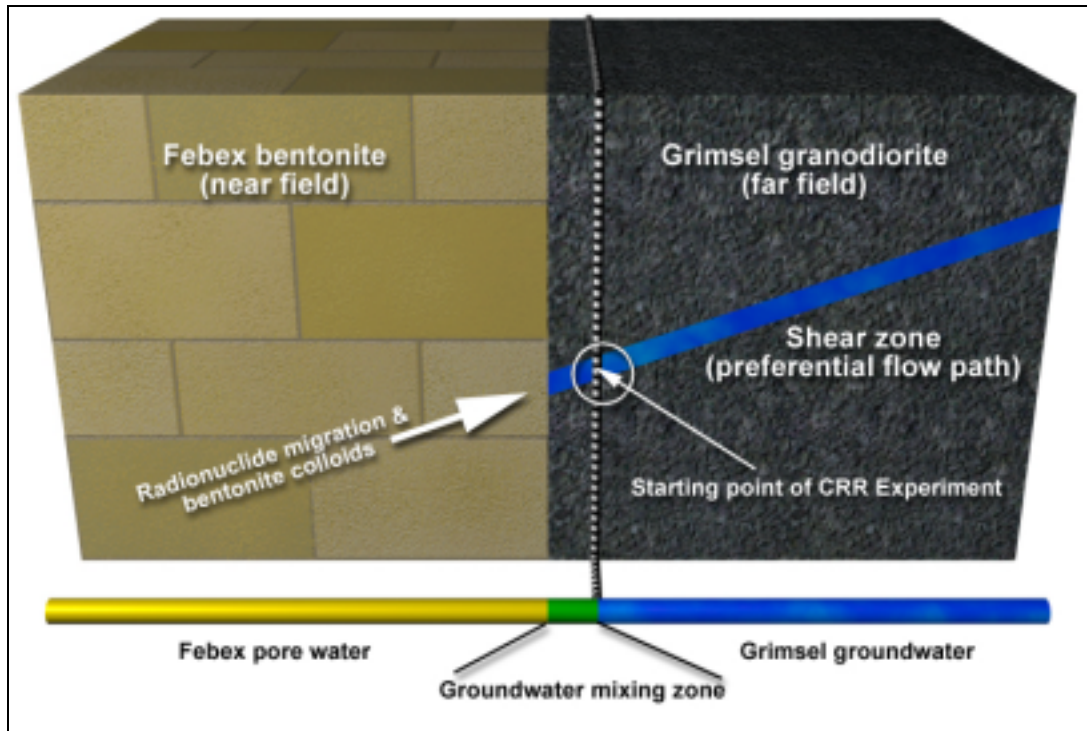


*Figure 4-11. Experimental concept of the CRR Project.*

### **Objectives**

The broad objective of the CRR experiment is to provide an improved understanding of the stability and in-situ retardation of colloid-bound safety-relevant radionuclides in the vicinity of the near-field/far-field interface. Prior to beginning the in situ experiment, three main questions had to be answered:

- is it likely that bentonite colloids will be generated at the bentonite / granite interface and are these colloids stable in the Grimsel Ground Water?
- which are the solubilities of the selected RN's in natural Grimsel Ground Water, can they be detected in solution and, if any sorption occurs in the flow field, can they be detected in the rock after excavation?
- can the tracer cocktail be safely handled in the field (sorption of nuclides on equipment, requirements for radioprotection)?

### **Experimental layout**

From the technical point of view, the in situ experiment of CRR is based on the preceding EP experiment, including injection of active tracers, resin impregnation and overcoring followed by subsequent core analysis. The main changes in the layout are the use of a Laser Induced Breakdown Detector (LIBD) for on site detection of colloids and the complete PEEK<sup>1</sup> coating of the equipment.

<sup>1</sup> PEEK (polyetheretherketone) is a flexible polymer material for tubings and fittings and is resilient to most chemicals.



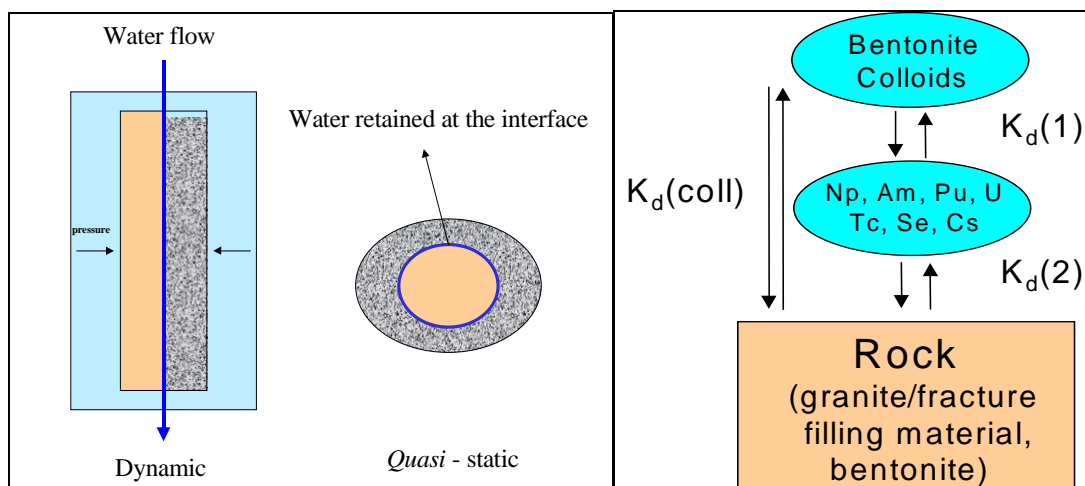


**Figure 4-12.** Schematic overview of the granite plus bentonite experiments simulating the near field / far field interface (left) and investigated sorption reactions for radionuclides and colloids in the Grimsel granodiorite.

AN intense modelling and laboratory programme was carried out in Phase 1 mainly by Ciemat (E), FZK (D), QuantiSci (E) and JNC (J) aimed to prove the feasibility of the planned field experiment. Modelling calculations regarding solubility, retardation and speciation of radionuclides were compared to literature data on the concentration, generation and stability of different colloid types such as the natural colloids found in the Grimsel Ground Water, bentonite colloids and radiocolloids (e.g.  $\text{PuO}_2$ ). A detailed laboratory programme with evaluation of solubility and sorption behaviour of radionuclides in different media as well as colloid generation, stability and labelling experiments were carried out (see Figure 4-12). A first field campaign served for site characterisation in order to define boundary conditions for the in-site experiment and for the development of conceptual models.

The final tracer injection will be divided into two injection runs: a first run with  $^{243}\text{Am}$ ,  $^{237}\text{Np}$ ,  $^{242}\text{Pu}$ ,  $^{238}\text{Pu}$ ,  $^{238}\text{U}$ ,  $^{85}\text{Sr}$  and  $^{232}\text{Th}$  in Grimsel groundwater in absence of bentonite colloids and a second injection with  $^{241}\text{Am}$ ,  $^{237}\text{Np}$ ,  $^{244}\text{Pu}$ ,  $^{238}\text{Pu}$ ,  $^{233}\text{U}$ ,  $^{99}\text{Tc}$ ,  $^{137}\text{Cs}$ ,  $^{85}\text{Sr}$ ,  $^{232}\text{Th}$  in Grimsel groundwater in presence of 20 mg of bentonite colloids per litre. The use of different isotopes for Am, U and Pu in both runs will guarantee to distinguish the sorbed nuclides between run 1 and 2 on the excavated samples. The migration/retardation behaviour will be observed via tracer breakthrough. Rock samples from the flow-field will be recovered for detailed definition of radionuclide/colloid sinks, in conjunction with definition of the flow system.

### **Preliminary results**

The work carried out in the Phase 1 laboratory and modelling exercises produced the following results and conclusions for the in situ injection in Phase 2 /for details see Möri ed., 2000b/:

The calculations based on laboratory sorption data (backed by literature data and experience from the RRP project) of Phase I indicate that, while keeping well within radioprotection limits and solubility limits (see Table 4-4), it is feasible to design a tracer cocktail which will still be possible to analyse using current techniques like ICP

MS and where the activities likely to be trapped in the shear zone will be detectable in the solid phase (e.g. autoradiography and total dissolution).

**Table 4-4. Calculated solubility limits for radionuclides in Grimsel Ground Water and Febex Pore Water with predicted dominant solid phases.**

RN	Febex		Grimsel
	Oxidising (458 mV)	Reducing (-190 mV)	(-70 / -200 mV)
Cs	nsl	nsl	Nsl
Ra	$5 \cdot 10^{-8}$ (RaSO <sub>4</sub> )	$5 \cdot 10^{-8}$ (RaSO <sub>4</sub> )	$10^{-6}$ (RaSO <sub>4</sub> )
Se	nsl	$10^{-9}$ (Se or FeSe)	$10^{-9}$ (Se)
Tc	nsl	$10^{-8}$ (TcO <sub>2</sub> )	$10^{-3}$ (TcO <sub>2</sub> , -70 mV) $10^{-8}$ (TcO <sub>2</sub> , -200 mV)
Am	$7 \cdot 10^{-7}$ (AmOHCO <sub>3</sub> (am))	$7 \cdot 10^{-7}$ (AmOHCO <sub>3</sub> (am))	$10^{-7}$ (AmOHCO <sub>3</sub> (am))
Th	$10^{-8}$ (Th(OH) <sub>4</sub> (am))	$10^{-8}$ (Th(OH) <sub>4</sub> (am))	$10^{-8}$ (Th(OH) <sub>4</sub> (am))
U	$10^{-4}$ (schoepite)	$10^{-9}$ to $10^{-8}$ (U(IV)solids)	$10^{-4}$ (Eh= -70 mV) $10^{-8}$ (Eh=-200 mV)
Np	$10^{-4}$ (NpO <sub>2</sub> OH)	$10^{-8}$ (Np(OH) <sub>4</sub> (am))	$10^{-8}$ (Np(OH) <sub>4</sub> (am))
Pu	$10^{-10}$ (Pu(OH) <sub>4</sub> (am))	$10^{-9}$ (PuOHCO <sub>3</sub> )	$10^{-10}$ (Pu(OH) <sub>4</sub> (am))

LIBD analysis on GGW showed that the natural colloid population is low and labelling natural colloids with safety relevant radionuclides is not feasible. Vitrified Waste-derived radiocolloids were found to be unstable in the GGW, especially in the presence of bentonite colloids. On the other hand, it was found that ground water flow at the host-rock bentonite interface indicate bentonite colloid generation. FEBEX bentonite colloids showed a range of size from 70 to 300 nm. The colloids remained stable in concentration of several tens of mg/litre in alkaline GGW even after several month, but not in the Febex pore water. It was also seen that waste derived radio colloids are unstable in the GGW, especially in the presence of bentonite colloids. The near-field (bentonite) colloids can be unambiguously labelled with radionuclides which will remain stable in solution for the duration of the field injection (see also Figure 4-13, influence of colloids on sorption properties of actinides on granite). A first in situ bentonite colloid injection in the GTS revealed that 50% of the colloids passed through the shear zone completely unretarded.

The strong sorption to fracture infill and granite of the actinides Am, Pu and the fission product Cs and Tc is expected to lead to a strong retardation or even immobilisation of these radionuclides. Np(V) will probably elute like a very weakly or non-sorbing tracer while U will probably behave as a weakly sorbing tracer due to the short contact time with the solid surface. However, due to the high sorption of Am, Pu, U and Cs to bentonite colloids, colloid facilitated transport of these radionuclide may occur.

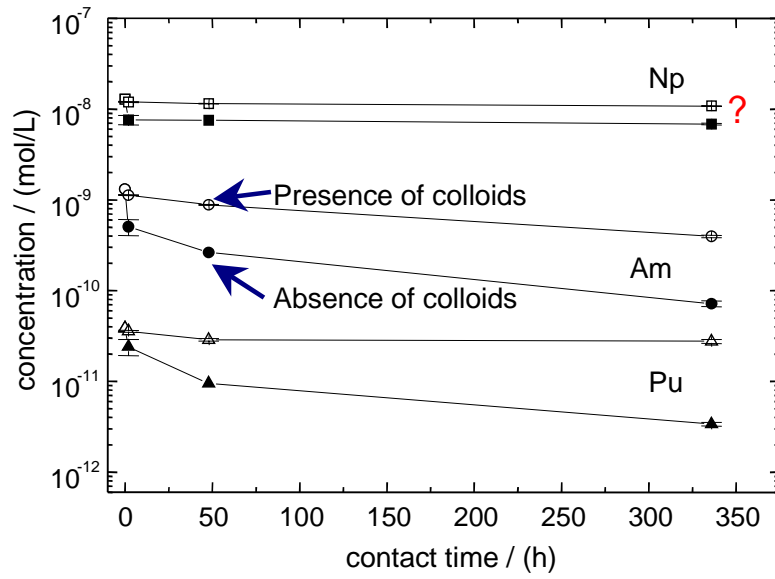


Figure 4-13. Sorption of Am, Np and Pu on granite in presence and absence of bentonite colloids.

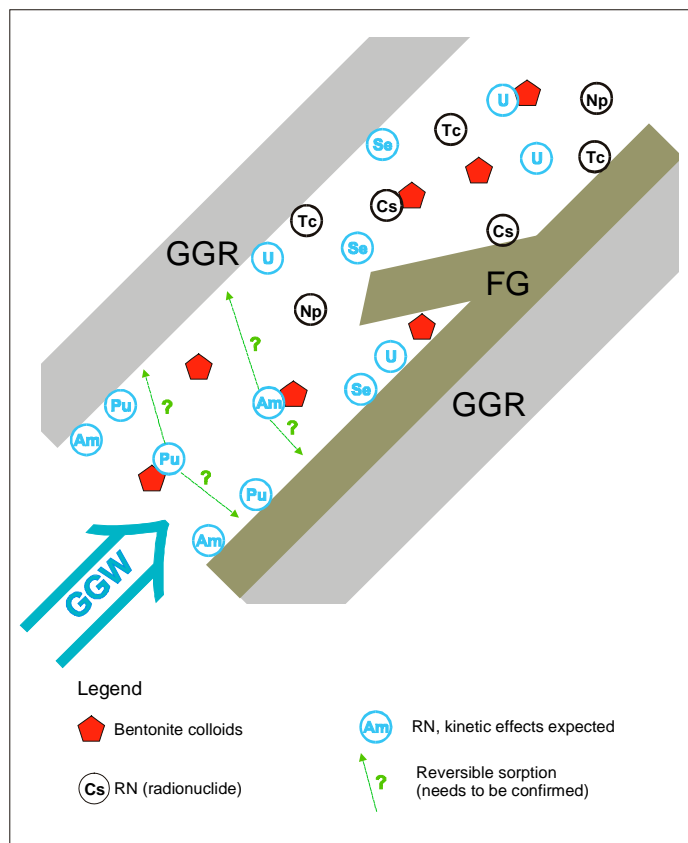


Figure 4-14. Preliminary conceptual model of radionuclide transport in a granitic shear zone in presence of bentonite colloids.

Significant sorption onto vial walls was observed for the actinides Pu and Am. Almost 90% loss of Pu and Am found in the case of low density polyethylene (LDPE) vials and less than 60% is lost in case of hard polyethylene, polypropylene material after ~10 days. No actinide losses can be detected in presence of 20 mg/L bentonite colloids. Additional laboratory experiments with PEEK vials are under way.

All these findings lead to the conclusion that a realistic field experiment is feasible at the GTS. A preliminary conceptual model of the behaviour of the nuclides within the flow field is shown in Figure 4-14.

## 5 Lessons learned and outlook

Given the scales of time and space that must be considered in a PA, direct testing of the realism, or conservatism, of a model in the system of interest is impossible. Field experiments, such as those performed at the GTS, are nevertheless of great value in that:

- the fundamental transport processes that operate in the system are expected to be the same or similar to those relevant to any fractured repository host rock;
- the structures present, though differing in detail, are also similar to those of potential fractured repository host rocks;
- the scales of time and space over which the experiments operate, though often considerably smaller than those of performance assessment, are larger than those achievable in the laboratory;
- the degree of characterisation of the system that is possible is greater than that achievable at a repository site (due to the smaller spatial scales involved in many field experiments and the need, at a repository site, to avoid perturbing the favourable properties of the system);
- field experiments, being performed in situ, are much less subject to experimental artefacts than laboratory experiments.

To look back on the last 15 years of radionuclide retardation experiments in the GTS, several things would almost certainly be changed from the days of MI (for example, in RRP a more complete hydrological characterisation of the experimental site was produced before beginning the in situ work and, for HPF/CRR, better structural and petrological descriptions of the flow paths have been produced). However, a more realistic question might be 'knowing now as little as you knew over ten years ago, at the beginning of MI/RRP, would you do it differently?'. In this case, it is likely that much less would be changed: the entire experiments have been a learning experience for most of the people involved and have certainly contributed to our views on blind predictive testing and the development and testing of conceptual models of groundwater flow. As noted in Alexander et al. /1997/ one weakness is that while the field experimenters, laboratory experimenters and transport modellers were in it together from the very beginning, the performance assessors were remarkable only by their absence. This would probably be the single greatest improvement possible to ensure the production of

PA relevant data from any field tracer experiment – and the eventual inclusion of such data in a repository PA.

Otherwise, the direction for future in situ experiments is clear: there must be greater integration of field experiments with appropriate natural analogues and laboratory data, everything being pulled together by the modelling of the systems /see Alexander et al., 1998 for comments/.

Overall, the field experiments at the GTS have enhanced confidence that the methodology adopted for:

- geological and hydrological characterisation of water-conducting features;
- simplification of this characterisation for modelling purposes;
- the adaptation of laboratory data (particularly sorption data) to field conditions;
- numerical solution of the governing equations for solute transport in dual-porosity media;

is indeed applicable to the modelling of solute transport through a fractured crystalline rock and have also been applied, at least in part, in the Kamaishi and Aspö rock laboratories.

## 6 Acknowledgements

Tasks as large as the joint Nagra / JNC Radionuclide Migration / Retardation Programme and the Colloid and Radionuclide Retardation Project have many players and the author would like to extend his thanks to all of them who have contributed in any form to the lessons learnt over the last 15 years. Special thanks are addressed to Russell Alexander and Wolfgang Kickmaier from Nagra, Kunio Ota from JNC and Walter Heer from PSI, all of whom played a leading role in the presented projects.

## References

**Alexander W R, Frieg B, Ota K, Bossart P, 1996.** The RRP Project: Investigating Radionuclide Retardation in the Host Rock. Nagra Bulletin No. 27 (June 1996), pp 43–55.

**Alexander W R, Frieg B, Ota K, Bossart P, 1997.** The assessment of radionuclide entrapment in repository host rocks. OECD Proceedings: Workshop on Field Tracer Experiments (role in the Prediction of Radionuclide Migration), Cologne, Germany, 28–30 August, 1996, NEA/OECD, Paris, France.

**Alexander W R, Gautschi A, Zuidema P, 1998.** Thorough testing of performance assessment models: the necessary integration of in situ experiments, natural analogues and laboratory work. Abstract in Sci. Basis Nucl. Waste Manag. XX, 1013–1014.

**Alexander W R, Kickmaier W, 2000.** Radionuclide retardation in water conducting systems – lessons learned in the research programme in the Grimsel Test Site. Presented at the workshop on “Chancen und Grenzen der geochemischen und Transport Modellierung bei der Verwahrung von Uranbergwerken und bei der Endlagerung radioaktiver Stoffe”, 18–19 May, 2000, Dresden, Germany.

**Berry J A, Boulton K A, Cowper M M, 2000.** Radionuclide retardation project: Analysis of radionuclide migration through a shear zone. Unpublished Nagra internal report, Nagra, Wettingen, Switzerland.

**Bossart P, Mazurek M, Hellmuth K-H, Schneebeili M, Siitari-Kauppi M, 1991.** GTS: structural geology and water flow paths in the Migration shear zone. Nagra Technical Report NTB 91-12, Nagra, Wettingen, Switzerland.

**Eikenberg J, Rützi M, Alexander W R, Frieg B, Fierz T, 1998.** The excavation project in the Grimsel Test Site: in situ high resolution gamma and alpha spectrometry of <sup>60</sup>Co, <sup>75</sup>Se, <sup>113</sup>Sn, <sup>152</sup>Eu, <sup>235</sup>U and <sup>237</sup>Np/<sup>233</sup>Pa. *Sci. Basis Nucl. Waste Manag.* XXI, 655–662.

**Frick U, Alexander W R et al., 1992.** The radionuclide migration experiment-overview of investigations 1985–1990. Nagra Technical Report NTB 91-04, Nagra, Wettingen, Switzerland.

**Heer W, Hadermann J, 1996.** Modelling Radionuclide Migration Field Experiments. Nagra Technical Report NTB 94-18, Nagra, Wettingen, Switzerland.

**Heer W, Hadermann J, 1996.** Grimsel Test Site – Modelling Radionuclide Migration Field Experiments. Nagra Tech. Report NTB 94-18, Nagra, Wettingen, Switzerland.

**McCombie C, Kickmaier W, McKinley I G, Thury M, 1997.** Swiss Underground Rock Laboratories in Crystalline and Clay: Rationale for Technical Programme Choice. Proceedings of the sixth international conference on Radioactive Waste Management and Environmental Remediation ICRM '97, Singapore (1997), pp 409–413.

**McKinley I G, Alexander W R, Bajo C, Frick U, Hadermann J, Herzog F A, Hoehn E, 1988.** The radionuclide migration experiment at the Grimsel rock laboratory, Switzerland. *Sci. Basis Nucl. Waste Manag.* XI, pp 179–187.

**Möri A, van Dorp F, 2000a.** Radionuclide Retardation Project: Excavation Project (EP), Grimsel Test Site, Mass balance of radionuclides injected into the MI experimental granitic shear zone in the GTS: degree of radionuclide recovery and radiological aspects. Unpublished Nagra internal report, Nagra, Wettingen, Switzerland.

**Möri A editor, 2000b.** CRR Experiment Phase 1, Status report. Unpublished Nagra internal report, Nagra, Wettingen, Switzerland.

**Nagra, 1994.** Kristallin-1, Nagra Technical Report Series, NTB 93-22, Nagra, Wettingen, Switzerland.

**Ota K, Alexander W R, Smith P A, Möri A, Frieg B, Frick U, Umeki H, Amano K, Cowper M M, Berry J A, 2000.** Building confidence in radionuclide transport models for fractured rock: the Nagra/JNC radionuclide retardation programme. *Sci. Basis Nucl. Waste Manag.* (in press).

**Smith P A, Alexander W R, Kickmaier W, Ota K, Frieg B, McKinley I G, 2000.** Development and Testing of Radionuclide Transport Models for Fractured Rock: Examples from the Nagra/JNC Radionuclide Migration Programme in the Grimsel Test Site, Switzerland. *J. Contam. Hydrol.* (in press).

**Smith P A, Alexander W R, Umeki H, Mazurek M, Heer W, Bayens B, Bradbury M H, McKinley I G, Kinzelbach W, 2000.** The radionuclide migration experiment-overview of investigations 1990–1997. Nagra Technical report NTB 00-09, Nagra, Wettingen, Switzerland.

# Classification and characterisation of water-conducting features at Äspö

*Martin Mazurek*

*Rock/Water Interaction Group (GGWW), University of Bern, Switzerland*

*Paul Bossart*

*Geotechnisches Institut, Bern, Switzerland*

*Jan Hermanson*

*Golder Grundteknik AB, Stockholm. Sweden*

## Executive summary

The objectives of the Fracture Classification and Characterization Project (FCC), a joint undertaking of Nagra (Switzerland) and SKB (Sweden), are

- to classify water-conducting features that occur in the Äspö tunnel system,
- to characterize and conceptualize these features with respect to radionuclide transport properties (e.g. structure, mineralogy, distribution of flow and matrix porosity),
- to develop and apply a methodology for the characterization of water-conducting features in crystalline rocks.

The methodology of investigation includes a stepwise procedure:

- Compilation of an inventory of existing data (geology, hydrogeology, hydro-chemistry) and of the boundary conditions on how water-conducting features can be explored (e.g. boreholes, open tunnel). Definition of scale at which the investigation should target.
- Preliminary characterization of a limited number of typical water-conducting features, with the objective to understand the processes that governed the evolution of water-conducting features and so to define a set of geologic parameters that adequately describe the features.
- Full characterization of a large number of water-conducting features and acquisition of a database containing all relevant parameters that can be observed or measured.
- Database analysis (which parameters are common to all features, which vary systematically ?) and derivation of a fracture classification scheme.
- Derivation of simplified conceptual models of all types of water-conducting features, including geometric and lithologic (mineralogic, porosimetric) information needed for transport modelling.



- Transport modelling and sensitivity analysis of parameters from the conceptual models.

The preliminary characterization stage indicated that on an observation scale of meters to decameters, all water-conducting features are related to faults. The fault geometries are consistent with the mechanistic principles of fault nucleation, propagation and linkage derived by Martel and Pollard /1989/. This model characterizes the anatomy of faults as interconnected systems of shear fractures (master faults) and tensile fractures (splay cracks).

The full characterization included 88 water-conducting features whose traces cross cut the entire tunnel cross-section (smaller features were not included in the study). Most of the faults dip steeply, and strike directions are NW-SE (dominant) and NE-SW (subordinate). Many of the faults follow pre-existing structural inhomogeneities, such as ductile shear-zones of lithified cataclastic shear-zones.

Fault geometries or any other parameters are indistinguishable in the Småland granite and in the Äspö diorite. Fracture frequencies are higher in the Fine-grained granite, and other fault characteristics contributing to the transport properties (e.g. lithologic units, mineralogy, distribution of pore-spaces) are also different. However, Fine-grained granite was never observed to be the dominating host rock of any of the features because it occurs as small intrusive bodies or dykes whose sizes are measured in meters to a few decameters. It is concluded that because (within the database of 88 water-conducting features) this rock type does not host faults over more than a few meters, it is not relevant for the larger-scale transport properties of the faults.

In the review process of this report, it was pointed out that the possibility exists that large bodies of Fine-grained granite could exist even if they were not observed in the part of the tunnel system on which this report is based. It is a topic of planned future investigations to explore and characterize faults hosted by Fine-grained granite.

The only striking difference between individual water-conducting features is the internal fault geometry, while no other distinguishing criteria (such as the arrangement of lithologic domains, mineralogy of fracture infills, transmissivity etc.) were identified and probably do not exist. On the basis of the geometric arrangement of master faults and splay cracks in faults, 5 types of water-conducting features are distinguished:

Type 1 – single fault

Type 2 – swarm of single faults

Type 3 – fault zone

Type 4 – fault zone with rounded geometries

Type 5 – parallel fault zones with long connecting splays.

Both direct observations and theoretical principles indicate that the internal geometry on which the classification is based is not a unique characteristic of a fault, i.e. the type may vary along the strike of a fault. The length of segments with constant properties (i.e. same type) is in the range of meters to many decameters. The application of the classification scheme is limited to smaller-scale considerations, while in the case of large-scale transport, the results of the study indicate that due to the common genetic history, water flow in the underground of Äspö is dominated by one single family of water-conducting features.

Conceptual models of the fault geometry are derived on the basis of the field database and laboratory analyses of mineralogy, porosity and pore-space distribution (Figure 4-15). Flow within faults occurs within the master faults and/or in the splay cracks. The lithologic domains adjacent to the flow porosity are

- fault gouge/breccia,
- lithified cataclasite,
- fracture coating,
- mylonite (altered or unaltered),
- granite (altered or unaltered).

The brittle fault rocks (i.e. fault gouge / breccia, see Figure 4-16) are expected to strongly interact with radionuclides or tracers transported in the flow porosity by means of sorption (presence of sorbing phases such as clay minerals and Fe-oxyhydroxides) and matrix diffusion (large interconnected porosity). These processes are weaker in mylonites due to the low porosity and the scarcity of low-temperature alteration products.

A conceptual representation of the expected transport paths of radionuclides between canister and the biosphere is shown in Figure 4-17.

## Reference

**Martel S J, Pollard D D, 1989.** Mechanics of slip and fracture along small faults and simple strike-slip fault zones in granitic rock. *J. Geophys. Res.* 94:9417–9428.

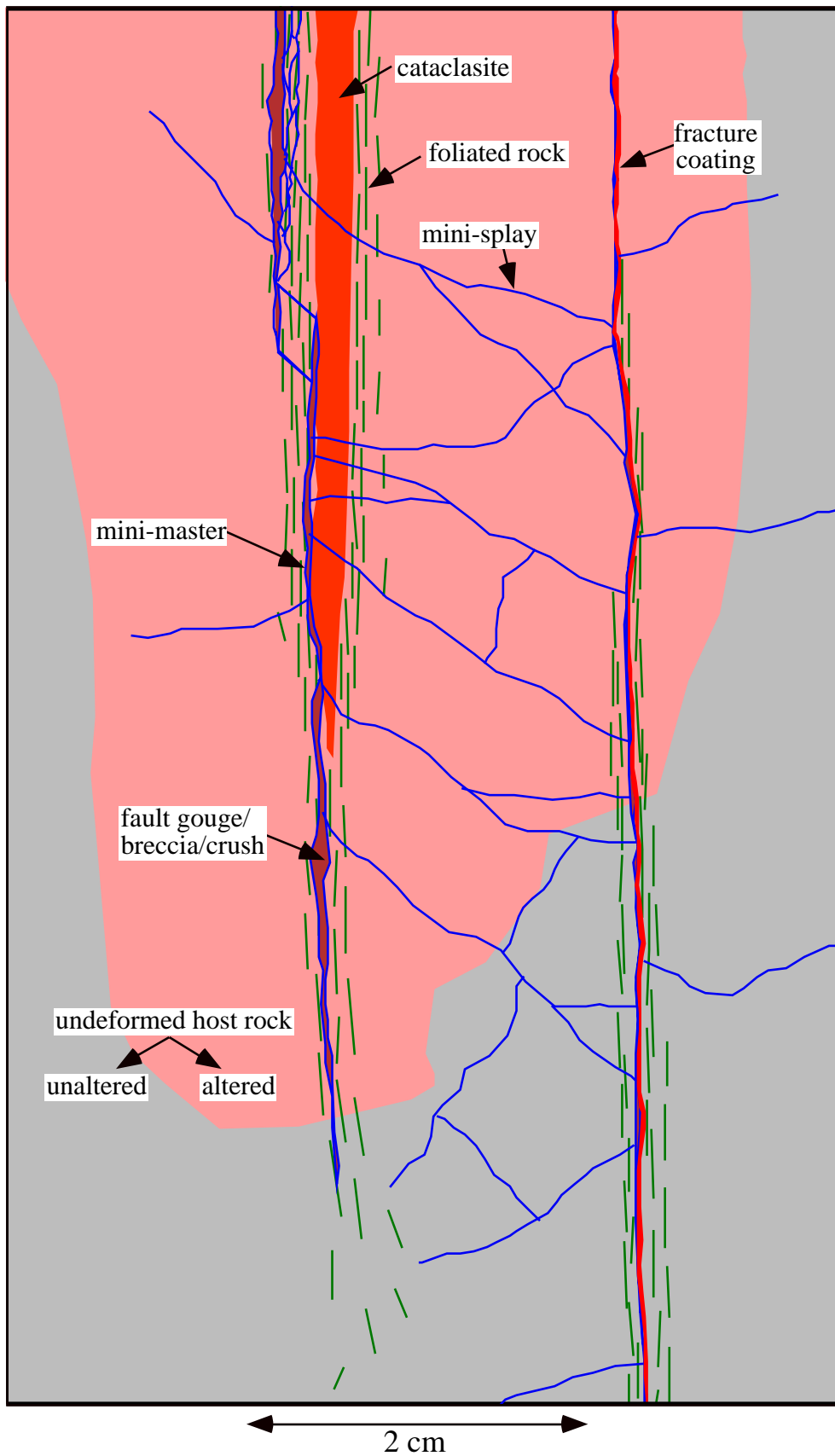
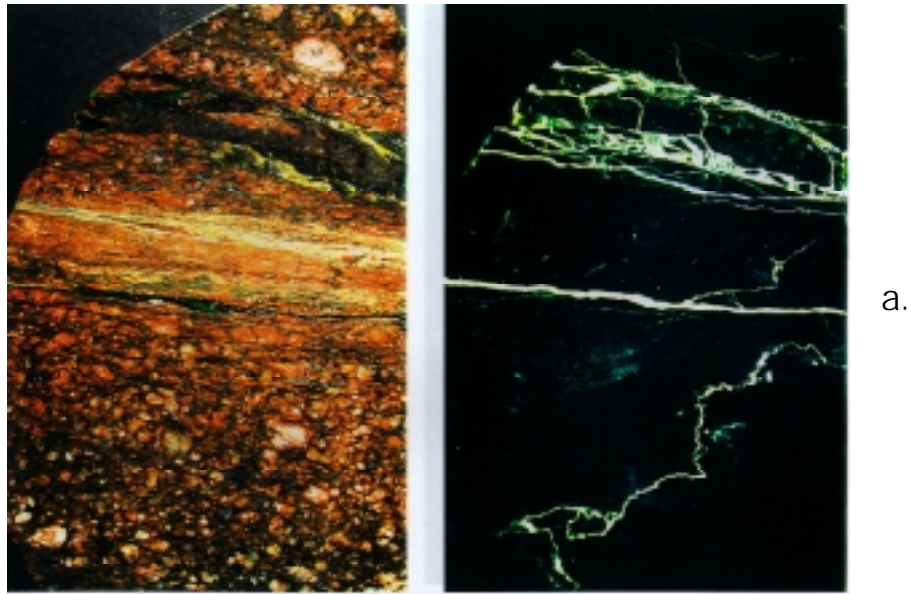
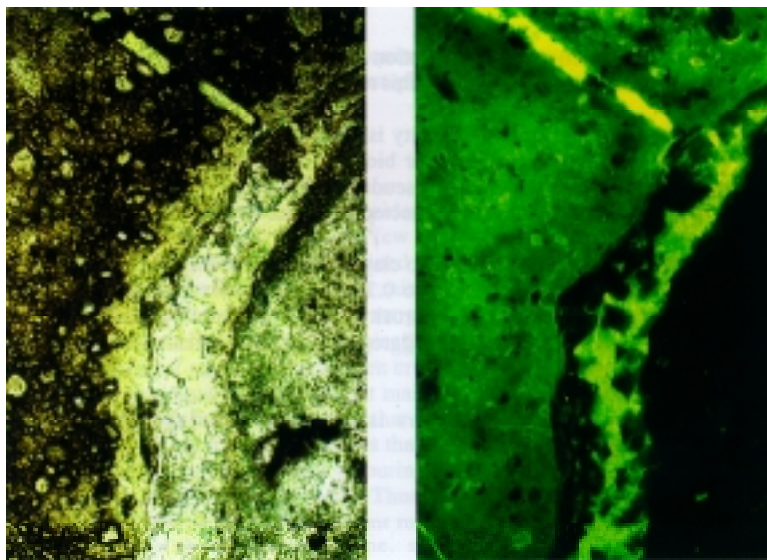


*Figure 4-15. Small-scale anatomy of a master fault.*



a.



b.

**Figure 4-16.** a) Photographs of cross-sections through a resin-impregnated master fault at 3124 m. Left: visible-light photograph; right: UV light. Height of photographs 12 cm, b) Close-up of the interface between fault gouge (left side in each photograph) and wallrock (right), showing a naturally open micro-fracture with idiomorphic crystals on the walls. Height of micrographs 0.5 mm.

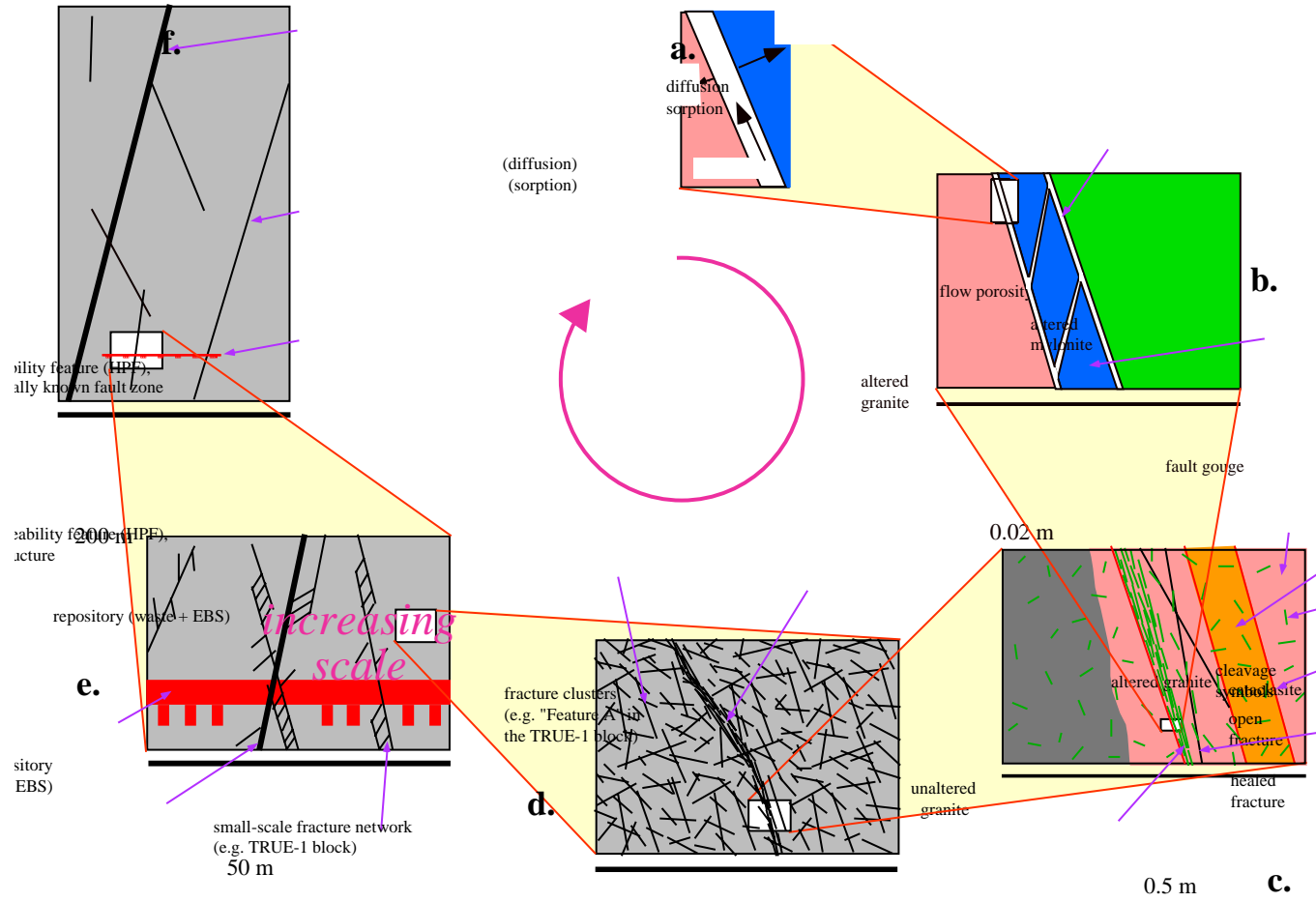


Figure 4-17. Series of conceptual models showing fracture geometries and water flow paths on a range of scales.

# **Appendices**

# Contents

	Page
Appendix A: References	211
Appendix B: Agenda of seminar	216
Appendix C: List of participants	219

### References

*The following list of references constitutes a collection of references to papers, reports and conference contributions related to the First TRUE Stage made by the SKB Project team and the participating modelling teams in the Äspö Task Force work (to be complemented during review process).*

**Andersson P, 1995.** Compilation of tracer tests in fractured rock. Äspö Hard Rock Laboratory Progress Report PR 25-95-05, Swedish Nuclear Fuel and Waste Management Co.

**Andersson P, 1996.** TRUE 1<sup>st</sup> stage tracer test programme. Experimental data and preliminary evaluation of the TRUE-1 radially converging tracer test (RC-1). Äspö Hard Rock Laboratory Progress Report HRL-96-24, Swedish Nuclear Fuel and Waste Management Co.

**Andersson P, Jönsson S, 1997.** TRUE 1<sup>st</sup> stage tracer test programme. Complementary Tracer Tests (RC-2, DP-5, DP-6). Experimental description and preliminary evaluation. Äspö Hard Rock Laboratory Progress Report HRL-97-23, Swedish Nuclear Fuel and Waste Management Co.

**Andersson P, Nordqvist R, Jönsson S, 1997.** TRUE 1<sup>st</sup> stage tracer test programme. Experimental data and preliminary evaluation of the TRUE-1 dipole tracer tests DP-1 – DP-4. Äspö Hard Rock Laboratory Progress Report HRL-97-13, Swedish Nuclear Fuel and Waste Management Co.

**Andersson P, Wass E, 1998.** TRUE 1<sup>st</sup> stage tracer test programme. Preliminary Design Tests for tests with radioactive sorbing tracers (PDT-1, PDT-2, PDT-3). Experimental description and preliminary evaluation. Äspö Hard Rock Laboratory Progress Report HRL-98-13, Swedish Nuclear Fuel and Waste Management Co.

**Andersson P, Johansson H, Nordqvist R, Skarnemark G, Skålberg M, Wass E (in prep).** TRUE 1<sup>st</sup> stage tracer test programme. Tracer tests with sorbing tracers STT-1. Experimental description and preliminary evaluation. Äspö Hard Rock Laboratory International Progress Report IPR-00-XX, Swedish Nuclear Fuel and Waste Management Co.

**Andersson P, Johansson H, Skarnemark G, Skålberg M, Wass E, 1999.** TRUE 1<sup>st</sup> stage tracer test programme. Tracer tests with sorbing tracers STT-1b. Experimental description and preliminary evaluation. Äspö Hard Rock Laboratory International Progress Report IPR-99-12, Swedish Nuclear Fuel and Waste Management Co.

**Andersson P, Byegård J, Johansson H, Skarnemark G, Wass E, 1999.** TRUE 1<sup>st</sup> stage tracer test programme. Tracer tests with sorbing tracers STT-2. Experimental description and preliminary evaluation. Äspö Hard Rock Laboratory International Progress Report IPR-99-15, Swedish Nuclear Fuel and Waste Management Co.



**Birgersson L, Gale J, Hakami E, 2000a.** First TRUE Stage – Pilot Resin Experiment – Summary Report. Äspö Hard Rock Laboratory International Progress Report IPR-00-04, Swedish Nuclear Fuel and Waste Management Co.

**Birgersson L, Gale J, Hakami E, 2000b.** First TRUE Stage – Pilot Resin Experiment – Background information. Äspö Hard Rock Laboratory International Progress Report IPR-00-05, Swedish Nuclear Fuel and Waste Management Co.

**Byegård J, 1993.** The possibility of using slightly sorbing cations in tracer experiments in the Äspö Hard Rock Laboratory. Äspö Hard Rock Laboratory Progress Report PR 95-93-14, Swedish Nuclear Fuel and Waste Management Co.

**Byegård J, Skarnemark G, Skålberg M, 1995.** The use of some ion-exchange sorbing tracer cations in in-situ experiments in high saline groundwaters. *Mat. Res. Soc. Symp. Proc.*, vol. 353, pp. 1077–1084.

**Byegård J, Johansson H, Skålberg M, Tullborg E-L, 1998.** The interaction of sorbing and non-sorbing tracers with different Äspö rock types – Sorption and diffusion experiments in the laboratory scale. SKB TR-98-18, Swedish Nuclear Fuel and Waste Management Co.

**Byegård J, Siitari-Kauppi M, Johansson H (in prep).** Complementary laboratory investigations of site-specific material from Feature A. Äspö Hard Rock Laboratory Progress Report IPR-00-XX, Swedish Nuclear Fuel and Waste Management Co.

**Cvetkovic V, Dagan G, Cheng H, 1998a.** Contaminant transport in aquifers with spatially variable flow and sorption properties, *Proc. R. Soc. Lond. A*, **454**, 2173–2207.

**Cvetkovic V, Cheng H, Selroos J-O, 1998b.** Lagrangian modelling of TRUE-1 reactive tracer tests at the Äspö Hard Rock Laboratory, Sweden, GQ'98 Groundwater Quality: Remediation and protection, IAHS Publication no. 250, pp. 375–379.

**Cvetkovic V, Selroos J-O, Cheng H, 1999.** Transport of reactive solute in single fractures, *J. Fluid Mech.*, **318**, 335–356.

**Cvetkovic V, Cheng H, Selroos J-O, 2000.** Evaluation of Tracer Retention Understanding Experiments (first stage) at Äspö. Äspö Hard Rock Laboratory International Cooperation Report ICR 00-01, Swedish Nuclear Fuel and Waste Management Co.

**Dershowitz W, Thomas A, Busse R, 1996.** Discrete fracture network analysis in support of the Äspö Tracer Retention Understanding Experiment (TRUE-1). Äspö Hard Rock Laboratory International Cooperation Report ICR 96-05, Swedish Nuclear Fuel and Waste Management Co.

**Dershowitz B, Cladouhus T T, Uchida M, 2001.** Tracer tests with sorbing tracers. Äspö Hard Rock Laboratory International Cooperation Report ICR 01-02, Swedish Nuclear Fuel and Waste Management Co.

**Elert M, 1999.** Evaluation of the TRUE-1 radially converging and dipole tests with conservative tracers. The Äspö Task Force on modelling of groundwater flow and transport of solutes. Tasks 4C and 4D. SKB TR-99-04, Swedish Nuclear Fuel and Waste Management Co.

**Elert M, Svensson H (in press).** Deconvolution of breakthrough curves STT-2 (Task 4F). The Äspö Task Force on modelling of groundwater flow and transport of solutes. Tasks 4F. Äspö Hard Rock Laboratory, SKB TR-01-12, Swedish Nuclear Fuel and Waste Management Co.

**Gylling B, Khademi B, Moreno L, 1998.** Modelling of the Tracer Retention Understanding Experiment Task 4C-D. Äspö Hard Rock Laboratory. International Cooperation Report ICR 98-01, Swedish Nuclear Fuel and Waste Management Co.

**Hakami E, Gale J, 1999.** First TRUE Stage – Pilot Resin Experiment – Pore space analysis. Äspö Hard Rock Laboratory International Progress Report IPR-99-14, Swedish Nuclear Fuel and Waste Management Co.

**Ittner T, Byegård J, 1997.** Äspö Hard Rock Laboratory First TRUE Stage. Test of tracer sorption on equipment. Äspö Hard Rock Laboratory Progress Report HRL-97-28, Swedish Nuclear Fuel and Waste Management Co.

**Johansson H, Siitari-Kauppi M, Skålberg M, Tullborg E-L, 1997.** Diffusion pathways in crystalline rocks – Examples from Äspö-diorite and fine-grained granite. *J. of Contaminant Hydrol.*, vol. 35, no. 1–3, pp. 41–53.

**Johansson H, Byegård J, Skarnemark G, Skålberg M, Andersson P, Wass E (submitted).** In-situ migration experiments at Äspö Hard Rock Laboratory, Sweden. Results of radioactive tracer migration studies in a single fracture. Paper submitted to *Radiochimica Acta*, March 2000.

**Johansson H, Haggerty R, Byegård J, Skålberg M (submitted).** In-situ migration experiments at Äspö Hard Rock Laboratory, Sweden: Application of laboratory-derived retardation and diffusivity data in modeling of sorbing tracer tests. Paper submitted to *J. Contaminant Hydrol.*, March 2000.

**Liedke L, Shao H, 1998.** Modelling of the tracer experiments in Feature A at Äspö HRL. Äspö Hard Rock Laboratory International Cooperation Report ICR 98-02, Swedish Nuclear Fuel and Waste Management Co.

**Mazurek M, Bossart P, Eliasson T. 1997.** Classification and characterisation of water-conducting features at Äspö. Results of investigations on the outcrop scale. Äspö Hard Rock Laboratory International Cooperation Report ICR-97-01, Swedish Nuclear Fuel and Waste Management Co.

**McKenna S A, 1999.** Solute transport modelling of the Äspö STT-1b tracer tests with multiple rates of mass transfer. Task 4E. Äspö Task Force on Modelling of Groundwater Flow and Transport of Solutes. Äspö Hard Rock Laboratory International Cooperation Report ICR-99-02, Swedish Nuclear Fuel and Waste Management Co.

**Moreno L, 2001.** Evaluation of sorbing tracer tests using the channel network model. Äspö Task Force , Task 4E and 4F. Äspö Hard Rock Laboratory International Cooperation Report ICR-99-02, Swedish Nuclear Fuel and Waste Management Co.

**Neretnieks I, Moreno L, in prep.** Analysis of the TRUE experiments considering a 3D flow-pattern, Manuscript in preparation.

**Painter S, Cvetkovic V, Selroos J-O, 1998.** Transport and retention in fractured rock : Consequences of a power-law distribution for fracture lengths. *Physical Review*, vol. 57, no. 6, pp. 6917–6922.

**Poteri A, Hautojärvi A, 1998.** Modelling of the tracer tests in radially converging and dipole flow fields in the first phase of the TRUE project. Äspö Hard Rock Laboratory International Cooperation Report ICR 98-03, Swedish Nuclear Fuel and Waste Management Co.

**Poteri A, 2001.** Modelling of the TRUE-1 sorbing tracer tests. Äspö Task Force, Task 4E and 4F. Äspö Hard Rock Laboratory International Cooperation Report ICR 01-01, Swedish Nuclear Fuel and Waste Management Co.

**Roberts R, 1998.** Data analyses using GTFM for selected flow and pressure buildup tests in the TRUE-1 borehole array. Äspö Hard Rock Laboratory Progress Report HRL-98-06, Swedish Nuclear Fuel and Waste Management Co.

**Selroos J O, Cvetkovic V, 1996.** On the characterisation of retention mechanisms in rock fractures. SKB TR 96-20, Swedish Nuclear Fuel and Waste Management Co.

**Selroos J-O, Cvetkovic V, 1998.** Prediction of the TRUE-1 radially and converging and dipole tracer tests, Äspö Task Force, Tasks 4C and 4D. Äspö Hard Rock Laboratory International Cooperation Report ICR-98-07, Swedish Nuclear Fuel and Waste Management Co.

**Shao H, Liedke L, 1999.** Modelling the reactive radioactive and sorbing tracer tests in fractured rock. Äspö Task Force, Task 4E and 4F. Äspö Hard Rock Laboratory International Cooperation Report ICR-99-03, Swedish Nuclear Fuel and Waste Management Co.

**Tanaka Y, Hasegawa T, Kawanishi M, 1997.** Numerical analysis with FEGM/FERM for TRUE-1 non-sorbing tracer tests. Äspö Hard Rock Laboratory International Cooperation Report ICR 97-07, Swedish Nuclear Fuel and Waste Management Co.

**Winberg A, 1994.** Tracer retention Understanding Experiments (TRUE) – Test plan for the First TRUE Stage. Äspö Hard Rock Laboratory Progress Report PR 25-94-35, Swedish Nuclear Fuel and Waste Management Co.

**Winberg A, Andersson P, Hermanson J, Byegård J, Cvetkovic V, Birgersson L, 2000.** Äspö Hard Rock Laboratory. Final report of the first stage of the Tracer Retention Understanding Experiments. SKB TR-00-07, Swedish Nuclear Fuel and Waste Management Co.

**Winberg A, 2001.** The Tracer Understanding Experiments (TRUE), Äspö Hard Rock Laboratory. In: Étude pour la Faisabilité des Stockages de Déchets Radioactifs. Actes des Journées Scientifiques ANDRA, Nancy, 7, 8 et 9 décembre 1999. EDP Sciences. ISBN : 2-86883-513-9.

**Winberg A (ed), 1996.** First TRUE Stage – Tracer Retention Understanding Experiments: Descriptive structural-hydraulic models on block and detailed scales on the TRUE-1 site. Äspö Hard Rock Laboratory International Cooperation Report ICR 96-04, Swedish Nuclear Fuel and Waste Management Co.

**Winberg A, Andersson P, Hermanson J, Stenberg L, 1996.** Results of the SELECT Project – Investigation Programme for Selection of Experimental Sites for the Operational Phase. Äspö Hard Rock Laboratory Progress Report PR HRL-96-01, Swedish Nuclear Fuel and Waste Management Co.

## Agenda of seminar

### International Seminar on First TRUE Stage

Äspö Hard Rock Laboratory, Sweden, September 11–13, 2000

#### Monday, September 11

##### Session 1 Introduction

- 13.30 Welcome address: Objective and scope of the seminar – Olle Olsson, Director of Repository Technology, SKB
- 13.45 Overview of TRUE Programme – Anders Winberg, Project manager for the TRUE programme

##### Session 2 SKB project team interpretation of experimental results

In following presentations the project group will convey their findings and experiences focused on “*main conclusions*” and “*lessons learned*”.

*Chairman: Peter Wikberg*

- 14.00 Introduction and overview of presentations – Anders Winberg, Conterra AB
- 14.05 Geology and structural geology – Jan Hermanson, Golder Associates
- 14.30 Mineralogy and geochemistry – Eva-Lena Tullborg, Terralogica AB
- 14.45 Hydraulic characterisation – Peter Andersson, GEOSIGMA AB
- 15.10 Questions/Discussion
- 15.30 Coffee
- 15.50 Laboratory transport experiments – Johan Byegård/Henrik Widestrand, Chalmers University of Technology
- 16.20 In situ transport experiments – Peter Andersson, GEOSIGMA AB
- 16.40 Detailed description of the studied fracture – Anders Winberg, Conterra AB
- 16.55 Model evaluation of in situ experiments – Vladimir Cvetkovic, Royal Institute of Technology
- 17.30 Implications to performance assessment and site characterisation – Anders Winberg, Conterra AB
- 17.50 Questions/Discussion
- 18.30 End of Day 1

## Tuesday, September 12

### Session 3 Alternative evaluation of TRUE-1 results and related studies

*Chairman: Olle Olsson and Mansueto Morosini*

#### *Session 3a Detailed characterisation of transport-related properties*

- 08.30 Assessment of in situ aperture using epoxy resin injection – Lars Birgersson (Kemakta Consultants AB), Eva Hakami (Itasca Geomekanik AB) and John Gale (Memorial University, Newfoundland).
- 08.50 Alteration and diffusion profiles in drill cores from Äspö – Ove Landström (Studsvik Nuclear) and Eva-Lena Tullborg (Terralogica AB).
- 09.10 “Laboratory Migration Experiments using Äspö Granitic Rock – Effects of Heterogeneity in Rock Properties”, Wörman A, Xu S, Dverstorp B.
- 09.30 Visualization and Quantification of Heterogeneous Diffusion Rates in Granodiorite Samples by X-Ray Absorption Imaging – Diffusion within Gouge Materials, Altered Rim and Intact Rock. – Susan J Altman (SANDIA), Masahiro Uchida (JNC), Vincent C. Tidwell (SANDIA).
- 09.50 Coffee

#### *Session 3b Alternative evaluation of TRUE-1 results*

- 10.20 When is a “Single Feature” a Fracture Network – Learning from Mass Recovery and Breakthrough Curves in the TRUE-1 Experiment – Bill Dershowitz (Golder Associates), Masahiro Uchida (JNC), Jan Hermanson (Golder Associates) and Aaron Fox (Golder Associates)
- 10.40 A simple flow channel model of TRUE-1 – Antti Poteri, VTT Energy
- 11.00 Integration of laboratory sorption and diffusivity data in modeling of sorbing tracer tests STT-1 and STT-1b – Henrik Widestrand, Johan Byegård (Chalmers University of Technology) and Roy Haggerty (Oregon State University).
- 11.20 Evaluation of tests with sorbing tracers using Chan 3D – Luis Moreno, Royal Institute of Technology
- 11.40 Lunch
- 12.40 Revisiting the Advection-Dispersion model – Testing an alternative – Ivars Neretnieks, Royal Institute of Technology
- 13.10 Discussion

*Session 3c Related studies*

- 13.40 Effects of combined matrix diffusion and small scale dispersion in a single fracture with spatially variable aperture – Jan-Olof Selroos, SKB.
- 14.00 The Moderately Fractured Rock Experiment Mass Transport in Fracture Networks – Experiment Overview. – Mark R Jensen, Ontario Power Generation.
- 14.20 Coffee
- 14.40 Anisotropy, Reversibility and Scale Dependence of transport properties in Single Fracture and Fractured Zone – Non-sorbing tracer experiment at the Kamaishi Mine. – Masahiro Uchida (JNC), Atsushi Sawada (JNC), Michito Shimo (Taisei Corporation), Hajime Yamamoto (Taisei Corporation), Hiroyuki Takahara (Nittetsu Mining Co) and Thomas W Doe (Golder Associates).
- 15.00 The TRUE Block Scale experiment – A status report. – Anders Winberg, Conterra AB
- 15.20 Underground visit (PW/AW)
- 17.30 End of Day 2

**Wednesday, September 13**

Session 4 Understanding of retention processes in a single fracture

*Moderator: Johan Andersson, Streamflow AB*

- 08.30 Session 4a: Themes 1 and 2 (see below)
- Synthesis of active transport processes over the time scales of the experiments – Vladimir Cvetkovic, Royal Institute of Technology
  - Swiss presentation of comparison between Grimsel and Äspö, Martin Mazurek, Res Möri
  - Discussion
- 10.30 Coffee
- 11.00 Session 4b: Themes 3 and 4
- 12.30 Lunch
- 13.30 Continued discussion, summing up
- 14.30 End of the seminar

## List of participants

Nr	Name	Surname	Org	Address	e-mail	Telephone
1.	Luis	Moreno	Chemical Engineering and Technology Royal Institute of Technology	100 44 Stockholm	lm@ket.kth.se	+46-8 790 6412
2.	Antti	Poteri	VTT Energy	P.O.Box 1604 FIN-02044 Finland	antti.poteri@vtt.fi	+358 9 456 5059 / fax +358 9 456 5000
3.	Karl-Heinz	Hellmuth	Radiation and Nuclear Safety Authority	P.O. Box 14 FIN-00881 Helsinki Finland	karl-heinz. hellmuth@stuk.fi	+ 358 9 759 88 307
4.	Kaisa-Leena	Hutri	Radiation and Nuclear Safety Authority	P.O. Box 14 FIN-00881 Helsinki Finland	karl-heinz. hellmuth@stuk.fi	+ 358 9 759 88 307
5.	Eva-Lena	Tullborg	Terralogica AB	Box 4140 443 14 Gråbo	evalena@swipnet. se	+46-302-420 66
6.	Ove	Landström		Styrmansv. 5 619 34 Trosa		+ 46-156-16165
7.	Ivars	Neretnieks	Royal Institute of Technology Dept. Chem. Engineering KTH	SE-100 44 Stockholm	niquel@ket.kth.se	08-7908229
8.	Mansueto	Morosini	SKB	Äspölaboratoriet PI 300 572 95 Figeholm	skbmm@skb.se	0491-767804
9.	Aimo	Hautojärvi	POSIVA OY	Töölönkatu 4 FIN-00100 Helsinki Finland	aimo.hautojarvi@ posiva.fi	+358-9-2280 3747
10.	Lutz	Liedtke	Federal Institute for Geosciences and Natural Resources	Stilleweg 2 D-30655 Hannover Germany	Lutz.Liedtke@ bgr.de	0049 511 643 2418



Nr	Name	Surname	Org	Address	e-mail	Telephone
11.	Emmanuel	Ledoux	Ecole des Mines de Paris, Centre d'Informatique Géologique	35 rue Saint Honoré, F-7305 Fontainebleau Cedex France	ledoux@cig. ensmp.fr	33 1 64 69 47 02 / fax 33 1 64 69 47 03
12.	Eckhard	Fein	GRS mbH	Theodor-Heuss-Str. 4, D-38122 Braunschweig, Germany	fei@grs.de	0049 531/8012- 292
13.	Mark	Jensen	Ontario Power Generation	700 University Ave Toronto, Ontario M5G 1X6 Canada	mark.jensen@ ontariopower generation.com	416-592-8672 / fax 416-592-7336
14.	William S	Dershowitz	Golder Associates Inc/JNO	18300 NE Union Hill Rd (Suite 200) Redmond WA 98052 USA	dersh@golder. com	+1 425 883 0777
15.	Masahiro	Uchida	JNC (Japan Nuclear Fuel Cycle Development Institute)	4-33, Muramatsu, Tokai-mura Ibaraki-ken 319-1194 JAPAN	uchida@tokai. jnc.go.jp	+81-29-287-1540
16.	Jan	Hermansson	Golder Associates	Box 20127 104 60 Stockholm	jhermansson@ golder.se	+46 8 506 30600 (Sthlm) +1 425 883 0777 (Seattle)
17.	Peter	Meier	Andra	???	peter.meier@ andra.fr	01 4611 8130
18.	John	Black	In Situ Solutions (UK) Ltd	24 Ludgate Drive East Bridgford NG13 8NW Nottingham UK	johnblack@ insitusolutions. co.uk	+44 1949 21379
19.	Johan	Andersson	Streamflow	???	johan.andersson@ streamflow.se	08-862228 Mobile : 070- 622 21 32

<b>Nr</b>	<b>Name</b>	<b>Surname</b>	<b>Org</b>	<b>Address</b>	<b>e-mail</b>	<b>Telephone</b>
20.	Jesús	Suso	Aitemin	C/Rio Valdemarías s/n 45007 Toledo Spanien	Jesus.suso@ aitemin.se	+34 925 241 162
21.	Anders	Winberg	Conterra AB	Ögärdesvägen 4, 433 30 Partille	anders.winberg@ mailbox.swipnet.se	031-44 32 90 Mob. 070- 674 32 90
22.	Johan	Byegård	Nuclear Chemistry, Chalmers University of Technology	412 96 Göteborg	byegard@nc. chalmers.se	031-772 29 16
23.	Henrik	Widestrand	Nuclear Chemistry, Chalmers University of Technology	412 96 Göteborg	henrikj@nc. chalmers.se	031-772 28 04
24.	Peter	Andersson	Geosigma AB	Box 894, 751 08 Uppsala	peter.andersson@ geosigma.se	018-65 08 15 Mob. 070- 640 00 41
25.	Vladimir	Cvetkovic	Water Resources Engineering, KTH	100 44 Stockholm	vdc@wre.kth.se	08-790 62 90
26.	Hua	Cheng	Water Resources Engineering, KTH	100 44 Stockholm	hcheng@ce. kth.se	
27.	Jan-Olof	Selroos	SKB	Box 5864, 102 40 Stockholm	skbjos@skb.se	08-459 84 25
28.	Peter	Wikberg	SKB	Box 5864, 102 40 Stockholm	skbpw@skb.se	08-459 85 63
29.	John E	Gale	Memorial University/ Fracflow Consultants	Dept. Earth Sciences, St. Johns, NF, CA, A1B3X5	ffc.nfld@thezone. net	709-739-7270 fax 709-753-5101
30.	Olle	Olsson	Äspö HRL	PI 300, 572 95 FIGEHOLM	Olle.olsson@ skb.se	0491-76 78 09 fax 0491-82 005

<b>Nr</b>	<b>Name</b>	<b>Surname</b>	<b>Org</b>	<b>Address</b>	<b>e-mail</b>	<b>Telephone</b>
31.	Atsushi	Sawada	JNC	4-33, Muramatsu, Tokai-mura, Ibaraki-ken 319-1194 JAPAN	<a href="mailto:sawada@tokai.jnc.go.jp">sawada@tokai.jnc.go.jp</a>	+81-29-287-0928
32.	Jane	Long	Mackay School of Mines	University of Nevada, Reno Nevada 89557-1766	<a href="mailto:jcslong@unr.edu">jcslong@unr.edu</a>	
33.	Lars	Birgersson	Kemakta Konsult AB	Box 12655, 112 93 Stockholm	<a href="mailto:lb@kemakta.se">lb@kemakta.se</a>	08-617 67 98
34.	Anders	Wörman	Inst. För Geovetenskaper / Uppsala Universitet	Villavägen 16 / 752 36 Uppsala	<a href="mailto:anders.worman@geo.uu.se">anders.worman@geo.uu.se</a>	018-471 25 23